The Dissertation Committee for Prince Nnamdi Azom certifies that this is the approved version of the following dissertation:

IMPROVED MODELING OF THE STEAM-ASSISTED GRAVITY DRAINAGE (SAGD) PROCESS

Committee:

Sanjay Srinivasan, Supervisor

Kishore Mohanty

Quoc Nguyen

Masa Prodanovic

Arjan Kamp

IMPROVED MODELING OF THE STEAM-ASSISTED GRAVITY DRAINAGE (SAGD) PROCESS

by

Prince Nnamdi Azom, B.S.Ch.E.; M.S.E.

Dissertation

Presented to the Faculty of the Graduate School of

The University of Texas at Austin

in Partial Fulfillment

of the Requirements

for the Degree of

Doctor of Philosophy

The University of Texas at Austin

May 2013

Dedication

To the memory of my late mum…words can't describe how much I would have wanted you to see this day…you started this journey with me, but still hurts you didn't wait to see its end…I couldn't have come this far without all the sacrifices you made…

To my wife, the unsung hero of this journey…without your patience and sacrifice, today would have been impossible…at least, we can now have our honeymoon…

To my son, I guess you have one less excuse not to pursue a doctorate degree…of course in any discipline of your choosing…I also hope you will one day read this dissertation and be proud of what I've tried to achieve…

Acknowledgements

I would like to acknowledge my dad for his unending support and belief in me. As a child, I couldn't understand why you pushed me the way you did, yet today, it has made all the difference.

To my siblings for such a beautiful and rewarding journey being your oldest brother. I've watched all of you make unbelievable strides in your different fields and I cannot be prouder. You have always outperformed my achievements and I know this will also be one of them.

To my uncle, Ignatius Onedibe, your financial support couldn't have come at a better time during my undergraduate studies and I cannot thank you enough. Today is also about your sacrifice of love and commitment you made to me more than a decade ago.

To my mentor and friend, Obi Imemba, you not only made me realize and believe I could pursue graduate studies in the US, but you have also redefined mentorship for me. I hold that definition very close to my heart and have tried to live up to it as I mentor others.

To all those who have impacted, in no small way, my improbable journey of getting a doctorate degree – the Oyenuga's, the Akinbode's, the Olaniyan's, the Aderibigbe's, the Akwukwegbu's, my Aunt, Mrs. Edith Ekezie and so many more too numerous to mention – I say a big thank you!

To my professor, Dr. Sanjay Srinivasan, for his excellent tutorship and supervision. I still remember the day I received the letter of funding from you back home in Nigeria. You probably don't know that if you hadn't sent that letter, I probably would not have attended UT. Your belief in me then and throughout my graduate studies has been remarkable. I've learnt so much from you and have watched myself grow both intellectually and emotionally since being your student. I recently looked at the first presentation I gave under your supervision during the 2007 Heavy Oil Joint Industry Project (JIP) at UT and my final PhD defense presentation, and couldn't help but be amazed at what time and a great supervisor can do with a young and naïve mind.

To members of my dissertation committee; Dr. Masa Prodanovic for the excellent discussions we had on fascinating ideas such as implicitly determining the steam chamber shape during SAGD and the Level Set Method, Dr. Arjan M. Kamp for your insights on the effect of capillarity during SAGD and the life changing research experience I had under your supervision during my 3 month stay at the Open and Experimental Centre for Heavy Oil (CHLOE), Dr. Kishore Mohanty for helping me understand the limitations of high temperature interfacial tension measurements and Dr. Quoc Nguyen for lending his invaluable experience in the design and running of the experimental part of this dissertation. Your comments during the final defense also helped produce a better dissertation and graduate.

One of the advantages of attending a renowned University like the University of Texas is that you get to learn and work with some of the best faculty in the world. Dr. Larry Lake's Enhanced Oil Recovery (EOR) class made me realize how much my research on proxy modeling was desperately needed as recoverable reservoirs and recovery processes become more complex for full blown numerical simulations to be economical, Dr. Steven Bryant's Advanced Transport Phenomena class taught me to

never trust results from a numerical simulator and be the worst critic of my own work, Dr. Gary Pope's EOR class taught me to always question any published work and seek out its underlying assumptions even if omitted by the author, Dr. Thomas Truskett's Advanced Fluid Flow and Heat Transfer class opened doors to analytically solving complex partial differential equations (PDE's) I didn't even know existed at the time – a skill that became invaluable in my research, Dr. Farzam Javadpour's class on Advanced Unconventional Reservoirs exposed me to the exciting world of Shale and Tight Gas reservoirs for which we published an interesting paper together and I intend to pursue as an additional research area post PhD. Of course there are other faculty I have not mentioned, not for lack of impacting my education, but for space constraints. To all of you, I say thank you for the great work that you do.

It is impossible to complete a dissertation that spanned experimental, simulation and theoretical work without the help of several support staff. My SAGD experiment was set up from scratch and such work would have been impossible to complete without the help and expertise of Glen Baum and Jon Holder. Dr. Roger Terzian was excellent with all my computer needs and support, our administrative assistant, Jin Lee, is probably the reason we can even get any research done in our group and I was fortunate to be served by two outstanding graduate coordinators – Cheryl Kruzie and more recently, Frankie Hart.

Very few events apart from your education prepare you for success in the oil and gas industry like an internship. At a time when it was almost impossible to get internship positions due to the recession, a company with a brave and kind heart – Afren Resources, USA – and its President, Shahid Ullah, took a huge gamble with me and few others and offered us an opportunity I will always be thankful for. My several internships with Afren, under the supervisions of Jim Ekstrand and George Zeito complimented

beautifully my graduate education with the kind of practical experience most of my peers seek but do not have.

To my fellow research group mates, both past and present; Kiomars Eskandridalvand, Juliana Leung, Cesar Mantilla, Alvaro Barrera, Ankesh Anupam, Selin Erzybek, Harpreet Singh, Darrin Madriz, Louis Forster, Tae Kim, John Littlepage, Sayantan Bhowmik, Brandon Henke, Aviral Sharma, Pradeep Anand-Govind, Donovan Kilmartin, Rami Abu-Rmaileh and the rest of the GAMMA team. Learning with and from you has been so much fun.

I've also had the unbelievable luck of mentoring some of the brightest young minds I've ever known during my doctoral studies through the Women-in-Engineering Program (WEP) and the Petroleum and Geosystems Engineering (PGE) undergraduate research internship program – Chris Yohe, Steven Fernandes, Travis Hampton, Dhananjay Kumar, Omar El-Batouty, Katie Ruf and Kristina Baltazar. Each of these great minds influenced my research in one way or the other and I will hold very fond memories of what we achieved together, constantly being on the lookout for the remarkable impact I know you will make in this world.

I would also like to appreciate several of my colleagues at the University of Texas, both past and present for the wonderful learning experiences we had together; Kelli Rankin, Abraham John, Olabode Ijasan, Lokendra Jain, Oluwagbenga Alabi, Amir Reza, Ola Adepoju, Siyavash Motella, Femi Ogunyomi, Mardy Shirdel and so many others I must have missed.

Improved Modeling of the Steam-Assisted Gravity Drainage (SAGD) Process

Prince Nnamdi Azom, Ph.D.

The University of Texas at Austin, 2013

Supervisor: Sanjay Srinivasan

The Steam-Assisted Gravity Drainage (SAGD) Process involves the injection of steam through a horizontal well and the production of heavy oil through a lower horizontal well. Several authors have tried to model this process using analytical, semi-analytical and fully numerical means. In this dissertation, we improve the predictive ability of previous models by accounting for the effect of anisotropy, the effect of heat transfer on capillarity and the effect of water-in-oil (W/O) emulsion formation and transport which serves to enhance heat transfer during SAGD.

We account for the effect of anisotropy during SAGD by performing elliptical transformation of the resultant gravity head and resultant oil drainage vectors on to a space described by the vertical and horizontal permeabilities. Our results, show that unlike for the isotropic case, the effect of anisotropy is time dependent and there exists a given time beyond which it ceases to have any effect on SAGD rates. This result will impact well spacing design and optimization during SAGD.

Butler et al. (1981) derived their classical SAGD model by solving a 1-D heat conservation equation for single phase flow. This model has excellent predictive capability at experimental scales but performs poorly at field scales. By assuming a linear saturation – temperature relationship, Sharma and Gates (2010b) developed a model that

accounts for multiphase flow ahead of the steam chamber interface. In this work, by decomposing capillary pressure into its saturation and temperature components, we coupled the mass and energy conservation equations and showed that the multi-scale, multiphase flow phenomenon occurring during SAGD is the classical Marangoni (or thermo-capillary) effect which can be characterized by the Marangoni number. At low Marangoni numbers (typical of experimental scales) we get the Butler solution while at high Marangoni numbers (typical of field scales), we approximate the Sharma and Gates solution. The Marangoni flow concept was extended to the Expanding Solvent SAGD (ES-SAGD) process and our results show that there exists a given Marangoni number threshold below which the ES-SAGD process will not fare better than the SAGD process.

Experimental results presented in Sasaki et al. (2002) demonstrate the existence of water-in-oil emulsions adjacent to the steam chamber wall during SAGD. In this work we show that these emulsions enhanced heat transfer at the chamber wall and hence oil recovery. We postulate that these W/O emulsions are principally hot water droplets that carry convective heat energy. We perform calculations to show that their presence can practically double the effective heat transfer coefficient across the steam chamber interface which overcomes the effect of reduced oil rates due to the increased emulsified phase viscosity. Our results also compared well with published experimental data.

The SAGD (and ES-SAGD) process is a short length-scaled process and hence, short length-scaled phenomena (typically ignored in other EOR or conventional processes) such as thermo-capillarity and in-situ emulsification should not be ignored in predicting SAGD recoveries. This work will find unique application in predictive models used as fast proxies for predicting SAGD recovery and for history matching purposes.

Table of Contents

List of Tables

List of Figures

Chapter 1: Introduction

It is largely accepted that the immediate future of the oil industry lies in unconventional resources, with heavy oil and bitumen as important classes of these deposits. The world's total resource of heavy oil in known accumulations is estimated by the US Geological Survey (Meyer et al. 2007) to be 3.396 billion barrels of original oil in place (OOIP) while that of bitumen is estimated to be 5,505 billion barrels OOIP. To put this into context, these reserves are at least three (3) times the size of the world's conventional light crude reserves and the oil sands deposit in Canada is believed to be larger than the oil reserves of Saudi Arabia. Even though the most talked about heavy oil and bitumen deposits are the oil sands of Canada, there are several places in the world where heavy oil and bitumen have been reported to exist (Meyer et al. 2007).

The classification of heavy crudes into heavy oil or bitumen is quite fuzzy and there is currently no universally accepted criterion which is also made worse by the existence of mini classifications like "extra-heavy oil" – used for bitumen that can flow at reservoir conditions. A frequently used classification is one in which heavy oil has an API gravity between 10^0API and 20^0API inclusive and a viscosity greater than 100cp while bitumen has an API gravity less than 10^0API and a viscosity greater than 10,000cp (Meyer et. al. 2007). **Fig. 1.1** shows the viscosity – temperature relationship of some known heavy oil reservoirs while **Fig. 1.2** shows an example viscosity – API – temperature correlation for typical heavy oils. For the purpose of this work, we will not distinguish between heavy oil and bitumen, and from now on, will use the word "bitumen" to describe both types of crudes unless otherwise stated.

There are several methods used to produce bitumen, one of the more popular methods is Steam-Assisted Gravity Drainage, SAGD, and generally involves the injection

of steam into the upper of two horizontal wells, usually located 3 – 5m apart and the production of the drained bitumen through the bottom well as shown in **Fig. 1.3**. The injected steam forms a steam chamber above the well pair, and bitumen is produced along the edges of the chamber to the producing well by the aid of gravity. Bitumen flow and hence production is initiated and enhanced by the flow of heat from the steam zone and through the condensate interface to the bitumen phase. The condensate interface is a mixture of condensed steam and bitumen of low viscosity (comparable in magnitude to the water at the interface temperature).

The SAGD process is a thermal enhanced oil recovery (EOR) technique whose basic physics is relatively simple and involves the growth of a steam chamber and the drainage of lower viscosity oil along the chamber wall by gravity. Hence, the *taller* the steam chamber, the larger the oil drainage rate and this was first mathematically described by Roger M. Butler and co-workers – who also invented the process – in their classical drainage equation (Butler et al. 1981). However, like all EOR processes, the basic physics is usually not enough and several other complex phenomena need to described and coupled to either completely describe the process or improve its predictability significantly. Some of these processes include, but not limited to

- **Permeability Anisotropy**: Butler's model assumes that the reservoir is both homogenous and isotropic. This is far from the case for most real reservoirs and it is unclear how anisotropy will affect SAGD rates since the steam chamber interface will most times lie in-between the principal axis of anisotropy during a typical SAGD process.
- **Capillarity**: Butler's model ignores capillary pressure and so does almost all other analytical and numerical models for the SAGD process. The reasoning has been that most bitumen reservoirs usually have high permeabilities and hence will

have small capillary pressures. However this reasoning is at best incomplete, because capillary pressure is also a function of temperature i.e. both interfacial tension and wettability are functions of temperature and thermal gradients in these can induce additional fluid flow currently not accounted for in any SAGD model.

- **Emulsification**: Just as emulsions are prone to form during chemical EOR due to the reduction of interfacial tension by the action of surfactants, emulsions are also prone to form during thermal EOR due to the reduction of interfacial tension with an increase in temperature. Both water-in-oil and oil-in-water emulsions have been reported in field scale recoveries but only water-in-oil emulsion formation has been proved to occur in-situ during SAGD (Sasaki et al. 2002). How the formation and transport of water-in-oil emulsions affects SAGD recovery is very poorly understood.

The challenge is that with increasing complexity, analytical models like Butler's model no longer remain valid and a transition has to be made to semi-analytical or fully numerical models.

1.1 Semi-Analytical vs. Fully Numerical Modeling

Since the earliest development of the SAGD process and its theory, several authors have attempted to better understand the process and account for other complex phenomena not included in the original Butler model. This has led to a plethora of models used to describe the process, ranging from simple analytical models to complex semi-analytical models. However, the inadequacies of these models together with the requirement to support operational considerations such as spacing of wells, the amount of steam injected etc. has led to the routine use of fully numerical models to predict its

recovery. The benefit of such numerical models is that they can be used to design field implementations of the SAGD process, but the challenge rests in their inadequacy to generate and test comprehensive theories that operate at different scales. This is a key strength of analytical approaches. Also, the cost of running such simulations and the accompanying numerical issues that affect the quality of the numerical solutions will continue to make the search for analytical or semi-analytical solutions to complex problems attractive. Another crucial reason to use semi-analytical models is that it is easier to investigate new physics that affect the recovery performance whereas in fully numerical models, this will require building a new simulator or significantly revamping the data architectures of an existing one.

Previous semi-analytical models have either been too complex to justify their use (Kamath et. al. 1993) or have included assumptions that are difficult to justify (Sharma and Gates 2010). In this work, we use semi-analytical models to investigate some physical characteristics of the SAGD process that have been inadequately studied in the past. We also attempt to characterize the different heat transfer mechanisms that are effective at the steam condensate-bitumen interface.

1.2 Motivation

Various researchers (Sasaki et al. 2001a), (Ito and Suzuki 1999), (Barillas et al. 2006) and (Donnelly 1998) have alluded to the difficulty in predicting the performance of the SAGD process using numerical simulators. In some cases, they have reported an under prediction of recovery while in others, overestimation of recovery have been reported using traditional modeling and simulation approaches. This has motivated our quest to include more physics in describing the SAGD process. In this work, we have

chosen to concentrate on the following three (3) aspects that affect SAGD recovery performance.

1.2.1 The Effect of Anisotropy

SAGD is a gravity dominated process. In fact, in the original concept, there is no other pressure gradient (Butler et al. 1981). This means that vertical permeability – hence anisotropy – will have a very strong influence on SAGD recovery. As will be shown later, it is very difficult to systematically vary k_v/k_h in a finite difference numerical simulator and get accurate results for the propagation of the steam chamber. This is because of the stair-step behavior of fluid flow when the ratio is too low.

1.2.2 The Effect of Capillarity (Multiphase Flow ahead of the Steam Chamber)

Almost all current SAGD simulations ignore capillary behavior and they are not included in any previous analytical or semi-analytical model. This is based on the consensus that bitumen reservoirs have quite uniform pore geometries and high permeabilities. However, capillary pressure is not only dependent on the radius of curvature of fluid contacts in the porous medium but also on interfacial tension and wettability, both of which can generally no longer be assumed constant especially for strongly non-isothermal processes like SAGD.

1.2.3 The Effect of Flow and Transport of Water-in-Oil (W/O) Emulsions

As far back as the early days of the invention of the SAGD process, it has been known that water-in-oil (W/O) emulsions are formed in-situ in the reservoir and produced together with separate phases of condensate and bitumen (Chung and Butler 1989). It was

also assumed that since the emulsion phase will be more viscous than the pure bitumen phase, that formation and transport of W/O emulsions will be detrimental to SAGD recovery. However Sasaki et al. (2001a, 2001b, 2002) demonstrated the formation of W/O emulsions at the walls of the steam chamber and hypothesized that this could provide an additional heat transfer mechanism that enhanced recovery. In this work, we will explain the reason for this supposed anomaly and the factors that influence it.

1.3 Contributions of this work

This work significantly enhances our understanding of the SAGD process as it relates to the effects described in the motivation. The chapters are also divided accordingly to reflect this.

In chapter 2, we give a thorough critique of available literature related to the SAGD process and relevant to this work.

In chapter 3, we develop the semi-analytical model used to account for anisotropy in both single layer and multilayered SAGD reservoirs. We show that conventional averaging techniques will be inaccurate for the unique geometry of the SAGD process and explain why we don't get the typical constant maximum SAGD rate as predicted by Butler's theory for anisotropic reservoirs. In an attempt to validate the results using numerical simulation, we will show why the results from finite difference based numerical simulators should not be trusted for modeling the SAGD process in strongly anisotropic reservoirs except in the impractical limit of infinitesimal grid sizes.

In chapter 4, we develop the semi-analytical model used to describe the effect of capillarity on the SAGD process by accounting for non-isothermal multiphase flow ahead of the steam chamber front using a physical effect called the Marangoni phenomena. We

also present an interesting discussion on why the Marangoni effect fundamentally explains the controversial issue of the nature of convection during the SAGD process.

In chapter 5, we extend the modeling procedure in chapter 4 to account for non-isothermal multiphase flow during the Expanding Solvent Steam-Assisted Gravity Drainage Process (ES-SAGD), a variant of the SAGD process.

In chapter 6, we present a mechanistic model that explains the enhanced heat transfer occurring at the steam chamber interface due to the formation of W/O emulsions. We utilize the experimental data of (Sasaki et al. 2001b) for this purpose.

We conclude the dissertation in chapter 7 with a review of the key research conclusions and future research issues.

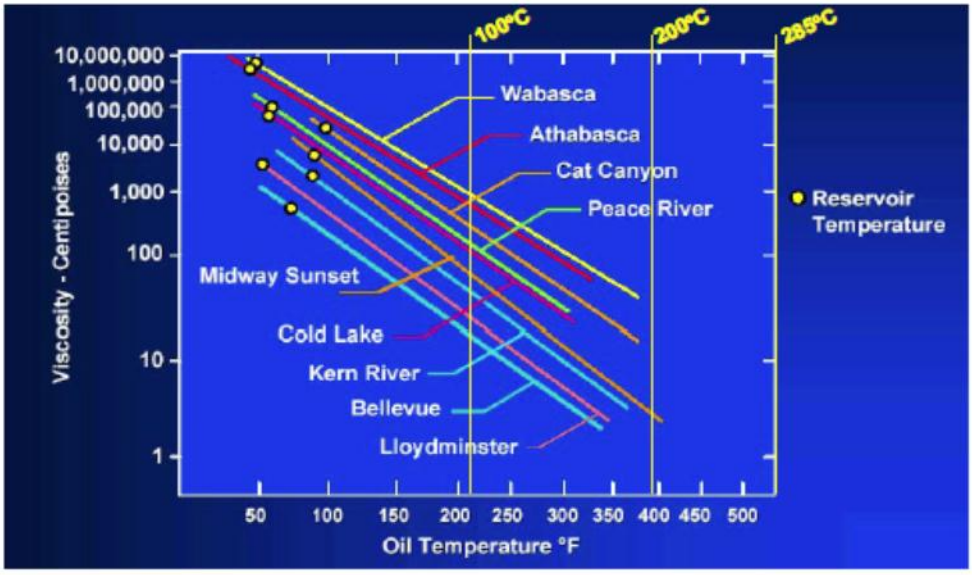

Figure 1.1: Viscosity – Temperature relationship for some heavy oil reservoirs (courtesy of Veil and Quinn 2008[1])

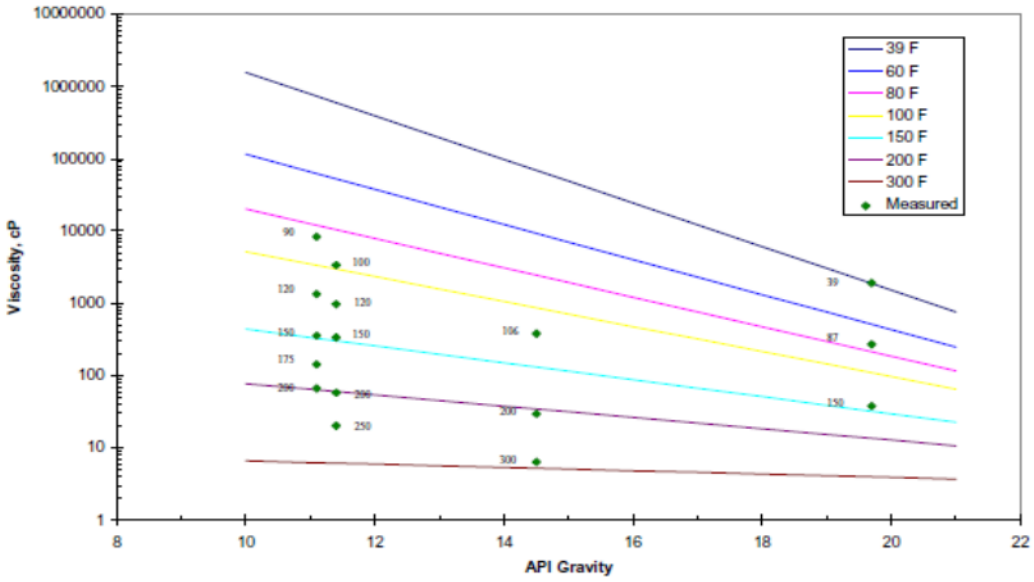

Figure 1.2: Viscosity – API – Temperature relationship for typical heavy oil reservoirs (courtesy of Bennison 1998[2])

[1] Veil and Quinn in their report cited personal communications with Dusseault M. B. as the source of this figure

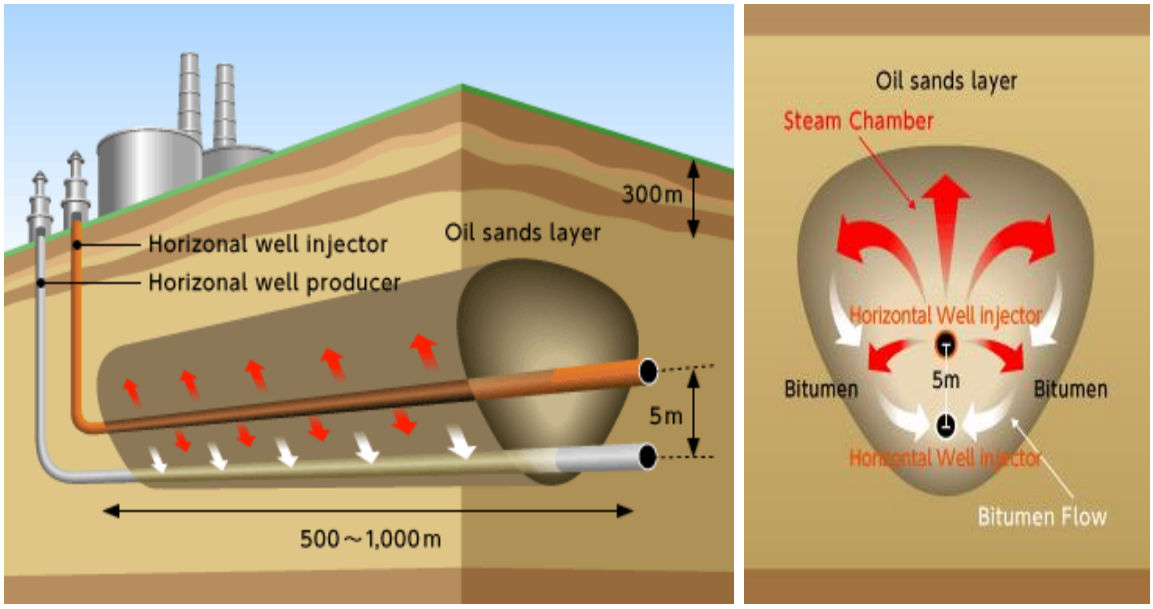

Figure 1.3: Schematic of a field scale application of the SAGD process with the general physics displayed on the front view by the right (courtesy of JAPEX[3]).

[2] This correlation is by Beggs and Robinson

[3] Japan Exploration's website page www.japex.co.jp/english/business/oversea/sadg.html

Chapter 2: Review and Critique of Relevant Literature

In this chapter, we will present a critique of past works on the SAGD process with emphasis on its modeling. We will also pay particular attention to works that tried to account for other complex phenomena apart from 1-D heat conduction, but restrict ourselves to the central themes of this dissertation which are permeability anisotropy, capillarity and water-in-oil (W/O) emulsion formation.

The SAGD process uses horizontal wells, hence permeability anisotropy will play a strong role in recovery (Peaceman, 1993) yet it is unclear how it will do so since the orientation of the fluid flow streamlines with respect to the principal axis of anisotropy during a typical SAGD process will change with time. This alone will make any static averaging technique i.e. arithmetic, harmonic etc. wrong. Also, numerical simulation alone does very little to explain or explore this phenomena.

Ignoring capillary pressure effects during SAGD could be detrimental in our understanding of the process as interfacial tension gradients – the so called Marangoni or thermo-capillary effect (Nield, 1998), (Castor and Somerton, 1977) – could be of similar order as that of thermal conduction. This is because for bitumen, the thermal conduction length scale is small and only the bitumen in this length scale is produced during SAGD. In fact, any short scale phenomena possibly occurring during SAGD should not be ignored but rather investigated for the SAGD process. This paradigm makes the SAGD process uniquely different from other thermal EOR processes or any other porous media recovery process for that matter.

In-situ emulsification is another short scaled phenomena occurring during the SAGD process since it comes about due to interfacial tension reduction at the steam chamber interface. Emulsions have phase viscosities greater than their component phases,

hence, it can be argued that the formation of W/O emulsions can be detrimental to SAGD recovery as some authors have stated (Chung and Butler, 1988), (Chung and Butler, 1989). However, these W/O emulsions are hot water droplets dispersed into the bitumen phase and hence, should be principal carriers of convective heat energy thereby improving recovery and not reducing it as has been shown to be the case by some authors (Sasaki et al., 2001a), (Sasaki et al., 2001b), (Sasaki et al., 2002). Clearly, the increase in both effective phase viscosity and heat transfer coefficient are competing physics and will need to be further studied.

2.1 Modeling the Steam-Assisted Gravity Drainage (SAGD) Process

The Steam-Assisted Gravity Drainage (SAGD) process involves the injection of steam and production of bitumen via pairs of horizontal wells that are usually separated 3 – 5 m apart, with the producer well at the bottom. The first attempt to model the SAGD process was by Butler et al. (1981) where they assumed the only transport mechanism was 1-D quasi-steady state heat conduction ahead of the steam chamber front and by combining this with Darcy's law gave the expression.

$$q_o = \sqrt{\frac{2\phi \Delta S_o k g \alpha H}{m \nu_{os}}} \tag{2.1}$$

where

$$m = \left[\nu_{os} \int_{T_s}^{T_R} \left(\frac{1}{\nu_o} - \frac{1}{\nu_{oR}} \right) \frac{dT}{(T - T_R)} \right]^{-1} \tag{2.2}$$

which is a parameter that relates how the viscosity-temperature curve changes from reservoir to steam temperature and varies from about 3 – 5 for typical heavy oil and bitumen reservoirs (Butler, 1991). The higher the value of m the lesser the viscosity-temperature curve changes from reservoir to steam temperature.

Equation (A.1) states that the bitumen drainage rates is directly proportional to the square root of porosity ϕ, mobile oil saturation ΔS_o, reservoir permeability k, acceleration due to gravity g, thermal diffusivity α and the thickness of the reservoir or bitumen column H, and inversely proportional to the square root of the Butler parameter m and the bitumen kinematic viscosity at steam temperature ν_{os}. This means that a change in each of these parameters will cause the same magnitude of change in the bitumen rates. This result is quite interesting because it suggests a rather simple way of improving SAGD rates – just increase any of the parameters in the numerator of (A.1) or decrease any of the parameters in the denominator of (A.1). Since nature fixes ϕ, g and H, we are left with 5 parameters as engineers to work with.

ΔS_o can be increased by delivering surfactants beyond the steam chamber interface, but this will hardly double SAGD rates and might not be too beneficial in a cumulative recovery sense since steam does a good job of reducing S_{or} by the mechanism of steam distillation (Hornbrook et al., 1991). Two important points to note here is that surfactants tend to reduce interfacial tension which we will show in chapter 4 of this dissertation diminishes recovery by the Marangoni or thermo-capillary effect, and surfactants also tend to emulsify oil-water systems which will complicate any analysis on SAGD recovery enhancement. In chapter 6, we will show that if water-in-oil emulsions are formed at the steam chamber interface, SAGD recovery can be enhanced irrespective of the increased bitumen phase viscosity (which by definition will be considerably less

than twice the bitumen component viscosity) because the thermal diffusivity can practically double in value.

Permeability k can be enhanced through the geo-mechanical process of dilation (Chalaturnyk and Li, 2004) or by hydraulic fracturing (Chen et al., 2008) while ν_{os} and m can be decreased by increasing steam temperature or co-injecting low viscosity solvent with steam. However, care must be taken while increasing steam temperature because there exists a temperature at a given pressure beyond which the latent heat of steam begins to decrease.

It is most times desired to design laboratory experiments that will perform like a given field scale recovery and for this, Butler et al. (1981) derived the dimensionless group B_2 useful for scaling laboratory experiments to field scale and given as

$$B_2 = \frac{mkgH}{\phi S_o \alpha \nu_s} \tag{2.3}$$

The value of B_2 for both the experimental model and field scale reservoir must match for both to be considered hydro-dynamically similar.

The factor m in equation (2.2) quantifies the effect of conductive heating on single phase bitumen viscosity during SAGD. Equation (A.1) predicts that the oil rate is constant and this equation only applies when the steam chamber has grown to the top of the formation and is expanding horizontally till it confines the boundary of the reservoir. This phase is called the horizontal or lateral growth phase in contrast to the vertical growth phase (steam chamber development) and the depletion phase (Llaguno et al., 2002). All parameters under the square root in equation (A.1) were assumed constant in

order to derive the analytical solution. Any attempt to make these parameters vary with space and/or time, will at least require a semi-analytical model.

The first semi-analytical SAGD model was by Butler and Stephens (1981) where they corrected equation (A.1) by replacing the 2 in (A.1) with 1.5 to account for the extra head needed to move bitumen from the base of the reservoir to the producer well. It required the approximation of drawing a tangent to the interface curves from the producer well and was consequently called the Tangential Drainage (TANDRAIN) approximation. We call this a semi-analytical model because it required an approximation (drawing of the tangent) to an analytical expression. Butler (1991) also obtained another equation which replaces the 2 in (A.1) with 1.3 and was called the Linear Drainage (LINDRAIN) approximation.

Equation (A.1) was derived employing a quasi-steady state temperature distribution assumption that allows a mass balance to be performed across a volume element along the steam-bitumen interface. Relaxing this quasi-steady state assumption, Butler (1985), developed a new approach to model the SAGD process using a heat penetration variable. This gave rise to a set of equations with an ordinary differential equation (ODE) that was solved for heat penetration, interface position and bitumen rates given as

$$q_{oD} = \gamma_D B_3 \sin\theta \tag{2.4}$$

$$U_D = -\frac{\partial q_{oD}}{\partial L_D} \tag{2.5}$$

$$\frac{d\gamma_D}{dt_D} = \frac{2}{B_3 \pi}\left(\frac{1}{\gamma_D} - B_3 U_D\right) \tag{2.6}$$

where q_{oD}, γ_D and U_D are the dimensionless rates, heat penetration and interface velocity respectively and B_3 is a new dimensionless group given as

$$B_3 = \sqrt{\frac{kgH}{\alpha\phi\Delta S_o m\nu_s}} \tag{2.7}$$

which essentially performs the same role as B_2 in the earlier theory. This new formulation could account for boundary effects and hence formed the basis for Butler's depletion phase equations.

Reis (1992; 1993) argued that the quasi-steady state assumption for temperature distribution used to derive (A.1) was incorrect due to its inadequacy for cases where the local interface velocity is low, resulting in accumulation of mass at the interface. Reis speculated that the interface velocity was not constant but changing in both magnitude and direction typical of the SAGD process. He proposed a solution for the recovery rate by assuming the local interface velocity to equal the maximum interface velocity at the top of the chamber which he assumed to be constant. He then accounted for the effect of lower velocities at other locations on the interface in an "average" sense by using an empirical fitting constant. The results performed better than the Butler models for the experimental data considered and his modified rate equation is given as

$$q_o = \sqrt{\frac{\phi\Delta S_o kg\alpha_T H}{2a_R m\nu_{os}}} \tag{2.8}$$

where a_R is the Reis constant which he determined from his history match to be 0.4.

Akin (2005) presented a model that accounts for asphaltene deposition during SAGD recovery by accounting for the increase in bitumen viscosity due to asphaltene content in a Butler-type model similar to Reis's development and it performed better than the Butler and Reis model for the experimental data he used. Table 2.1 summarizes the modifications to Butler's equation for the flow rate in terms of the Butler m parameter to account for the velocity and viscosity variations along the steam chamber interface.

Table 2.1: Showing the values of the modified Butler m parameter m^* for the different SAGD models

Model	m^*
Butler	m
Tandrain	$1.33m$
Lindrain	$1.54m$
Reis	$1.6m$
Akin	$4m$

Nukhaev et al. (2006) corrected the Butler models by using shape factors that took the geometry and approximation of chamber velocity into account. Their model considered the case before steam break-through by accounting for the additional bitumen rate due to the liquid head between the base of the steam chamber and the producer well. Their model might be more accurate for situations where steam circulation was done before initiating the SAGD process.

Najeh et al. (2009) presented a model that corrected the Butler models for transient effects (i.e. the rate of propagation of the steam chamber) but however, their

approach will at best work for history matching purposes since there is currently no way to explicitly model the interface velocity which is a critical and necessary parameter in their formulation unlike the Butler models. Their results did better than the Butler models only after fine tuning with the interface velocity dimensionless number.

2.1.1 The Effect of Anisotropy

While it is widely accepted that permeability anisotropy has a strong effect on recovery processes that utilize a horizontal well such as SAGD (Peaceman, 1993), very few studies have attempted to quantify anisotropy on SAGD process performance.

Najeh et al. (2009) used a geometric average of the vertical and horizontal permeability for developing their semi-analytical SAGD model. No attempt was however made to validate this assumption in their paper. It is our observation that the approximate triangular shape of the steam chamber during the horizontal growth phase indicates that the influence of the vertical permeability on bitumen rates should decrease just as the influence of the horizontal permeability increases. The influence of permeability anisotropy should therefore be time dependent.

Sharma et al. (2002) used a thermal simulator to perform a study of several thermal recovery techniques including the SAGD process. They showed that anisotropy influences SAGD bitumen rate, and their plots reveal a definite time component to this phenomenon i.e., not only is the rate reduced for decreasing k_v/k_h ratios, but the shape of the plots though similar appear shifted in time as k_v/k_h varies. One of these plots (**Fig. 9** in their paper) is presented here for clarity in **Fig. 2.1**.

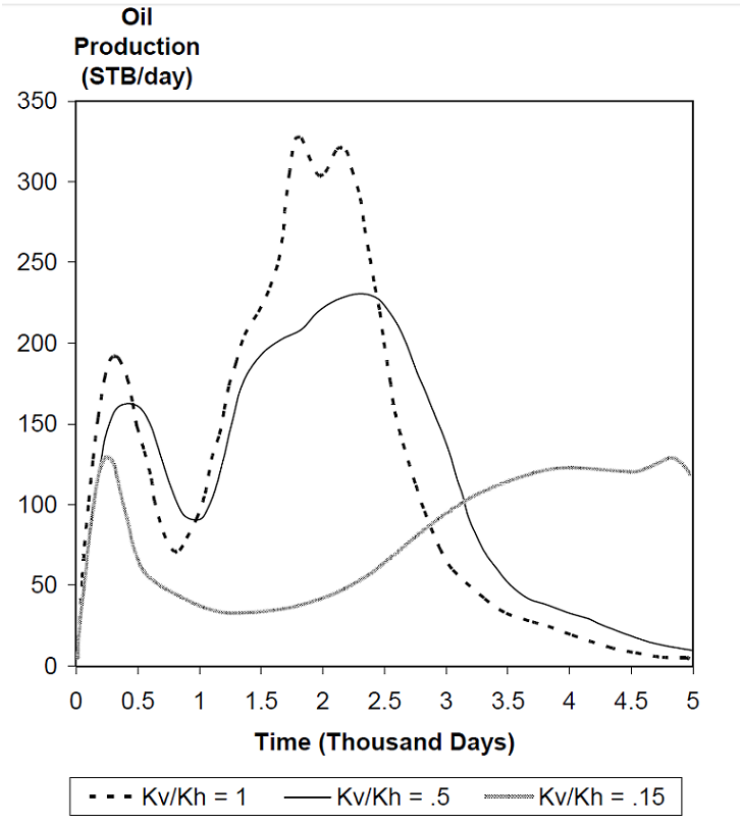

Figure 2.1: Comparison plot showing the effect of anisotropy on SAGD oil production rate[4]

This result further suggests that any static averaging of the vertical and horizontal permeabilities will be inadequate to model this phenomenon.

McLennan and Deutsch (2006) used accurately computed distribution of k_v/k_h ratios from mini-models to simulate steam chamber growth for the Surmount Lease in Northern Alberta. Their results are quite interesting because **Fig. 16** of their paper shows a very irregular steam chamber shape as a result of heterogeneity and anisotropy. They concluded that SAGD flow performance is quite sensitive to the spatial distribution of permeability and to the contrast in vertical and horizontal permeability.

[4] Courtesy of (Sharma et al., 2002), copyright, SPE.

Barillas et al. (2006) found that both heterogeneity and vertical permeability has a major influence on SAGD oil recovery and optimal steam injection. However, their work showed that cumulative oil recovery increases with a decrease in vertical permeability. They commented on the non-intuitive nature of their results especially when compared with the results in Sharma et al. (2002). They attributed the difference to steam breakthrough and it is not clear if they used a steam trap in their simulations as that would have significant impact on their conclusions. Their work reveals the difficulty of comparing results from analytical and semi-analytical models with full numerical simulations because events such as steam breakthrough that can entirely alter process physics are not accounted for in analytical and semi-analytical models.

Sharma et al. (2002) also observed that when the vertical permeability was increased beyond 200md for the given reservoir they modeled, it had no influence on cumulative oil recovery. This suggests that there might be a specific combination of reservoir and fluid properties for which the effect of anisotropy is unimportant to the performance of the SAGD process. This conclusion is also supported by the work of Kisman and Yeung (1995) who observed that lower k_v/k_h ratios gave about 32% lower production rates initially then gradually increased to about 8% of the isotropic base case after about 8 years. This is not surprising from a purely geometric point of view because as the steam chamber expands, depending on the lateral extent of the reservoir, there will be a steam chamber angle for which the horizontal permeability influence on bitumen rates dominates that of vertical permeability and this will also depend on the k_v/k_h ratio. We will prove this formally in a dimensionless framework in this dissertation.

Kamath et al. (1993) developed a 2D SAGD model based on Butler's (1985) modified SAGD model to account for factors such as heterogeneity, presence of shale barriers and anisotropy. They found that the nature of heterogeneity has a complex effect

on the SAGD process as for any given heterogeneity index, it is better, in terms of bitumen recovery, to have the horizontal producer in a higher permeability layer than in a lower one. This is a consequence of using a transient formulation as the speed of withdrawing bitumen by the producer can become a rate limiting step for the overall SAGD process. This result can't be obtained from a quasi-steady state model like the Butler models. They also varied the Dykstra Parsons (DP) coefficient (Dykstra and Parsons, 1950) and concluded that DP has a strong effect on recovery even though they obtained a case (DP = 0.753) which had a higher recovery than for a purely homogenous reservoir with same average permeability (DP = 0). The reason for this anomaly is that their recovery prediction was responding to the multivariate distribution of the relative location of the layers, the layer permeabilities and their thickness. They also presented simulation results that showed the effect of anisotropy to be insignificant on recovery for the reservoir and fluid properties studied. However, their well spacing of 200ft might have been too small for a 900,000cp bitumen reservoir to see the full range of the anisotropic rates as it varies from that due to mainly the vertical permeability to that due to mainly the horizontal permeability. We will show in chapter 3 that the effect of anisotropy is time dependent and there exists a dimensionless time after which its effect ceases to affect SAGD rates. There might have also been numerical or other issues with their simulation as their results show that close to the end of the simulation, the cumulative oil recovery for $k_v/k_h = 0.75$ is greater than that for the isotropic case.

Azad and Chalaturnyk (2010) and Azad (2012) were the first to present a physically plausible analytic model for anisotropy used to account for oil saturation evolution ahead of the steam chamber front due to geomechanics which they called the Geomechanical Azad Butler (GAB) model. However, their intent was not to study the effect of anisotropy but rather to quantify geomechanical effects during SAGD and hence

did not present any sensitivity to the k_v/k_h ratio in their work. We will discuss their anisotropy model further in this work and show that it is strictly not consistent with the Butler type models.

What causes anisotropy is the presence of stochastic shales (Begg and Chang, 1985) laterally in the porous media (Deutsch, 2010) and these are shale barriers with dimensions smaller than the size of a typical grid block. The k_v/k_h ratio has been calculated for these systems by considering the streamline path of a fluid particle as it traverses a porous medium embedded with stochastic shales (Haldorsen and Lake, 1984). If these shale barriers become larger than the size of a grid block, they lead to a heterogeneous porous media which can also strongly affect the SAGD process (Yang and Butler, 1992); (Chen et al., 2008); (Le Ravalec et al., 2009); (Shin and Choe, 2009). Donnelly (1998) also claims that since the shale barriers are saturated with water, they will be disintegrated under high temperatures due to the creation of internal stresses during SAGD and this will cause anisotropy to be enhanced, making it a dynamic (instead of the usual static) parameter. This claim is yet to be verified.

2.1.2 The Effect of Capillarity (Multiphase Flow ahead of the Steam Chamber)

Capillary pressure has been explicitly ignored from most analysis of the SAGD process. In fact it is generally considered a secondary effect. Indirectly, it has been taken into account mostly in numerical simulations of the SAGD process through relative permeability curves. This also gives a sense of accounting for multiphase flow during the SAGD process. We will distinguish between two kinds of multiphase flow during SAGD – parallel to the steam chamber wall (condensate flow) and ahead of it (that controls the transfer of heat to the bitumen). In the absence of other flow phenomena like the flow of

emulsions, SAGD fluid streamlines ahead of the steam chamber interface will be largely parallel to the walls of the steam chamber, making multiphase flow parallel to the steam chamber walls to be less important. Hence we will only consider capillarity ahead of the steam chamber front (capillary imbibition).

As stated earlier, correcting the Butler models for multiphase flow effects started with Butler himself in his second model (Butler and Stephens, 1981) and the LINDRAIN (linear drainage) model (Butler, 1991). This was followed by models from Reis (1992; 1993) and Akin (2005). One characteristic of these multiphase flow corrections is the use of an empirical constant to characterize its effect on the SAGD process. The inadequacy of such an assumption is apparent as k in (A.1) has historically been used as a history match parameter to capture the effective oil permeability (Butler, 1991).

More serious attempts to understand the phenomena of multiphase flow ahead of the steam chamber front started – albeit unknowingly – with the work of Ito and Suzuki (1999) where they used numerical simulation to conclude that the principal mechanism of heat transfer during SAGD was by convection. It is still not clear how this is possible as they stated their simulation runs had a pressure difference less than 40kPa between the injector and the producer which is quite small compared to the specified maximum bottomhole pressure (BHP) of 5000kPa to cause any appreciable convective fluid flux ahead of the steam chamber interface. They also used small grid blocks to minimize numerical dispersion which could cause a saturation gradient ahead of the steam chamber interface. Their work was quite controversial, supported by (Farouq-Ali, 1997) and disagreed with by (Edmunds, 1999) who argued that fluid streamlines during a typical SAGD process should be nearly parallel to the steam chamber interface and hence should have zero fluid flux orthogonal to it.

(Gotawala and Gates, 2008) argued that convection can occur ahead of the steam chamber interface by the mechanism of steam fingering. They demonstrated that the interface between the steam and the bitumen is generally hydro dynamically unstable. However, the length scale of such instability is not expected to be considerable compared to the reservoir thickness since gravity acts as a strong stabilizing force (Lake, 1996).

Sharma and Gates (2010b) inspired by the work of Ito and Suzuki (1999) modeled multiphase flow effects explicitly by assuming a linear saturation-temperature profile ahead of the steam chamber front with respect to temperature and included this in the Butler-type model framework. Their model gave rise to a correction to the rate equation that is a function of the Corey exponent of the oil relative permeability curve a, and the Butler parameter m as in the following:

$$q_o = \sqrt{\left(\frac{2\phi\Delta S_o kg\alpha H}{m\nu_{os}}\right)\left(\frac{\Gamma(m+1)\Gamma(a+1)}{\Gamma(m+a+1)}\right)} \tag{2.9}$$

The Sharma and Gates model is flawed because it inherently assumes that thermal diffusivity scales similarly as saturation diffusivity. As will be presented later, this cannot be true because the principal mechanism of multiphase flow ahead of the steam chamber front must be due to capillarity and not fluid convection (Edmunds, 1999, see also response from Ito and counter-response).

Sharma and Gates (2011) also used this linear transport model to obtain an effective thermal diffusivity ahead of the steam chamber interface due to convection and was based on the work of Birrell (2003). Their model however gave a very poor fit to Birrell's data (see **Fig. 10** of their paper) especially at the steam chamber interface. This is because Birrell's data has two parts to it – the thermal diffusivity at the steam chamber

interface, which will be mostly condensate saturated and the thermal diffusivity of the oil sand ahead of the steam chamber interface, which will be mostly bitumen saturated. Sharma and Gates (2011) model fit the bitumen saturated part – because this will just be the thermal diffusivity of the oil sand – but did not fit the condensate saturated part.

McCormack (2001) observed a correlation between oil sand quality and recovery as lower than theoretical average rates were obtained for average to poor sands. Since factors that determine the quality of sands (for example grain size distribution) can be linked to capillarity, this leads to the suggestion that capillary behavior can play an important role during SAGD. **Fig. 2.2** shows the histogram of available SAGD recoveries and their predictions using several analytical models compared to the observed data. We see that almost analytical models perform well at the experimental scale but perform poorly at field scales. In contrast, the Sharma and Gates (S&G) model performs well at field scales but poorly for the experimental data. This shows that multiphase flow during SAGD is a multi-scale process and any method used to account for it should be accurate across scales.

Most published works on the numerical simulation of the SAGD process ignore capillary effects. The argument has been that the pore size distribution for most heavy oil reservoirs is quite uniform (hence, negligible gradient in the Leverett J function) and permeability high (hence, low capillary pressure). This assumption can only be adequate for isothermal systems and fails considerable for non-isothermal systems such as SAGD. This is because both interfacial tension and wettability can change with temperature in a porous medium (Flock et al., 1986), (Bowman, 1967), (Serhat et al., 1999), (Torabzadey, 1984), (Castor and Somerton, 1977).

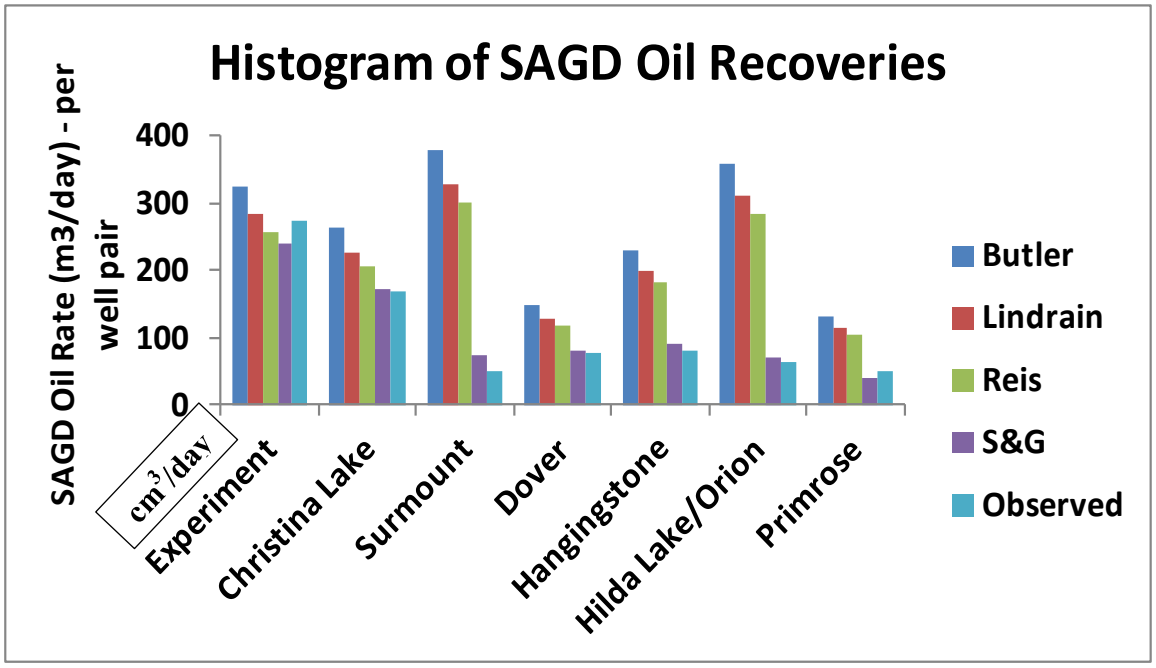

Figure 2.2: Histogram of SAGD oil recoveries and their predictions using different analytical models compared to the observed data[5]

In fact, the gradient in interfacial tension and wettability due to temperature (and solvent concentration in the case of injecting steam with solvent) can be greater than the gradient in the Leverett *J* function (Leverett, 1941) due to non-uniform pore size distributions. This is because at high water saturations, the Leverett *J* function has an almost zero gradient while interfacial tension curves are fairly linear with temperature (Bowman, 1967). Also, the capillary transport mechanism will change the saturation of the wetting phase which in turn will create a gradient in the Leverett *J* function. These three gradients (interfacial tension, wettability and saturation) sum up to give the total capillary gradient with respect to temperature which will significantly impact the transport characteristics during SAGD and can explain several discrepancies between experiment and field scale recoveries. Several authors have termed this "multiphase flow

[5] Courtesy of Sharma and Gates (2010b)

effects" and have tried to quantify it using fudge factors and other simplifying assumptions as stated earlier. In this work, we will attempt to present a cohesive theory to explain and quantify this phenomenon based on the classical Marangoni or thermo-capillary effect.

If thermo-capillarity is to play a role during SAGD, it must do so via a mechanism, and its effect can only be important near the steam chamber interface. The concept of capillary imbibition as a transport mechanism during SAGD has been reported by several authors (Butler et al., 1994). Nasr et al. (2000) argued there must be coupled flow going on at the steam chamber interface, and this coupled flow is countercurrent in nature. Even though they did not give a mechanism for such coupled flow, their results suggests such a mechanism can be countercurrent capillary imbibition with condensate imbibing into the bitumen phase. Al-Bahlani and Babadagli (2009) mentioned water imbibition as a flow mechanism during the SAGD process and Aherne and Maini (2008) gave proof that water can move horizontally through an oil sand with the Dover project where water was consciously injected into the reservoir without it being produced concurrently. The challenge however, is to model this physics in a realistic framework. Some authors have rightly questioned the ability of current commercial simulators to model this effect (Nasr et al., 2000), and it is also our conclusion that current simulators cannot adequately model this effect, and may only be able to do so via very complicated indirect means. To give validity to these indirect methods will require a calibration or history match. However, such model calibration will be non-unique and no explicit conclusions regarding the occurrence or absence of such capillary mechanisms may be possible.

2.1.3 The Effect of Flow and Transport of Water-in-Oil (W/O) Emulsions

The in-situ formation and transport of emulsions in porous media is not a new phenomenon (Raghavan and Marsden., 1971a) and both oil-in-water (O/W) and water-in-oil (W/O) emulsions are known to form depending on the state of the porous media. Mehdizadeh (2005) suggests only the formation of O/W emulsions during SAGD in their discussion of adequate flowmeters for the SAGD process while Arendo et al. (2005) suggest both O/W and W/O emulsions form during SAGD and flowmeters should be designed to handle both types of emulsions. Dalmazzone et al., (2010) stated they received W/O emulsions from a heavy oil field in describing their de-emulsification process while Sanyi et al. (2004) stated that only O/W emulsions always form during SAGD. Noik et al. (2005) and Beetge (2005) went a step further to state that in addition to W/O and O/W emulsions, other complex emulsion systems like water-in-oil-in-water (W/O/W) and oil-in-water-in-oil (O/W/O) emulsions also do form during SAGD. Bosch et al. (2004) argued only for the formation of O/W emulsions by stating that the high temperatures and small density difference between bitumen and water at typical SAGD operating conditions helps stabilize O/W emulsions. Georgie and Smith (2012) paper suggests that W/O emulsions do form downhole during SAGD but can "invert" to O/W emulsions during transport to surface facilities.

These field scale observations suggests the possibility of forming both types of emulsions at some point during bitumen production, but it is not clear if both emulsions are formed in-situ in the reservoir during SAGD. Also, they suggest that the quality of injected steam and initial water saturation of the reservoir play significant roles in deciding which of W/O or O/W emulsions are formed during a given SAGD operation. This is because it is thermodynamically unfavorable for W/O emulsions to exist at high

water cuts characteristic of high initial water saturation reservoirs or low quality steam injection processes. The reverse is also true for O/W emulsions.

Some experimental work has been done to study emulsion characteristics during SAGD and it is worth noting that only the in-situ formation of W/O emulsions has been reported experimentally. This shouldn't discount the possibility of the in-situ formation of O/W emulsions during SAGD because most field scale recoveries will be characterized by lower steam quality and higher water cut than experimental scale recoveries. This might explain why only W/O emulsions have been reported at experimental scales.

The study of the flow and transport of water-in-oil (W/O) emulsions during SAGD started with the work of Chung and Butler (1988) where they showed that injecting steam from the top of the reservoir minimizes the formation of W/O emulsions unlike the typical SAGD process of injecting steam just a few meters above the production well. This result is quite interesting as it indicates that the mechanism of the formation of W/O emulsions might be shear induced.

Chung and Butler (1988) also stated that oil recovery in the well will be reduced because the emulsified phase will have a higher viscosity than the bitumen phase. However, such analysis generally fails to take into account the complex mechanism of fluid flow and heat transfer at the steam/bitumen interface. Water-in-oil (W/O) emulsions are non-equilibrium, thermodynamically unstable phases (Sasaki et al., 2002), and differ in this regard from the thermodynamically stable micro emulsions of chemical flooding EOR. The presence of such emulsion was seen clearly for the first time in the work of Sasaki et al. (2002) where they used an optical fiber scope to visualize the flow of the W/O emulsion droplets and showed that it was impossible to match the experimental data without accounting for their in-situ flow characteristics (Sasaki et al., 2001b); (Sasaki et

al., 2001a). We speculate in this work that such emulsions are formed at the steam/bitumen interface due to shear induced instability (Raghavan and Marsden, 1971b) and subsequently, the emulsion droplets are transported into the bitumen phase by dispersion.

Chung and Butler (1989) extended their initial model to study the effect of initial water saturation, steam quality, reservoir grain size and injection pressure. They found that the lower the initial water saturation, the greater the degree of emulsification which they explained on thermodynamic grounds to be the consequence of having a connected water film in the reservoir. They also concluded that steam quality, reservoir grain size and injection pressure do not significantly affect the emulsification process. It is however important to note that the steam conditions they used was superheated to about 10 – 15^0C above saturated steam, clearly creating conditions favorable for the formation of W/O emulsions and hence their conclusions.

Cuthiell et al. (1995) studied W/O emulsification behavior in heavy oils and determined that there exists a threshold point for emulsification which is characterized by the capillary number N_c given by

$$N_c = \frac{u\mu_o}{\sigma_{ow}} \tag{2.10}$$

and this value is about 10^{-3} to 10^{-4} which is easily attained for heavy oils. It is important to note that their work did not consider non-isothermal systems like SAGD, and it is easy to see from (2.10) that even for typical values at the steam chamber interface, N_c will be in the order of 10^{-5} to 10^{-6} which should not give rise to emulsification based on Cuthiell et al.'s theory. This also suggests that in-situ emulsification during SAGD might be occurring at a small, but finite distance away from the interface where oil viscosities are

larger, or a different mechanism is needed to explain W/O emulsification for non-isothermal bitumen recovery processes.

Modeling this process of in-situ emulsification is quite challenging, because the physics of emulsion formation and transport in porous media is not yet fully understood. Current knowledge describes the process as induced by the difference in viscosity of two adjacent liquid phases (Raghavan and Marsden, 1971b); (Raghavan, 1982); (Chuoke et al., 1959).

2.2 Modeling the Solvent-Aided Steam-Assisted Gravity Drainage (SA-SAGD) Processes

Solvent-Aided Steam-Assisted Gravity Drainage (SA-SAGD) processes were developed to mitigate some of the limitations of the traditional SAGD process. These limitations include high heat loss to the overburden and low thermal efficiencies. There are several classifications of this modification of the SAGD process (Mohammadzadeh et al., 2010) but we will classify the SA-SAGD process in this work by the intended purpose of the aiding solvent. Based on this, only two commercially successful types of the SA-SAGD process currently exists.

2.2.1 The Steam and Gas Push (SAGP)

This involves the co-injection of non-condensable gases ($C_1 - C_2$) with steam so as to minimize heat losses to the overburden. It generally gives slightly lower drainage rates (Butler, 1999) but conserves heat significantly. This is an extremely complicated process from a modeling point of view because of the existence of 3-phase flow (gas/oil/condensate) beyond the edge of the steam chamber unlike the SAGD process

where only oil/condensate flow occurs ahead of the steam chamber. The three phase region exists because the non-condensable gas generally tends to diffuse appreciably beyond the steam chamber edge. This can be seen clearly from the numerical simulations of Al-Murayri et al. (2011) and very few models have been presented to analyze this process from an analytical point of view.

To adequately model this process will not only require 3-phase relative permeability curves but also gas/oil or gas/water capillary pressure curves in addition to the oil/water curves. This difficulty can easily be seen in the work of Sharma et al. (2012) where they accounted for the diffusion of the non-condensable gas and its partitioning into the bitumen phase but had to assume linear oil saturation-temperature profiles and linear gas saturation-distance profiles in their model. A model that incorporates the full suite of capillary pressure models would have avoided such an assumption and yielded a more accurate rate equation.

2.2.2 The Expanding Solvent Steam-Assisted Gravity Drainage Process (ES-SAGD)

This involves the co-injection of condensable gases (C_3 – C_8) with steam to provide additional viscosity reduction of bitumen, thereby requiring less steam for the same drainage rates which makes the ES-SAGD process more thermally efficient than the traditional SAGD process. The ES-SAGD process is a blend of the Vapor Extraction (VAPEX) process developed by Butler and Mokrys (1991) and the SAGD process. It was initially conceived by Nasr et al. (2003) and has been shown to be quite successful in recent pilot studies (Gupta and Gittins, 2006). Most of the modeling work done on the ES-SAGD process have used numerical simulators (Ananth Govind et al., 2008) and very few analytical models exist.

Sharma and Gates (2010a) noted the cross-dependencies of the solvent diffusion coefficient and the bitumen phase viscosity and accounted for them in their steam-solvent coupled model but did not present equations for enhanced bitumen rates due to solvent dilution. **Fig. 7** and **Fig. 10** of their paper reveal that they could have assumed the diffusion coefficient to be constant without adversely affecting the prediction of bitumen rates. They also did not account for multiphase flow ahead of the steam chamber interface in this work.

Rabiei Faradonbeh et al. (2012) coupled the quasi-steady state energy equation with the transient component mass balance equation using the Heat Integral Method (HIM) to develop a semi-analytical ES-SAGD model. Their model was however, not fully dimensionless and this limited the generality of their conclusions. From their plots, it also seems that they could have obtained similar results if they completely worked in a quasi-steady state space i.e. using the snapshot of the mass transfer process at a particular instant in time. This is because the length scale of mass transfer is so small compared to that of heat transfer for its transient to have any significant impact on such a coupled solution. They also did not account for multi-phase flow effects in their model.

Gupta and Gittins (2012) combined the SAGD and VAPEX equations in a quasi-steady state framework to derive their semi-analytical ES-SAGD (which they call the solvent-aided process (SAP)) model. Their model was quite unique in its simplicity and showed the need to define a diffuse solvent layer ahead of the steam chamber to accurately capture ES-SAGD physics. They also did not account for multi-phase flow effects in their model.

To summarize, we have explored the current state of knowledge with respect to modeling the SAGD and ES-SAGD processes and have identified three (3) effects – anisotropy, capillarity and emulsification – that are currently weakly understood and

loosely accounted for, if at all, in current SAGD models. In chapter 3, we will extend the Butler models to account for anisotropy during SAGD and show that it is a time dependent phenomenon which depending on the scale of the well spacing, its effect might be masked just as seen in the results (and hence conclusions) of (Kamath et al., 1993). In chapter 4, we will extend the Butler models to account for the effect of heat transfer on capillarity (multiphase flow ahead of the steam chamber) during the SAGD process. We will show that the Marangoni (thermo-capillary) effect can be used to explain the saturation – temperature distribution results of (Ito and Suzuki, 1999) and also explain why the (Sharma and Gates, 2010b) model does well at predicting field scale recoveries but performs poorly for experimental scale recoveries just as the reverse is true for the Butler models. In chapter 5, we will extend the Marangoni concept to model the ES-SAGD process and also give a unified model that explains other important physics like the ineffectiveness of any solvent with a viscosity lower than the bitumen viscosity at steam temperature for the ES-SAGD process. In chapter 6, we will account for the heat transport effect of W/O emulsions and use it to explain the enhanced rate results of the experimental data of (Sasaki et al., 2001b).

Chapter 3: The Effect of Anisotropy

The SAGD process utilizes horizontal wells to collect oil draining along the inclined steam chamber wall and consequently permeability anisotropy can play a very strong role in recovery. In fact, it has been well documented that poor vertical permeability kills the SAGD process because it curtails the vertical growth of the steam chamber. Several authors have attempted to model this phenomenon by computing the average permeability of the medium using time-independent averaging (e.g. harmonic, geometric averaging etc.) methods only to discover the inadequacy of such an approach as the field data in several instances reveal a definite time component to this effect. Most studies on the effect of anisotropy on SAGD performance have been based on commercial simulators. However, there exists a need to describe this phenomenon quantitatively prior to any numerical simulation and delineating conditions where it can be considered important or not.

Isotropy of permeability can be geometrically represented as a sphere (or circle in 2D) where the permeability magnitude is the same in all directions. Anisotropy can be represented as an ellipsoid (or ellipse in 2D) with varying magnitudes of permeability in different directions and the principal axes representing principal permeability directions (Ekwere J. Peters 2012). In this work, we assume that the principal axes point in the vertical and horizontal directions. We will show that the SAGD process has a unique geometry that allows a meaningful mapping of the steam chamber wall to the coordinate frame of such an ellipsoid. We will then use this transformation to incorporate permeability anisotropy within the framework of the Butler type models. This will be done in dimensionless space and the results obtained can be used as type curves for correcting any isotropic SAGD model for anisotropic effects.

Our results show that the effect of anisotropy is time dependent (generally obeying a sigmoid function) and there exists a unique time corresponding to a given set of reservoir and fluid properties, after which the effect of permeability anisotropy ceases to influence the performance of the SAGD process.

Our results also explain why most other static averaging methods for representing permeability anisotropy fail. The analytical expression can be used as a fast SAGD predictive model suitable for history matching purposes.

3.1 Model Development – Single Layer Reservoir

Butler's equation (2.1) relating recovery to various reservoir and fluid parameters was derived for a purely isotropic permeable medium. To account for the effect of anisotropy, permeability k in (2.1) will have to be modified as in (3.1) and replaced with an effective permeability due to anisotropy. We will assume that the principal directions of permeability anisotropy are in the horizontal and vertical directions and hence permeability k can be decoupled into its vertical (k_v) and horizontal (k_h) components.

$$q_o = \sqrt{\frac{2\phi\Delta S_o k_{eff} g\alpha_T H}{m\nu_{os}}} \tag{3.1}$$

An anisotropic system can be represented by a permeability ellipsoid in 3D or ellipse in 2D. The key to accounting for anisotropy during SAGD is to come up with a transformation function that relates the chamber geometry at any instant in time to the permeability ellipsoid. Such a function must not only take into account the physics of the SAGD process, but must also become equal to the isotropic case in the limit of $k_v/k_h \to 1$

. In this work, we will consider only the horizontal growth phase, which is the most likely to conform to the classical inverted triangular shape assumed in Butler's derivation. The assumption of an inverted triangular steam chamber is critical for the derivation presented below. We also assume the k_v / k_h ratio to be constant for the layer being considered.

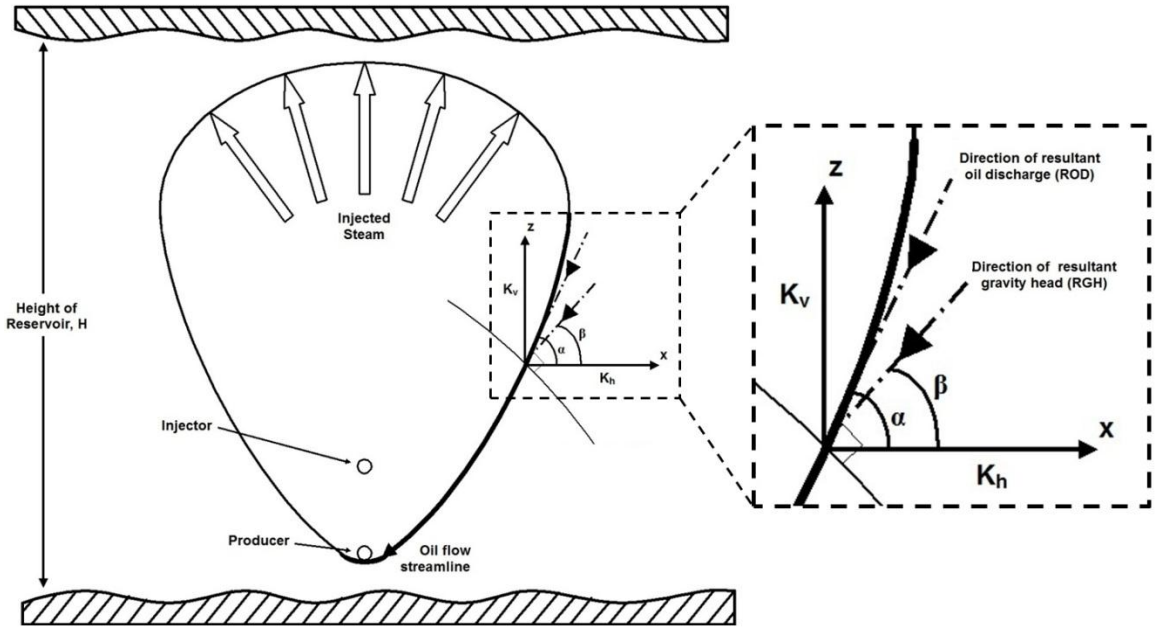

Figure 3.1: Schematic of a typical SAGD steam chamber showing important flow directions

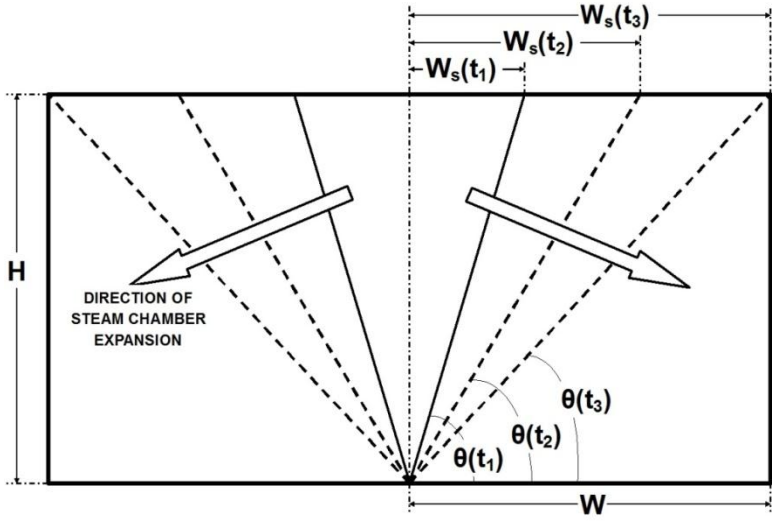

Figure 3.2: Schematic of an idealized SAGD steam chamber during horizontal growth

A schematic of the SAGD horizontal growth phase is shown in **Fig. 3.2** from which we see that the steam chamber angle is a function of time i.e.

$$\theta = \theta(t) = \arctan\left(\frac{H}{W_s(t)}\right) \tag{3.2}$$

Hence from (3.2), for the horizontal growth phase, the time dependence of the steam chamber angle is transferred to the horizontal expansion of the steam chamber W_s. We also see that as $W_s \to W$, the flow of condensate and bitumen along the chamber wall becomes more and more horizontal. This leads us to conclude that the influence of the vertical permeability on the movement of the mobilized bitumen decreases as $W_s \to W$, while the influence of the horizontal permeability increases. Any function we choose to represent anisotropy during SAGD must reflect this characteristic. We also require the formulation to converge to the isotropic case in the limit of $k_v/k_h \to 1$. Two excellent choices that obey both criteria are

$$k_{eff_{RGH}} = k_v \sin^2\theta + k_h \cos^2\theta \tag{3.3}$$

$$\frac{1}{k_{eff_{ROD}}} = \frac{\sin^2\theta}{k_v} + \frac{\cos^2\theta}{k_h} \tag{3.4}$$

Both choices are not arbitrary, but result from resolving SAGD flow both in the direction of resultant gravity head (RGH) and resultant oil discharge (ROD) respectively (see **Fig. 3.1**). The ROD model assumes that bitumen flow occurs tangential to the steam chamber interface while the RGH model assumes that bitumen flow occurs in the direction perpendicular to the equipotential surface or in the direction of the resultant hydraulic gradient.

The formal proof to equations (3.3) and (3.4) are given by Das (2013) and briefly reproduced in appendix A. It is important to note that unlike for an isotropic media, the equipotential line is not orthogonal to the oil flow streamline in an anisotropic media, hence, the ROD direction does not necessarily coincide with the RGH direction (Das 2013) in an anisotropic media as shown in **Fig. 3.1**. The difference between both models is that for the RGH model, an effective oil velocity (since it is the direction of resultant gravity head) defined by

$$\begin{aligned} v_{RGH} &= -k_{eff_{RGH}} \frac{\partial h}{\partial \psi_{RGH}} \\ &= k_v \frac{\partial h}{\partial z}\sin\beta + k_h \frac{\partial h}{\partial x}\cos\beta \end{aligned} \tag{3.5}$$

is used for its derivation. Here, ψ is the direction parallel to the steam chamber interface. The resultant gravity head can in turn be resolved in the horizontal and vertical direction as:

$$\frac{\partial h}{\partial x} = \frac{\partial h}{\partial \psi_{RGH}} \cos\beta \tag{3.6}$$

$$\frac{\partial h}{\partial z} = \frac{\partial h}{\partial \psi_{RGH}} \sin\beta \tag{3.7}$$

Substituting $k_{eff_{RGH}} = k_v \sin^2\beta + k_h \cos^2\beta$ obtained by projecting k_v and k_h in the direction of the gravity head inclined at an angle β (see appendix A) together with equation (3.6) and (3.7) in the expression for the velocity yields:

$$v_{RGH} = -\left(\frac{\partial h}{\partial x} k_H \cos\beta + \frac{\partial h}{\partial z} k_v \sin\beta\right) \tag{3.8}$$

For the ROD model, an effective gravity head (in the direction of resultant oil discharge) is defined by

$$\frac{\partial h}{\partial \psi_{ROD}} = \frac{\partial h}{\partial z} \sin\alpha + \frac{\partial h}{\partial x} \cos\alpha \tag{3.9}$$

corresponding to the angle α subtended by the resultant oil discharge direction. The components of the oil velocity are given by

$$v_x = v_{ROD} \cos\alpha \tag{3.10}$$

$$v_z = v_{ROD} \sin\alpha \tag{3.11}$$

Substituting $\frac{1}{k_{eff_{ROD}}} = \frac{\sin^2\alpha}{k_v} + \frac{\cos^2\alpha}{k_h}$ obtained by projecting k_v and k_h in the direction of the oil discharge inclined at an angle α (see appendix A) together with equations (3.9) to (3.11) for the velocity and gradient expressions yields:

$$v_{ROD} = -\left(\frac{\partial h}{\partial x} \frac{k_H}{\cos\alpha} + \frac{\partial h}{\partial z} \frac{k_v}{\sin\alpha} \right) \tag{3.12}$$

Comparing equations (3.8) and (3.12) reveals why the RGH and ROD models will give different bitumen rates.

Determining which of the two expressions would give a more accurate representation of the SAGD recovery performance is difficult. All analytical (and semi-analytical) SAGD models such as Butler et al.'s (1981) original model implicitly assume the RGH model as they obtain bitumen rates as a function of the resultant gravity potential gradient in the direction parallel to the steam chamber interface.

An implicit assumption made in both these models accounting for permeability anisotropy is that at every specific time, k_{eff} is a constant for all fluid streamlines parallel to the steam chamber interface. This is clearly seen from a step in the derivation of Butler's equation (2.1) where the production rate q is written as:

$$q = k_{eff} g \sin\theta \int_0^\infty \left(\frac{1}{\nu} - \frac{1}{\nu_R} \right) d\xi \tag{3.13}$$

where the coordinate ξ is perpendicular to the chamber wall. We speculate that in the presence of anisotropy, the derivation of flow rate is written better as:

$$q = g\sin\theta\int_0^\infty k_{eff}\left(\frac{1}{\nu}-\frac{1}{\nu_R}\right)d\xi \tag{3.14}$$

since k_{eff} will vary ahead of the steam chamber interface. However, for most bitumen reservoirs, viscosities are high enough such that the activated volume ahead of the steam chamber front is small, and hence (3.13) can be used without much error.

In **Fig. 3.3**, we plot the difference in effective permeability using both models for varying steam chamber angles (to the horizontal axis) and anisotropy ratio. The difference in effective permeability using both models is more pronounced at lower steam chamber angles and anisotropy ratios reaching a value of more than 81% for anisotropic ratio of 0.1 and steam chamber angle of 20 degrees. Hence, we should expect some significant difference in results from modeling the effect of anisotropy using both the RGH and ROD models with any Butler type model. It is important to note here that Azad and Chalaturnyk (2010) used the ROD model in their work. It will be helpful if a recommendation can be made as to which model to use, but we will defer to comment on such recommendation until we validate the models using numerical simulation.

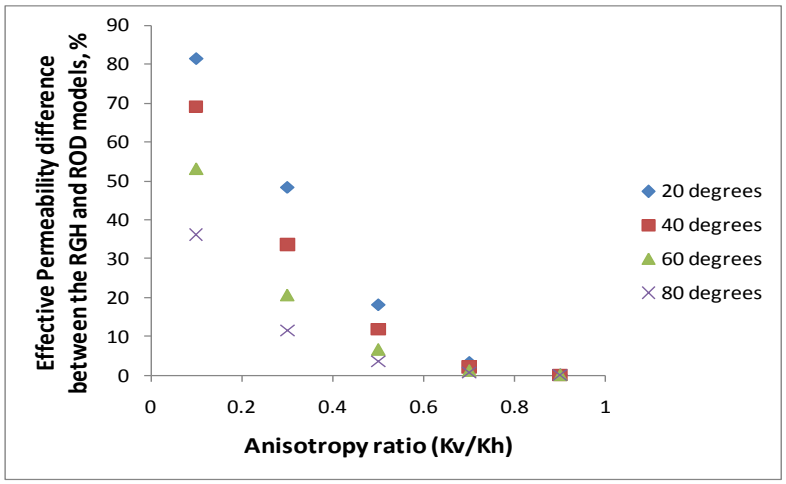

Figure 3.3: Plot of the % difference between the RGH and ROD models

3.1.1 Computing Oil Production Rate Accounting for Permeability Anisotropy

Using the RGH model and substituting (3.3) into (2.1) gives

$$q_{o_{RGH}} = \sqrt{\frac{2\phi\Delta S_o\left(k_v \sin^2\theta + k_h \cos^2\theta\right) g\alpha_T H}{m\nu_{os}}} \tag{3.15}$$

From (3.2) and writing $W_s(t)$ at any given time instant as W_s, we get

$$\cos^2\theta = \frac{W_s^2}{W_s^2 + H^2} \tag{3.16}$$

$$\sin^2\theta = \frac{H^2}{W_s^2 + H^2} \tag{3.17}$$

Substituting (3.16) and (3.17) into (3.15) gives

$$q_{o_{RGH}} = \sqrt{\frac{2\phi\Delta S_o \left(\frac{k_v H^2 + k_h W_s^2}{W_s^2 + H^2} \right) g\alpha_T H}{m\nu_{os}}} \tag{3.18}$$

We have assumed that the steam chamber during horizontal growth is an inverted triangle, then, similar to Reis's (1992) development, mass balance gives

$$q_o = \frac{d}{dt}\left(\phi\Delta S_o \frac{1}{2} H W_s \right) \tag{3.19}$$

Combining (3.18) and (3.19) gives

$$\frac{dW_{s_{RGH}}}{dt} = \sqrt{\frac{8\left(\frac{k_v H^2 + k_h W_{s_{RGH}}^2}{W_{s_{RGH}}^2 + H^2} \right) g\alpha_T}{\phi\Delta S_o H m\nu_{os}}} \tag{3.20}$$

The constant "8" in (3.20) is a consequence of using Butler's original equation (2.1). If we had used Reis's model (1992), the constant would be "5" and similarly for other models. We will replace this value with the constant "C^2". As in the previous works by Reis (1992) and others, C^2 is basically a correction for multiphase flow that occurs at the edge of the steam chamber. It accounts for the retardation in the expansion of the steam chamber due to the presence of condensed water at the edge of the steam chamber.

Non-dimensionalizing (3.20) yields

$$\frac{dW_{sD_{RGH}}}{dt_D} = C\sqrt{\frac{\left(\left(k_v / k_h \right) + W_{sD_{RGH}}^2 \right)}{W_{sD_{RGH}}^2 + 1}} \tag{3.21}$$

where

$$t_D = \sqrt{\frac{k_h g \alpha_T}{\phi \Delta S_o m \nu_{os} H^3}} t \tag{3.22}$$

$$W_{sD} = \frac{W_s}{H} \tag{3.23}$$

The corresponding non-dimensional form of the rate equation (3.19) is:

$$q_{oD_{RGH}} = \frac{q_{o_{RGH}}}{q_{o_{\frac{k_v}{k_h}=1}}} = \frac{\dfrac{dW_{sD_{RGH}}}{dt_D}}{\dfrac{dW_{sD}}{dt_D}_{\frac{k_v}{k_h}=1}} = \sqrt{\frac{k_v/k_h + W_{sD_{RGH}}^2}{W_{sD_{RGH}}^2 + 1}} \tag{3.24}$$

Similarly, using the ROD model and repeating the above procedure with (3.4) substituted into (3.1) yields:

$$q_{o_{ROD}} = \sqrt{\frac{2\phi \Delta S_o \left(k_v k_h / k_v \sin^2\theta + k_h \cos^2\theta\right) g \alpha_T H}{m \nu_{os}}} \tag{3.25}$$

Substituting (3.16) and (3.17) into (3.25), the rate of growth of an inverted triangular chamber yields:

$$\frac{dW_{sD_{ROD}}}{dt_D} = C \sqrt{\frac{W_{sD_{ROD}}^2 + 1}{W_{sD_{ROD}}^2 + \left(\dfrac{k_v}{k_h}\right)^{-1}}} \tag{3.26}$$

$$q_{oD_{ROD}} = \frac{q_{o_{ROD}}}{q_{o_{\frac{k_v}{k_h}=1}}} = \sqrt{\frac{W_{sD_{ROD}}^2 + 1}{W_{sD_{ROD}}^2 + \left(\frac{k_v}{k_h}\right)^{-1}}} \tag{3.27}$$

Equations (3.21) and (3.26) are non-linear ordinary differential equations (ODE's) and can be integrated analytically to give complex elliptic functions that will be difficult to evaluate. We will rather solve (3.21) and (3.26) by finite differences. We will also utilize the implicit finite-difference scheme due to its unconditional stability criterion and hence overcome solution difficulties with the elliptic functions. Discretizing (3.21) and (3.26) in such a manner gives

$$W_{sD_{RGH}}^{n+1} = W_{sD_{RGH}}^{n} + C\Delta t_D \sqrt{\frac{k_v/k_h + \left(W_{sD_{RGH}}^{n+1}\right)^2}{\left(W_{sD_{RGH}}^{n+1}\right)^2 + 1}} \tag{3.28}$$

$$W_{sD_{ROD}}^{n+1} = W_{sD_{ROD}}^{n} + C\Delta t_D \sqrt{\frac{\left(W_{sD_{ROD}}^{n+1}\right)^2 + 1}{\left(W_{sD_{ROD}}^{n+1}\right)^2 + \left(\frac{k_v}{k_h}\right)^{-1}}} \tag{3.29}$$

In order to access the impact of anisotropy on the steam chamber expansion, it might be useful to compute the ratio:

$$W_{S_{D_D}} = \frac{W_{S_D}}{W_{S_{D_{\frac{k_v}{k_h}=1}}}} \tag{3.30}$$

that is the ratio of the anisotropic steam chamber expansion to the isotropic case. The isotropic steam chamber expansion is obtained from (3.21) or (3.26) by integrating the corresponding expressions after substituting $k_v/k_h = 1$

$$W_{s_{D_{\frac{k_v}{k_h}=1}}} = Ct_D \tag{3.31}$$

Substituting (3.31) into (3.30) gives

$$W_{s_{D_D}} = \frac{W_{s_D}}{Ct_D} \tag{3.32}$$

3.1.2 Model Validation

We will use numerical simulation and the CMG – STARS^{TM} non-isothermal compositional simulator to validate our model for anisotropy during horizontal growth for the SAGD process. To be successful, we will have to eliminate all physics not accounted for in the Butler models (Roger M. Butler 1991) and are described below;

a. **No overburden heat losses:** The amount of heat injected during SAGD is used to raise bitumen temperature as well as heat up the reservoir overburden. At steady state, the amount of steam injected is the total required to raise the bitumen temperature as well as to account for heat loss to the overburden. This is the scenario assumed by Reis (1992). However, a fully numerical model is transient and will generally couple both these heat transfer processes. We will eliminate this effect in our validation by assuming zero overburden heat losses.
b. **Zero pressure gradient other than gravity:** There are situations where it is desirable to operate the SAGD process under a pressure gradient other than

gravity (Edmunds and Gittins 1993). However, the Butler models does not take any additional pressure gradient other than gravity into account, hence, in our validation, we will operate the horizontal wells under zero pressure gradient.

c. **Zero multiphase flow effects and (numerical) dispersion:** As stated in the literature review, the Butler models were derived assuming only single phase non-isothermal flow of the bitumen phase. Several constants and fudge factors have historically been used to account for multiphase flow effects in most Butler type analytical models. However, multiphase flow is coupled to permeability anisotropy as we will show in subsequent sections and in the absence of a reliable model to quantify such coupling, multiphase flow effects should be eliminated in our validation. To do this, we will use straight line relative permeability curves with zero end points. This will eliminate multiphase flow effects parallel to the steam chamber interface. We minimized numerical dispersion by using very small grid sizes within reasonable computational limits and will discuss its effect in the results section. In chapter 4, we will present a model that accounts for multiphase flow ahead of the steam chamber interface by coupling the mass and energy conservation equations. Table 3.1 gives the reservoir parameters used for the validation study.

Table 3.1: Showing the values of reservoir parameters used in the anisotropic model validation

Reservoir Parameter	**Value**
Horizontal Permeability, k_h	7000 mD
Thermal diffusivity, α_T	1.15942 x 10^{-6} m^2/s
Viscosity, μ	$Ae^{(B/T)}$
A	8.13 x 10^{-9} cp
B	8871.026 K
m	5.2546
Porosity, ϕ	0.33
ΔS_o	1
Bitumen density	980 kg/m^3
Reservoir thickness, H	25.7186 m
Number of grid block in x direction, N_x	149
Number of grid block in y direction, N_y	2
Number of grid block in z direction, N_z	49
Size of grid block in x direction, Δx	0.5253441 m
Size of grid block in y direction, Δy	10 m
Size of grid block in z direction, Δz	0.5253441 m

The Butler parameter m was computed by performing the integration in (2.2).

3.2 Model Development – Multiple Layered Reservoirs

The above models are only valid for single layered reservoirs where the k_v/k_h ratio is constant throughout the reservoir. However, most bitumen reservoirs are not single – layered and the k_v/k_h ratio is usually spatially varying. In the limit of the reservoir being layered i.e. having layers of rocks exhibiting different permeability anisotropies, the above model can be extended to account for the effect of such multi-layered reservoirs.

Consider the SAGD process during horizontal growth for a layered reservoir as shown in **Fig. 3.4**

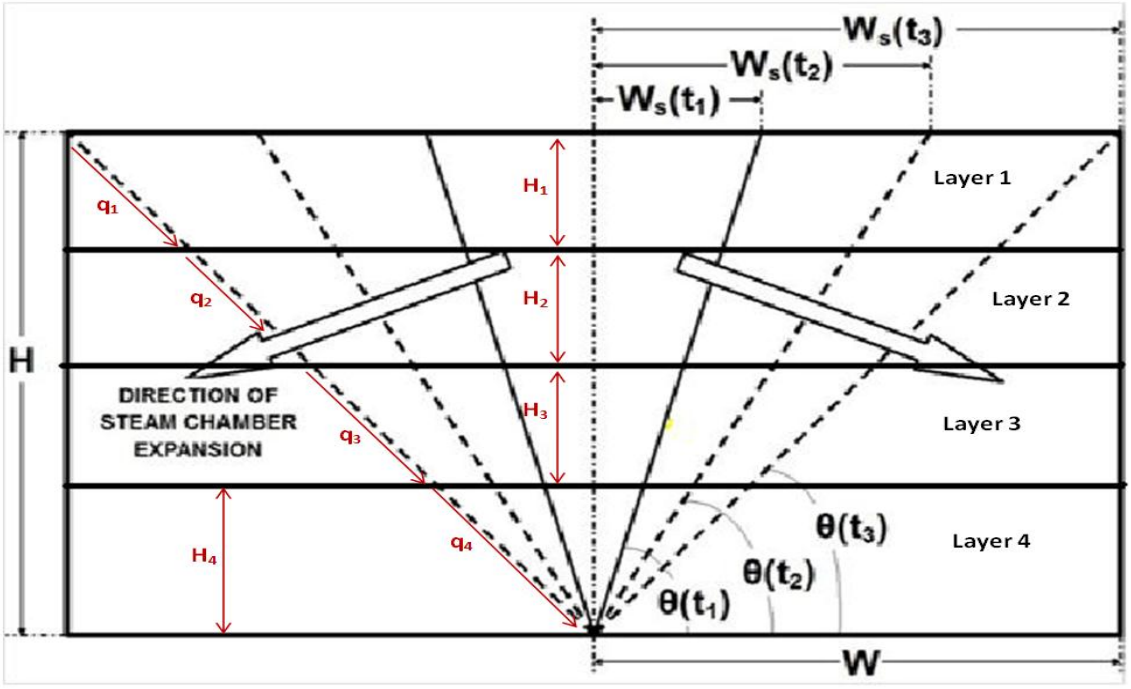

Figure 3.4: Schematic of an idealized SAGD steam chamber during horizontal growth for a layered reservoir

Both the RGH and ROD models apply. From **Fig. 3.4** and noting that the Butler type models assume quasi-steady state flow, then the following relationship holds

$$q_o = q_{o_1} + q_{o_2} + q_{o_3} + ... + q_{o_N} \tag{3.33}$$

Equation (3.33) basically treats each layer as a separate SAGD process and has its basis on the assumption of quasi-steady state i.e. the fluid entering any layer exits the layer without any accumulation. Hence if conditions exist that makes Butler's model valid (high viscosity oil, injection at reservoir pressure, etc.), then (3.33) is also valid. For each layer, (3.15) can be written for the RGH model as

$$q_{o_{i_{RGH}}} = \sqrt{\frac{2\phi\Delta S_o \left(k_{v_i} \sin^2\theta + k_{h_i} \cos^2\theta\right) g\alpha_T H_i}{m\nu_{os}}} \qquad i = 1,2,...,N \tag{3.34}$$

From (3.1), (3.33) and (3.34) we get

$$k_{eff_{RGH}} = \frac{\sum_{i=1}^{N} \left(k_{v_i} \sin^2\theta + k_{h_i} \cos^2\theta\right) H_i}{H} \qquad i = 1,2,...,N \tag{3.35}$$

If we assume that the steam chamber angle θ to the horizontal is the same for each layer (this assumption is strictly valid for gravity stabilized flows), we can use the results of the previous section that gives the angle θ as a function of reservoir and steam chamber dimensions which will be the same as (3.16) and (3.17) to give the effective permeabilities as

$$k_{eff_{RGH}} = \frac{k_v H^2 + k_h W_s^2}{W_s^2 + H^2} \tag{3.36}$$

which also applies to each layer due to the principle of geometric self-similarity to give

$$k_{eff_{iRGH}} = \frac{k_{v_i} H^2 + k_{h_i} W_s^2}{W_s^2 + H^2} \qquad i = 1,2,...,N \tag{3.37}$$

In (3.37), we have used the assumption of an invariant θ with respect to each layer. As noted earlier, this assumption breaks down in the presence of high permeability streaks, impermeable barriers or strong capillary heterogeneities since for such situations, gravity will likely not be strong enough to stabilize any advancing front orthogonal to the drainage direction.

Substituting (3.37) into (3.35) and non-dimensionalizing W_s gives

$$k_{eff_{RGH}} = \frac{1}{\left(W_{sD_{RGH}}^2 + 1\right)} \sum_{i=1}^{N} \left(k_{v_i} + k_{h_i} W_{sD_{RGH}}^2\right) H_{D_i} \qquad i = 1,2,...,N \tag{3.38}$$

where

$$H_{D_i} = \frac{H_i}{H} \qquad i = 1,2,...,N \tag{3.39}$$

and W_{S_D} is given by (3.23). Substituting (3.38) into (3.1) and non-dimensionlaizing q_o gives

$$q_{oD_{RGH}} = \frac{q_{o_{RGH}}}{q_{o_{\left(\frac{K_v}{K_h}\right)_i = 1}}} = \sqrt{\frac{\sum_{i=1}^{N} \left(W_{sD_{RGH}}^2 + \left(\frac{k_v}{k_h}\right)_i\right) k_{h_i} H_{D_i}}{\left(W_{sD_{RGH}}^2 + 1\right) \sum_{i=1}^{N} k_{h_i} H_{D_i}}} \qquad i = 1,2,...,N \tag{3.40}$$

Combining (3.1), (3.38) and (3.19) in dimensionless space gives the corresponding rate of growth of the steam chamber as:

$$\frac{dW_{sD_{RGH}}}{dt_D} = C\sqrt{\frac{\sum_{i=1}^{N}\left(W_{sD_{RGH}}^2 + \left(\frac{k_v}{k_h}\right)_i\right)k_{h_i}H_{D_i}}{\left(W_{sD_{RGH}}^2+1\right)\sum_{i=1}^{N}k_{h_i}H_{D_i}}} \qquad i=1,2,...,N \qquad (3.41)$$

where

$$q_{o_{\left(\frac{k_v}{k_h}\right)_i=1}} = \sqrt{\frac{2\phi\Delta S_o g\alpha_T H\sum_{i=1}^{N}k_{h_i}H_{D_i}}{m\nu_{os}}} \qquad i=1,2,...,N \qquad (3.42)$$

$$t_D = \sqrt{\frac{g\alpha_T\sum_{i=1}^{N}k_{h_i}H_{D_i}}{\phi\Delta S_o m\nu_{os}H^3}}t \qquad i=1,2,...,N \qquad (3.43)$$

In (3.42), we have used the same analysis in (3.35) to (3.40) for its derivation but for isotropic conditions. In the special limit where the horizontal permeability is the same across the layers (3.40) to (3.43) becomes

$$q_{oD_{RGH}} = \frac{q_{o_{RGH}}}{q_{o_{\left(\frac{k_v}{k_h}\right)_i=1}}} = \sqrt{\frac{\sum_{i=1}^{N}\left(W_{sD_{RGH}}^2 + \left(\frac{k_v}{k_h}\right)_i\right)H_{D_i}}{\left(W_{sD_{RGH}}^2+1\right)}} \qquad i=1,2,...,N \qquad (3.44)$$

$$\frac{dW_{sD_{RGH}}}{dt_D} = C\sqrt{\frac{\sum_{i=1}^{N}\left(W_{sD_{RGH}}^2 + \left(\frac{k_v}{k_h}\right)_i\right)H_{D_i}}{\left(W_{sD_{RGH}}^2 + 1\right)}} \qquad i = 1,2,...,N \qquad (3.45)$$

$$q_{o_{\left(\frac{k_v}{k_h}\right)_i=1}} = \sqrt{\frac{2\phi\Delta S_o k_h g\alpha_T H}{m\nu_{os}}} \qquad (3.46)$$

The assumption of constant horizontal permeability across layers is not necessary but used here to reduce the amount of parameters required to solve the model. Similar derivations as above using the ROD model yields

$$q_{oD_{ROD}} = \frac{q_{o_{ROD}}}{q_{o_{\left(\frac{k_v}{k_h}\right)_i=1}}} = \sqrt{\frac{\left(W_{sD_{ROD}}^2 + 1\right)\sum_{i=1}^{N}\frac{k_{h_i}H_{D_i}}{W_{sD_{ROD}}^2 + \left(\frac{k_v}{k_h}\right)_i^{-1}}}{\sum_{i=1}^{N}k_{h_i}H_{D_i}}} \qquad i = 1,2,...,N \qquad (3.47)$$

$$\frac{dW_{sD_{ROD}}}{dt_D} = C\sqrt{\frac{\left(W_{sD_{ROD}}^2 + 1\right)\sum_{i=1}^{N}\frac{k_{h_i}H_{D_i}}{W_{sD_{ROD}}^2 + \left(\frac{k_v}{k_h}\right)_i^{-1}}}{\sum_{i=1}^{N}k_{h_i}H_{D_i}}} \qquad i = 1,2,...,N \qquad (3.48)$$

If we also assume the horizontal permeability to be the same across the layers, (3.47) and (3.48) becomes

$$q_{oD_{ROD}} = \frac{q_{o_{ROD}}}{q_{o_{\left(\frac{k_v}{k_h}\right)_i=1}}} = \sqrt{\left(W_{sD_{ROD}}^2+1\right)\sum_{i=1}^{N}\frac{H_{D_i}}{W_{sD_{ROD}}^2+\left(\frac{k_v}{k_h}\right)_i^{-1}}} \qquad i=1,2,...,N \qquad (3.49)$$

$$\frac{dW_{sD_{ROD}}}{dt_D} = C\sqrt{\left(W_{sD_{ROD}}^2+1\right)\sum_{i=1}^{N}\frac{H_{D_i}}{W_{sD_{ROD}}^2+\left(\frac{k_v}{k_h}\right)_i^{-1}}} \qquad i=1,2,...,N \qquad (3.50)$$

Equations (3.40) to (3.50) reveal that the effect of anisotropy on recovery from multi-layered reservoirs during horizontal growth of the SAGD process is not only dependent on the vertical permeability, but also on the combination of vertical permeability and thickness of each layer. This renders the use of variance based reservoir heterogeneity measures like the Dykstra-Parsons or Lorenz coefficient to characterize the SAGD response at best fortuitous as seen in the unexplainable results of Kamath et al. (1993) discussed in chapter 2. However, it will be interesting to attempt such characterization by determining a simple and yet suitable parameter for the unique flow geometry of the SAGD process. A clue to this can be seen from (3.40) to (3.50) where it can be reasonably hypothesized that all layered reservoirs having an equivalent anisotropy ratio $\left(k_v/k_h\right)_{eq}$ defined as

$$\left(k_v/k_h\right)_{eq} = \frac{\sum_{i=1}^{N}\left(k_v/k_h\right)_i k_{h_i} H_i}{\sum_{i=1}^{N} k_{h_i} H_i} \qquad i=1,2,...,N \qquad (3.51)$$

should have the same dimensionless bitumen rate response during the horizontal SAGD growth phase. If each layer has the same horizontal permeability, (3.51) becomes

$$\left(k_v/k_h\right)_{eq} = \sum_{i=1}^{N} \left(k_v/k_h\right)_i H_{D_i} \qquad i = 1,2,\ldots,N \qquad (3.52)$$

It should be understood that the equivalent permeability model is just a way to convert the multi-layered model to the single layer model. We will use (3.52) to verify the above hypothesis in an example problem below.

3.2.1 Example Problem

In this section, we will consider two cases – a high permeability anisotropy case (left table) and a low permeability anisotropy case (right table) for a 6 layered reservoir. The reservoir parameters for both cases are given in Table 3.2. We have chosen both cases to have the same distribution for the thickness of each layer for convenience. We are also assuming for both cases that the horizontal permeability is the same in all the layers.

Table 3.2: The k_v/k_h ratio for each layer and the dimensionless thickness distribution. The higher permeability anisotropy case is shown on the left and the lower permeability anisotropy case is shown on the right.

$(k_v/k_h)_i$	H_{D_i}
0.05	0.25
0.01	0.1
0.1	0.05
0.04	0.2
0.02	0.15
0.07	0.25

$(k_v/k_h)_i$	H_{D_i}
0.6	0.25
0.7	0.1
1	0.05
0.5	0.2
0.4	0.15
0.9	0.25

Based on the data in Table 3.2, and using (3.52), the equivalent anisotropy ratio is calculated for both cases as

$$(k_v/k_h)_{eq} = 0.047 \tag{3.53}$$

for the high permeability anisotropy case and

$$(k_v/k_h)_{eq} = 0.655 \tag{3.54}$$

for the low permeability anisotropy case.

3.3 Results and Discussion

Fig. 3.6 shows the plot of the dimensionless oil production rate as a function of dimensionless time for the RGH model. Notice that for all practical purposes, the effect of anisotropy disappears at $t_D > 3$ for all anisotropy ratios. This is a very interesting result because it suggests that there exists a combination of reservoir and fluid parameters for which the effect of anisotropy becomes unimportant at times that are small enough to be ignored. This is however not the case if the ROD model is used especially for lower anisotropy ratios as seen in **Fig. 3.9**. Both models reveal that the general effect of anisotropy is to introduce a time component to the maximum SAGD oil rate. **Figs. 3.6** and **3.9** exhibit a discontinuity at $t_D = 0$ and this is because at the start of the SAGD horizontal growth phase, there will be a finite non-zero rate response. Also, form **Figs. 3.6** and **3.9** and for $k_v/k_h = 0.01$ there is a dramatic difference between the RGH and the ROD models. The reason for this can be understood better from **Fig. 3.3** where the difference in effective permeabilities can be as high as 90% depending on the steam chamber angle.

Figs. 3.7 and **3.10** plots the dimensionless steam chamber half width for both the RGH and ROD models respectively and we see that while the effect of anisotropy on steam chamber expansion is short-lived (about $t_D \le 1$ for $k_v/k_h \le 0.01$) for the RGH model, the ROD model predicts that anisotropy ratios less than 0.1 is likely to impact the rate of growth of the steam chamber through-out the duration of the process.

Figs. 3.8 and **3.11** show more clearly the loss in size of the steam chamber with time due to anisotropy. While the RGH model predicts that given sufficient time (and if the reservoir aspect ratio allows), the steam chamber will recover to its isotropic size for all anisotropic ratios. For lower values of anisotropy ratio, the time after which the

chamber geometry will coincide with that for the isotropic case may be substantially large and it may be that the physical boundaries of the layer may be experienced prior to that time. The ROD model predicts that convergence to the isotropic case might happen at infinite time for $k_v/k_h \le 0.01$. This result might lead to the conclusion that the ROD model is the more physically appropriate choice since it is generally agreed that the SAGD process will fail for any reservoir with such low anisotropic ratios because the steam chamber will simply not grow. It is important to note however, that the results we show here are only strictly valid during horizontal growth of the steam chamber and hence, implicit in them is the assumption that the steam chamber has *already grown* to reach the top of the reservoir. **Figs. 3.12** to **3.14** are comparison plots and reveal both models are indistinguishable when $k_v/k_h > 0.7$.

Fig. 3.15 shows the validation plot comparing both the RGH and the ROD models with numerical simulation results using CMG-Stars™. The input model for the numerical simulation is given in Table 3.1. As discussed earlier, modifications have been proposed to Butler's model to account for multiphase flow effects. However, these modifications are mostly empirical and most likely have to be calibrated against the actual characteristics of the process as represented in a simulation result or as measured in the field. For this reason, in **Fig. 3.15** we calculated a multiphase flow factor for the isotropic case by dividing the simulation average bitumen rate with the theoretical Butler model rate obtained using (2.1). This calibration multiphase flow factor was subsequently used for all k_v/k_h ratios. However as observed in **Fig. 3.15**, the application of this multiphase flow factor results in a poor match between the simulation and semi-analytical results. This can be explained further by writing the orthogonal components of the effective permeabilities in the presence of anisotropy for both the RGH and ROD models as

$$k_{eff_{RGH\rightarrow}} = k_v \cos^2\theta + k_h \sin^2\theta \tag{3.55}$$

$$\frac{1}{k_{eff_{ROD\rightarrow}}} = \frac{\cos^2\theta}{k_v} + \frac{\sin^2\theta}{k_h} \tag{3.56}$$

where $k_{eff_{RGH\rightarrow}}$ and $k_{eff_{ROD\rightarrow}}$ are the effective permeabilities for both the RGH and ROD models orthogonal to the steam chamber interface.

From (3.55) and (3.56) we see that the effective permeability orthogonal to the steam chamber interface will decrease with a decrease in the k_v/k_h ratio which will generally give lower multiphase flow factors at lower k_v/k_h ratios. Even though in chapter 4, we will describe a model accounting for multiphase flow during SAGD horizontal growth, we have not coupled such to anisotropy in this dissertation. Hence, we will treat the anisotropic multiphase flow factors as a history match parameter and the results are shown in **Fig. 3.16**. An excellent match between our anisotropy models and numerical simulation result is seen in **Fig. 3.16** and the anisotropic multiphase flow factors used to obtain the match is given in Table 3.3. **Fig 3.16** also shows that the ROD model is more accurate than the RGH model at lower k_v/k_h ratios. It is important to note that in **Fig. 3.16**, we are only plotting the SAGD rates during horizontal growth from the numerical simulation.

Figs. 3.17 to **3.19** reveal that the history matched multiphase flow factors shown in Table 3.3 are not necessarily fudge factors. **Fig. 3.17** shows the temperature profile close to the end of the horizontal growth period for the isotropic case using the validation parameters in Table 3.1. The plot shows that the heat transfer length scale varies from about 1m at the top of the chamber to about 5m at the base of the chamber. **Figs 3.18** and **3.19** give the water saturation profiles for the isotropic and $k_v/k_h = 0.3$ cases respectively

and from which we see that the saturation diffusivity length scale is similar to the heat transfer length scale and the degree of saturation diffusion for the anisotropic case is slightly greater than that of the isotropic case, thereby giving rise to smaller multiphase flow factors. It is important to note that saturation diffusion here is caused by numerical dispersion and in chapter 4, we will show that saturation diffusion similar to that from numerical simulation, is evident from laboratory and field scale recoveries but are rather caused by the Marangoni or thermo-capillary effect.

There is however an alternative explanation to the mismatch of **Fig. 3.15**. The mismatch between the simulation and semi-analytical results may be due to grid orientation effects that are inherent in structured grid based finite difference simulators. Due to the unique geometry of the SAGD process, the effective permeability parallel to the steam chamber wall is always underestimated because of the stair-step flow that is simulated on the grid. This effect is shown in **Fig. 3.5** where the effective permeability parallel to the steam chamber wall is driven largely by the vertical permeability (since we have used a zero pressure gradient between the wells, the horizontal permeability effect will be small and will only arise due to pressure perturbations in the simulation). This is a consequence of not using the full permeability tensor in formulating the finite difference equations in most commercial simulators. Even though we have used very small grid sizes to minimize this effect, it is likely it was not eliminated. Also, using dynamic grid refinement around the steam chamber interface didn't help much as the structure of the problem doesn't change beyond a particular refinement level – beyond this point, what is needed is a change in the grid orientation relative to the steam chamber interface and not the grid size. To resolve this problem, and hence determine the more accurate model between the RGH and ROD model will require either experimentation or a gridding technique relatively insensitive to the grid orientation effect like the finite element

method (FEM). FEM has been applied to the SAGD process (Bogdanov et al. 2007), but only for a homogenous reservoir.

Before the grid orientation issue is resolved, we recommend that any semi-analytical model developed to analyze the effect of anisotropy on SAGD performance should include sensitivities to using both the RGH and ROD models. If such sensitivities reveal significant differences in recovery performance, then a choice will have to be made taking into account the nature of the phenomenon itself, and at the very least, the difference in results using both models can be used to inform uncertainty due to anisotropy.

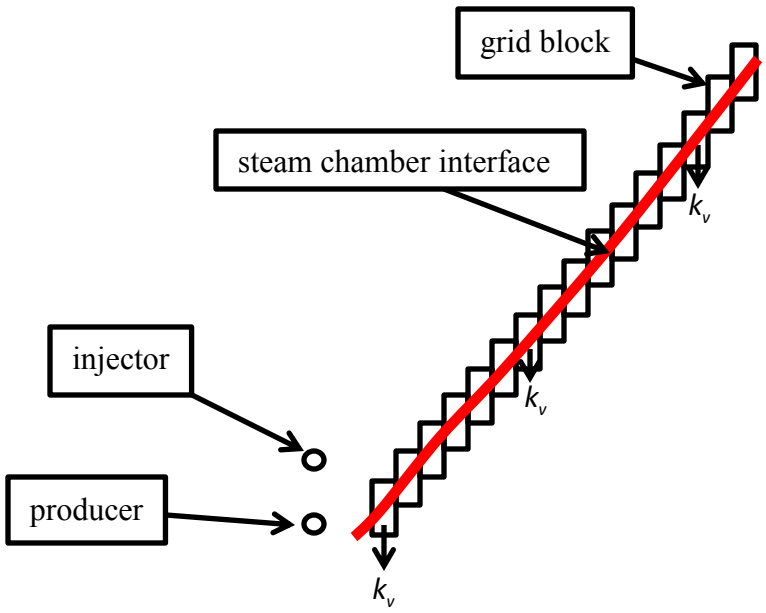

Figure 3.5: Showing a finite difference based grid orientation during SAGD horizontal growth with an effective permeability parallel to the steam chamber wall similar to the vertical permeability

Table 3.3: Showing the multiphase flow factor for each k_v/k_h ratio suitable for comparing the semi-analytical model with numerical simulation results

k_v/k_h **ratio**	**Multiphase Flow Factor**
1	0.76
0.7	0.61
0.3	0.46

Figs. 3.20 to **3.22** show the results for the layered models which give similar results as the single layer case as at high equivalent anisotropy ratios, the RGH and ROD models are indistinguishable approaching the asymptotic limit of the isotropic case for $t_D > 3$, while at low equivalent anisotropy ratios, significant differences between both models exist. They also reveal that the equivalent anisotropy ratio $(k_v/k_h)_{eq}$ is an exact characterization parameter for the RGH model, but is not for the ROD model especially at low $(k_v/k_h)_{eq}$ ratios. This is because $(k_v/k_h)_{eq}$ was derived using the Butler's model which in turn was derived implicitly assuming the RGH model, not the ROD model.

Since this work was entirely done in dimensionless space, **Fig. 3.6** or **3.9** can be used as type curves to predict the effect of anisotropy on SAGD rates. As mentioned earlier, these curves are strictly valid for the horizontal growth phase of the steam chamber but they can still be used with caution for both the vertical growth and the depletion phases with a slight modification to the governing equations. This modification includes rescaling the models presented in this chapter by using $H = H(t)$ (with the respective definitions for both the vertical growth and depletion phases) instead of H. This will require an elaborate procedure different from (especially for the depletion

phase) that described by Llaguno et al. (2002) and which is beyond the scope of this dissertation.

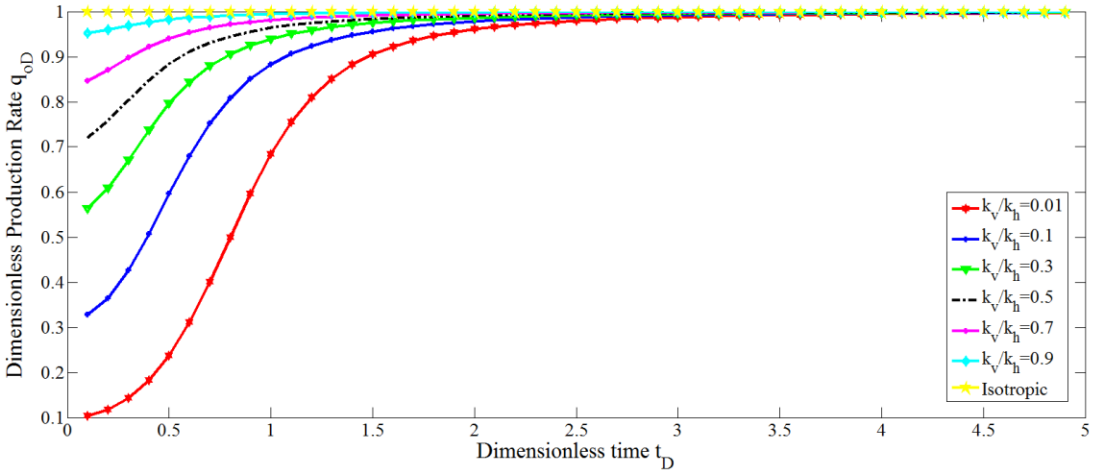

Figure 3.6: Plot of dimensionless rate vs. dimensionless time for the RGH model

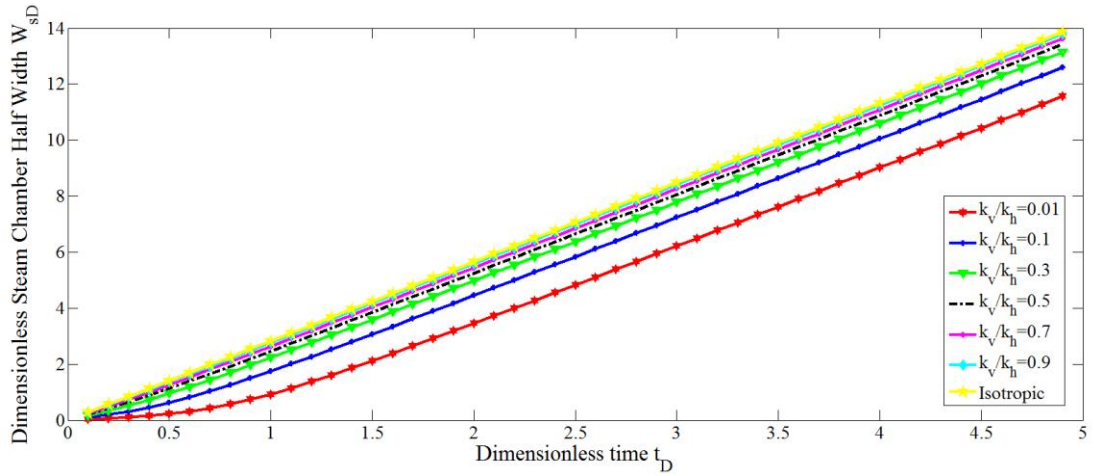

Figure 3.7: Plot of dimensionless steam chamber half width vs. dimensionless time for the RGH model

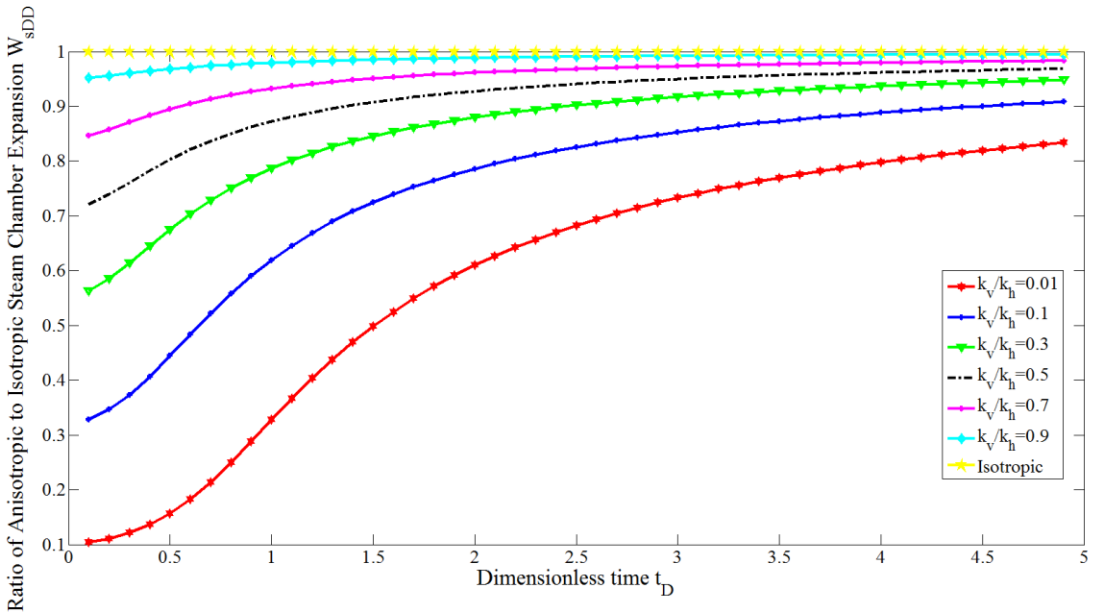

Figure 3.8: Plot of ratio of anisotropic to isotropic dimensionless steam chamber expansion vs. dimensionless time for the RGH model

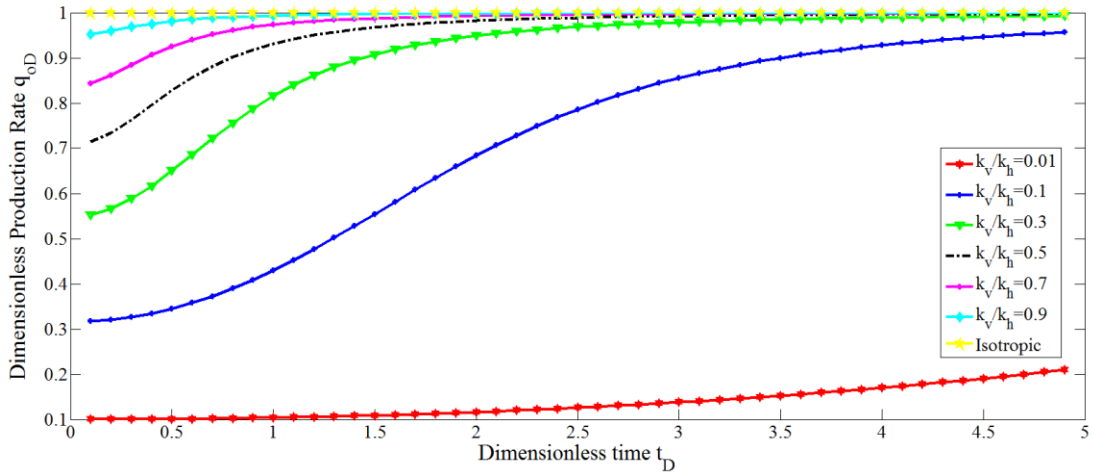

Figure 3.9: Plot of dimensionless rate vs. dimensionless time for the ROD model

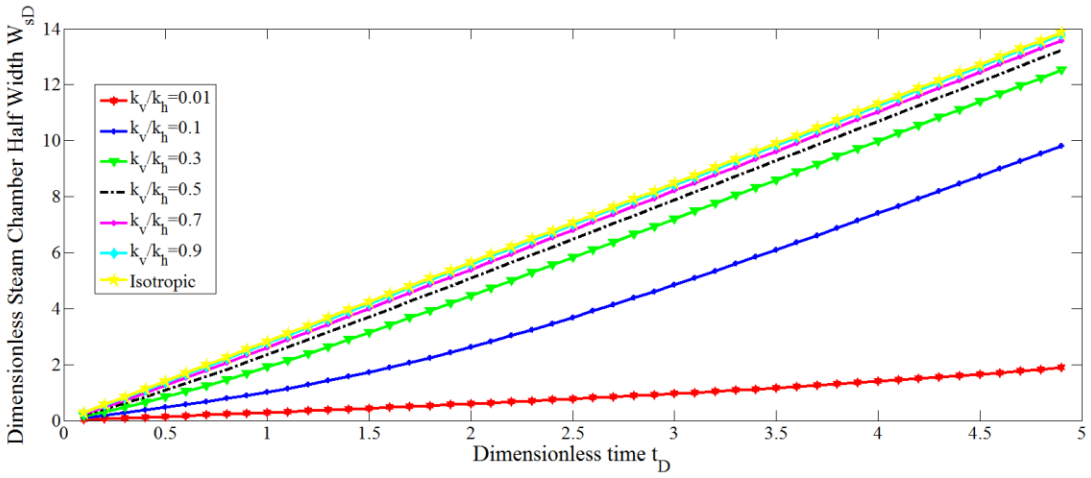

Figure 3.10: Plot of dimensionless steam chamber half width vs. dimensionless time for the ROD model

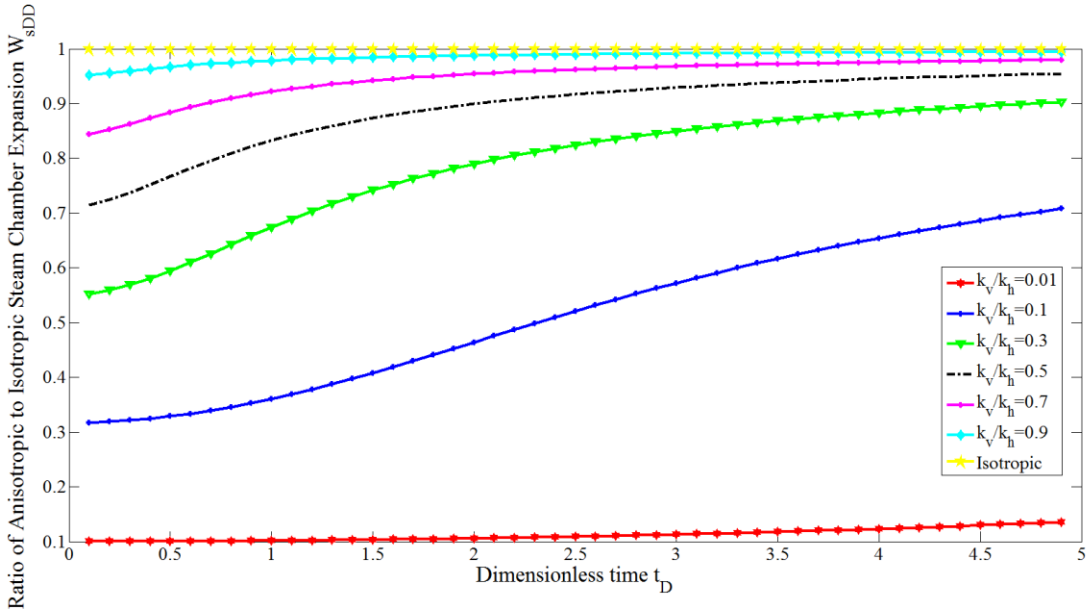

Figure 3.11: Plot of the ratio of anisotropic to isotropic dimensionless steam chamber expansion vs. dimensionless time for the ROD model

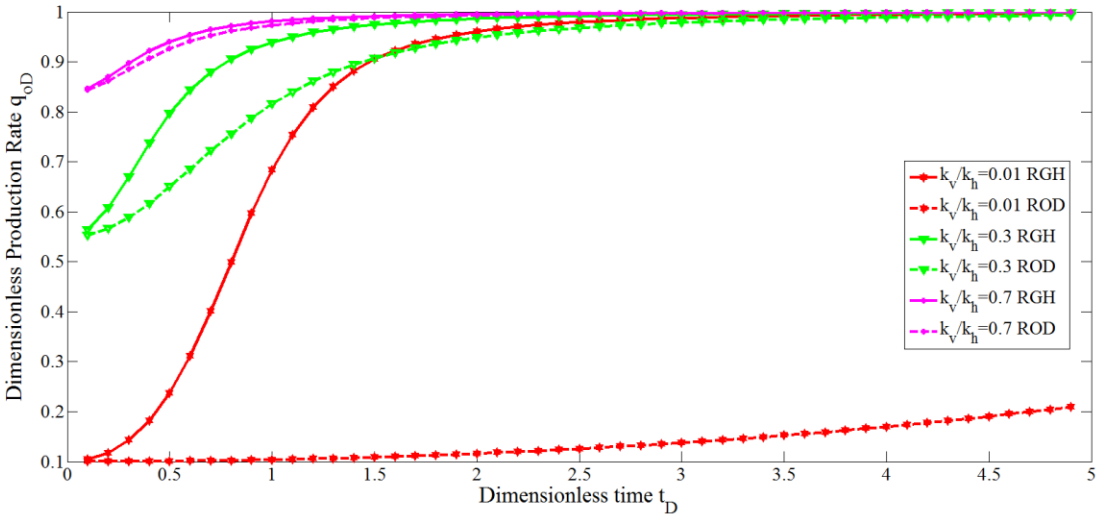

Figure 3.12: Comparison plot of dimensionless rate vs. dimensionless time for the RGH and ROD models

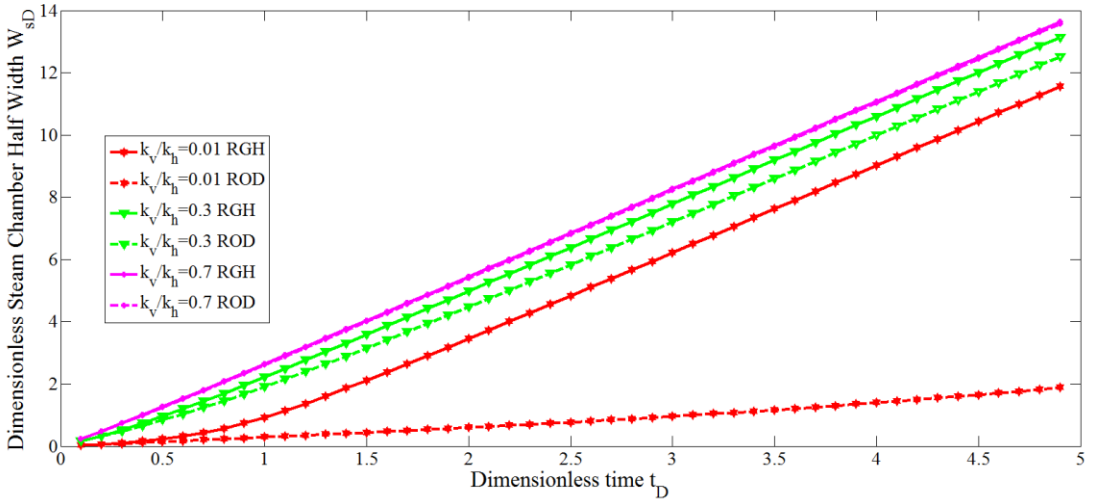

Figure 3.13: Comparison plot of dimensionless steam chamber half width vs. dimensionless time for the RGH and ROD model

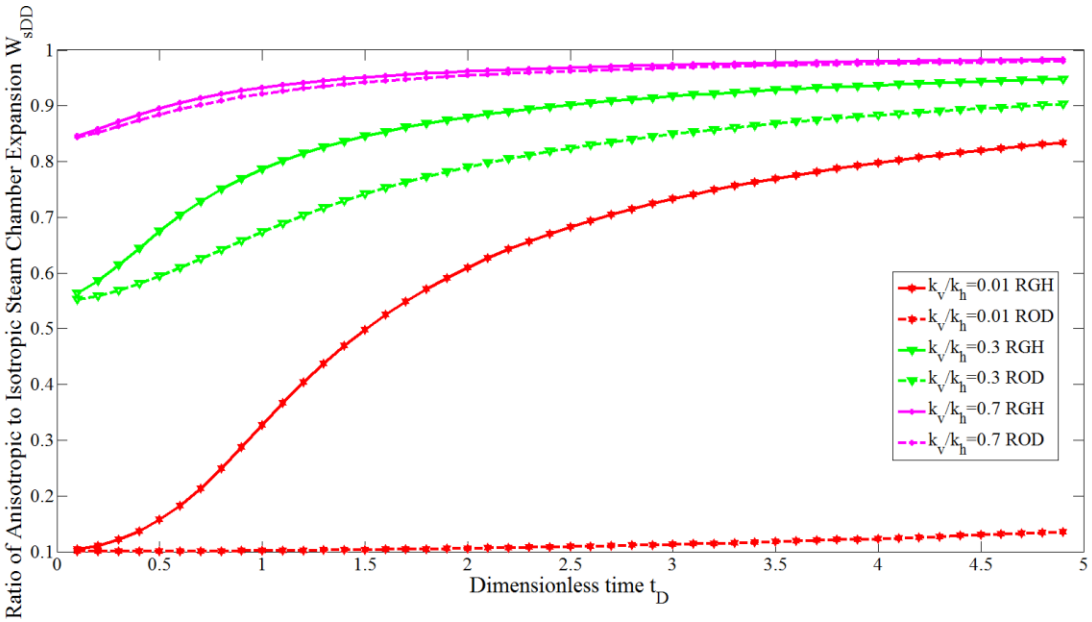

Figure 3.14: Comparison plot of the ratio of anisotropic to isotropic dimensionless steam chamber expansion vs. dimensionless time for the ROD model

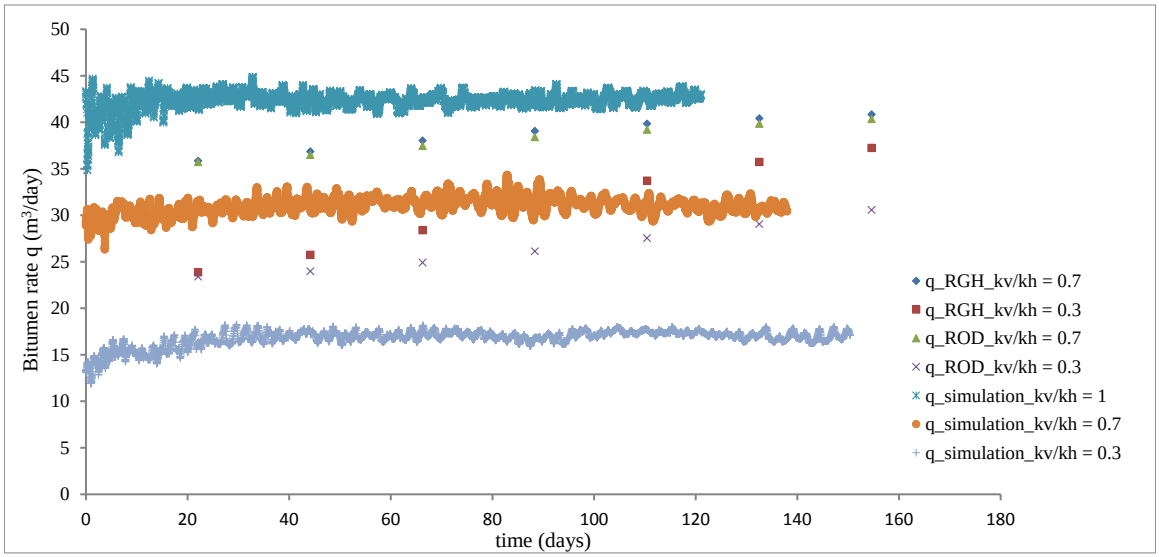

Figure 3.15: Comparison plot of bitumen rate vs. time for the RGH, ROD and numerical simulation models for constant multiphase flow calibration factors

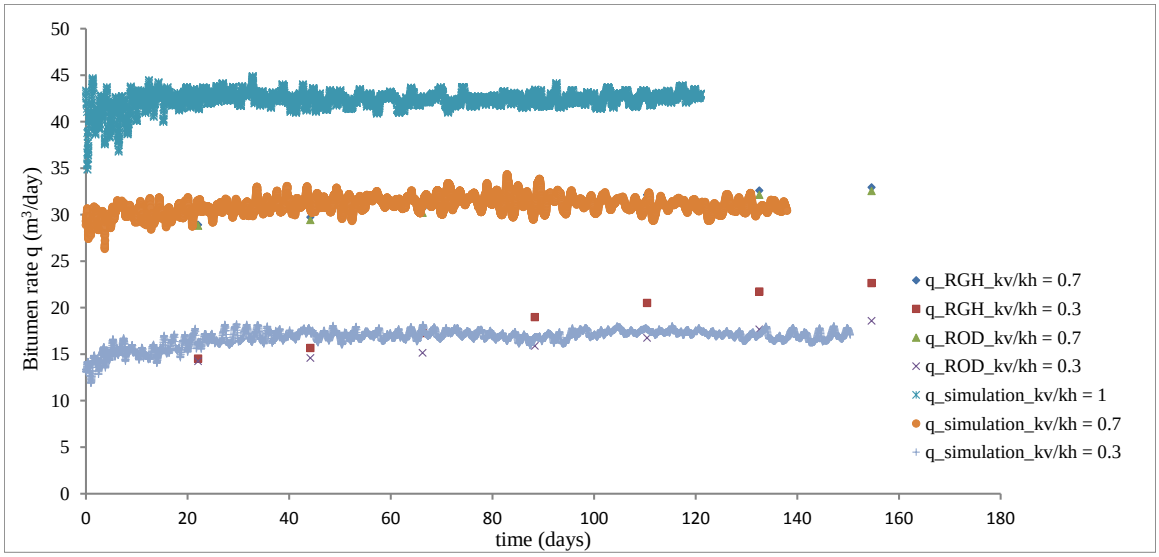

Figure 3.16: Comparison plot of bitumen rate vs. time for the RGH, ROD and numerical simulation models for varying multiphase flow calibration factors

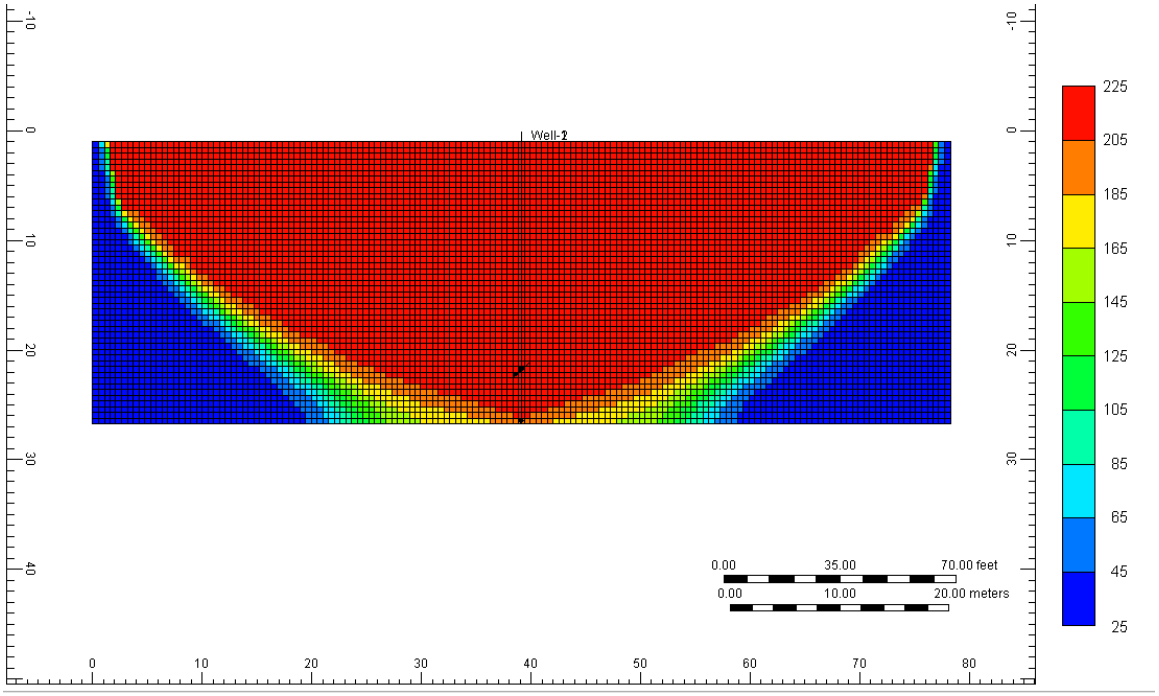

Figure 3.17: Temperature profile from numerical simulation validation for $k_v/k_h = 1$

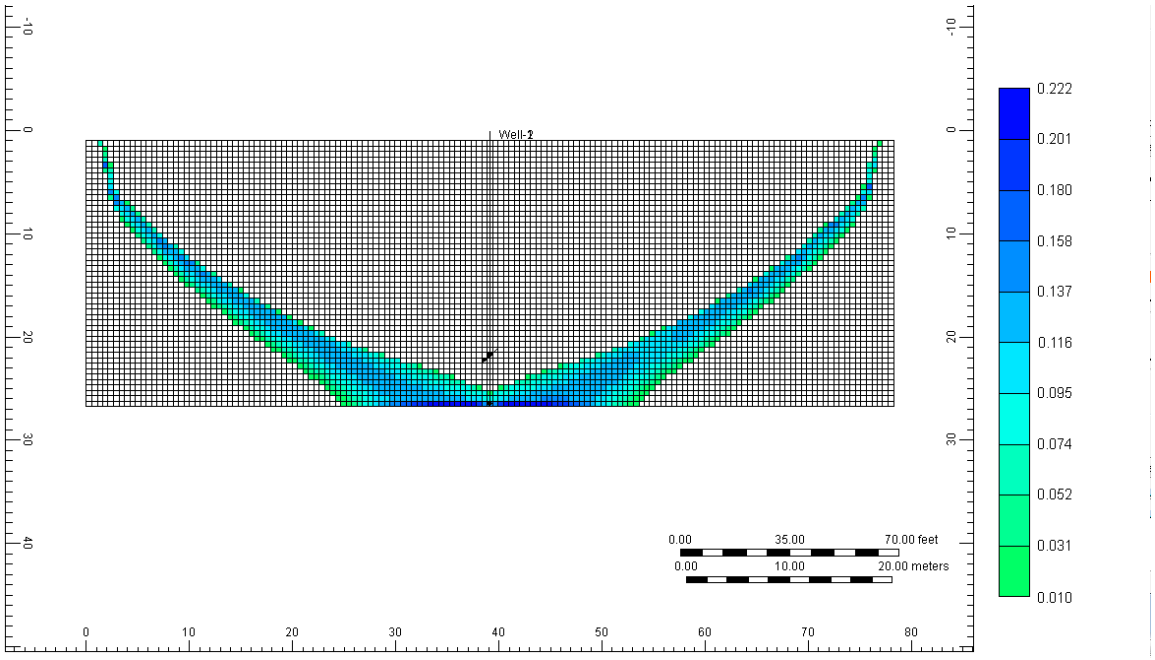

Figure 3.18: Water Saturation profile from numerical simulation validation for $k_v/k_h = 1$

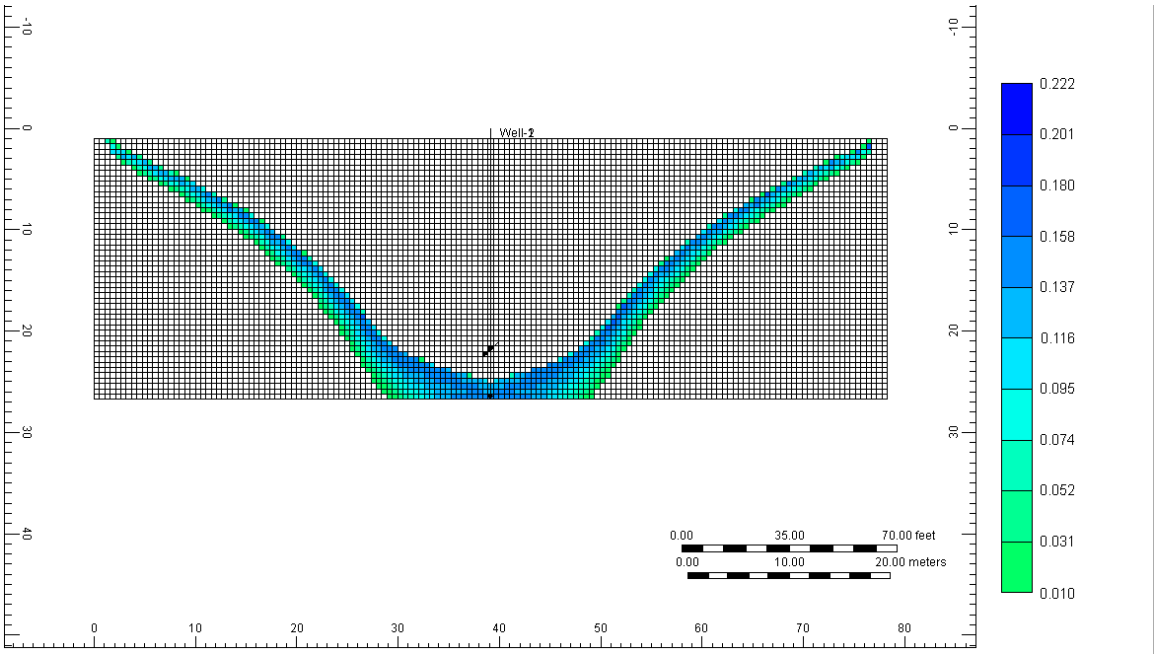

Figure 3.19: Water Saturation profile from numerical simulation validation for $k_v/k_h = 0.3$

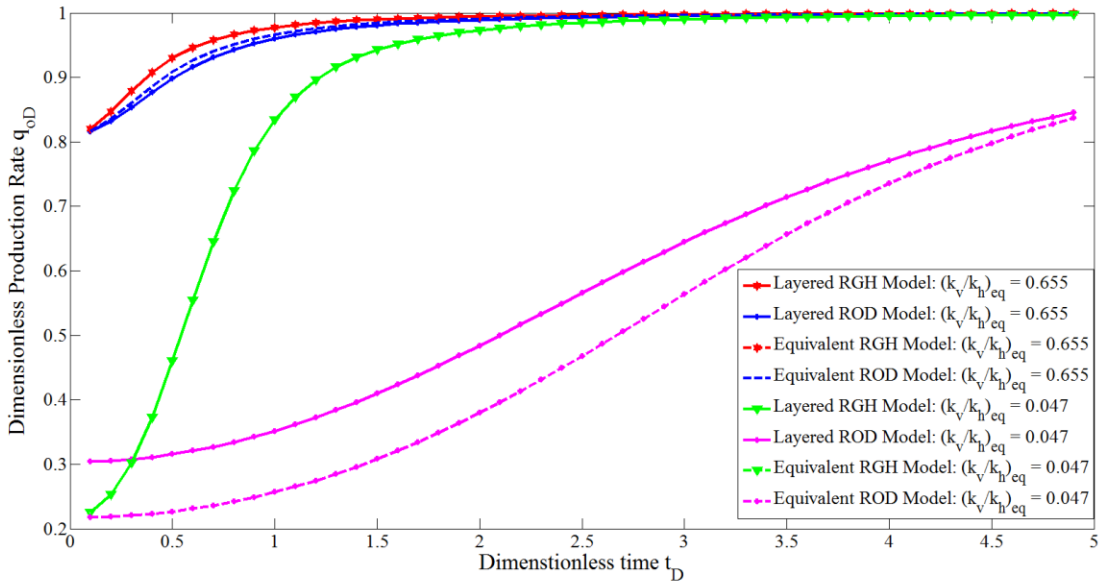

Figure 3.20: Comparison plot of dimensionless rate vs. dimensionless time for the layered and equivalent RGH and ROD models

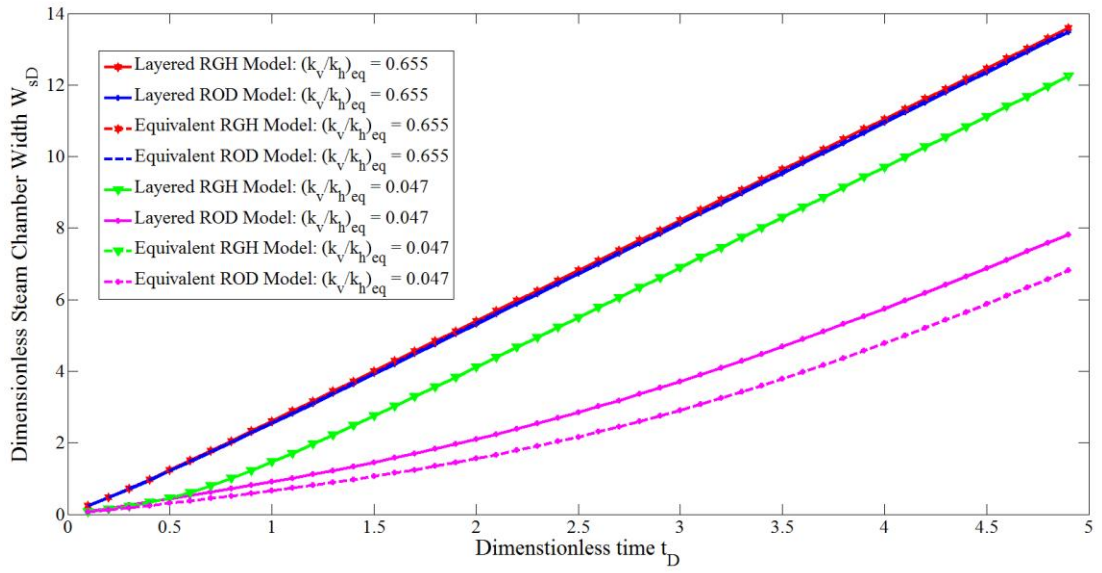

Figure 3.21: Comparison plot of dimensionless steam chamber half width vs. dimensionless time for the layered and equivalent RGH and ROD models

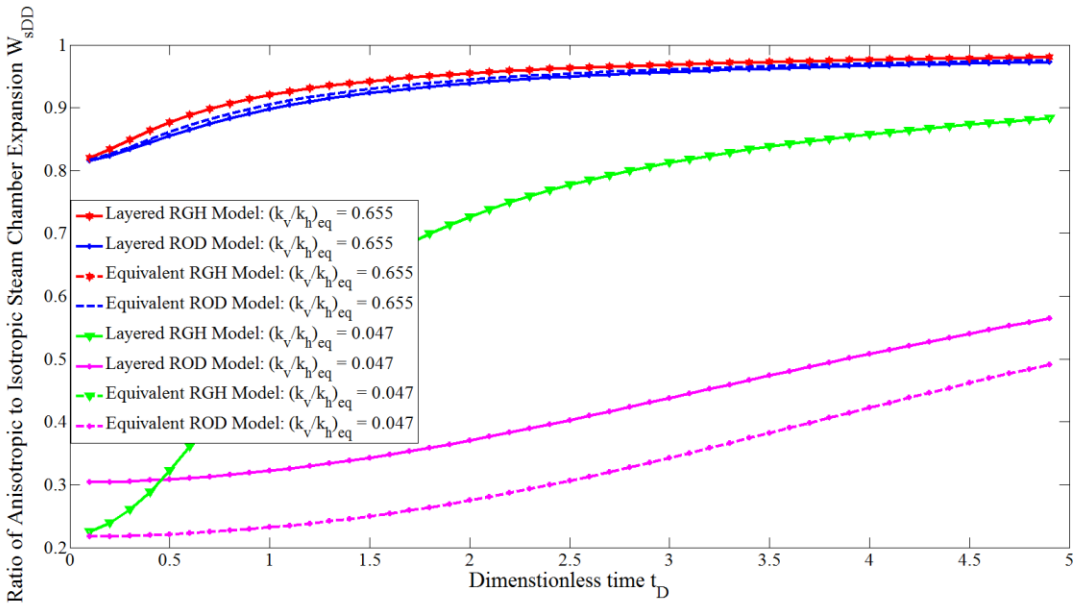

Figure 3.22: Comparison plot of the ratio of anisotropic to isotropic dimensionless steam chamber expansion vs. dimensionless time for the layered and equivalent RGH and ROD models

3.4 Summary and Significance of Work

We have developed and validated a semi-analytical model that takes into account the effect of anisotropy during the SAGD process for both single and multi-layered reservoirs. This was done using both the resultant gravity head (RGH) and the resultant oil discharge (ROD) models which mimic natural flow directions that generally do not coincide for anisotropic reservoirs.

This work gives a viable model that accounts for anisotropy in a Butler type model framework and explains the observed phenomena of bitumen rates gradually ramping up to isotropic levels for anisotropic reservoirs as shown in the work of Kisman and Yeung (1995) and discussed in chapter 2.

This work will find great utility in proxy based history matching of the SAGD process and also in optimal well spacing design because it reveals that if the well spacing is such that you are past the horizontal growth phase by dimensionless time $t_D = 3$ for any given anisotropy ratio, then your wells will probably never produce at its maximum possible rate. Economics will ultimately drive the decision of well spacing but understanding how anisotropy influences it is an invaluable contribution of this work.

This work has also helped illuminate on the weakness of grid based finite difference simulators in capturing the correct effective permeabilities for the propagation of fluid interfaces that are inclined to the simulator's grid orientation such as observed in the SAGD process. More research still needs to be done to understand the grid orientation effect as it relates to anisotropic SAGD flow.

Chapter 4: The Effect of Heat Transfer on Capillarity during SAGD

By solving a 1-D heat conservation equation for single phase flow along the steam chamber wall, Butler et al. (1981) derived their classical SAGD model. Their equation has excellent predictive capability at experimental scales but performs poorly at field scales. Several authors have postulated that multiphase flow along the steam-bitumen boundary that was not accounted for in the Butler's original model has an important impact on recovery. They have proposed rate multipliers to bring the model predictions closer to observations and related these multipliers to multiphase flow effects, but in practice, the multipliers seem to vary for each reservoir or experiment. Another reason why the Butler models perform poorly at field scales is because it only takes into account flow due to gravity neglecting other pressure gradients. However, at field scales, other pressure gradients are known to exist (Ito and Suzuki 1999).

Recently, by making the prior assumption that fluid saturations ahead of the steam chamber vary linearly with temperature, Sharma and Gates (2010b) derived a SAGD equation that accounts for multiphase flow ahead of the steam chamber, which performs excellently at field scales but poorly at experimental scales. In this work, we proceed by decomposing capillary pressure change into its temperature and saturation components. Our premise is that though capillary pressure changes due to saturation, these changes are likely to be negligible given the unconsolidated nature of the reservoir. However, the large temperature changes associated with the process can induce significant changes to the interfacial tension between the oil and water and that in turn can induce significant capillary pressure changes. This phenomenon is the classical Marangoni (or thermo-capillary) effect where interfacial tension driven flows are triggered by temperature (or concentration gradients) (Lyford et al. 1998), (Flock et al., 1986). We also show how the

Marangoni number can be used to characterize this effect. At low Marangoni numbers (typical of experimental scales) we get the Butler solution while at high Marangoni numbers (typical of field scales), we approximate the Sharma and Gates solution. The entire modeling was done in dimensionless space so our results can be used as a fast SAGD predictive model within a proxy-based history matching process.

4.1 Model Development

We now present the detailed development of our model that quantifies thermo-capillary behavior during SAGD. Note that we interchangeably use the term thermo-capillarity for what is known as the Marangoni effect through this chapter and the rest of the dissertation.

4.1.1 Transport equations in a fixed frame

The SAGD process is a moving boundary problem, but we present the basic mass and energy transport equations in a fixed coordinate (Eulerian) frame in this section and then transform these equations into a moving coordinate (Langrangian) frame in the next section. There are three phases flowing simultaneously during SAGD – water vapor, liquid water and bitumen – however, water vapor will usually be non-wetting in the porous medium, hence, it will not imbibe into the pore space containing bitumen. The wetting phase – usually liquid water – will preferentially imbibe into the pore space containing the intermediate wetting phase – bitumen. Furthermore, water vapor will condense at the steam chamber boundary, and ahead of this boundary, no vapor remains. This implies that for all practical purposes, it suffices to study the two-phase (liquid water and bitumen) problem when studying capillary imbibition during SAGD. We assume in

the foregoing analysis that water is the wetting phase. The conservation equations are now presented.

Mass conservation for the water phase is given as

$$\frac{\partial}{\partial t}\left(\phi\rho_w S_w\right)+\nabla\cdot\left(\rho_w \mathbf{u}_w\right)=0 \tag{4.1}$$

and for the bitumen phase as

$$\frac{\partial}{\partial t}\left(\phi\rho_o S_o\right)+\nabla\cdot\left(\rho_o \mathbf{u}_o\right)=0 \tag{4.2}$$

The velocities are given by Darcy's law

$$\mathbf{u}_w=-\frac{kk_{rw}}{\mu_w}\left(\nabla p_w+\rho_w \mathbf{g}\right)=-\lambda_w\left(\nabla p_w+\rho_w \mathbf{g}\right) \tag{4.3}$$

$$\mathbf{u}_o=-\frac{kk_{ro}}{\mu_o}\left(\nabla p_o+\rho_o \mathbf{g}\right)=-\lambda_o\left(\nabla p_o+\rho_o \mathbf{g}\right) \tag{4.4}$$

Pressure in the water and bitumen phases are related through capillary pressure

$$p_o=p_w+P_c\left(S_w,T\right) \tag{4.5}$$

Note that capillary pressure is expressed explicitly as a function of both wetting phase saturation as well as temperature T. If we assume constant phase densities for the water and bitumen phases, (4.1) and (4.2) becomes

$$\frac{\partial}{\partial t}(\phi S_w)+\nabla\cdot(\mathbf{u}_w)=0 \tag{4.6}$$

$$\frac{\partial}{\partial t}(\phi S_o)+\nabla\cdot(\mathbf{u}_o)=0 \tag{4.7}$$

Adding (4.6) and (4.7) and noting that for two phase flow

$$S_o+S_w=1 \tag{4.8}$$

we can derive:

$$\nabla\cdot(\mathbf{u})=0 \tag{4.9}$$

where $\mathbf{u}=\mathbf{u}_o+\mathbf{u}_w$ is the total velocity which is given by

$$\mathbf{u}=-\left[\lambda(\nabla p+\rho\mathbf{g})+\lambda_o\nabla P_c\right] \tag{4.10}$$

where $\lambda=\lambda_o+\lambda_w$ is the total mobility and we have assumed that $\rho_o\approx\rho_w\equiv\rho$ which is a good assumption for heavy oils. Substituting (4.3) and (4.4) into (4.6) and (4.7) respectively gives

$$\frac{\partial}{\partial t}(\phi S_w)-\nabla\cdot\left[\lambda_w(\nabla p_w+\rho\mathbf{g})\right]=0 \tag{4.11}$$

$$\frac{\partial}{\partial t}(\phi S_o)-\nabla\cdot\left[\lambda_o(\nabla p_o+\rho\mathbf{g})\right]=0 \tag{4.12}$$

If we assume that water is always a connected phase, we can choose to take the pressure in the water phase as the reference pressure variable, hence $p \equiv p_w$. Using this definition and assuming constant porosities, (4.5), (4.11) and (4.12) can be written respectively as

$$\phi \frac{\partial S_w}{\partial t} - \nabla \cdot \left[\lambda_w \left(\nabla p + \rho \mathbf{g} \right) \right] = 0 \tag{4.13}$$

$$\phi \frac{\partial S_o}{\partial t} - \nabla \cdot \left[\lambda_o \left(\nabla p + \rho \mathbf{g} + \nabla P_c \right) \right] = 0 \tag{4.14}$$

The next transport equation to consider is that of energy. In the absence of the other phenomena like emulsification and well bore flow effects, the only heat transfer mechanism operating during SAGD is thermal conduction. Hence, energy conservation for the two phase system and porous media gives

$$\begin{aligned} &\left[\phi \left(S_o C_o + S_w C_w \right) + \left(1 - \phi \right) \frac{\rho_s}{\rho} C_s \right] \frac{\partial T}{\partial t} \\ &- \nabla \cdot \left[\left(\lambda_o C_o + \lambda_w C_w \right) \left(\nabla p + \rho \mathbf{g} \right) T + \lambda_o C_o \nabla P_c T + \frac{k_{TH}}{\rho} \nabla T \right] = 0 \end{aligned} \tag{4.15}$$

where k_{TH} is the thermal conductivity of the reservoir and C_o, C_w and C_s are the specific heat capacities of the bitumen, condensate and reservoir solid rock phases. Equations (4.13), (4.14) and (4.15) are the transport equations in a fixed frame. As is, these equations can be solved using a numerical scheme (by making finite difference approximations). However, our goal is to derive an analytical or semi-analytical solution

for the above. For this, we will transform the same set of equations to a moving reference frame.

4.1.2 Transport equations in a moving reference frame

In a moving reference frame (see appendix B) in which we assume that the steam chamber is expanding in a quasi-steady state manner (Butler, 1991), (4.13), (4.14) and (4.15) become

$$\phi \mathbf{U} \cdot \nabla' S_w + \nabla' \cdot \left[\lambda_w \left(\nabla' p + \rho \mathbf{g}' \right) \right] = 0 \tag{4.16}$$

$$\phi \mathbf{U} \cdot \nabla' S_o + \nabla' \cdot \left[\lambda_o \left(\nabla' p + \rho \mathbf{g}' + \nabla' P_c \right) \right] = 0 \tag{4.17}$$

$$\begin{aligned} &\mathbf{U} \cdot \nabla' \left[\left\{ \phi \left(S_o C_o + S_w C_w \right) + \left(1 - \phi \right) \frac{\rho_s}{\rho} C_s \right\} T \right] \\ &- \nabla' \cdot \left[\left(\lambda_o C_o + \lambda_w C_w \right) \left(\nabla' p + \rho \mathbf{g}' \right) T + \lambda_o C_o \nabla P_c T + \frac{k_{TH}}{\rho} \nabla' T \right] = 0 \end{aligned} \tag{4.18}$$

where $\nabla' = \left(\partial \xi, \partial \psi \right)^T$ is the gradient operator in the moving reference frame and $\mathbf{U}$ is the velocity with which the steam-bitumen interface moves (see **Fig. 4.1**). Flow in the direction parallel to the front (ψ direction) will be fast relative to that in the direction orthogonal to the front (ξ direction) and hence, we can neglect variations in saturation pressure (note that we have assumed equal densities for water and bitumen, hence gravity will not be a factor here) and temperature in the direction parallel to the front. This allows us to ignore the gradients in the ψ direction and write:

$$\phi U_f \frac{dS_w}{d\xi} + \frac{d}{d\xi}\left[\lambda_w\left(\frac{dp}{d\xi} + \rho g \sin\theta\right)\right] = 0 \tag{4.19}$$

$$\phi U_f \frac{dS_o}{d\xi} + \frac{d}{d\xi}\left[\lambda_o\left(\frac{dp}{d\xi} + \rho g \sin\theta + \frac{dP_c}{d\xi}\right)\right] = 0 \tag{4.20}$$

$$\begin{aligned} &U_f \frac{d}{d\xi}\left\{\left[\phi\left(S_o C_o + S_w C_w\right) + \left(1-\phi\right)\frac{\rho_s}{\rho} C_s\right] T\right\} \\ &+ \frac{d}{d\xi}\left[\left(\lambda_o C_o + \lambda_w C_w\right)\left(\frac{dp}{d\xi} + \rho g \sin\theta\right) T + \lambda_o C_o \frac{dP_c}{d\xi} T + \frac{k_{TH}}{\rho}\frac{dT}{d\xi}\right] = 0 \end{aligned} \tag{4.21}$$

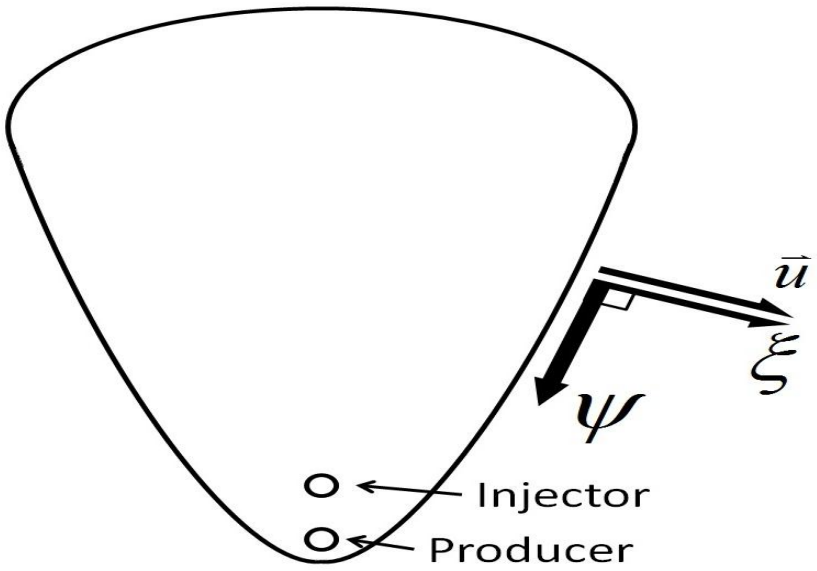

Figure 4.1: Schematic of the SAGD steam chamber showing important flow directions and the steam chamber front velocity vector

where U_f is the front velocity in the ξ direction. Since we have assumed U_f is independent of ξ,(4.19), (4.20) and (4.21) can be integrated with respect to ξ between an arbitrary

value ξ (corresponding to any location away from the interface) and ∞ (corresponding to the undisturbed reservoir) to yield the mass and energy balances within a given volume of the reservoir as

$$\phi U_f \int_{S_{wi}}^{S_w} dS_w = -\left[\lambda_w \left(\frac{dp}{d\xi} + \rho g \sin\theta \right) \right]_{\infty}^{\xi} \tag{4.22}$$

$$\phi U_f \int_{1-S_{wi}}^{S_o} dS_o = -\left[\lambda_o \left(\frac{dp}{d\xi} + \rho g \sin\theta + \frac{dP_c}{d\xi} \right) \right]_{\infty}^{\xi} \tag{4.23}$$

$$\begin{aligned} &\phi U_f \int_{S_{wi},T_R}^{S_w,T} d\left\{ \left[\frac{1-\phi}{\phi} \frac{\rho_s}{\rho} C_s + \left(S_o C_o + S_w C_w \right) \right] T \right\} \\ &= -\left[\left(\lambda_o C_o + \lambda_w C_w \right) \left(\frac{dp}{d\xi} + \rho g \sin\theta \right) T + \lambda_o C_o \frac{dP_c}{d\xi} T + \frac{k_{TH}}{\rho} \frac{dT}{d\xi} \right]_{\infty}^{\xi} \end{aligned} \tag{4.24}$$

The right hand sides of these equations are fluxes that approach zero when ξ approaches infinity. In this limit, S_w approaches S_{wi}, S_o approaches $1 - S_{wi}$ and T approaches T_R, the reservoir temperature. The integration is thus straightforward and gives:

$$\phi U_f \left(S_w - S_{wi} \right) = -\lambda_w \left(\frac{dp}{d\xi} + \rho g \sin\theta \right) \tag{4.25}$$

$$\phi U_f \left(S_o + S_{wi} - 1 \right) = -\lambda_o \left(\frac{dp}{d\xi} + \rho g \sin\theta + \frac{dP_c}{d\xi} \right) \tag{4.26}$$

$$\phi U_f \left\{ \left(C_o + \frac{1-\phi}{\phi} \frac{\rho_s}{\rho} C_s \right) (T - T_R) + (C_w - C_o)(S_w T - S_{wi} T_R) \right\} = \\ -(\lambda_o C_o + \lambda_w C_w) \left(\frac{dp}{d\xi} + \rho g \sin\theta \right) T - \lambda_o C_o \frac{dP_c}{d\xi} T - \frac{k_{TH}}{\rho} \frac{dT}{d\xi} \tag{4.27}$$

Summing (4.25) and (4.26) gives

$$0 = (\lambda_o + \lambda_w) \left[\frac{dp}{d\xi} + \rho g \sin\theta \right] + \lambda_o \frac{dP_c}{d\xi} \tag{4.28}$$

Simplifying (4.28) gives

$$\frac{dp}{d\xi} + \rho g \sin\theta = -\frac{\lambda_o}{\lambda_o + \lambda_w} \frac{dP_c}{d\xi} \tag{4.29}$$

Substituting (4.29) in (4.25), (4.26) and (4.27) allows for the elimination of the pressure gradient term to give

$$\phi U_f (S_w - S_{wi}) = \Lambda \frac{dP_c}{d\xi} \tag{4.30}$$

$$\phi U_f \left\{ \left(C_o + \frac{1-\phi}{\phi} \frac{\rho_s}{\rho} C_s \right) (T - T_R) + (C_w - C_o)(S_w T - S_{wi} T_R) \right\} = (C_w - C_o) \Lambda \frac{dP_c}{d\xi} T - \frac{k_{TH}}{\rho} \frac{dT}{d\xi} \tag{4.31}$$

where

$$\Lambda(S_w, T) \equiv \frac{\lambda_w \lambda_o}{\lambda_o + \lambda_w} = f_\lambda (S_w, T) \frac{k}{\mu_s} \tag{4.32}$$

in which

$$\mu_s = \mu_o\left(T = T_s\right) \tag{4.33}$$

$$f_\lambda \equiv \frac{k_{rw}k_{ro}\mu_s}{k_{ro}\mu_w + k_{rw}\mu_o} \tag{4.34}$$

Expanding (4.32) using Corey relative permeability curves gives

$$\Lambda\left(S_w, T\right) = \left(\frac{k_{rwro}\left(S_{wD}\right)^b k_{rocw}\left(1-S_{wD}\right)^a \mu_s}{k_{rocw}\left(1-S_{wD}\right)^a \mu_w + k_{rwro}\left(S_{wD}\right)^b \mu_o}\right)\frac{k}{\mu_s} \tag{4.35}$$

where a and b are the Corey exponents of oil and water phases respectively and

$$S_{wD} = \frac{S_w - S_{wc}}{1 - S_{wc} - S_{or}} \tag{4.36}$$

Bitumen viscosities are usually order of magnitudes higher than water viscosities throughout the temperature space, hence – for all practical purposes

$$k_{rwro}\left(S_{wD}\right)^b \mu_o >> k_{rocw}\left(1-S_{wD}\right)^a \mu_w \tag{4.37}$$

Substituting condition (4.37) into (4.35) gives

$$\Lambda\left(S_w,T\right)\approx\frac{k_{rocw}k}{\mu_s}\left(\frac{\left(1-S_{wD}\right)^a\mu_s}{\mu_o}\right) \tag{4.38}$$

Equation (4.38) implies a weak dependence of mobility on the water relative permeability exponent b i.e. the curvature of the water relative permeability curve. It is interesting to note that this weak dependence was also implicitly assumed albeit without proof in Sharma and Gates (2010b).

The bitumen viscosity-temperature relationship can be approximated by (Butler 1991)

$$\frac{\mu_s}{\mu_o}=\left(T^*\right)^m \tag{4.39}$$

where

$$T^*=\frac{T-T_R}{T_s-T_R} \tag{4.40}$$

Substituting (4.39) into (4.38) gives

$$\Lambda\left(S_w,T\right)=\frac{k_{rocw}k}{\mu_s}\left(\left(1-S_{wD}\right)^a\left(T^*\right)^m\right) \tag{4.41}$$

Equation (4.31) can be simplified further to give

$$-\frac{dT}{d\xi}=\phi U_f\frac{\left(T-T_R\right)}{\alpha_T} \tag{4.42}$$

where α_T is the reservoir's thermal diffusivity and given as

$$\alpha_T \equiv \frac{k_{TH}}{\rho C} \tag{4.43}$$

with

$$\rho C \equiv \frac{1-\phi}{\phi}\rho_s C_s + S_{wi}\rho C_w + \left(1-S_{wi}\right)\rho C_o \tag{4.44}$$

The thermal diffusivity defined in (4.42) through (4.44) is quite different from the apparent diffusivity of Sharma and Gates (2011) where S_w was used in place of S_{wi} in (4.44), hence, their theory predicts that thermal diffusivity will be a function of the current saturation state S_w. The reason for this difference is that our model is one of thermo-capillary counter-current imbibition (hence, the convective fluxes cancel out) while Sharma and Gates (2011) explicitly accounted for condensate convection in their model. Condensate convection ahead of the steam chamber front as a transport mechanism during SAGD is still open for debate because even if the steam injection pressure is higher than the original reservoir pressure, fluid streamlines are still expected to be parallel to the steam chamber interface and hence, there should be no convective flow orthogonal to the steam chamber interface (Edmunds 1999).

Capillary pressure will depend on both the wettability of the porous medium and the interfacial tension between water and bitumen. These in turn will depend on temperature (Flock et al., 1986), hence, we can write that

$$\frac{dP_c}{d\xi} = P_{S_w}\frac{dS_w}{d\xi} + P_T\frac{dT}{d\xi} \tag{4.45}$$

The functions $P_{S_w} \equiv \left(\partial P_c / \partial S_w\right)_T$ and $P_T \equiv \left(\partial P_c / \partial T\right)_{S_w}$ account for the effect of temperature on interfacial tension and wettability and will be defined shortly. Substituting (4.41) and (4.45) into (4.30) gives

$$\frac{k_{rocw}k}{\mu_s}\left(\left(1-S_{wD}\right)^a\left(T^*\right)^m\right)\left(P_{S_w}\frac{dS_w}{d\xi} + P_T\frac{dT}{d\xi}\right) = \phi U_f\left(S_w - S_{wi}\right) \tag{4.46}$$

A complex non-linear relationship between the saturation and the temperature gradient is indicated in (4.46). This is in distinct contrast to the assumption in Sharma and Gates (2010b) that the saturation gradient is identical to the thermal gradient. Substituting (4.42) into (4.46) and simplifying yields

$$-\frac{dS_w}{d\xi} = \phi U_f\left[-\frac{\left(S_w - S_{wi}\right)\mu_s}{k_{rocw}k\left(\left(1-S_{wD}\right)^a\left(T^*\right)^m\right)P_{S_w}} - \frac{\left(T-T_R\right)P_T}{\alpha_T P_{S_w}}\right] \tag{4.47}$$

The system composed of (4.42) and (4.47) is a coupled system of two non-linear ordinary differential equations. It can also be written in vector form as

$$-\frac{d\mathbf{Y}}{d\xi} = \mathbf{b} \tag{4.48}$$

where

$$\mathbf{Y} = \left(S_w, T\right)^T \tag{4.49}$$

and

$$\mathbf{b} = \phi U_f \left[-\frac{\left(S_w - S_{wi}\right)\mu_s}{k_{rocw} k \left(\left(1 - S_{wD}\right)^a \left(T^*\right)^m \right) P_{S_w}} - \frac{\left(T - T_R\right) P_T}{\alpha_T P_{S_w}}, \frac{T - T_R}{\alpha_T} \right]^T \tag{4.50}$$

where the superscript T is the transpose. From (4.50), we see that in the limit $\xi \to \infty$, both $\mathbf{b}$ and the derivatives go to zero as expected, which is an important heuristic check on our derivations. Another important observation from (4.50) is that the system of equations cannot be solved if the front velocity – which appears at the right hand side of (4.50) – is unknown. This is often generally the case, and in order to calculate it, an equation for the interface motion is needed. Also, the front velocity will not be constant at all locations within the interface as it will be dependent on its local curvature. Using the same transformation as in Butler (1991) (which is basically the chain rule of differential calculus) which follows from (4.42) as

$$-\frac{d}{d\xi} = \phi U_f \frac{\left(T - T_R\right)}{\alpha_T} \frac{d}{dT} \tag{4.51}$$

Substituting (4.51) into (4.48) gives

$$\frac{dS_w}{dT} = -\frac{\alpha_T \left(S_w - S_{wi}\right)\mu_s}{k_{rocw} k \left(\left(1 - S_{wD}\right)^a \left(T^*\right)^m \right) P_{S_w} \left(T - T_R\right)} - \frac{P_T}{P_{S_w}} \tag{4.52}$$

Equation (4.52) is a non-linear ordinary differential equation that describes the change of saturation with respect to temperature ahead of the steam chamber front and reveals that such change (for non-isothermal multiphase flow) is a function of the thermal, viscous and capillary properties of the flowing fluids and the porous medium. Before we simplify (4.52), let us define some useful constitutive relations.

4.1.3 Constitutive equations

The first constitutive equation we will describe is that of capillary pressure itself. Leverett (1941), defined the J function as

$$P_c = \frac{\sigma(T)\cos\theta(T)}{\sqrt{k/\phi}} J(S_w) \tag{4.53}$$

where P_c is the capillary pressure, σ is the interfacial tension and θ is the wetting angle. A wetting angle of 0 corresponds to a medium that is fully water-wet. For solids that are preferentially water-wet, the Leverett J function is a decreasing function of water saturation. For this work, we will use the model for $J(S_w)$ given by El-Khatib (1995) because of its closed form and ease of computing its gradient:

$$J(S_w) = \frac{\left(\frac{1}{\sqrt{4\kappa+2}}\right)}{S_{wD}^{\kappa}} \tag{4.54}$$

where κ is a constant related to the tortuosity of the porous medium. Equation (4.54) is simply a generalization of the Brooks-Corey model to account for tortuosity effects and the numerator of (4.54) plays this role. Differentiating (4.54) with respect to S_w yields

$$J'(S_w) = \frac{\left(\frac{-\kappa}{\sqrt{4\kappa+2}}\right)}{S_{wD}^{\kappa+1}\left(1-S_{wc}-S_{or}\right)} \tag{4.55}$$

It is important to state here that other J functions like that of Van Genuchten (1980) can be used or even specific field data – if available – and it doesn't change the analysis that follows. However, we found that (4.54) and (4.55) are more stable numerically and specific experimental or field data should first be fit with (4.54) – whenever possible – and only when unsuccessful should more sophisticated models or raw data be used. The change in $J(S_w)$ with saturation is usually assumed to be instantaneous in porous media flows and this assumption will be important in this analysis.

The general trend for interfacial tension is to decrease with temperature and this can be described by the Eötvös' correlation (Eötvös 1886) which assumes interfacial tension to be a linearly decreasing function of temperature. This trend has also been observed by other researchers (Flock et al., 1986), (Bowman 1967). In the absence of thermodynamic data needed to use Eötvös' equation and also to account for the deviations from linearity frequently observed in experiments, we will write this correlation as

$$\frac{\sigma_R - \sigma}{\sigma_R - \sigma_s} = \left(T^*\right)^n \tag{4.56}$$

where n is a positive constant σ_R is the interfacial tension at reservoir conditions and σ_s is the interfacial tension at steam conditions. The form of (4.56) ensures that Eötvös' rule is obeyed when $n=1$ and also accounts for deviations from linearity when $n\neq 1$.

The next parameter to consider is wettability. We could write a similar constitutive equation to (4.56) for the change in wettability with temperature, but this would assume that wettability and interfacial tension change with temperature at the same time-scale. This becomes important given the quasi-steady state assumption employed to derive the equations. In the absence of any data validating such an assumption, we will assume that wettability is constant throughout the recovery process.

4.1.4 Dimensionless saturation profile

Substituting (4.53) and (4.56) into (4.52) and rendering the resulting equation dimensionless using the scaled variables (4.40) and

$$S_w^* \equiv \frac{S_w - S_{wi}}{\Delta S_o} \tag{4.57}$$

where

$$\Delta S_o = S_{oi} - S_{or} \tag{4.58}$$

we get

$$\frac{dS_w^*}{dT^*} = \frac{\left(\sigma_R - \sigma_s\right)\left(T^*\right)^{n-1}}{J'\left(S_w\right)\left(\sigma_R - \left(\sigma_R - \sigma_s\right)\left(T^*\right)^n\right)}\left(\frac{nJ\left(S_w\right)}{\Delta S_o} - \frac{N_1 S_w^*}{\left(1-S_{wD}\right)^a\left(T^*\right)^{m+n}}\right) \tag{4.59}$$

where

$$N_1 = \frac{1}{M_g} = \frac{\alpha_T \mu_S}{k k_{rocw} \Delta P_c} = \frac{\alpha_T \mu_S}{k_{rocw} \Delta\sigma \cos\theta \sqrt{k\phi}} \tag{4.60}$$

$$M_g = -\frac{d\sigma}{dT}\frac{1}{\mu\alpha} L\Delta T = \frac{\Delta\sigma}{\mu_s \alpha} k_{rocw} \cos\theta \sqrt{k\phi} \tag{4.61}$$

$$\Delta\sigma = \sigma_{_R} - \sigma_{_s} \tag{4.62}$$

and L is a characteristic length scale. N_1 is a dimensionless number that is the inverse of the Marangoni number $\left(M_g\right)$ which relates thermal-interfacial tension effects to viscous effects. We call N_1 the thermo-capillary number with ΔP_c equal to the change in capillary pressure due to temperature change. A further look at (4.59) reveals that the Marangoni behavior during SAGD can be effectively characterized by the following dimensionless functional relationship

$$\frac{dS_w^*}{dT^*} = f\left(N_1, a, m, n, J\left(S_w\right), \sigma_f, \Delta S_{wD}\right) \tag{4.63}$$

where

$$\Delta S_{wD} = \frac{S_{wi} - S_{wc}}{1 - S_{wc} - S_{or}} \tag{4.64}$$

and

$$\sigma_f = \frac{\sigma_R - \sigma_S}{\sigma_R} \tag{4.65}$$

is the fractional decrease of interfacial tension from the undisturbed reservoir to the steam front. Also from (4.54) and (4.55), the effect of the Leverett J function $J(S_w)$ and its gradient $J'(S_w)$ can be effectively characterized by κ. Equation (4.63) then becomes

$$\frac{dS_w^*}{dT^*} = f\left(N_1, a, m, n, \kappa, \sigma_f, \Delta S_{wD}\right) \tag{4.66}$$

Note that from (4.59), (4.63) and (4.66) should also show a dependence on ΔS_o but ΔS_o is not independent of ΔS_{wD} hence its seclusion from the functional relationship. Equation (4.66) is sufficient to characterize the Marangoni effect on the SAGD oil rate. It is more interesting to describe this effect in terms of a saturation-distance relationship rather than the more abstract saturation-temperature function in (4.66). To do this will require a description of the interface velocity U_f as previously discussed. If we assume U_f to be constant,(4.48), (4.49) and (4.50) can be non-dimensionalized with the same dimensionless groups to give

$$\frac{dS_w^*}{d\xi^*} = Pe\left(\frac{\sigma_R - \sigma_S}{J'(S_w)\left(\sigma_R - (\sigma_R - \sigma_S)(T^*)^n\right)}\right)\left(\frac{S_w^* N_1}{\left((1 - S_{w_D})^a T^{*m}\right)} - \frac{nT^{*n} J(S_w)}{\Delta S_o}\right) \tag{4.67}$$

$$\frac{dT^*}{d\xi^*} = -PeT^* \tag{4.68}$$

where

$$Pe = \frac{\phi U_f H}{\alpha_T} \tag{4.69}$$

is the Peclet number. The functional saturation – distance relationship is then given as

$$\frac{dS_w^*}{d\xi^*} = f\left(N_1, Pe, a, m, n, \kappa, \sigma_f, \Delta S_{wD}\right) \tag{4.70}$$

4.1.5 A note on boundary conditions

In order to solve (4.59), (4.67) and (4.68), appropriate boundary conditions have to be specified. Recognizing that when $T = T_s$ then $T^* = 1$, the possible choices for the boundary conditions are:

$$S_w^* = 1 \qquad \left(\text{at} \quad T^* = 1\right) \tag{4.71}$$

$$S_w^* = 1 \qquad \left(\text{at} \quad \xi^* = 0\right) \tag{4.72}$$

$$T^* = 1 \qquad \left(\text{at} \quad \xi^* = 0\right) \tag{4.73}$$

However, (4.71) and (4.72) will be physically incorrect due to our initial assumption of the physics of thermo-capillary counter-current imbibition. At the interface, both bitumen and water can co-exist in equilibrium and consequently, there will be an equilibrium water saturation that might not necessarily be equal to $1 - S_{or}$.

4.1.6 Oil rate

Following Butler (1991), but accounting for relative permeability (Marangoni or multi-phase flow) effects, the oil (which drains down along the chamber wall with Darcy velocity) rate equation is given by

$$u_o = \frac{dq_o}{d\xi} = \frac{kk_{ro}(S_o)\rho_o g}{\mu_o(T)}\sin\theta \tag{4.74}$$

The derivative with respect to position ξ in the moving coordinate frame can also be transformed into a derivative with respect to temperature, using (4.51)

$$-\frac{dq_o}{dT} = \frac{\alpha kk_{ro}(S_o)\rho_o g}{\phi(T-T_R)\mu_o(T)}\frac{\sin\theta}{U_f} \tag{4.75}$$

This equation still contains unknowns, namely the inclination angle θ of the interface and the front velocity U_f. The angle θ is a constant for a given position of the front. Therefore, (4.75) can be integrated to yield the total oil rate that goes through that plane given by

$$q_o = -\frac{kg\alpha}{\phi m_{TC}\nu_s}\frac{\sin\theta}{U_f} \tag{4.76}$$

where

$$\frac{1}{m_{TC}} \equiv \nu_s \int_{T_R}^{T_s}\left(\frac{k_{ro}(S_o)}{\nu_o(T)} - \frac{k_{ro}(S_{wi})}{\nu_R}\right)\frac{dT}{(T-T_R)} \tag{4.77}$$

is similar to Butler's $1/m$ parameter, but also accounts for multi-phase flow effects. It is also possible to let the thermal diffusivity α_T depend on temperature in which case it has to appear inside the integral. Also notice that, like Butler did, we've subtracted the so called "infinite cold flow" from the solution. This infinite cold flow correction accounts for the overestimation of equations (4.22) to (4.24) due to the integration to infinity which is outside the reservoir range.

Butler (1991) determined the quotient $\sin\theta/U_f$ from the equation that describes the motion of the interface as

$$\left(\frac{\partial q_o}{\partial x_f}\right)_t = \phi\Delta S_o\left(\frac{\partial y_f}{\partial t}\right)_{x_f} \tag{4.78}$$

where $\left(x_f, y_f\right)$ indicates an arbitrary position on the interface. It can be shown also that

$$\left(\frac{\partial q_o}{\partial y_f}\right)_t = -\phi\Delta S_o\left(\frac{\partial x_f}{\partial t}\right)_{y_f} \tag{4.79}$$

Furthermore, the front velocity U_f is a projection of the horizontal or vertical velocity of a point on the interface on a unit normal to the interface

$$U_f = \sin\theta\left(\frac{\partial x_f}{\partial t}\right)_{y_f} = -\cos\theta\left(\frac{\partial y_f}{\partial t}\right)_{x_f} \tag{4.80}$$

Equations (4.79) and (4.80) can be combined to yield

$$\frac{U_f}{\sin\theta} = -\frac{1}{\phi \Delta S_o}\left(\frac{\partial q_o}{\partial y_f}\right)_t \tag{4.81}$$

Substituting (4.81) in (4.76) yields

$$q_o\left(\frac{\partial q_o}{\partial y_f}\right)_t = \frac{\Delta S_o k g \alpha_T}{m_{TC} \nu_s} \tag{4.82}$$

Equation (4.82) can now be integrated between the top of the oil zone and an arbitrary position y to give

$$q_o = \left(\frac{2\Delta S_o k g \alpha_T (H - y)}{m_{TC} \nu_s}\right)^{1/2} \tag{4.83}$$

If y is set to zero in order to determine the flow rate at the bottom of the reservoir, (4.83) becomes

$$q_o = q_o(y = 0) \equiv \sqrt{\frac{2\Delta S_o k g \alpha_T H}{m_{TC} \nu_s}} \tag{4.84}$$

This expression is identical to that obtained by Butler (1991), except for two small differences. The first is that the porosity has been incorporated in the expression for the thermal diffusivity, and the second is that the definition of the Butler m parameter now incorporates the additional effect of thermo-capillarity in m_{TC}.

4.1.7 Dimensionless oil rate

Equation (4.84) can be written in dimensionless form by dividing by the Butler rate (2.1) to give

$$q_{o_D} = \frac{q}{q_B} = \sqrt{\frac{m}{m_{TC}}} \tag{4.85}$$

Substituting (4.77) into (4.85) and simplifying further using (4.40) gives

$$q_{o_D} = \sqrt{\frac{m}{k_{rocw}} \int_0^1 k_{ro} T^{*m-1} dT^*} \tag{4.86}$$

where we have assumed that

$$\frac{k_{ro}(S_{wi})\nu_s}{\nu_R} \approx 0 \tag{4.87}$$

Note that, using our current (or any Butler-type) formulation, it will not be appropriate for non-zero $k_{ro}(S_{wi})$ to compute ν_s/ν_R since this will give a discontinuity because mathematically $\nu_s/\nu_R = T_R^{*m} = 0$ even though it is strictly not physically correct. However, for most heavy oils, (4.87) is a good assumption. Combining (4.86) and (4.66) gives the functional relationship of the parameters and dimensionless groups influencing the dimensionless oil rate as

$$q_{oD} = f\left(N_1, a, m, n, \kappa, \sigma_f, \Delta S_{wD}\right) \tag{4.88}$$

To study how the oil flux varies spatially, we can also compute the dimensionless oil mobility ahead of the steam chamber front defined as

$$\lambda_o^* = \frac{k_{ro}\nu_s}{k_{rocw}\nu_o} = \frac{k_{ro}}{k_{rocw}} T^{*m} \tag{4.89}$$

4.2 Model Validation

The only accurate way to validate the above multiphase flow model currently is by performing an experiment. However, in order to ascertain the role of thermo-capillarity, we would require high resolution imaging capability (such as using a C-T (computed tomography) scan) connected to the SAGD experimental setup. This is extremely difficult to implement and hence we attempted to validate our model by using the data of Ito and Suzuki (1999), which was also used by Sharma and Gates (2010a; 2011) to develop their models.

Ito and Suzuki (1999) used numerical simulation to predict SAGD recovery from the Hanging-stone Oil Sands reservoir near Fort McMurray Canada. Their results showed significant condensate transport in the direction orthogonal to the steam chamber interface. Since the condensate is basically hot condensed steam, they attributed the enhanced convective heat transfer to this condensate flow. Edmunds (1999) argued against this hypothesis since fluid streamlines during a typical SAGD process are expected to be parallel to the steam chamber interface. Ito and Suzuki's claim was helped by Farouq-Ali (1997) who discounted the influence of numerical dispersion to produce such phenomena. Our hypothesis is that heat transfer creates low but measureable

thermo-capillary imbibition giving rise to saturation diffusion similar to that seen in Ito and Suzuki's (1999) simulation results.

4.3 Results and Discussion

In this section, we will discuss the results obtained from our thermo-capillary model and compare with previous models describing multiphase flow during the SAGD process. We first present a base case using parameters tabulated in Table 4.1 and later present a sensitivity analysis around these base case values.

Fig 4.2 shows the plot of dimensionless temperature vs. dimensionless distance from the steam chamber interface for different thermo-capillary numbers compared to the Butler and Sharma and Gates models. The models all overlap because the temperature profile is obtained by solving (4.66) and we have assumed that thermal conductivity is independent of temperature and fluid saturation, hence the physics of thermo-capillarity does not influence the temperature profile. Also, from **Fig 4.2**, we see that the length scale of thermal conduction for the base case Peclet number of 100 is about 0.01 the reservoir thickness.

Fig 4.3 shows the plot of the dimensionless water saturation vs. the dimensionless distance away from the steam chamber interface for different values of the thermo-capillary number. It also compares these with Butler's (1981) model and the Sharma and Gates model. At infinite thermo-capillary number there is a discontinuous condensate/bitumen interface that is consistent with Butler's assumption. At lower thermo-capillary numbers, but typically larger than order of 1, the saturation profile is more spread due to imbibition. The saturation vs. distance curve takes a concave shape. The Sharma and Gates model is seen to approximate the $N_1 = 0.1$ plot.

At field scales, thermo-capillary numbers are usually lower and of the order of about 0.01 to 5. At the scale of laboratory experiments, the thermo-capillary number is quite large and the saturation profile approaches that of Butler et al. (1981). Butler's model was developed and validated using laboratory experiments. We also see from **Fig 4.3** that at lower thermo-capillary numbers, the capillary length scale is of the same order as the thermal conduction length scale from **Fig 4.2**. This is because a capillary pressure gradient is created ahead of the steam chamber interface due to a thermal induced gradient in interfacial tension. Note also that the saturation profile using Sharma and Gates model in **Fig. 4.3** mirrors the temperature profile in **Fig 4.2**. As stated earlier, the correspondence between the length scales exhibited by the temperature and saturation profile is a crucial assumption in that model.

One important point to note from the thermo-capillary number, equation (4.60) is that since $\sqrt{k\phi}_{lab}$ is usually greater than $\sqrt{k\phi}_{field}$, then, $N_{1_{field}}$ should be greater than $N_{1_{lab}}$. As Butler (1991) states "In order to obtain dimensionless similarity, it is necessary to employ a much more permeable medium in the model than is present in the field". A much more permeable medium may lead to smaller capillary effects (larger thermo-capillary number). The reason why this is not generally so is because of other parameters in the definition of the thermo-capillary number. An order of magnitude analysis can help to explain why the reverse is rather generally true. First, for typical laboratory experiments and field scale recoveries, $\sqrt{k\phi}_{lab}$ will only be greater than $\sqrt{k\phi}_{field}$ by about 1 order of magnitude. Second, $k_{rocw}\Delta\sigma\cos\theta_{field}$ will be greater than $k_{rocw}\Delta\sigma\cos\theta_{lab}$ by about 1 order of magnitude because of higher injection temperatures at field scales (making $\Delta\sigma$ larger) and most reservoirs will be more water-wet than most experiments, since experiments are usually not water saturated before steam injection. This effectively cancels both effects in the denominator. Hence, the controlling effect to determine larger

thermo-capillary numbers between laboratory and field scales will largely fall on thermal diffusivity and bitumen viscosity at steam conditions. Most experiments, even though insulated will be exposed to air, which has a thermal diffusivity of about an order of magnitude less than sandstone or most reservoir rocks. The viscosity effect is more complex as for experiments that use the same oil as reservoir oil, the bitumen viscosity at steam temperature for laboratory scales will be greater than that at field scales since field scales typically inject steam at higher temperatures. However, for experiments that use different oils, the bitumen viscosity at steam conditions could be similar or even smaller than that at field scales. The $k_{rocw}\Delta\sigma\cos\theta$ values could also behave quite differently for laboratory and field scales, thereby complicating this analysis further. Hence, the above analysis shows that $N_{1_{lab}}$ could be greater than $N_{1_{field}}$ by about 1 order of magnitude, consistent with **Fig. 4.6**, or could be greater by as much as 3 orders of magnitude as seen in **Fig. 4.13** or both scales could have similar values as seen with the Christina Lake pilot plotting close to the experimental scale values in **Fig. 4.13**.

Fig 4.4 shows the plot of the dimensionless water saturation vs. dimensionless temperature for different thermo-capillary numbers. It carries the same information as **Fig 4.3** and also shows that all curves asymptote to the $S_w^* = 1$ at $T^* = 1$ boundary. This plot also reveals that the effect of thermo-capillarity is limited in spatial extent for most cases, however, when the thermo-capillary number approaches zero, the capillary diffusion will be so large that the entire reservoir orthogonal to the steam chamber interface will be flooded by condensate. The assumption of the semi-infinite reservoir boundary condition may get violated in that case. As expected, the Sharma and Gates profile is linear because of the assumption of equivalence in length scales of thermal and saturation diffusivity.

Fig 4.5 shows the plot of the dimensionless oil mobility vs. dimensionless distance from the steam chamber interface. This plot is interesting because it shows that

at low thermo-capillary numbers, there exists a maximum oil mobility which is some distance away from the steam chamber interface as also predicted by the Sharma and Gates model and also observed by Ito and Suzuki (1999). The difference however with our model and these works is that our model also predicts that the position of this maximum mobility – seen more clearly through the insert plot – depends on the thermo-capillary number as the higher the thermo-capillary number, the closer is the location of the maximum mobility to the steam chamber interface. This result indicates that neither the Ito and Suzuki (1999) observation nor the Butler model is wrong but rather are two extremes of the thermo-capillary phenomenon. The reason why this maximum occurs is not due to convection as alluded to by Ito and Suzuki (1999) but due to the Marangoni effect. At the steam chamber interface, the temperature is highest but so also is the water saturation, hence, there is zero bitumen flux. As we move away from the steam chamber interface, bitumen saturation begins to increase causing an increase in oil relative permeability but then, the temperature decreases causing higher bitumen viscosities and hence lower rates. Far away from the steam chamber interface, bitumen saturations are high but temperatures are also low which gives rise to an almost zero bitumen flux. Hence in between, there will exist a certain location where these effects combine to give a maximum bitumen rate as seen in **Fig 4.5**.

Fig 4.6 shows the plot of the dimensionless oil rate vs. the thermo-capillary number comparing our model to previous models. These models provide different expressions for the oil rate (that has been standardized against the rate predicted by Butler's model) and because they do not explicitly account for thermo-capillarity, the rate is a constant regardless of the thermo-capillary number. The variation in rates predicted by the different models can be explained on the basis of the thermo-capillary number. Butler's first model is clearly seen as the maximum possible SAGD rate and our model

converges to it at infinite thermo-capillary number. This is not surprising because Butler's first model was derived assuming single phase flow of bitumen ahead of the steam chamber which will give the maximum SAGD rate possible for any given fluid and reservoir properties. **Fig 4.6** also confirms that models that perform well at the experimental scale plot near the top of the thermo-capillary curve while those that perform well at the field scale plots lower on the thermo-capillary curve.

Fig 4.7 gives the model validation plot obtained my manual history matching while **Fig. 4.8** shows the same results but via automatic history matching using a modified Levenberg Marquardt technique called OCCAM minimization with a reference solution (Aster, 2012). **Figs. 4.7** and **4.8** shows that our thermo-capillary model fits the Ito and Suzuki (1999) data excellently. As stated earlier, Ito and Suzuki's data is a consequence of numerical dispersion rather than capillary diffusion but their effects are similar (Lantz 1971) and we have taken advantage of this similarity in this validation attempt.

Fig 4.9 shows that the capillary length scale obtained from the match is quite small and of extent comparable to numerical dispersion. **Figs 4.7** and **4.9** also show the inadequacy of the Sharma and Gates model to describe this phenomenon even though they based their linear transport model on the Ito and Suzuki data. **Figs 4.10** and **4.11** show the Leverett J function and its derivative respectively with sensitivities around the match values. These Leverett J values are typical of porous media flows (El-Khatib 1995). Table 4.2 shows the parameters used to obtain the match and are seen to be consistent with Ito and Suzuki's data.

Fig 4.12 shows a column chart of the dimensionless oil rate computed for two experimental data and different available field data taken from Sharma and Gates (2010b) which reveals the trend that experimental data tend to have higher dimensionless

oil rates while field scale data tend to have lower dimensionless oil rates. Our conjecture is that, this decreasing trend in recovery is due to thermo-capillarity but to test our conjecture we will require that all the parameters in Table 4.1 be known for the given experiment or reservoir. Fortunately, only 3 of the 9 parameters (the Peclet number is not a true experiment or reservoir variable as it also depends on the assumed steam chamber interface velocity) in Table 4.1 are unknown for these experiments and reservoirs. Hence a viable model validation procedure will be to compute the thermo-capillary number for these experiments and field data using the known parameters and assuming realistic values for the unknown parameters. To improve the integrity of such a correlation, we will assume the same values for the assumed parameters regardless of whether we are fitting the experiment or the field data. These assumed parameters are shown in Table 4.3. The trend in the thermo-capillary number shown in **Fig 4.13** conforms to the trend in bitumen recovery that we observed in **Fig. 4.12**. The correspondence between the bitumen rate and thermo-capillary number is shown clearly in **Fig 4.14**. The high correlation coefficient obtained from **Fig 4.14** confirms further that the Marangoni or thermo-capillary number can provide a viable explanation for the trend in oil recovery that we see for different reservoirs at both experimental and field scales.

Table 4.1: Showing the base case parameters used for SAGD[6]

Parameter	Values
S_{wc}	0.2
S_{wi}	0.25
S_{or}	0.2
k_{rocw}	0.5
a	1
n	1.5
m	4
σ_f	0.033
κ	1
Pe	100

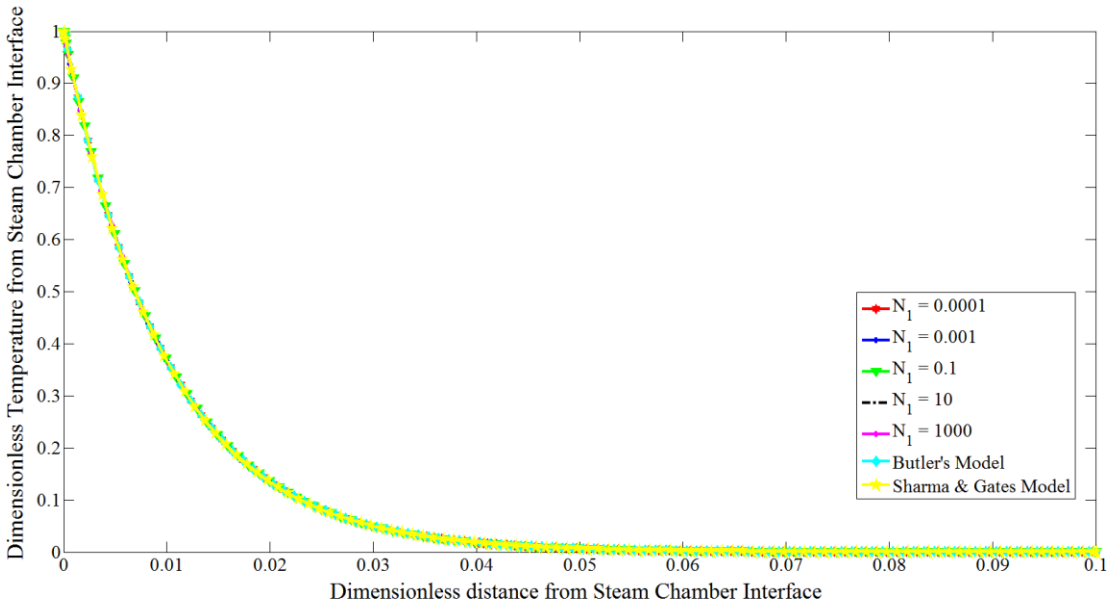

Figure 4.2: Plot of the dimensionless temperature – distance profile ahead of the steam chamber interface for base case

[6] The value of $Pe = 100$ here is consistent with the results reported in Sharma and Gates (2010b)

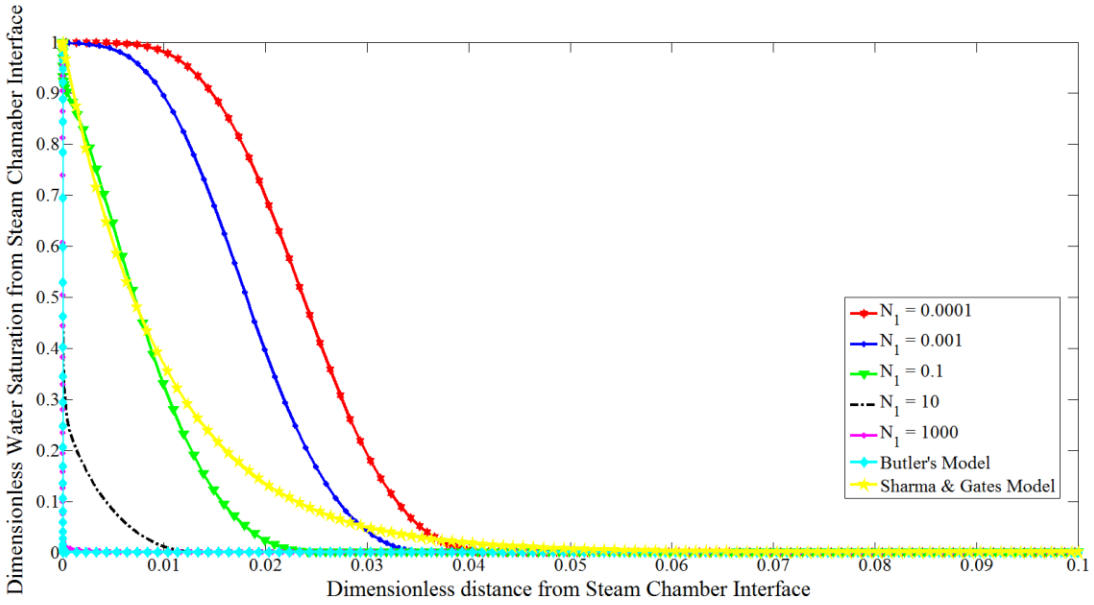

Figure 4.3: Plot of the dimensionless water saturation – distance profile ahead of the steam chamber interface for base case

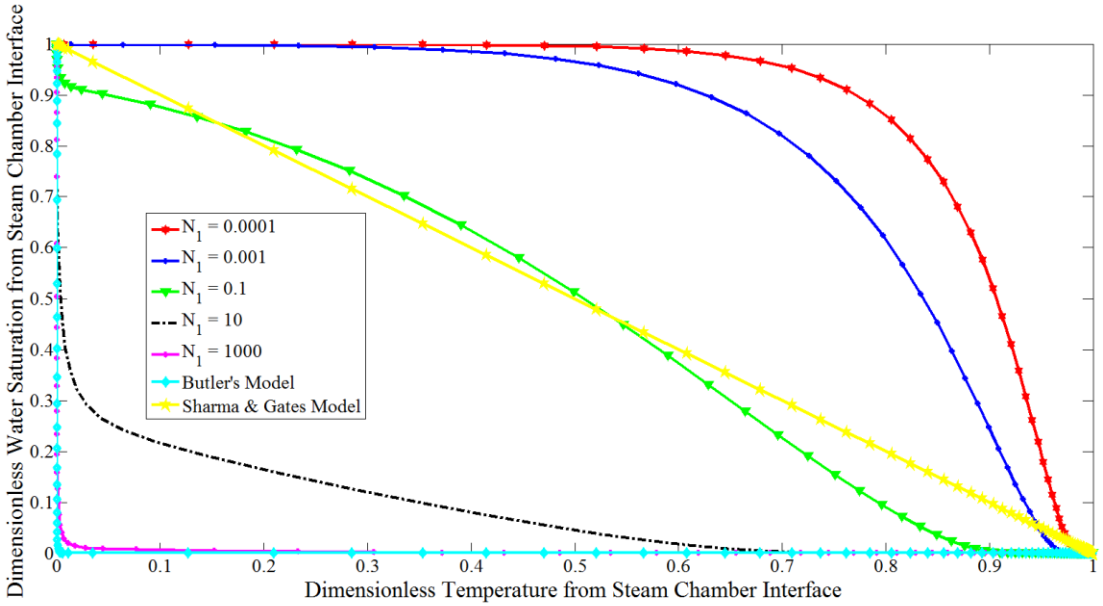

Figure 4.4: Plot of the dimensionless water saturation – temperature profile ahead of the steam chamber interface for base case

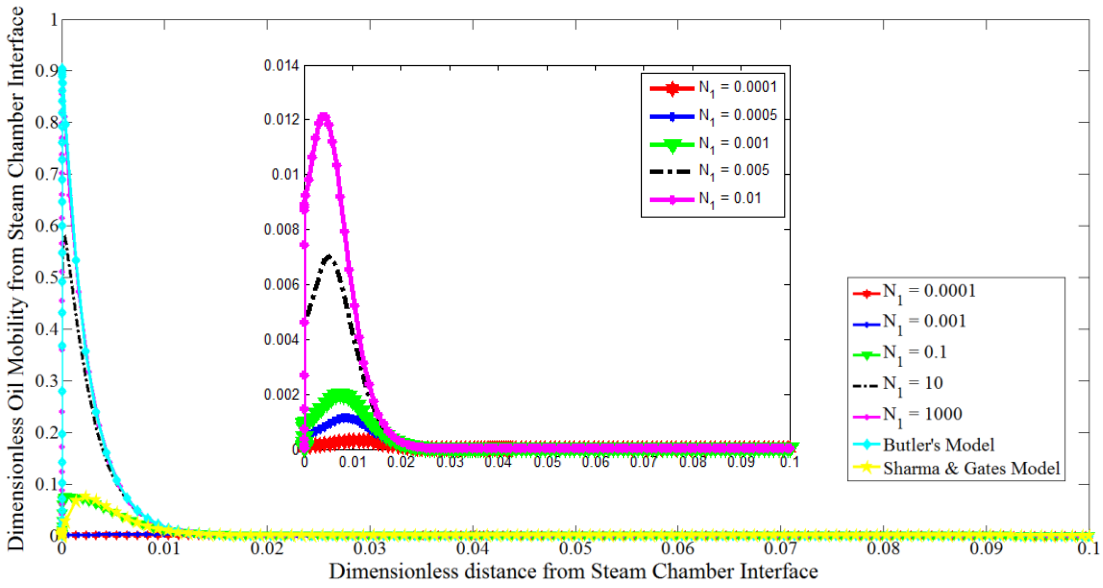

Figure 4.5: Plot of the dimensionless oil mobility – distance profile ahead of the steam chamber interface for base case

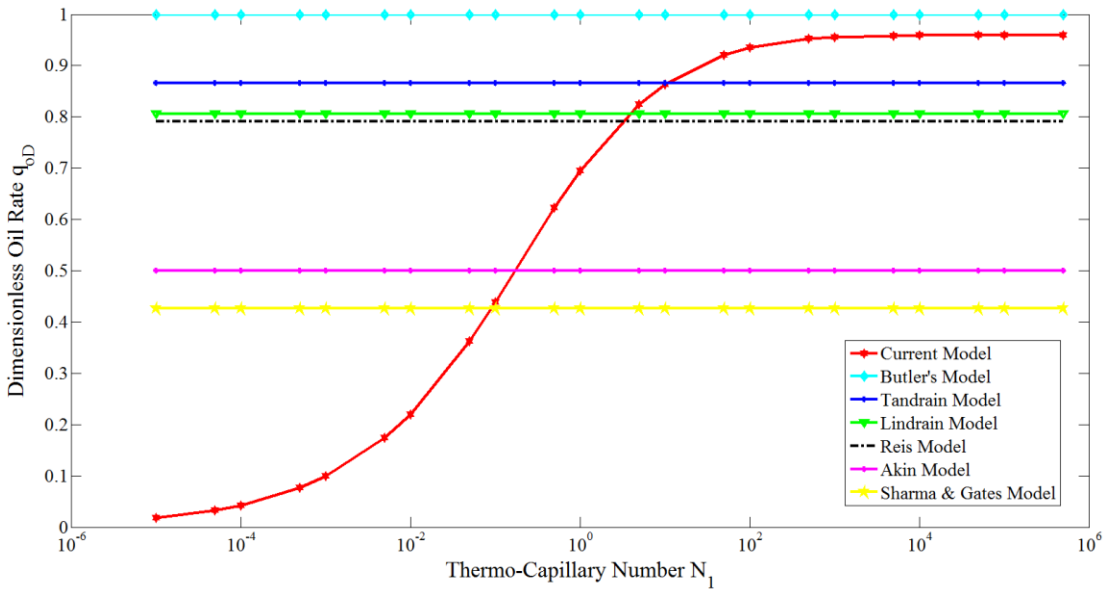

Figure 4.6: Plot of the dimensionless oil rate vs. thermo-capillary number for base case

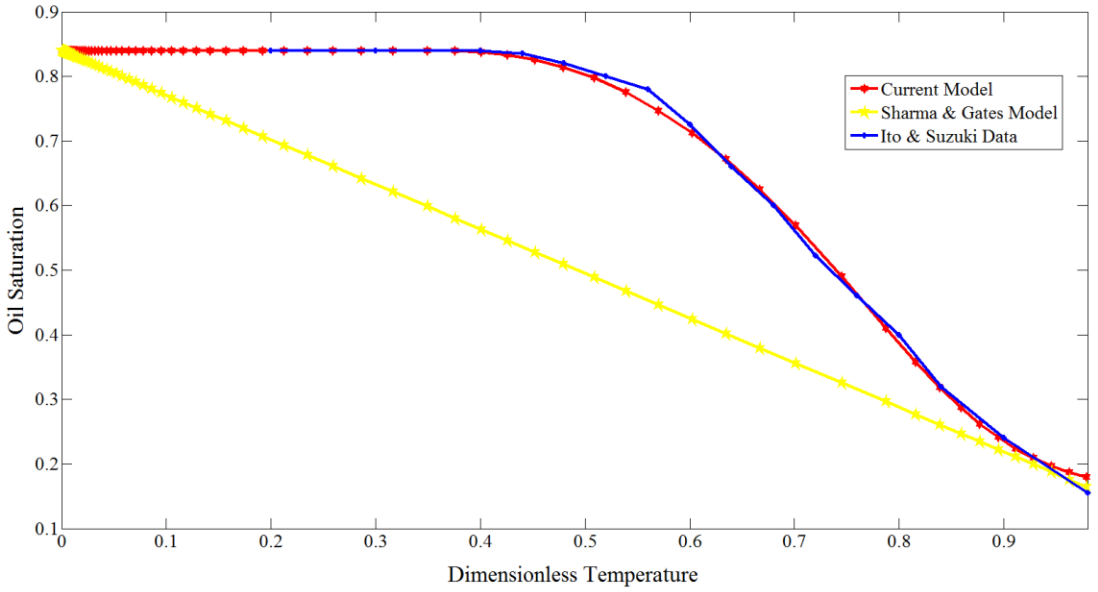

Figure 4.7: Plot of the oil saturation vs. dimensionless temperature for model validation

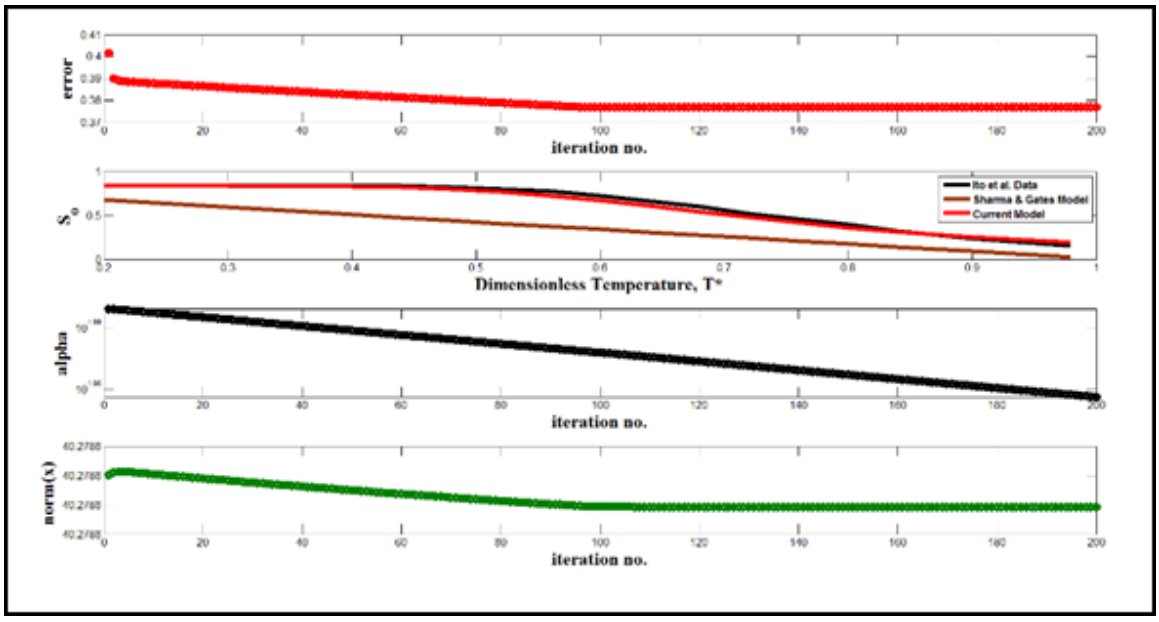

Figure 4.8: Inversion plots for oil saturation vs. dimensionless temperature by a modified Levenberg Maqardt technique

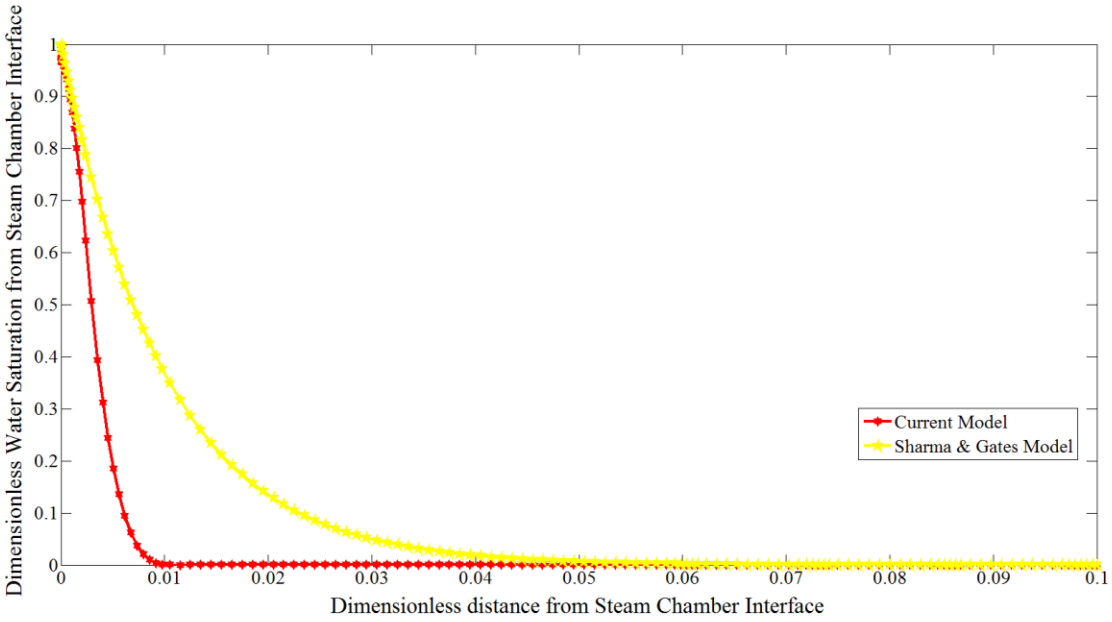

Figure 4.9: Plot of the dimensionless water saturation – distance profile ahead of the steam chamber interface for model validation

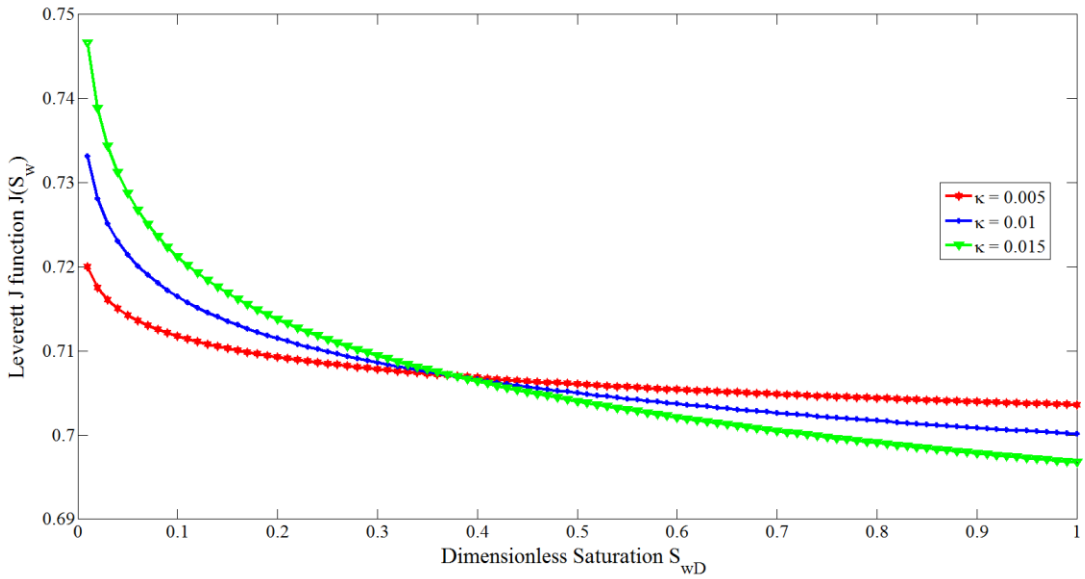

Figure 4.10: Plot of the Leverett *J* function used for model validation and sensitivities around it

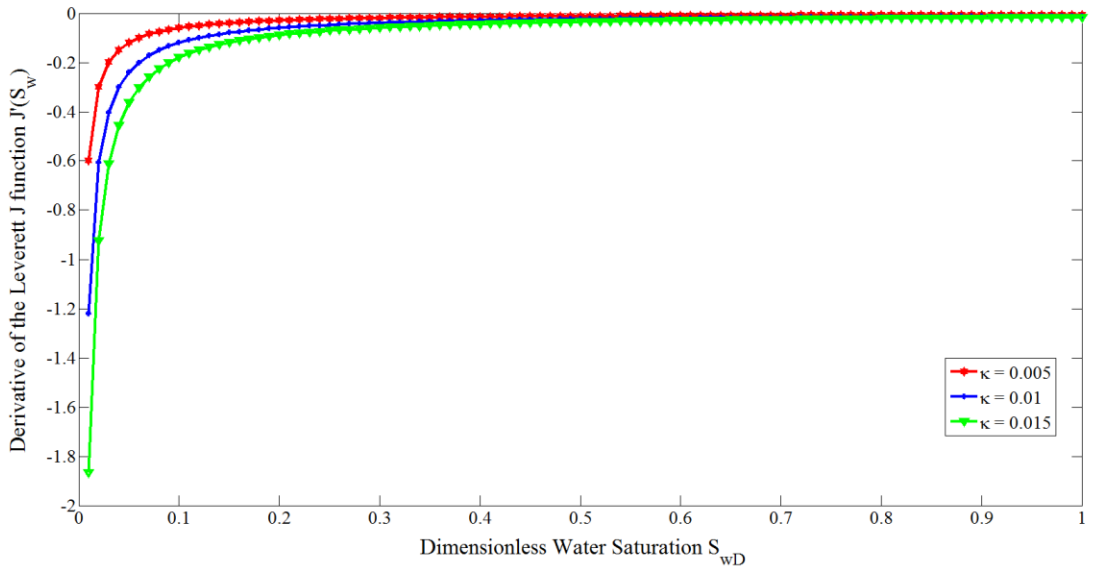

Figure 4.11: Plot of the derivative of the Leverett *J* function used for model validation and sensitivities around it

Table 4.2: Showing the history match parameters used to match Ito and Suzuki (1999)[7] data

Parameter	Estimate	Data	Source
S_{wc}	0.082	0.083	Ito and Hirata (1999)
S_{wi}	0.159	0.16	Ito and Hirata (1999)
a	2	1.92	Ito and Hirata (1999)
n	5	0.5	Bowman (1967)
m	4	4	Sharma and Gates (2010b)
σ_{oR}	35.3	35.3	Bowman (1967)
σ_{os}	18.2	18.2	Bowman (1967)
κ	0.0101	N/A	N/A
N_1	0.154	N/A	N/A

[7] The reservoir parameters obtained are consistent with the Hangingstone data reported in (Ito and Hirata 1999)

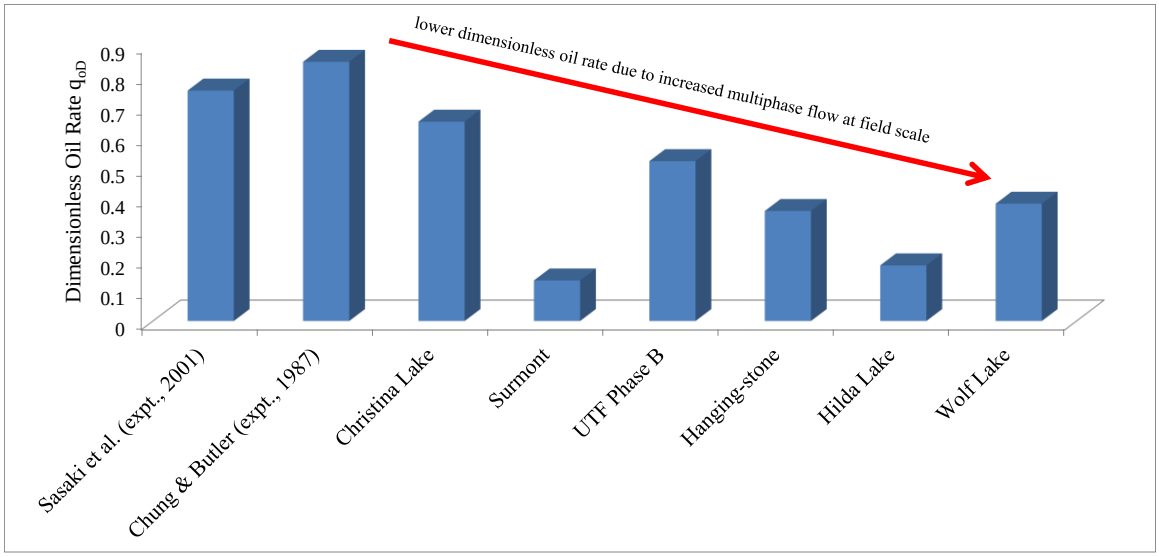

Figure 4.12: Column chart showing the distribution of dimensionless oil rate for available experiment and field data[8]

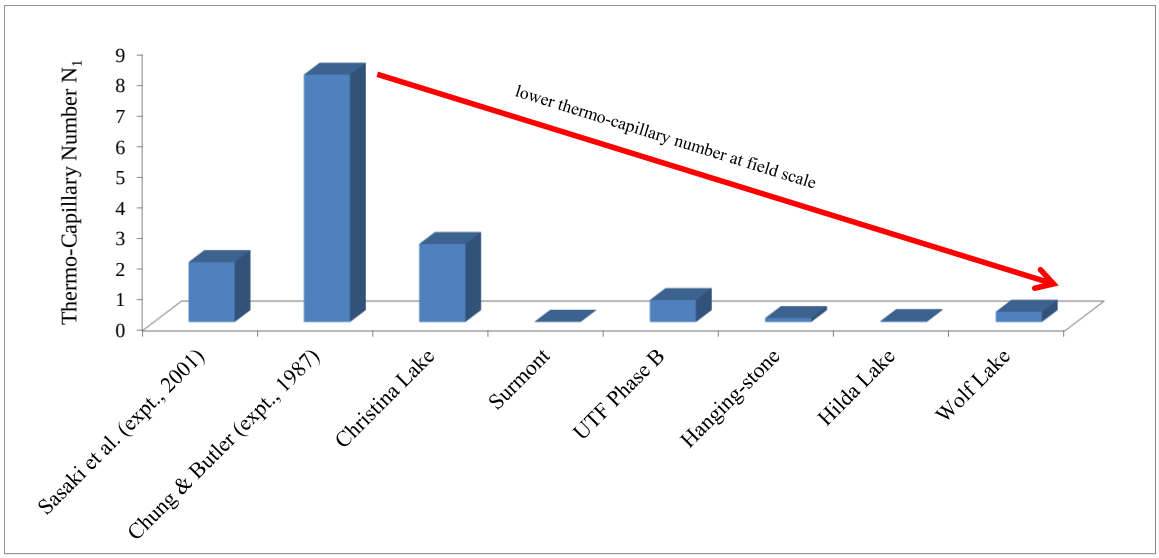

Figure 4.13: Column chart showing the distribution of computed thermo-capillary numbers for available experiment and field data

[8] Data taken from Tables 2 & 3 of Sharma & Gates (2010b)

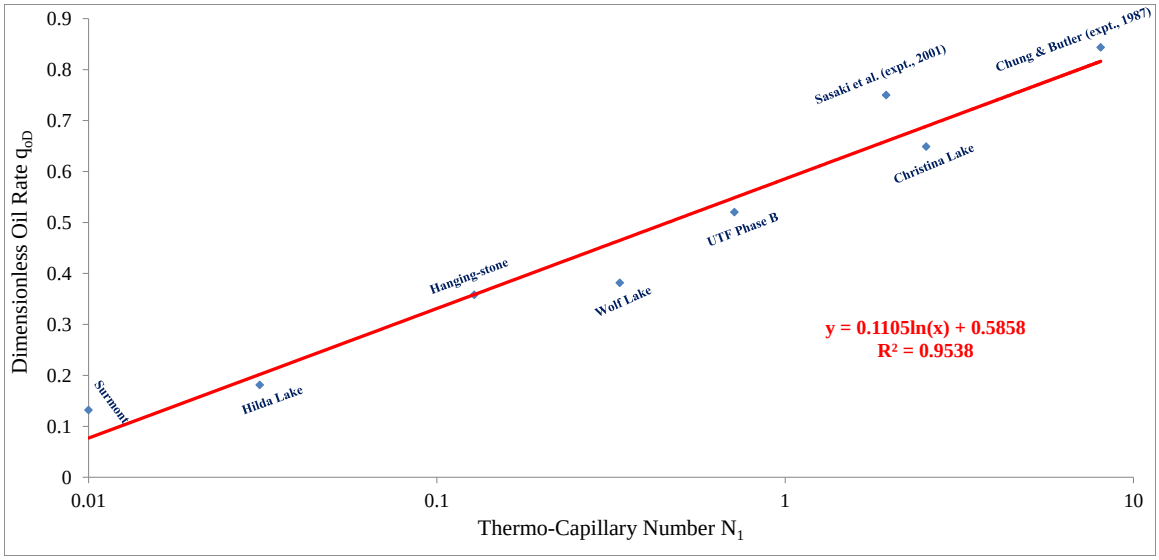

Figure 4.14: Plot showing the correlation between the dimensionless oil rate and computed thermo-capillary number for available experiment and field data

Table 4.3: Showing the unknown parameters used to compute the thermo-capillary numbers shown in **Figs 4.12** & **4.13** of available experimental and field data[9]

Parameter	Value
n	1
σ_f	0.5
κ	1

4.3.1 Sensitivity analysis

We now present a sensitivity analysis of the parameters describing the thermo-capillary phenomenon. The parameters are not only varied around the base case values

[9] These values are consistent with data reported in (Bowman 1967) for n and σ_f and also in (El-Khatib 1995) for κ

but also restricted to realistic values that can be expected at both experimental and field scales. The parameters were varied one at a time.

Fig 4.15 shows the effect of varying the Corey exponent a and reveals that as the Corey exponent is increased, the dimensionless oil rate decreases keeping the thermo-capillary number constant. This is not surprising as higher Corey exponent means larger curvature of the oil relative permeability curve and hence reduced bitumen rates. However, what is surprising is that the spread in oil rates with varying Corey exponents is higher at higher thermo-capillary numbers and lower at lower thermo-capillary numbers. This explains why single constants proposed by different researchers did a good job of characterizing multiphase flow for a variety of experimental data while performing poorly at field scales.

Fig 4.16 shows that varying the Butler m parameter has little effect across scales on the dimensionless oil rate. This is in remarkable contrast to the linear transport model of Sharma and Gates (2010b) where they predict the dimensionless oil rate is a strong function of both m and a through a gamma function combining both parameters (see equation (2.9)). The reason for this is that we have implicitly assumed through equation (4.37) of our model that the bitumen viscosity does not influence the thermo-capillary imbibition of the condensate into the bitumen phase.

Fig 4.17 shows the complicated effect of the exponent of the interfacial tension – temperature curve n on the dimensionless oil rate. It shows that even if an experimental analysis reveals the value of n to not influence recovery, it should not be ignored in designing scaled experiments as n influences recovery at field scales. This is a consequence of the non-linear relationship describing thermo-capillary behavior during SAGD.

Fig 4.18 reveals that varying the exponent κ of the capillary pressure curve results in a very non-linear variation in the dimensionless oil rate. As κ increases, q_{oD} approaches its asymptotic limit at higher thermo-capillary numbers. This means that the thermal diffusivity of the reservoir will have to be progressively higher to attain the theoretical Butler rates for higher values of κ. This is because as κ increases, capillary pressure and hence, its gradient increases thereby enhancing capillary diffusion for any given thermal diffusivity. This plot also relates to the effect of heterogeneity because as κ increases, the reservoir pore size becomes more heterogeneous. Hence reservoir heterogeneity will enhance thermo-capillary imbibition.

Fig 4.19 shows that varying the fractional decrease in interfacial tension also gives a non-linear response in the dimensionless oil rate. The larger the fractional decrease in interfacial tension, the higher the dimensionless oil rate. At first, this might seem counter-intuitive since, higher σ_f should give rise to more capillary diffusion and hence less bitumen rates, but higher capillary diffusion also gives rise to higher absolute values of $J'(S_w)$ by moving farther along the asymptotic part of the $J(S_w)$ curve (see **Figs 4.10** and **4.11**) and from equation (4.67) we see that both parameters have opposite effects on the saturation gradient.

Fig 4.20 shows the interesting result that an uncertainty in ΔS_{wD} is very important at the experimental scale and that the dimensionless oil rate reduces as the dimensionless initial water saturation increases. This conclusion is supported by the experimental work of Javad et al. (2010) where they showed that bitumen recovery dropped by as much as 7% when the initial water saturation was increased from 14.7 to 32.2%. However, **Fig 4.20** also shows that sensitivity to ΔS_{wD} is minimal at field scales.

Fig 4.21 gives the sensitivity of the Peclet number to the dimensionless water saturation – distance plot. Peclet number is not influenced by the thermo-capillary

number and hence the dimensionless oil rate but will influence the value of bitumen saturation ahead of the steam chamber interface. **Fig 4.21** shows that the higher the Peclet number, the lower the dimensionless water saturation at any given location ahead of the steam chamber interface.

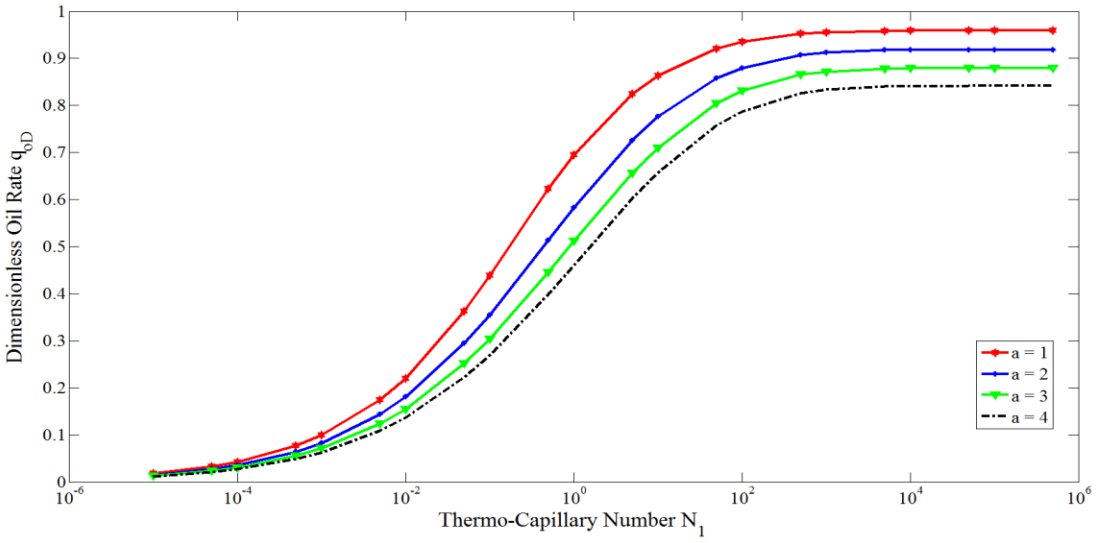

Figure 4.15: Plot showing the sensitivity of the dimensionless oil rate vs. thermo-capillary number to the Corey exponent a

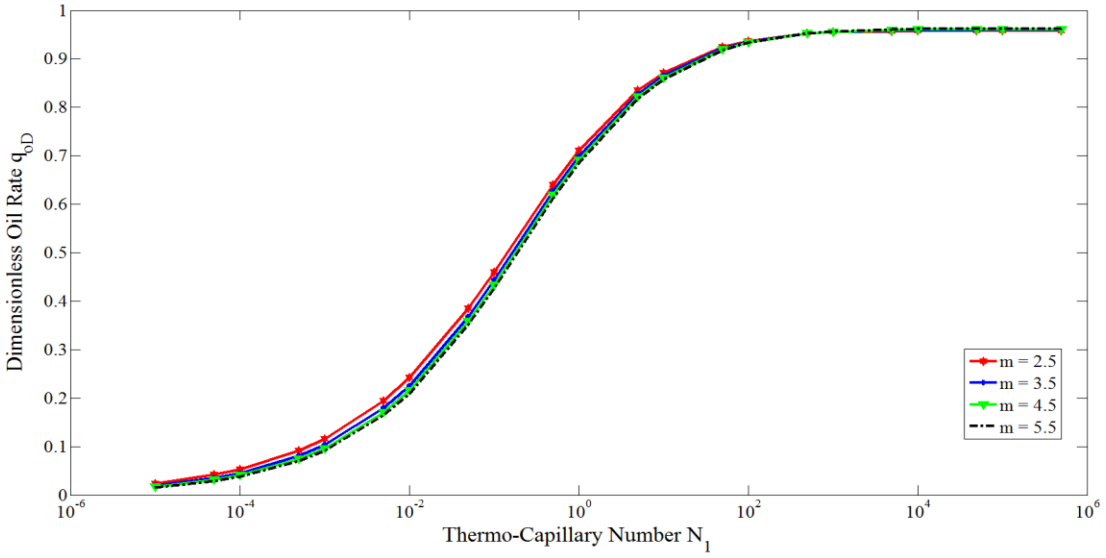

Figure 4.16: Plot showing the sensitivity of the dimensionless oil rate vs. thermo-capillary number to the Butler *m* parameter

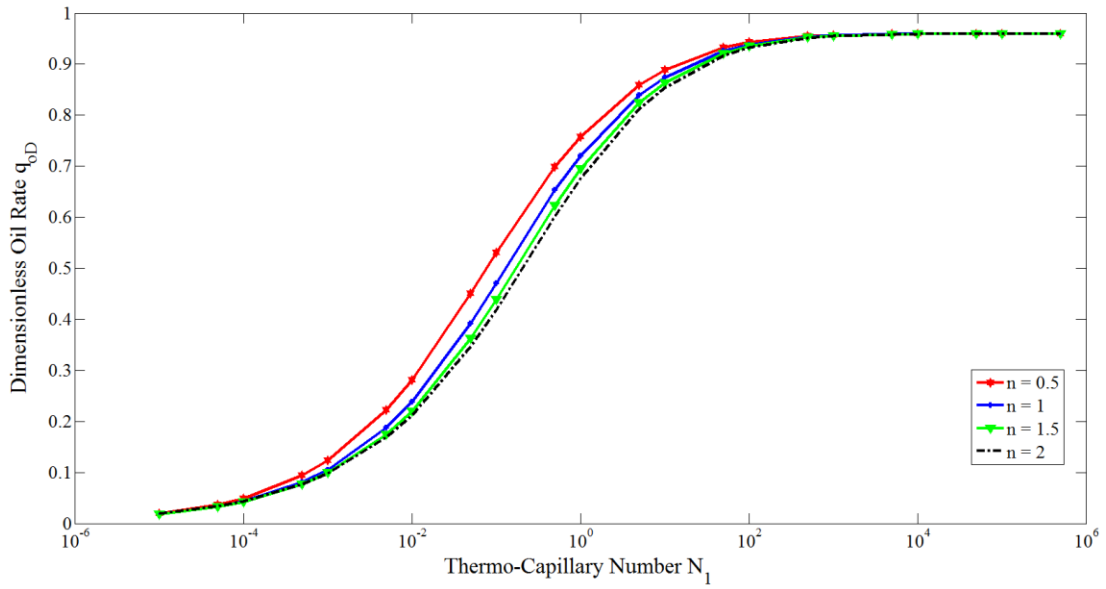

Figure 4.17: Plot showing the sensitivity of the dimensionless oil rate vs. thermo-capillary number to the exponent of the interfacial tension – temperature curve *n*

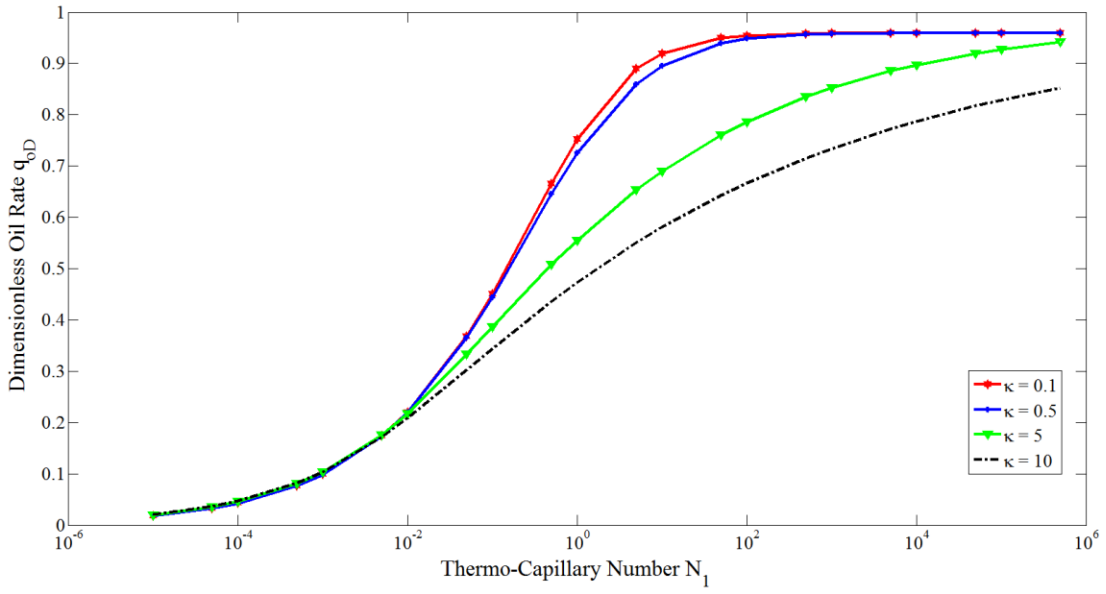

Figure 4.18: Plot showing the sensitivity of the dimensionless oil rate vs. thermo-capillary number to the Leverett *J* curve parameter κ

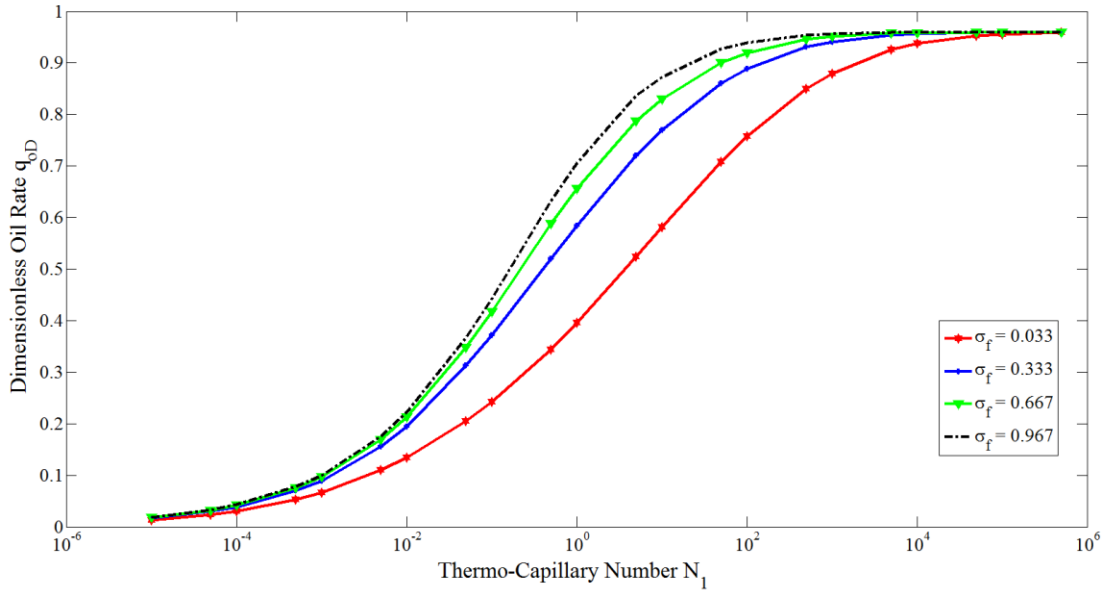

Figure 4.19: Plot showing the sensitivity of the dimensionless oil rate vs. thermo-capillary number to the fractional decrease in interfacial tension σ_f

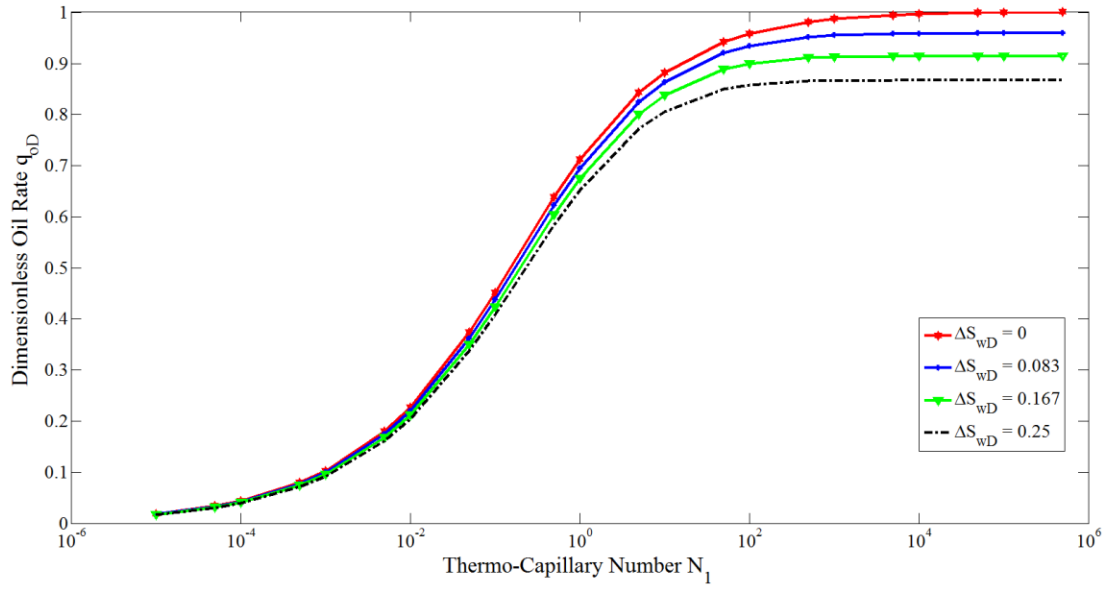

Figure 4.20: Plot showing the sensitivity of the dimensionless oil rate vs. thermo-capillary number to the dimensionless initial mobile saturation ΔS_{wD}

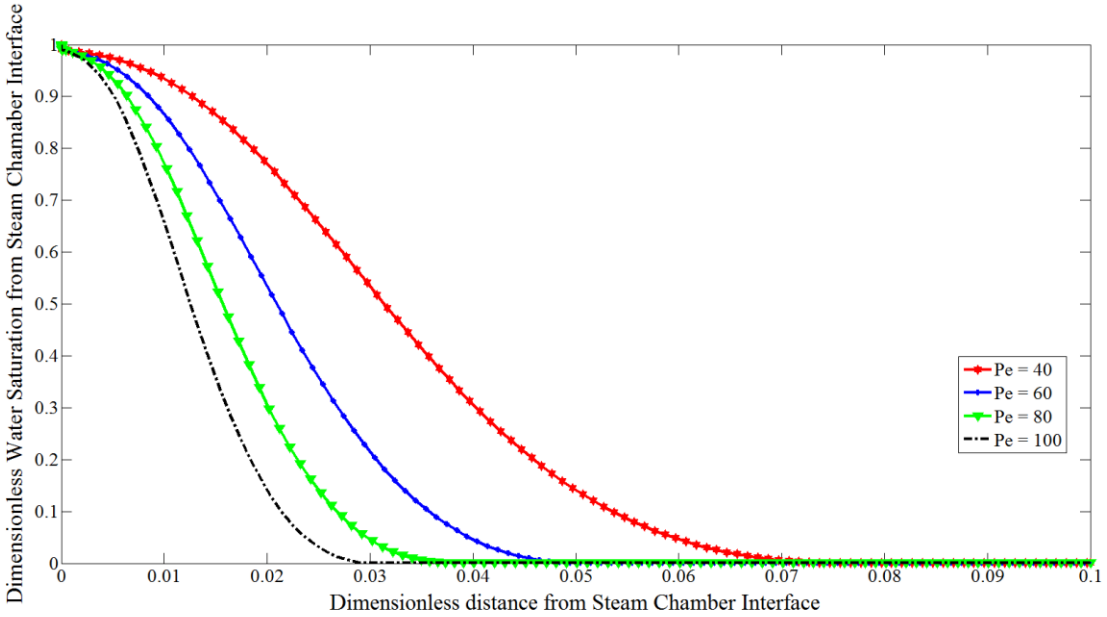

Figure 4.21: Plot showing the sensitivity of the dimensionless water saturation with distance from the steam chamber interface for thermo-capillary number $N_1 = 0.01$ to the Peclet number Pe

4.4 Summary and Significance of Work

In this work, we have developed a model that accounts for capillary imbibition at the boundary of the steam chamber brought about by the change in interfacial tension between water and bitumen due to temperature change. Our results show that this phenomenon is a very complex multi-scale process that can be characterized by a dimensionless group we call the thermo-capillary number which can also be interpreted as an inverse of the Marangoni number. An important observation is that thermo-capillarity behaves differently at experimental scales compared to field scales and hence conclusions made from incompletely scaled experiments should not be used to predict field scale recovery. A complete scaling of experiments will require using previous Butler scaling groups described in Chapter 2 together with all the parameters and dimensionless groups characterizing temperature-induced capillary behavior during SAGD. It was also found that heterogeneity enhances this effect.

This work will find strong application in SAGD proxy model development.

Chapter 5: The Effect of Heat Transfer on Capillarity during ES-SAGD

The Expanding-Solvent Steam-Assisted Gravity Drainage (ES-SAGD) Process is a variant of the SAGD process (Nasr et al., 2003) and involves the injection of hydrocarbon solvent together with steam in the vapor phase to improve bitumen recovery by diluting and hence reducing the viscosity of the bitumen. During ES-SAGD, the solvent condenses out of the vapor phase into the bitumen phase thereby diluting it. Hence the key to a successful ES-SAGD process is the effective partitioning of solvent into the bitumen phase and the consequent lowering of viscosity of the bitumen phase. The lower the viscosity of the solvent, the better the recovery of bitumen (due to solvent mixing), but, from a thermodynamic point of view, lower viscosity solvents generally partition less into bitumen. This then creates an optimization problem with the key variables being the solvent partitioning coefficient and its viscosity.

This problem has been studied extensively experimentally and numerically but a quantitative description and analysis of the ES-SAGD process in an analytical or semi-analytical framework has eluded the SAGD community since it was invented. In this chapter, we will develop such a model and demonstrate that the ES-SAGD process is quite similar to that of SAGD but with the added physics of solvent partitioning, dispersion and bitumen dilution. Because the solvent injected is a hydrocarbon, it is not expected to change the capillary characteristics of the porous media and the modeling procedure in the previous chapter can easily be extended to quantify multiphase flow (thermo-capillarity or the Marangoni effect) during the ES-SAGD process.

Our results predict recovery factors of the same order of magnitude as reported in experiments and field data. They also show that there exists a threshold value of the thermo-capillary number below which the ES-SAGD process will not fare better than the

SAGD process. Sensitivities performed with the semi-analytical model further indicate that the dispersion of the solvent plays a crucial role in recoveries at the experimental and field scales. We also show that the ratio of the solvent viscosity to bitumen viscosity at steam temperature is a critical parameter in determining the success of the ES-SAGD process over SAGD. The smaller this ratio is than unity, the better the ES-SAGD rates will be over SAGD.

5.1 Model Development

The difference between a model for the ES-SAGD process and SAGD will be the addition of a component mass balance for the solvent and a mixing rule for representing the solvent dilution effect on bitumen. This component balance equation can then be added to the phase mass balance and energy equation to give the complete model for the ES-SAGD process. We will assume that the solvent component doesn't influence capillary behavior or thermal properties of the porous rock, hence only the mass balance and thermal energy equation will be coupled for the effect of capillarity just like the SAGD model in Chapter 4. However, unlike the SAGD model in Chapter 4, where the mass balance equation of the condensate and the bitumen were written separately, these equations will be coupled for ES-SAGD because the solvent interacts with both the condensate and bitumen phases. We now present the detailed model that will form the basis of quantifying the horizontal growth phase of the ES-SAGD process and the effect of capillarity on it.

5.1.1 Transport equations in a fixed frame

As stated above, the mass balance and energy equations will be the same as that of the SAGD process presented in Chapter 4 and we will only present below the solvent component mass balance equation.

Solvent mass conservation for a two phase system in porous media is given by

$$\frac{\partial}{\partial t}\left(\phi\left(\rho_w S_w w_i + \rho_o S_o x_i\right)\right) + \nabla\cdot\left(\rho_w \mathbf{u}_w w_i - \rho_w S_w D_w \nabla w_i\right) + \nabla\cdot\left(\rho_o \mathbf{u}_o x_i - \rho_o S_o D_o \nabla x_i\right) = 0 \qquad (5.1)$$

where w_i and x_i are the mole fractions of the solvent in the condensate and bitumen phases respectively. The additional mass transfer due to the dispersion of the solvent in the bitumen and condensate phases is accounted for through the dispersion coefficients D_o and D_w respectively. If we assume local equilibrium of the flowing phases, w_i and x_i are related by the equilibrium relationship

$$w_i = K_i^{w/o} x_i \qquad (5.2)$$

where $K_i^{w/o}$ is the water – oil partition coefficient or equilibrium constant and is a thermodynamic quantity that determines component distributions between two fluid phases in equilibrium (Sandler 2006). Substituting (5.2) into (5.1) gives

$$\begin{aligned}&\frac{\partial}{\partial t}\left(\phi\left(\rho_w S_w K_i^{w/o} + \rho_o S_o\right)x_i\right) + \nabla\cdot\left(\rho_w \mathbf{u}_w K_i^{w/o} x_i - \rho_w S_w D_w \nabla\left(K_i^{w/o} x_i\right)\right) \\ &+\nabla\cdot\left(\rho_o \mathbf{u}_o x_i - \rho_o S_o D_o \nabla x_i\right) = 0\end{aligned} \qquad (5.3)$$

If we assume that the solvent doesn't alter the density of the phases or if the average of the bitumen and solvent mixture density is still close to that of water, then we can

substitute constant phase densities for the condensate and bitumen phases just as we did in Chapter 4 and (5.3) becomes

$$\frac{\partial}{\partial t}\left(\phi\left(S_w K_i^{w/o} + S_o\right)x_i\right) + \nabla\cdot\left(\mathbf{u}_w K_i^{w/o} x_i - S_w D_w \nabla\left(K_i^{w/o} x_i\right)\right) + \nabla\cdot\left(\mathbf{u}_o x_i - S_o D_o \nabla x_i\right) = 0 \qquad (5.4)$$

For two phase flow, (4.8) still holds and substituting it into (5.4) and simplifying yields

$$\begin{aligned} &\frac{\partial}{\partial t}\left(\phi\left(\left(K_i^{w/o} - 1\right)S_w + 1\right)x_i\right) \\ &+\nabla\cdot\left(\left(\mathbf{u}_w K_i^{w/o} + \mathbf{u}_o\right)x_i + \left(\left(D_o - D_w K_i^{w/o}\right)S_w - D_o\right)\nabla x_i - S_w D_w x_i \nabla K_i^{w/o}\right) = 0 \end{aligned} \qquad (5.5)$$

Equations (5.5), (4.13), (4.14) and (4.15) are the transport equations in a fixed frame. We will now derive the transport equations in the moving frame.

5.1.2 Transport equations in a moving reference frame

In a moving reference frame, just as we did in chapter 4, we use the transformations in appendix B to transform (5.5) to

$$\begin{aligned} &\phi\mathbf{U}\cdot\nabla'\left(\left(\left(K_i^{w/o} - 1\right)S_w + 1\right)x_i\right) \\ &-\nabla'\left(\left(\mathbf{u}_w K_i^{w/o} + \mathbf{u}_o\right)x_i + \left(\left(D_o - D_w K_i^{w/o}\right)S_w - D_o\right)\nabla x_i - S_w D_w x_i \nabla K_i^{w/o}\right) = 0 \end{aligned} \qquad (5.6)$$

where $\mathbf{U}$ is the velocity with which the steam chamber expands when the vapor phase contains both steam and solvent. Using the same assumptions as the SAGD case in Chapter 4, (5.6) is reduced to the 1-D case as

$$\begin{aligned}&\phi U_f \frac{d}{d\xi}\left(\left(\left(K_i^{w/o}-1\right)S_w+1\right)x_i\right)\\&-\frac{d}{d\xi}\left(\left(u_w K_i^{w/o}+u_o\right)x_i+\left(\left(D_o-D_w K_i^{w/o}\right)S_w-D_o\right)\frac{dx_i}{d\xi}-S_w D_w x_i\frac{dK_i^{w/o}}{d\xi}\right)=0\end{aligned} \tag{5.7}$$

Equation (5.7) can similarly be integrated between an arbitrary value ξ (corresponding to any location away from the interface) and ∞ (corresponding to the undisturbed reservoir) to give

$$\begin{aligned}&\phi U_f \int_{S_{wi},0,0}^{S_w,K_i^{w/o},x_i} d\left(\left(\left(K_i^{w/o}-1\right)S_w+1\right)x_i\right)\\&-\int_{S_{wi},0,0}^{S_w,K_{i0}^{w/o},x_{i0}} d\left(\left(u_w K_i^{w/o}+u_o\right)x_i+\left(\left(D_o-D_w K_i^{w/o}\right)S_w-D_o\right)\frac{dx_i}{d\xi}-S_w D_w x_i\frac{dK_i^{w/o}}{d\xi}\right)=0\end{aligned} \tag{5.8}$$

The upper limit of the integral represents any location in the reservoir domain away from the steam chamber interface. To further perform the integration and simplify (5.8), the phase velocities need to be determined. Equations (4.3) and (4.4) still apply and yield

$$u_w K_i^{w/o}+u_o=\frac{\lambda_w\lambda_o}{\lambda_w+\lambda_o}\left(K_i^{w/o}-1\right)\frac{dP_c}{d\xi} \tag{5.9}$$

Substituting (5.9) into (5.8) and completing the integration gives

$$\begin{aligned}&\phi U_f\left(\left(\left(K_i^{w/o}-1\right)S_w+1\right)x_i\right)-\frac{\lambda_w\lambda_o}{\lambda_w+\lambda_o}\left(K_i^{w/o}-1\right)x_i\frac{dP_c}{d\xi}\\&-\left(\left(D_o-D_w K_i^{w/o}\right)S_w-D_o\right)\frac{dx_i}{d\xi}+S_w D_w x_i\frac{dK_i^{w/o}}{d\xi}=0\end{aligned} \tag{5.10}$$

The equilibrium constant can be expanded using the product rule as

$$\frac{dK_i^{w/o}}{d\xi} = \frac{dK_i^{w/o}}{dT}\frac{dT}{d\xi} \tag{5.11}$$

Equation (5.11) explicitly utilizes the dependence of the partition coefficient on temperature. Substituting (4.42) into (5.11) gives

$$\frac{dK_i^{w/o}}{d\xi} = -\phi U_f K_i'^{\,w/o}\frac{\left(T-T_R\right)}{\alpha_T} \tag{5.12}$$

where

$$K_i'^{\,w/o} = \frac{dK_i^{w/o}}{dT} \tag{5.13}$$

Substituting (4.30) and (5.12) into (5.10) and simplifying gives

$$\frac{dx_i}{d\xi} = \frac{\phi U_f\left(\left(1-S_{wi}+K_i^{w/o}S_{wi}\right)-S_w D_w K_i'^{\,w/o}\dfrac{\left(T-T_R\right)}{\alpha_T}\right)x_i}{\left(\left(D_o-D_w K_i^{w/o}\right)S_w-D_o\right)} \tag{5.14}$$

Non-dimensionalizing (5.14) using (4.40) and (4.57) just as for the SAGD case gives

$$\frac{dx_i^*}{d\xi^*} = \frac{Pe\left(Le_w\left(1-S_{wi}+K_i^{w/o}S_{wi}\right)-\left(S_w^*\Delta S_o+S_{wi}\right)K_i'^{\,w/o}T^*\Delta T\right)x_i^*}{\left(D^*-K_i^{w/o}\right)\left(S_w^*\Delta S_o+S_{wi}\right)-D^*} \tag{5.15}$$

where Le_w is the condensate Lewis number defined as

$$Le_w = \frac{\alpha_T}{D_w} \tag{5.16}$$

and

$$D^* = \frac{D_o}{D_w} \tag{5.17}$$

$$x_i^* = \frac{x_i}{x_{i_s}} \tag{5.18}$$

where x_{i_s} is the mole fraction of the solvent in the bitumen phase at steam temperature. The functional relationship for the composition – distance space is then given as

$$\frac{dx_i^*}{d\xi^*} = f\left(Pe, Le_w, D^*, \Delta T^*, S_{wiD}, \Delta S_{wD}, K_i^{w/o}(T)\right) \tag{5.19}$$

where

$$S_{wiD} = \frac{S_{wi}}{1 - S_{wc} - S_{or}} \tag{5.20}$$

$$\Delta T^* = \Delta T_R^* = \frac{\Delta T}{T_s} = \frac{T_s - T}{T_s} \tag{5.21}$$

if the temperature difference is taken with respect to T_R side. If instead the temperature difference is taken with respect to T_s then

$$\Delta T^* = \Delta T_s^* = \frac{\Delta T}{T_R} = \frac{T - T_R}{T_R} \tag{5.22}$$

Equation (5.15) is completely dimensionless but not completely parameterized because $K_i^{w/o}$ and $K_i^{'w/o}$ are functions of temperature, not dimensionless temperature. To parameterize $K_i^{w/o}$ and $K_i^{'w/o}$ with any reasonable degree of accuracy will be extremely complex, requiring lots of data, if at all possible, because the equilibrium constant strongly depends on the chemical properties of the fluids in contact. We will circumvent this problem by applying our model to the best single component hydrocarbon solvent for the ES-SAGD process – hexane (Nasr et al. 2003). Hexane has this quality because its vapor pressure is closest to water and yet light enough to dilute bitumen (Tawfik Nasr and Ayodele 2006).

There is a subtle but very important distinction between this work and other works. All previous works (Rabiei et al. 2012), (Sharma and Gates, 2010a) and (Gupta Gittins, 2012) consider only the gas/oil equilibrium constant $K_i^{g/o}$ in modeling the ES-SAGD process because of the implicit assumption that the hydrocarbon solvent does not partition into the condensate phase. Thimm (2001) and (2006) however has shown that this assumption is incorrect and that the pressures and temperatures of a typical SAGD process are high enough to cause appreciable dissolution of the hydrocarbon solvent in water. This means that the gas/water equilibrium constant $K_i^{g/w}$ should be used to account for this extra dissolution. This becomes more necessary when accounting for the effect of thermo-capillary imbibition during the ES-SAGD process because the only mechanisms

that can transport the hydrocarbon solvent through the bitumen phase beyond the steam chamber interface will be dispersion and imbibition, and throughout the imbibition length scale, both condensate and bitumen will be in thermodynamic equilibrium, hence requiring the water/oil equilibrium constant $K_i^{w/o}$. If the gas, condensate and bitumen phases are in thermodynamic equilibrium at the steam chamber interface, then the condensate and bitumen phases will maintain that same equilibrium away from the steam chamber interface and the three phase interface equilibrium can be used to determine the two phase equilibrium anywhere else away from the interface. This means that $K_i^{w/o}$ is not independent of $K_i^{g/o}$ and $K_i^{g/w}$ and is given by (Wu et al. 1997)

$$K_i^{w/o} = \frac{K_i^{g/o}}{K_i^{g/w}} \tag{5.23}$$

What is left are the constitutive equations needed to determine $K_i^{g/o}$ and $K_i^{g/w}$ and will be described in the next subsection.

Equation (5.15) is one more dimensionless equation to be added and solved with the SAGD system of equations. Even though (4.68) will still hold for the ES-SAGD process, the dimensionless water saturation equation (4.67) will no longer be valid because the viscosity of bitumen will now not only be a function of temperature but also a function of solvent composition. We will also describe the constitutive equation needed to determine such a function in the next subsection. It is important to note that the above formulation accounts for the effect of heat transfer on the imbibition of hot condensate/water into the bitumen phase by capillary forces as well as the enhanced mass transfer of solvent into the bitumen phase through dispersion and thermo-capillarity.

5.1.3 Constitutive equations

The first constitutive equations to consider are those for the equilibrium constants. The water/oil equilibrium constant can be defined in the following forms

$$K_i^{w/o} = \frac{w_i}{x_i} = \frac{y_i}{x_i} \Big/ \frac{y_i}{w_i} = \frac{K_i^{g/o}}{K_i^{g/w}} \tag{5.24}$$

This form is very useful because it means that the very difficult to compute liquid/liquid equilibrium formulation can be computed from just knowing the simpler vapor/liquid equilibrium constants. The vapor/liquid equilibrium constants can be computed using the Raoult and Henry's laws (Sandler 2006).

The gas/oil equilibrium equation is based on Raoult's law and given by (CMG 2011)

$$K_i^{g/o} = \left(\frac{K_{V_1}}{P} + K_{V_2} P + K_{V_3} \right) e^{\left(\frac{K_{V_4}}{T - K_{V5}} \right)} \tag{5.25}$$

where K_{V_1}, K_{V_2}, K_{V_3}, K_{V_4} and K_{V_5} are constants specific to the given solvents. For most practical cases (CMG 2011),

$$K_{V_2} = K_{V_3} = 0 \tag{5.26}$$

Substituting (5.26) into (5.25) gives

$$K_i^{g/o} = \frac{K_{V_1}}{P} e^{\left(\frac{K_{V_4}}{T - K_{V5}} \right)} \tag{5.27}$$

If we assume an ideal solution has been formed between the solvent and oil component, then the constants K_{V_1}, K_{V_4} and K_{V_5} will be unique and dependent only on the type of solvent and is the basis for the values found in CMG (2011), reproduced in table 5.1 and used for most numerical simulations of the ES-SAGD process (Rabiei et al. 2012), (Sharma and Gates 2010a).

Table 5.1: $K_i^{g/o}$ - value parameters for Hexane from CMG (2011)

Parameter	Values
K_{V_1}	9.9305×10^3 atm
K_{V_4}	-2697.55 K
K_{V_5}	48.78 K

However, no solution is ideal, and prediction can be significantly improved if the constants are obtained by regressing on equilibrium data. An example of equilibrium data can be obtained for the Athabasca type reservoir from Xu (1990) and by performing non-linear regression on the data using Microsoft Excel™ solver, the parameters in Table 5.2 were obtained. This should give better results than CMG (2011) and was used for the rest of this work.

Table 5.2: $K_i^{g/o}$ - value parameters for Hexane obtained by regressing data from Xu (1990)

Parameter	Values
K_{V_1}	9.47×10^3 atm
K_{V_4}	-2839.815 K
K_{V_5}	47.7844 K

The gas/water equilibrium equation is based on Henry's law and given by (Al-Murayri et al. 2011)

$$K_i^{g/w} = \frac{K_H}{\varphi P} \tag{5.28}$$

where K_H is the Henry's law constant and φ is the fugacity coefficient that accounts for non-idealities. If we assume that

$$\varphi = 1 \tag{5.29}$$

which is usually a good assumption, then the only parameter that is needed for $K_i^{g/w}$ is the Henry's law constant K_H. For large temperature ranges typical of the SAGD process, the best and most used correlation for determining K_H is that of Harvey (1996) given by

$$\ln K_H = \ln P_{\text{sat}} + \frac{A}{T^{**}} + \frac{B\left(1-T^{**}\right)^{0.355}}{T^{**}} + \frac{Ce^{\left(1-T^{**}\right)}}{T^{**0.41}} \tag{5.30}$$

where

$$T^{**} = \frac{T}{T_c} \tag{5.31}$$

and A, B and C are constants specific to the given solvent and P_{sat} is the saturation pressure obtained using the correlation of Wagner and Pruss (1993). Even though Harvey (1996)

did not give the value of these constants for hexane, Thimm (2006) gave K_H values for hexane using the more complex method of Plyasunov and Shock (2003). We circumvent this problem by regressing on Thimm (2006) data to obtain the values of A, B and C for hexane and given in Table 5.3.

Substituting (5.30) and (5.29) into (5.28) gives

$$K_i^{g/w} = \frac{e^{\ln P_{sat} + \frac{A}{T^{**}} + \frac{B\left(1-T^{**}\right)^{0.355}}{T^{**}} + \frac{Ce^{\left(1-T^{**}\right)}}{T^{**0.41}}}}{P} \tag{5.32}$$

Table 5.3: the K_H - value parameters for Hexane obtained by fitting data in Thimm (2006)

Parameter	Values
A	-12.1512
B	7.5278
C	11.3839

Substituting (5.27) and (5.32) into (5.24) gives

$$K_i^{w/o} = K_{V_1} e^{\left(\left(\frac{K_{V4}}{T-K_{V5}}\right) - \ln P_{sat} - \frac{A}{T^{**}} - \frac{B\left(1-T^{**}\right)^{0.355}}{T^{**}} - \frac{Ce^{\left(1-T^{**}\right)}}{T^{**0.41}}\right)} \tag{5.33}$$

Equation (5.33) indicates that the water/oil equilibrium constant $K_i^{w/o}$ is explicitly independent of pressure. However, the composition of the solvent in the bitumen and condensate phases will be dependent on pressure because the solvent mole fraction in the bitumen phase at steam temperature x_{i_s} will be computed from the injected gas composition and $K_i^{g/o}$.

The next constitutive equation to consider is that of bitumen viscosity and its dependence on both temperature and solvent concentration. We will use the same formulation used for most numerical simulations described in CMG (2011) and given by

$$\ln \mu_o = x_i \ln \mu_{\text{sol}} + (1 - x_i) \ln \mu_{o_d} \tag{5.34}$$

where μ_{sol} is the viscosity of the solvent which we will assume to be constant and μ_{o_d} is the dead oil viscosity of bitumen which will be dependent on temperature only and given by (4.39). Substituting (4.39) for μ_{o_d} into (5.34) and simplifying gives

$$\frac{\mu_o}{\mu_s} = \left(\frac{\mu_{\text{sol}}}{\mu_s} \right)^{x_i} T^{*m(x_i - 1)} \tag{5.35}$$

In (5.35), μ_s is the dead oil viscosity of bitumen at steam temperature.

5.1.4 Dimensionless saturation profile

Because (4.37) will still be valid for the ES-SAGD process, substituting (5.35) into (4.38) gives

$$\Lambda(S_w, T) = \frac{k_{rocw} k}{\mu_s} \left((1 - S_{wD})^a \left(\frac{\mu_s}{\mu_{\text{sol}}} \right)^{x_i} T^{*m(1 - x_i)} \right) \tag{5.36}$$

Equation (5.36) is the ES-SAGD equivalent of (4.41). Because (4.45) will still be valid for the ES-SAGD process, substituting (5.36) into (4.30) gives

$$\frac{k_{rocw}k}{\mu_s}\left(\left(1-S_{wD}\right)^a\left(\frac{\mu_s}{\mu_{\text{sol}}}\right)^{x_i}T^{*m(1-x_i)}\right)\left(P_{c,S_w}\frac{dS_w}{d\xi}+P_{c,T}\frac{dT}{d\xi}\right)=\phi U_f\left(S_w-S_{wi}\right) \tag{5.37}$$

Substituting (4.42) into (5.37) and simplifying:

$$-\frac{dS_w}{d\xi}=\phi U_f\left[-\frac{\left(S_w-S_{wi}\right)\mu_s T^{*m(x_i-1)}}{k_{rocw}k\left(1-S_{wD}\right)^a P_{c,S_w}}\left(\frac{\mu_{\text{sol}}}{\mu_s}\right)^{x_i}-\frac{\left(T-T_R\right)P_{c,T}}{\alpha_T P_{c,S_w}}\right] \tag{5.38}$$

The system composed of (4.42), (5.38) and (5.14) is a coupled system of three non-linear ordinary differential equations. It can also be written in vector form as (4.48) where for the ES-SAGD process

$$\mathbf{Y}=\left(x_i,S_w,T\right)^T \tag{5.39}$$

and

$$\mathbf{b}=\phi U_f\left[\begin{array}{c}\dfrac{\left(\left(1-S_{wi}+K_i^{w/o}S_{wi}\right)-S_wD_wK_i^{'w/o}\dfrac{\left(T-T_R\right)}{\alpha_T}\right)x_i}{\left(\left(D_o-D_wK_i^{w/o}\right)S_w-D_o\right)},\\ -\dfrac{\left(S_w-S_{wi}\right)\mu_s T^{*m(x_i-1)}}{k_{rocw}k\left(1-S_{wD}\right)^a P_{c,S_w}}\left(\dfrac{\mu_{\text{sol}}}{\mu_s}\right)^{x_i}-\dfrac{\left(T-T_R\right)P_{c,T}}{\alpha_T P_{c,S_w}},\dfrac{T-T_R}{\alpha_T}\end{array}\right]^T \tag{5.40}$$

where just like for the SAGD case the superscript T is the transpose and from (5.40), we see that in the limit $\xi\to\infty$, both $\mathbf{b}$ and the derivatives go to zero as expected. Also, just like the SAGD case, the system of equations cannot be solved if the front velocity – which appears at the right hand side of (5.40) – is unknown. It is interesting to note that

the system of equations reduces to the SAGD case for $x_i = 0$ i.e. zero solvent concentration in the injected steam.

Substituting (4.53) and (4.56) into (5.38) and non-dimensionalizing using (4.40), (4.57) and (5.18) gives

$$\frac{dS_w^*}{d\xi^*} = Pe\left(\frac{\sigma_{o_R} - \sigma_{o_S}}{J'(S_w)\left(\sigma_{o_R} - \left(\sigma_{o_R} - \sigma_{o_S}\right)\left(T^*\right)^n\right)}\right)\left(\frac{S_w^* N_1 T^{*m\left(x_i^* x_{i_S} - 1\right)}}{\left(1 - S_{w_D}\right)^a}\left(\frac{\mu_{sol}}{\mu_s}\right)^{x_i^* x_{i_S}} - \frac{nT^{*n} J(S_w)}{\Delta S_o}\right) \quad (5.41)$$

The functional relationship for the saturation – distance space for the ES-SAGD process is given as

$$\frac{dS_w^*}{d\xi^*} = f\left(N_1, Pe, a, m, n, \kappa, \sigma_f, \Delta S_{wD}, x_{i_{sD}}\left(T_s, P\right), \left(\frac{\mu_{sol}}{\mu_s}\right)\right) \quad (5.42)$$

where

$$x_{i_{sD}} = \frac{x_{i_s}}{y_i} \quad (5.43)$$

Equation (5.42) gives two important insights. The first is that the success of the ES-SAGD process will be dependent on the reservoir or operating pressure and since this determines the amount of solvent that will partition into the bitumen and condensate phases at the steam chamber interface. From (5.27), we see that higher pressures are preferred. The second is that the effectiveness of the ES-SAGD process will be dependent on how much the solvent viscosity is smaller than the bitumen only viscosity at steam

temperature. This can be used as a screening parameter to determine if the ES-SAGD process should be preferred over the SAGD process. This can also be used to optimize the solvent design to maximize ES-SAGD recovery. Equations (4.68), (5.41) and (5.15) now form the complete system of equations in dimensionless space.

We can also transform (5.15) and (5.41) into temperature space by using the dimensionless form of (4.51) to give

$$\frac{dx_i^*}{dT^*} = \frac{\left(\left(S_w^*\Delta S_o + S_{wi}\right)K_i'^{w/o}\Delta T - \frac{Le_w}{T^*}\left(1 - S_{wi} + K_i^{w/o}S_{wi}\right)\right)x_i^*}{\left(D^* - K_i^{w/o}\right)\left(S_w^*\Delta S_o + S_{wi}\right) - D^*} \tag{5.44}$$

$$\frac{dS_w^*}{dT^*} = \left(\frac{\sigma_{o_R} - \sigma_{o_S}}{J'(S_w)\left(\sigma_{o_R} - \left(\sigma_{o_R} - \sigma_{o_S}\right)\left(T^*\right)^n\right)}\right)\left(\frac{nT^{*n-1}J(S_w)}{\Delta S_o} - \frac{S_w^* N_1 T^{*m\left(x_i^* x_{i_S} - 1\right) - 1}}{\left(1 - S_{w_D}\right)^a}\left(\frac{\mu_{\text{sol}}}{\mu_s}\right)^{x_i^* x_{i_S}}\right) \tag{5.45}$$

Equations (5.44) and (5.45) now give the system of equations in dimensionless temperature space. The functional relationships in the temperature space now becomes

$$\frac{dx_i^*}{dT^*} = f\left(Le_w, D^*, \Delta T, S_{wiD}, \Delta S_{wD}, K_i^{w/o}(T)\right) \tag{5.46}$$

$$\frac{dS_w^*}{dT^*} = f\left(N_1, a, m, n, \kappa, \sigma_f, \Delta S_{wD}, x_{i_{SD}}(T_s, P), \left(\frac{\mu_{\text{sol}}}{\mu_s}\right)\right) \tag{5.47}$$

5.1.5 Dimensionless oil rate

The oil rate for the ES-SAGD process will still be given by (4.84) but with the important difference that m_{TC} given by (4.77) will also take into account the bitumen

phase viscosity dependence on the solvent concentration. Substituting (5.35) and (4.77) into (4.85) gives the dimensionless oil rate for the ES-SAGD process as

$$q_{o_D} = \sqrt{\frac{m}{k_{rocw}} \int_0^1 k_{ro}\left(1-c_i\right) T^{*m(1-x_i)-1} \left(\frac{\mu_s}{\mu_{\text{sol}}}\right)^{x_i} dT^*} \tag{5.48}$$

where the $1-c_i$ factor inside the integral is used to account for only the bitumen production excluding solvent and c_i is the volume fraction of solvent in the bitumen phase given as

$$c_i = \frac{\dfrac{x_i M_{sol}}{\rho_{sol}}}{\dfrac{x_i M_{sol}}{\rho_{sol}} + \dfrac{\left(1-x_i\right) M_o}{\rho_o}} \tag{5.49}$$

where M_{sol} and M_o are the molecular weights of solvent and bitumen components respectively and ρ_{sol} is the density of solvent in the bitumen phase. Equation (5.49) can be simplified further to give

$$c_i = \frac{x_i}{x_i + \left(1-x_i\right)\dfrac{\rho_{sol}^m}{\rho_o^m}} \tag{5.50}$$

where ρ_{sol}^m and ρ_0^m are the molar densities of solvent and bitumen components respectively in the bitumen phase. Ideally, both molar densities will not be constants but will be functions of temperature, pressure, the isobaric and isothermal compressibilities of the individual components. We will however assume the ratio to be constant in this work and

hence utilize its average value as a process parameter. This choice should not be confused with our earlier assumption of ignoring the effect of solvent on bitumen phase density as that deals with a bulk phase property while (5.50) deals with a ratio of component properties.

Combining (5.48), (5.46) and (5.47) gives the functional relationship for the dimensionless oil rate of the ES-SAGD process as

$$q_{oD} = f\left(N_1, a, m, n, \kappa, \sigma_f, \Delta S_{wD}, x_{i_{SD}}\left(T_s, P\right), \left(\frac{\mu_{\text{sol}}}{\mu_s}\right), Le_w, D^*, \Delta T^*, S_{wiD}, K_i^{w/o}\left(T\right), \frac{\rho_{sol}^m}{\rho_o^m} \right) \quad (5.51)$$

$x_{i_{SD}}\left(T_s, P\right)$ and $K_i^{w/o}\left(T\right)$ are not independent, hence (5.51) can be simplified to give

$$q_{oD} = f\left(N_1, a, m, n, \kappa, \sigma_f, \Delta S_{wD}, P, \left(\frac{\mu_{\text{sol}}}{\mu_s}\right), Le_w, D^*, \Delta T^*, S_{wiD}, K_i^{w/o}\left(T\right), \frac{\rho_{sol}^m}{\rho_o^m} \right) \quad (5.52)$$

where the dependence on $x_{i_{SD}}\left(T_s, P\right)$ is replaced with a dependence on pressure P because

$$K_i^{w/o}\left(T\right) \neq f\left(P\right) \quad (5.53)$$

Notice that in (5.49), we have not non-dimensionalized pressure as there is clearly no meaningful way to do this because even though the ES-SAGD process is pressure dependent, the typical SAGD process is not and hence there exists no clear reference for non-dimensionalization. One way to make (5.49) strictly dimensionless is to replace P with $K_i^{g/o}\left(T, P\right)$ but this won't be helpful from a sensitivity analysis point of view. If the solvent is fixed, (5.49) will be the most useful functional relationship in the absence of

parameterizing the equilibrium constants. The sensitivity of q_{oD} on $K_i^{w/o}(T)$ will be determined indirectly from temperature data.

The dimensionless mobility for the ES-SAGD process is similarly given as

$$\lambda_o^* = \frac{k_{ro}\nu_s}{k_{rocw}\nu_o} = \frac{k_{ro}}{k_{rocw}}\left(T^{*m(1-x_i)}\left(\frac{\mu_s}{\mu_{\text{sol}}}\right)^{x_i}\right) \tag{5.54}$$

5.2 Results and Discussion

In this section, we will discuss the results obtained from our ES-SAGD model and compare it to the SAGD results of Chapter 4. We first define a base case of the parameters we will use in our simulations and later present a sensitivity analysis around these base values.

Fig 5.1 shows the dimensionless temperature – distance profile for both the ES-SAGD and SAGD processes. The profiles overlap because in our model, the presence of the hydrocarbon solvent does not influence heat transfer i.e. we have assumed the heat capacities and thermal conductivities of both the condensate and bitumen phases to be constant irrespective of solvent concentration. The thermal conductivity length scale is also the same for ES-SAGD like SAGD and about 0.05 times the reservoir thickness.

Fig 5.2 shows the dimensionless water saturation – distance plot compared with that for the SAGD plot. The plot reveals that the presence of the solvent does not alter the saturation – distance profiles significantly for the base case considered. This is also seen in **Fig 5.3** the dimensionless water saturation – temperature plot, but with some separation between the ES-SAGD and SAGD plots at temperatures closest to steam temperature. This separation is due to the increased dispersive transport of the solvent

through the condensate phase resulting in increased water saturation during the ES-SAGD process.

Fig 5.4 shows the dimensionless hydrocarbon solvent concentration – distance profile in the bitumen phase. The plot reveals that the thermo-capillary number significantly influences the solvent concentration distribution. At lower thermo-capillary numbers, you have relatively higher concentration distributions than at higher thermo-capillary numbers because of the combined effect of lower bitumen saturations and mass transfer of solvent from the condensate to the bitumen phase due to increased condensate transport ahead of the steam chamber interface at lower thermo-capillary numbers. **Fig 5.5** shows similar results but in dimensionless temperature space. One key point to infer from **Figs 5.1, 5.4** and **5.5** is that the combined dispersion length scale is about one order of magnitude less than the thermal conductivity length scale. This is typical and a consequence of our choice of the Lewis number Le_w and dimensionless dispersion coefficient in the bitumen phase D^*. This is important because just like the SAGD process, the ES-SAGD is a short length-scaled process (the heat transfer length scale in bitumen is short) and hence, any phenomena that is short-scaled (like thermo-capillarity) should not be ignored during the SAGD or ES-SAGD process.

Fig 5.6 shows the dimensionless bitumen mobility – distance profile for the base case. Significant differences only exist between the ES-SAGD case and the SAGD case at high thermo-capillary numbers as the insert plot shows that the ES-SAGD and SAGD plots give same results at low thermo-capillary numbers. This is a consequence of having the same saturation profiles, and hence same relative permeability curves and the water saturation so high that the effect of solvent dilution is not significantly felt. At this point, the thermo-capillary length scale will be of the same order as the solvent dispersive length scale, thereby reducing the dilution effect of the solvent to just residual oil. This

suggests that there exists a critical thermo-capillary number for a given set of dimensionless parameters below which the ES-SAGD process performs no better than the SAGD process. This is also more clearly seen in **Fig 5.7** where the dimensionless oil rate is plotted against the thermo-capillary number and from $N_1 < 1$, the ES-SAGD and SAGD processes are indistinguishable. The Sharma and Gates assumption plotted was obtained by using their linear transport model and re-deriving the ES-SAGD equations like we did in this work. Clearly a linear saturation-temperature profile also fails to capture the multi-scale physics of thermo-capillarity during the ES-SAGD process. One last point about **Fig 5.7** is that it shows the ES-SAGD process gives recoveries about 20% higher than for SAGD for the base case process parameters and is consistent with the results of Tawfik Nasr and Ayodele (2006) where they reported about 25% increase in rates for ES-SAGD over SAGD in their experiments. Orr (2009) reported about 17 – 24% increase in bitumen rates for the Long Lake pilot and 0% increase in rates for the Firebag reservoir. These results are consistent with the effect of thermo-capillarity on the ES-SAGD process.

Table 5.1 summarizes the reservoir and fluid parameters used for developing these base case results.

Table 5.4: Base case reservoir and fluid parameters used for developing the ES-SAGD results[10]

Parameter	Values
S_{wc}	0.2
S_{wi}	0.25
S_{or}	0.2
k_{rocw}	0.5
a	1
n	1.5
m	4
σ_f	0.033
κ	1
Pe	100
Le_w	5
D^*	0.5
μ_{sol}/μ_s	0.1
y_i	0.3
T_s	350 ^{0}C
T_R	50 ^{0}C
ρ_{sol}^m/ρ_o^m	500

[10] Some of these data values correspond to those found in the works of Sharma and Gates (2010a), Rabiei et al. (2012) and Bowman (1967)

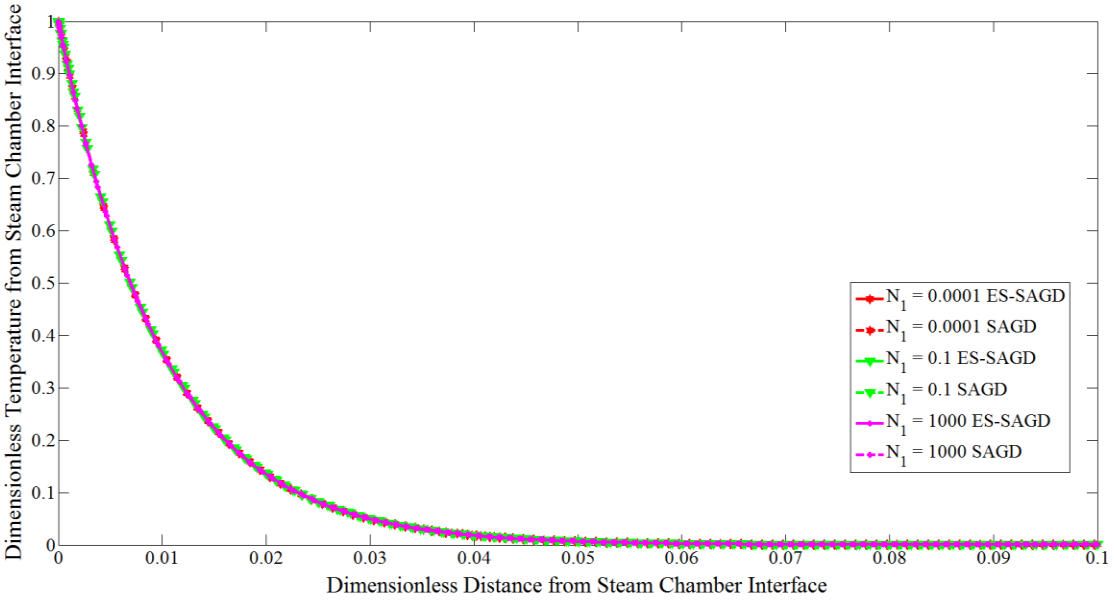

Figure 5.1: Plot of the dimensionless temperature – distance profile ahead of the steam chamber interface for the base case

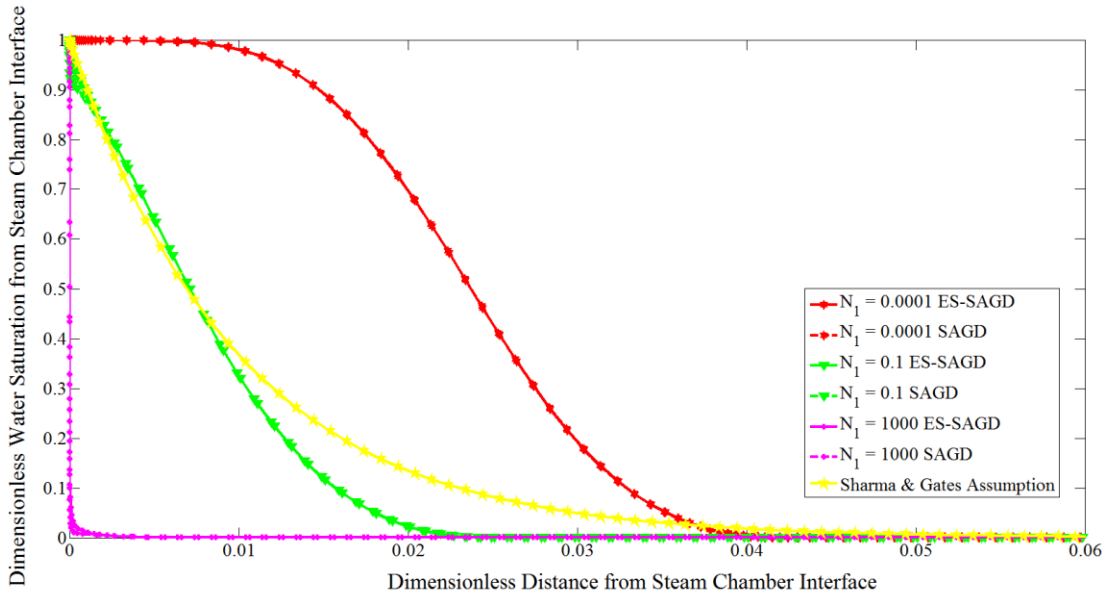

Figure 5.2: Plot of the dimensionless water saturation – distance profile ahead of the steam chamber interface for the base case

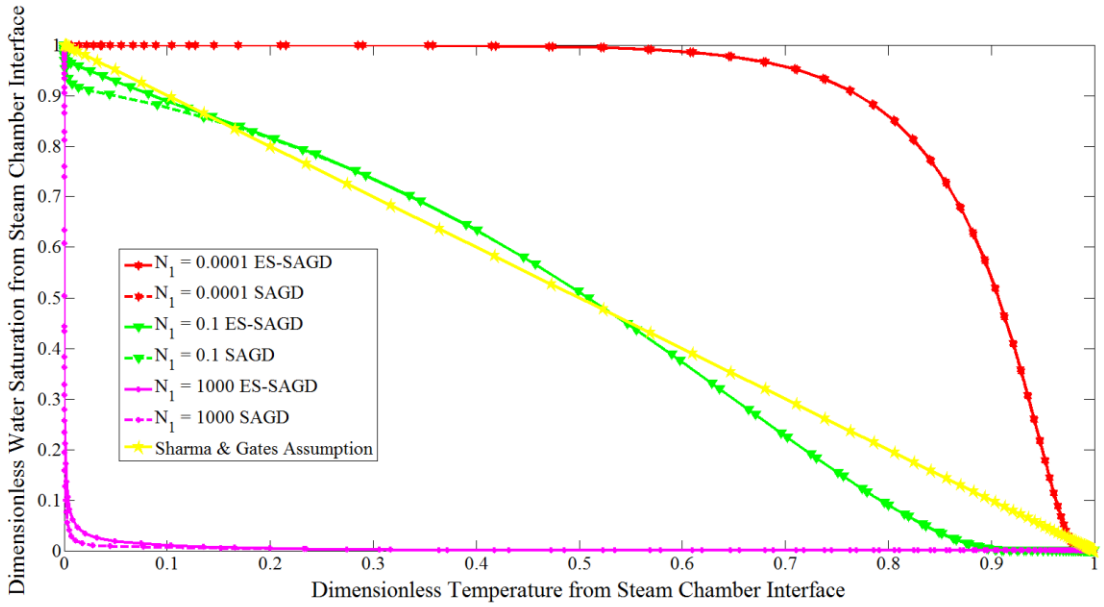

Figure 5.3: Plot of the dimensionless water saturation – temperature profile ahead of the steam chamber interface for the base case

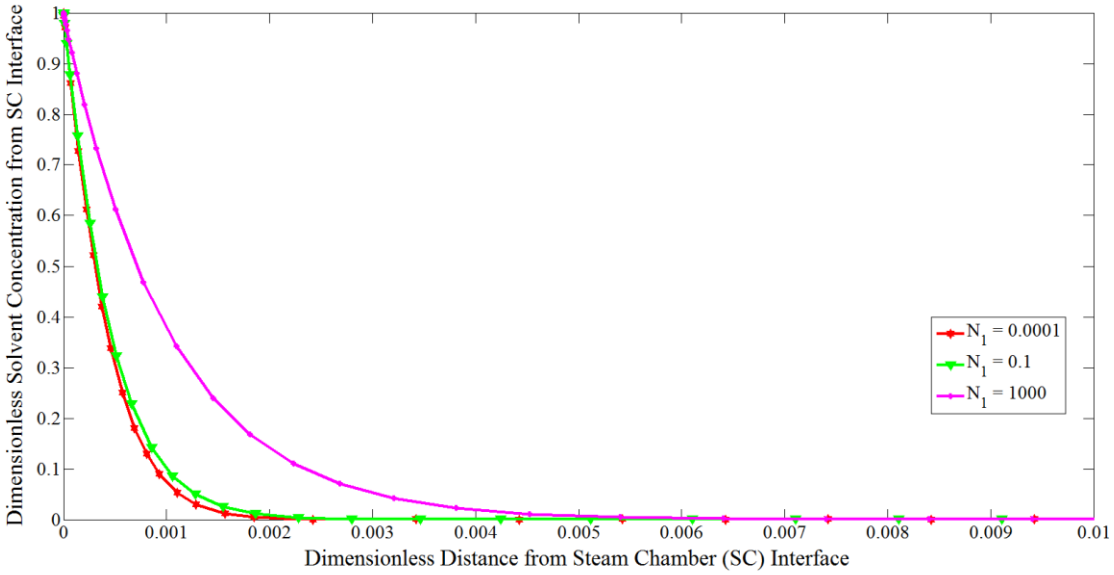

Figure 5.4: Plot of the dimensionless molar solvent concentration – distance profile in the bitumen phase ahead of the steam chamber interface for the base case

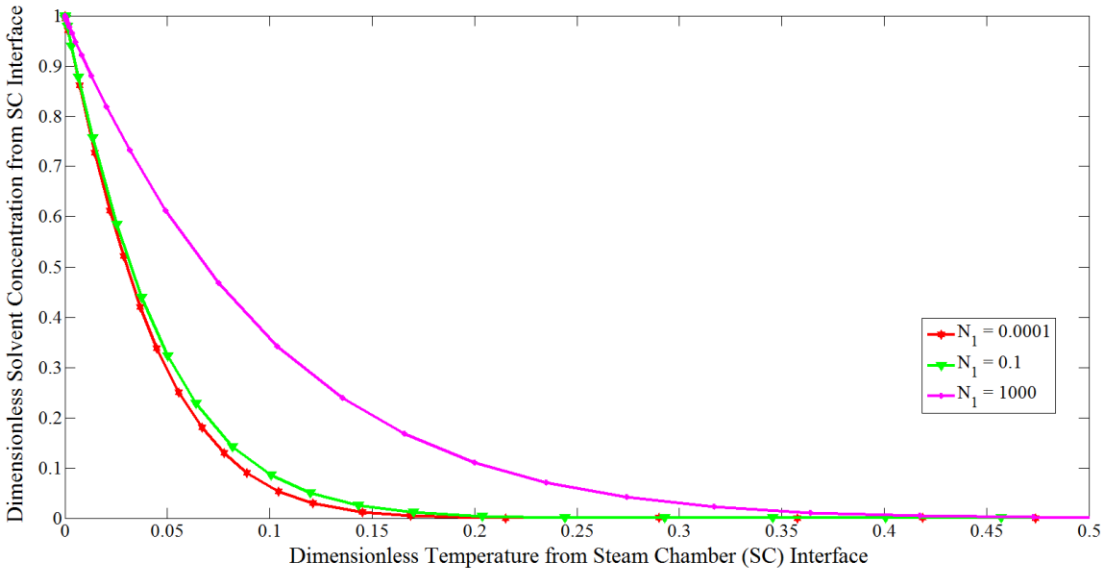

Figure 5.5: Plot of the dimensionless molar solvent concentration – temperature profile in the bitumen phase ahead of the steam chamber interface for the base case

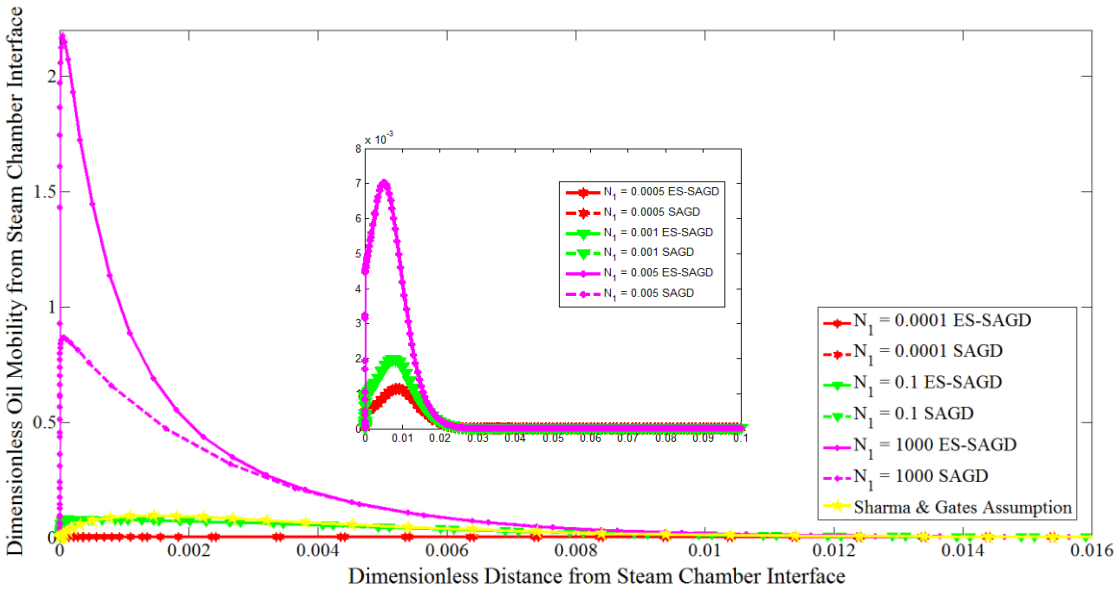

Figure 5.6: Plot of the dimensionless oil mobility – distance profile ahead of the steam chamber interface for the base case

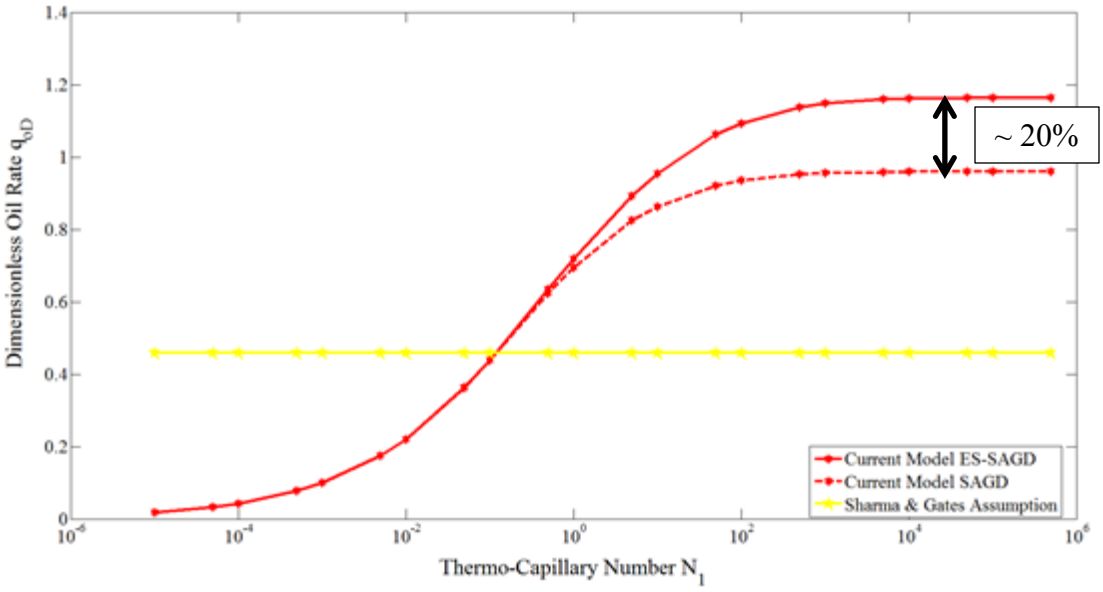

Figure 5.7: Plot of the dimensionless oil rate vs. thermo-capillary number for the base case

5.2.1 Sensitivity analysis

Fig 5.8 shows the sensitivity of the oil rate – thermo-capillary number plot to the Corey exponent a. The plot reveals that the flow of solvent does not affect the influence of a on bitumen rates. This is expected because we have assumed in our model that the hydrocarbon solvent does not change the porous media properties of the reservoir rock.

Fig 5.9 shows the sensitivity to the Butler m parameter. The ES-SAGD results are quite different from the SAGD case as at very low thermo-capillary numbers, the ES-SAGD model predicts slightly higher rates at lower values of m as expected for $N_1 < 1$, but also gives the counter-intuitive result of predicting higher dimensionless bitumen rates for higher values of m for $N_1 > 1$. This is due to the action of the hydrocarbon solvent. At higher thermo-capillary numbers, there exists appreciable bitumen to be produced ahead of the steam chamber interface. However, if m is small, then the viscosity difference

between at steam and reservoir conditions will be small, hence there will be so little the solvent can do, however, the higher the value of m, the larger the viscosity difference, and then the solvent more significantly influences bitumen rates. This result reveals an important screening criteria for choosing the ES-SAGD process over SAGD – the value of m needs to be high and the higher it is, the more successful the ES-SAGD process will be. Since nature will always fix the native bitumen viscosity – temperature relationship, the only way to increase m is to use lower viscosity solvent and the lower the solvent viscosity, the higher the value of m due to dilution effects.

Fig 5.10 shows the sensitivity to the capillary pressure curve exponent κ. It reveals a similar behavior as the SAGD process but also shows that as κ increases, the difference in bitumen rates between the ES-SAGD and SAGD process decreases. This is because as κ increases, there is more capillary diffusion, hence lower bitumen saturations for the solvent to act on. **Fig 5.11** shows the sensitivity to the fractional decrease in interfacial tension σ_f and reveals similar behavior to the SAGD case. Again, this is because we have assumed that the solvent does not influence the interfacial tension between condensate and bitumen and this result is expected.

Fig 5.12 shows the sensitivity to the dimensionless initial mobile water saturation and reveals similar behavior to the SAGD case. This is because we have assumed complete thermodynamic equilibrium of the phases and hence, the amount of condensate present doesn't affect solvent dilution.

Fig 5.13 shows the sensitivity to the condensate Lewis number Le_w and shows that the lower the value of Le_w the higher the bitumen recovery will be and at $Le_w > 50$ you get the SAGD rates i.e. there exists a value of Le_w for which the ES-SAGD process does not fare better than SAGD for a given set of dimensionless parameters. Since heterogeneity gives rise to larger dispersion in porous media (Arya et al. 1988), **Fig 5.13** reveals that

heterogeneous formations, which have lower Le_w, will produce higher ES-SAGD rates. The reason for this is the enhanced transport qualities of the condensate phase at it carries the hydrocarbon solvent beyond the steam chamber interface where temperatures are lower and hence equilibrium shifted to favor more dissolution of solvent in the bitumen phase (see **Fig 5.19**). This result is an interesting observation made with the semi-analytical model.

Fig **5.14** shows the sensitivity to the dimensionless dispersion coefficient in the bitumen phase $D*$ and shows that the higher the value of D^* the greater the bitumen recovery. It also reveals that for a given set of dimensionless parameters, there exists a low enough bitumen dispersion for which the ES-SAGD process does not fare better than SAGD. These results are expected as the greater the dispersion in the bitumen phase, the more volume of bitumen contacted by the bitumen and, hence more dilution. **Figs 5.14** and **5.13** also show that only the dimensionless bitumen dispersion coefficient D^* and the condensate Lewis number Le_w control the value of the thermo-capillary number N_1 at which the ES-SAGD and SAGD processes are indistinguishable.

Fig 5.15 shows the sensitivity to the viscosity ratio $\frac{\mu_{sol}}{\mu_s}$ and reveals that the smaller this ratio is the better the bitumen recovery. It also reveals another screening criterion for choosing the ES-SAGD process over SAGD as, if this ratio is unity or greater, then the ES-SAGD process should not be attempted and the smaller the ratio is than unity the more effective the ES-SAGD process will be. This is because for $\frac{\mu_{sol}}{\mu_s} \geq 1$, there will be no dilution effect at the steam chamber interface, and even though solvent can be transported beyond the steam chamber interface where bitumen viscosities will be higher, the length scale of dispersion is so small to overcome the adverse effect of zero dilution at the steam chamber interface.

Fig 5.16 shows the sensitivity to the solvent mole fraction in the injected vapor phase y_i and reveals a very uniform variation of bitumen rates with y_i for $N_1 > 1$. This is because for a given solvent, $K_i^{w/o}$ behaves quite uniformly as seen from **Fig 5.19** throughout the temperature space and the increased rates are expected since more solvent in the steam phase will give rise to more solvent partitioning into the bitumen and condensate phases, thereby aiding recovery.

Fig 5.17 shows the sensitivity to the dimensionless temperature difference ΔT_R^* and reveals that the ES-SAGD process is in-sensitive to variations in practical reservoir temperatures. This is because of the effect of the dispersive length scale being an order of magnitude smaller than the thermal conductivity length scale (see **Figs 5.1** and **5.5)**, i.e. at T_R, there is clearly zero concentration of the solvent. This situation is different for **Fig 5.18** the sensitivity to ΔT_s^* where we see that at low ΔT_s^*, equivalent to lower steam temperature T_s values, the bitumen rates are higher than those at higher ΔT_s^*. The reason for this is seen from **Fig 5.19** the water/oil equilibrium ratio plot as lower $K_i^{w/o}$ values and hence higher solvent concentrations in the bitumen phase x_i are obtained at lower temperatures.

Fig 5.20 shows the sensitivity to the reservoir pressure and reveals the higher the steam chamber pressure the higher the ES-SAGD rates. This result is expected because at higher pressures you get lower $K_i^{g/o}$ which in turn gives higher dissolution of solvent in the bitumen phase. Also notice that at $P = 1\ \text{atm}$, the ES-SAGD and SAGD rates are indistinguishable and this suggests a way to now completely dimensionalize (5.49) as

$$q_{oD} = f\left(N_1, a, m, n, \kappa, \sigma_f, \Delta S_{wD}, P^*, \left(\frac{\mu_{\text{sol}}}{\mu_s}\right), Le_w, D^*, \Delta T^*, S_{wiD}, K_i^{w/o}(T), \frac{\rho_{sol}^m}{\rho_o^m}\right) \quad (5.55)$$

where

$$P^* = \frac{P}{P = 1 \text{ atm}} \tag{5.56}$$

Fig 5.21 shows that the ES-SAGD rates are insensitive to the dimensionless initial water saturation S_{wiD} provided $\Delta S_{wD} = 0$. This result is very helpful as it eliminates S_{wiD} as a parameter in (5.55) and is a consequence of our assumption of complete thermodynamic equilibrium irrespective of initial phase volumes.

Fig 5.22 shows the sensitivity of the ES-SAGD rates to the ratio of solvent to bitumen molar densities $\frac{\rho_{sol}^m}{\rho_o^m}$ and reveals that the smaller this ratio is, the smaller the ES-SAGD rates will be. This is because as the solvent volumetric concentration in the bitumen phase gets larger, it reduces the effective bitumen component volumetric concentration in the bitumen phase. **Fig 5.22** also shows that at about $\frac{\rho_{sol}^m}{\rho_o^m} \geq 10$ for the base case parameters chosen the ES-SAGD rates begin to be indistinguishable and is a consequence of the solvent volumetric concentration becoming so small to appreciably have any effect on equation (5.48).

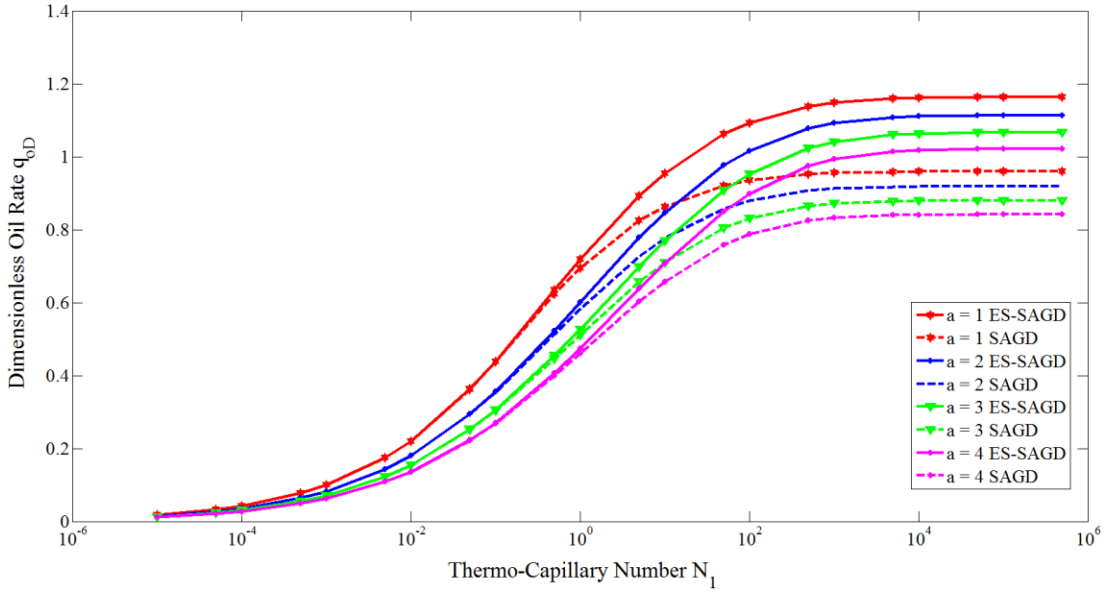

Figure 5.8: Plot showing the sensitivity of the dimensionless oil rate vs. thermo-capillary number to the Corey exponent a

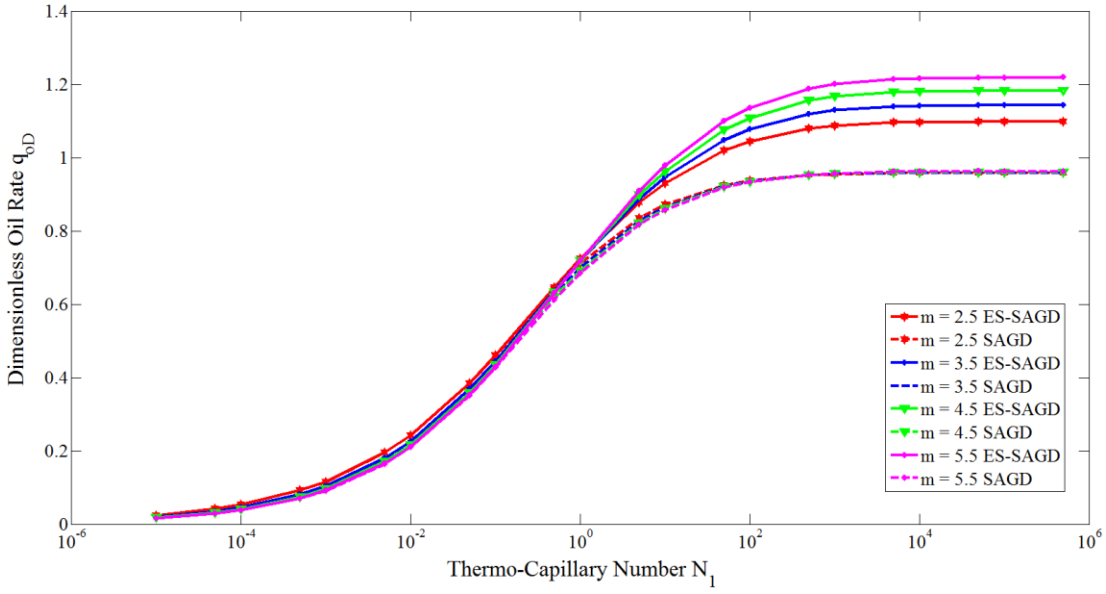

Figure 5.9: Plot showing the sensitivity of the dimensionless oil rate vs. thermo-capillary number to the Butler m parameter

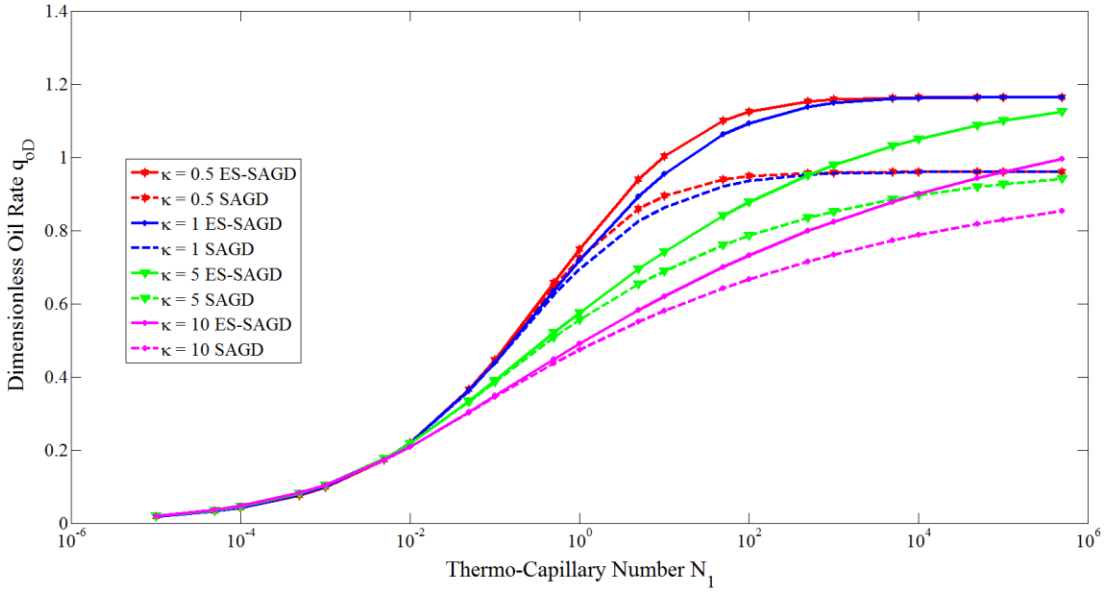

Figure 5.10: Plot showing the sensitivity of the dimensionless oil rate vs. thermo-capillary number to the Leverett *J* curve parameter κ

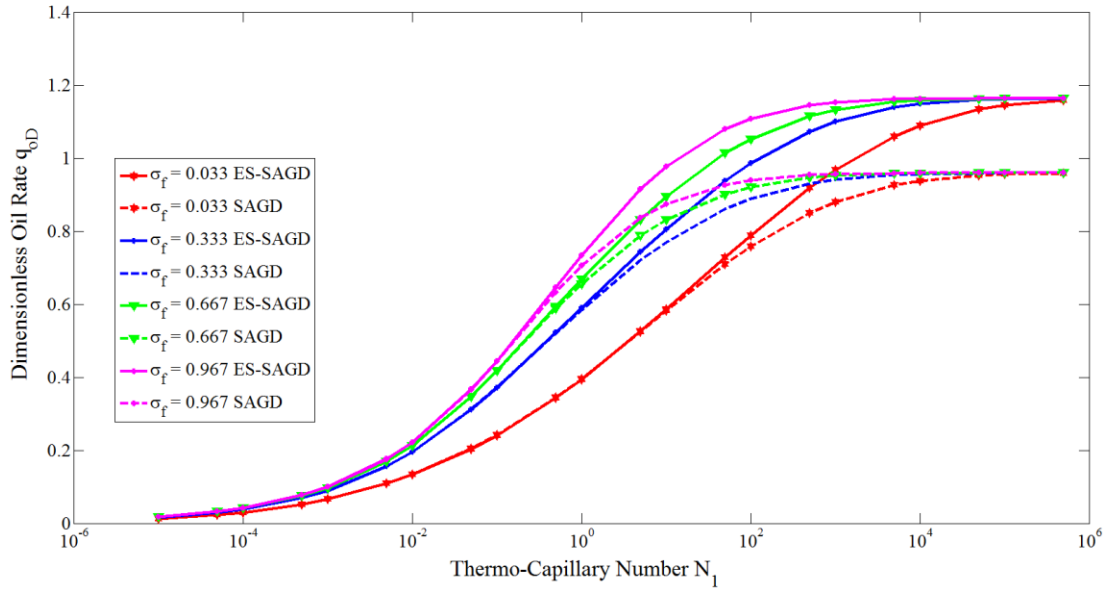

Figure 5.11: Plot showing the sensitivity of the dimensionless oil rate vs. thermo-capillary number to the fractional decrease in interfacial tension σ_f

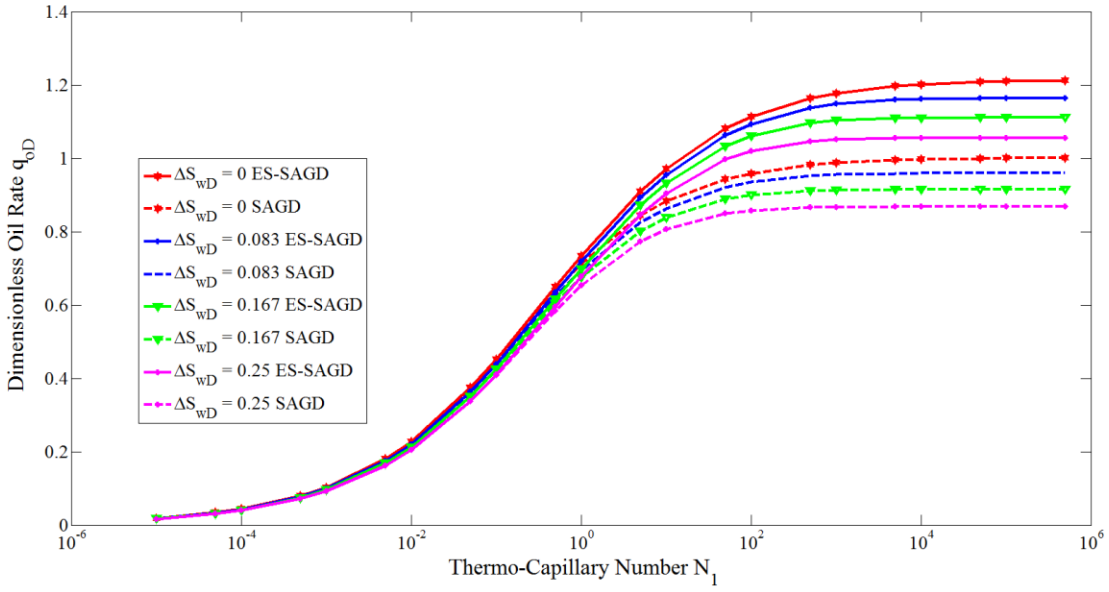

Figure 5.12: Plot showing the sensitivity of the dimensionless oil rate vs. thermo-capillary number to the dimensionless initial mobile water saturation ΔS_{wD}

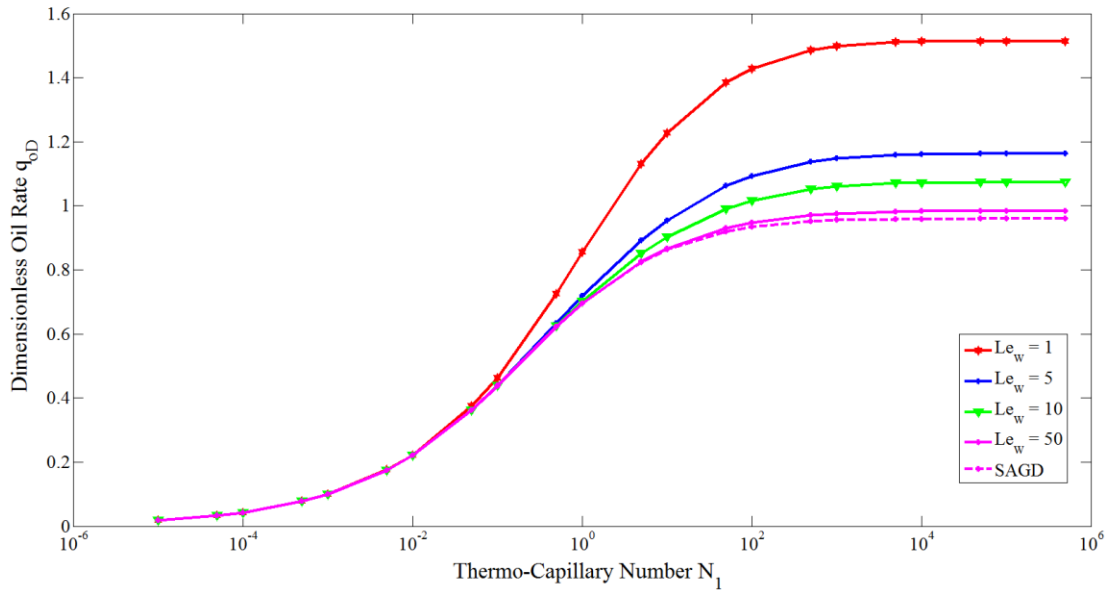

Figure 5.13: Plot showing the sensitivity of the dimensionless oil rate vs. thermo-capillary number to the condensate Lewis number Le_w

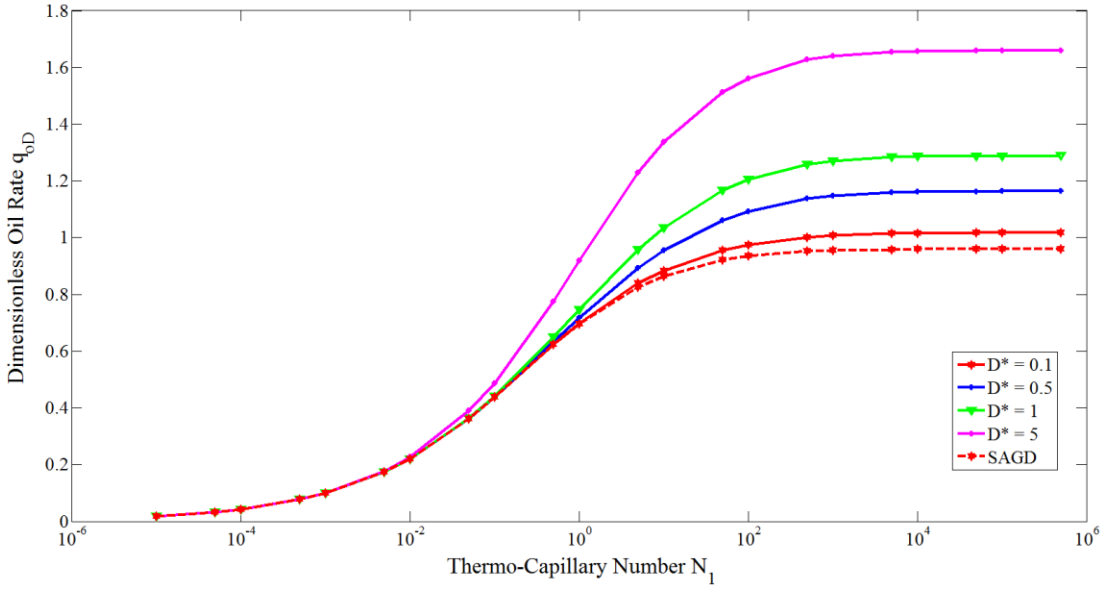

Figure 5.14: Plot showing the sensitivity of the dimensionless oil rate vs. thermo-capillary number to the dimensionless dispersion number D^*

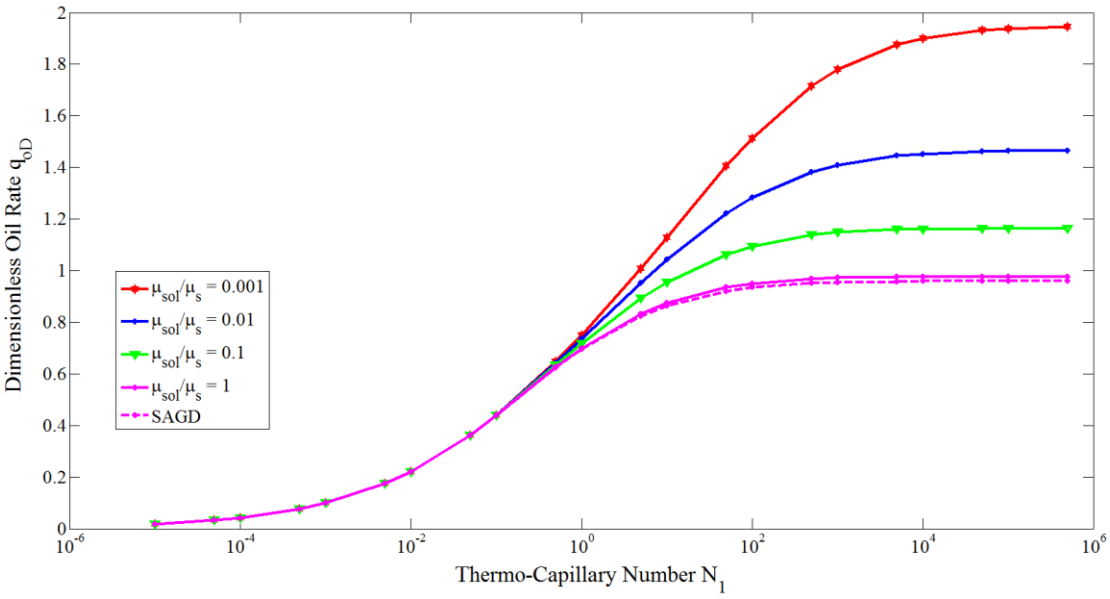

Figure 5.15: Plot showing the sensitivity of the dimensionless oil rate vs. thermo-capillary number to the viscosity ratio $\frac{\mu_{sol}}{\mu_s}$

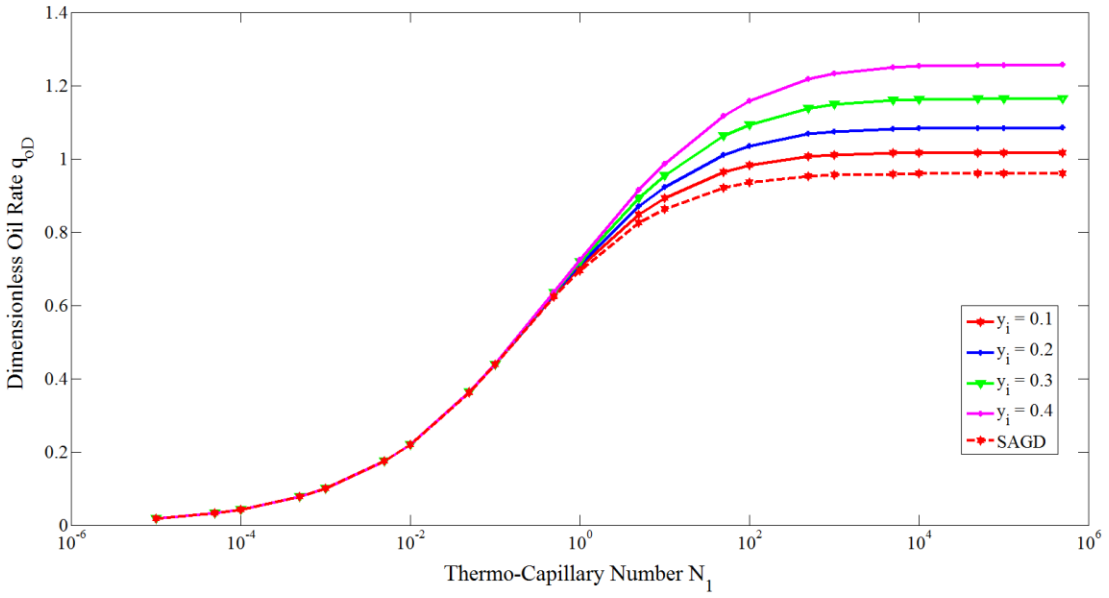

Figure 5.16: Plot showing the sensitivity of the dimensionless oil rate vs. thermo-capillary number to solvent concentration in the vapor phase y_i

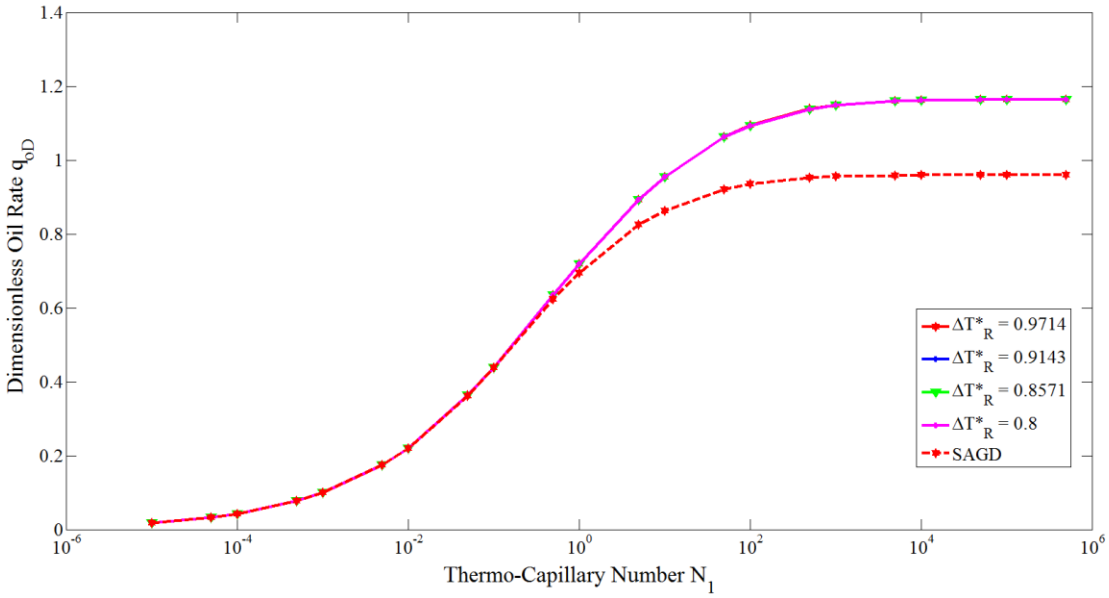

Figure 5.17: Plot showing the sensitivity of the dimensionless oil rate vs. thermo-capillary number to the dimensionless temperature difference ΔT_R^*

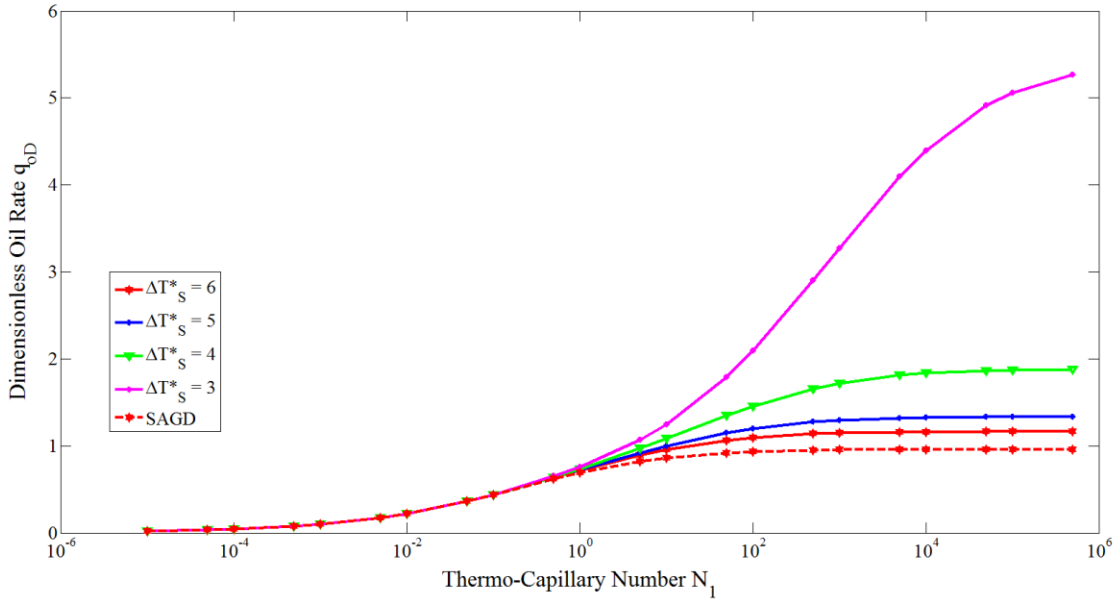

Figure 5.18: Plot showing the sensitivity of the dimensionless oil rate vs. thermo-capillary number to the dimensionless temperature difference ΔT_S^*

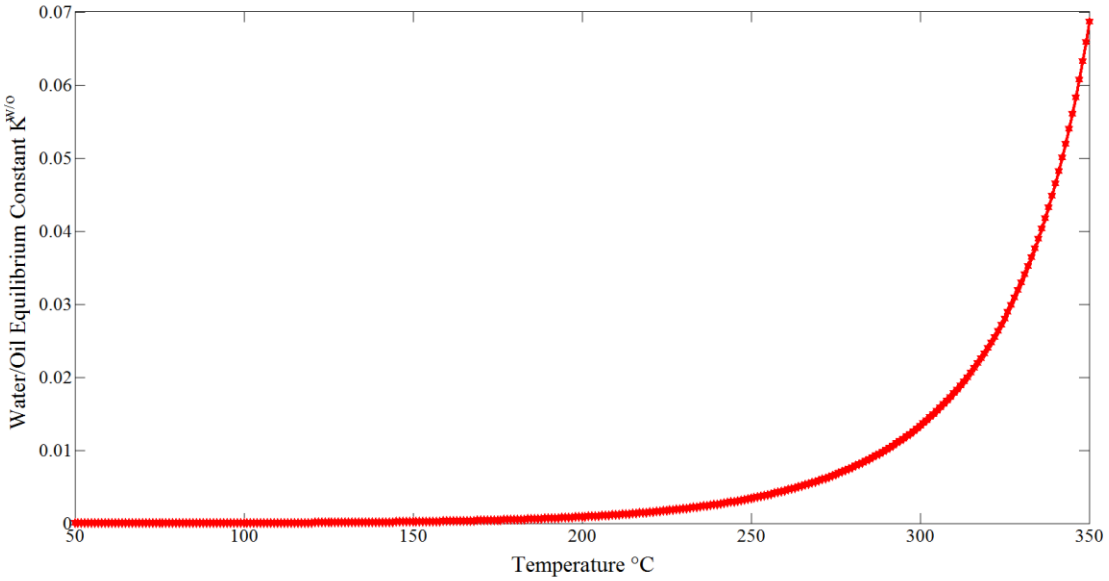

Figure 5.19: Plot showing the water/oil equilibrium constant $K_i^{w/o}$ from reservoir to steam temperature

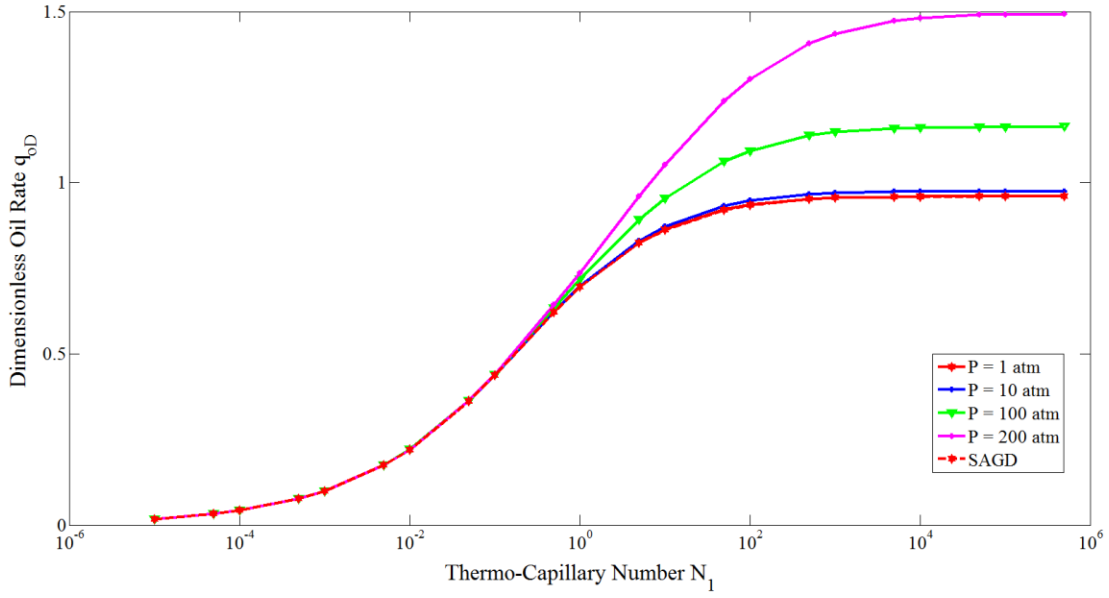

Figure 5.20: Plot showing the sensitivity of the dimensionless oil rate vs. thermo-capillary number to reservoir/injection pressure P

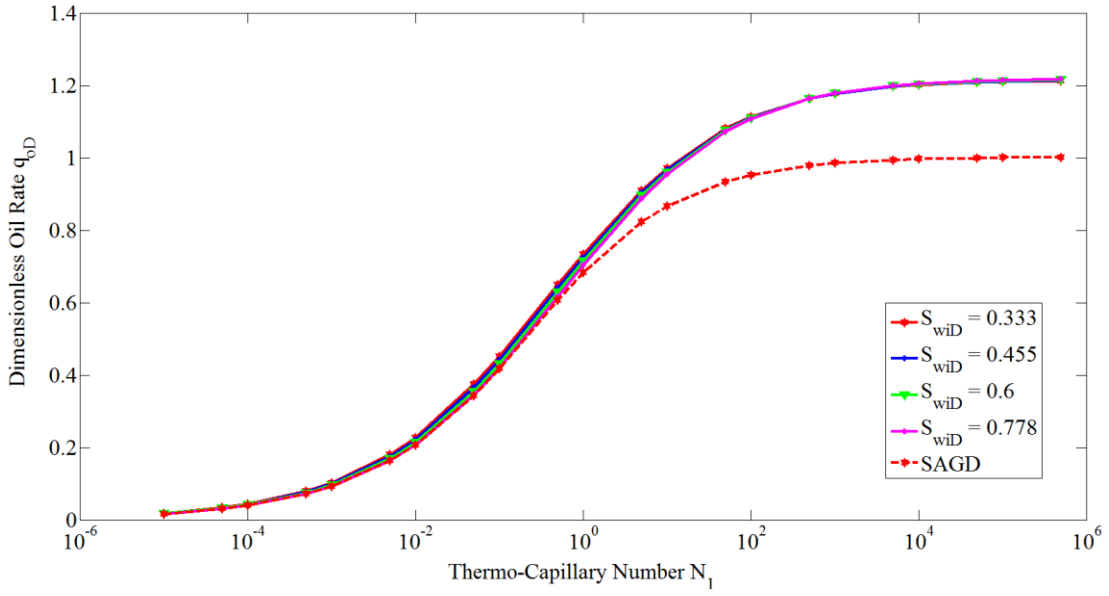

Figure 5.21: Plot showing the sensitivity of the dimensionless oil rate vs. thermo-capillary number to the dimensionless initial water saturation S_{wiD}

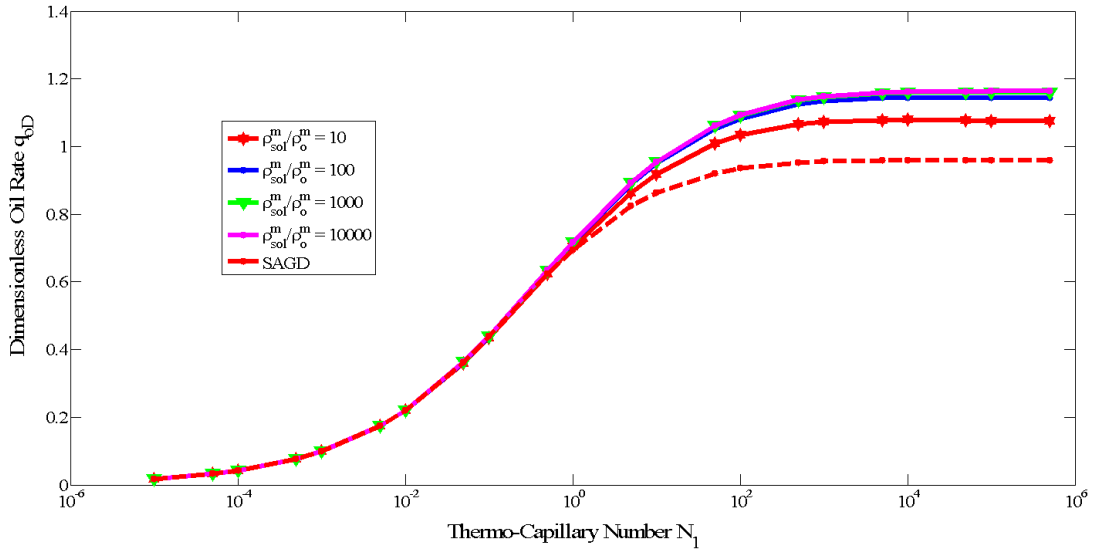

Figure 5.22: Plot showing the sensitivity of the dimensionless oil rate vs. thermo-capillary number to the ratio of molar densities $\frac{\rho^m_{sol}}{\rho^m_o}$

5.3 Summary and Significance of Work

In this work, we have developed a model for the ES-SAGD process that accounts for the transport of solvent into the bitumen phase by the Marangoni or thermo-capillary imbibition. Our results indicate that there exists a thermo-capillary number corresponding to a given set of reservoir parameters below which the ES-SAGD process does not fare better than the SAGD process. This is a crucial conclusion from this work and illustrates the importance of the physics of thermo-capillarity during the ES-SAGD process.

Our results show that certain dimensionless groups control the degree of additional recovery from the ES-SAGD process over SAGD. One of these dimensionless groups is the condensate Lewis number Le_w which revealed that heterogeneity can aid the ES-SAGD process by transporting the hydrocarbon solvent beyond typical dispersive

length scales of a homogenous reservoir, thereby aiding increased solvent transfer from the condensate to the bitumen and consequently improved bitumen recovery. This effect of the condensate Lewis number is also enhanced by the dimensionless solvent dispersion coefficient in the bitumen phase D^* where the higher this number is, the higher the bitumen recovery we get since more bitumen volume is contacted by the solvent. Unlike the SAGD process, the ES-SAGD rates are sensitive to the Butler m parameter because of the effect of solvent coupling with bitumen viscosity behavior. If m is small, there is little room for the solvent to influence the bitumen viscosity, and hence the dimensionless bitumen rates is hardly changed, while the larger the value of m, the more room the solvent has to influence bitumen viscosity and hence its dimensionless rates. This result is quite counterintuitive and would have been difficult to obtain through any other means.

Another dimensionless group that produced very interesting results is the viscosity ratio μ_{sol}/μ_s where it is seen that the closer this value is to or greater than unity, the less effective the ES-SAGD process will be over SAGD.

Not all dimensionless groups were found to influence bitumen rates and these results can be summarized by updating (5.55) as

$$q_{oD} = f\left(N_1, a, m, n, \kappa, \sigma_f, P^*, \left(\frac{\mu_{\text{sol}}}{\mu_s}\right), Le_w, D^*, \Delta T_s^*, K_i^{w/o}(T), \frac{\rho_{sol}^m}{\rho_o^m}\right) \tag{5.57}$$

and shows that the ES-SAGD process has eight (8) more parameters over the SAGD process to completely describe its physics.

This work will also find strong application in scaled experiment design and improved field scale recovery predictions and can be used as a fast ES-SAGD proxy for history matching, optimization and uncertainty analysis.

Chapter 6: The Effect of Emulsion Formation and Transport on Heat Transfer during SAGD

Even in the absence of flow barriers and other reservoir heterogeneities, current SAGD models underestimate heavy oil recovery, and are generally seen to be inaccurate for predicting important production characteristics like steam oil ratio (SOR) and water oil ratio (WOR), when compared against experimental or field data. Sasaki et al. (2001a) report that the simulation model for their laboratory set up yielded lower oil recovery than what was measured in the laboratory. They further observed that water-in-oil (W/O) emulsions are formed at the steam-oil interface in their experiments (Sasaki et al. 2002). It is our premise that transport of these emulsion droplets into the bitumen phase facilitates convective heat transfer resulting in improved recovery. Incorporating these effects is crucial to accurately modeling the SAGD process.

Unfortunately, the physics of emulsion formation and transport in porous media is not well understood, and current simulators do not have the capability to directly model such effects. We present a new approach that approximates the effect of emulsion droplets on heat transfer. In this approach, the emulsion droplets are modeled as additional chemical species and the dispersion of these species and adsorption phenomena is implemented in this paper. This model utilizes the features available in most commercial simulators in order to model emulsion generation, propagation and coalescence in porous media. The results from such a mechanistic simulation are compared against published SAGD experimental data. Our results show significant improvement from previous SAGD models and bolster the argument that emulsions are responsible for a key heat transport mechanism during SAGD.

6.1 Background

The mechanisms of heat transfer and hence heavy oil production by application of thermal recovery methods has been the subject of extensive research (Marx and Langenheim 1959), (Mandl and Volek 1969). Two main heat transfer mechanisms have been identified;

- Conductive heat transfer from the steam and condensate interface to the heavy oil and reservoir rock.
- Convective heat transfer at the interface of the flowing fluids and also at the producing well bore, due to fluid acceleration. The convective heat transfer at the interface, especially at the sides of the chamber, is due to the countercurrent flow of steam at the condensate interface and hence quite efficient resulting in the thickness of the condensate interface being larger at the base (near the producer) than at the top (Butler, 1987).

The period of purely conductive heating is quite short and several authors have attempted to quantify the time over which the predominant mode of heat transfer transitions from conductive to convective (Mandl and Volek 1969). However, such analysis generally fail to take into account complex mechanisms at the steam/oil interface such as the formation of water-in-oil (W/O) emulsions (Sasaki et al., 2002), which are non-equilibrium, thermodynamically unstable phases, and differ in this regard from the thermodynamically stable micro-emulsions of chemical flooding EOR. It is speculated that these emulsions are formed at the steam/oil interface due to shear induced instability (Raghavan and Marsden 1971a) at the interface and then transported into the bitumen phase by convection (dispersion) as discussed later.

Modeling this process of in-situ emulsification is quite challenging, because the physics of emulsion formation and transport in porous media is not yet fully understood. We have attempted to model this process mechanistically, accounting for its formation, propagation and coalescence in the reservoir. Our assumption is that the emulsions form at time $t > 0$, and then, its effect on production is allowed to vary with time. The incipient conditions leading to the formation of the emulsions e.g. the slope of the walls of the steam chamber are not taken into consideration for the formation of the emulsion. The slope of the chamber wall determines the extent of shear experienced by the fluid at the interface and thus would control the rate of emulsion formation. However, to model the details of that process would require sophisticated analytical modeling such as that by Raghavan and Marsden (1971b). The objective of this chapter is to develop a viable numerical modeling scheme that would serve as a tool for studying the sensitivity of emulsion formation to various reservoir and fluid parameters.

Sasaki et al. (2002) used an optical fiber scope to visualize the interface of the steam chamber and their results showed that W/O emulsions formed at the interface as seen in **Fig. 6.1**. The emulsions are seen to track the walls of the steam chamber interface and do not travel far into the undisturbed bitumen phase. If this is the case, then W/O emulsification will also be a short length-scale process and hence is expected to influence SAGD process performance.

Our goal is to develop a model that can be implemented in current, commercial simulators. The challenge would be to approximately represent the physical processes involved during emulsification by the closest analogous processes available in current simulators. For this work, we decided to use the thermal simulator CMG-Stars™ since we are more interested in the heat transfer effect of the emulsions on heavy oil recovery.

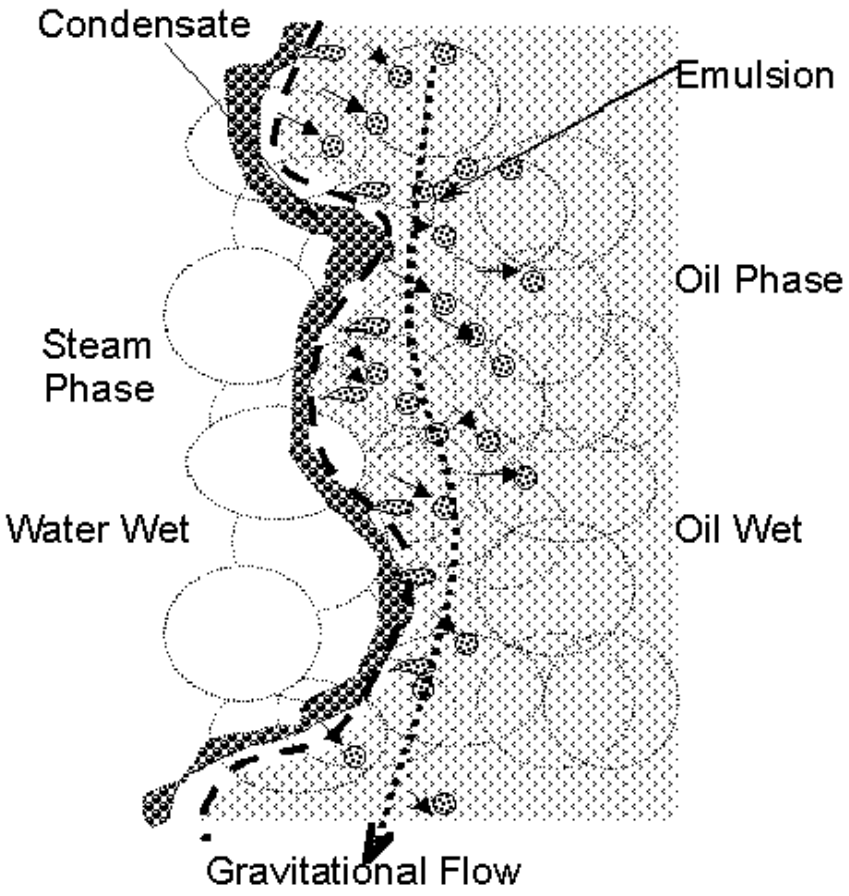

Figure 6.1: Schematic representation of the steam chamber interface showing the presence of W/O emulsions at the steam chamber interface courtesy of Sasaki et al. (2002)

6.2 Mechanistic Model

A black-oil model is used to describe the fluids. Since steam is injected in the vapor phase and it subsequently condenses along the wall of the steam chamber, water is allowed to exist both in the aqueous and gaseous phases. Two components, EMULSW and EMULSO are used to describe the state of the emulsion droplets i.e. EMULSW is the fraction of injected steam that condenses and has the potential to form emulsions, while

EMULSO forms the water-in-oil (W/O) emulsions and is the emulsion component in the bitumen phase. The conversion of EMULSW to EMULSO occurs in the aqueous (condensed) phase, and only EMULSO is allowed to partition into the bitumen phase, and also be adsorbed on the rock surface. Adsorption of EMULSO on the rock surface signals the destruction of that species i.e. its adsorption is irreversible and is modeled as such. This adsorbed water is not added to the immobile water phase, but exists as water species in the adsorbed phase. EMULSW and EMULSO have the same properties as water. We decided to separate EMULSW from water to better control and hence effectively introduce the kinetics of conversion to EMULSO. This mimics the dynamics of emulsion formation.

A choice has to be made for the reference phase of EMULSO and this choice is determined by two critical factors affecting the emulsification process. The first process is enhancement of oil relative permeability due to the coalescence of EMULSO. This can be modeled more effectively if the reference phase for EMULSO is aqueous, and if we can model relative permeability curves as a function of phase composition (this can be done by defining several interpolation sets as a function of composition, for relative permeability curves in CMG-Stars^{TM}). The second process is the increase in phase viscosity due to emulsification. If this is to be modeled accurately, then the reference phase for EMULSO should be oleic. CMG-Stars^{TM} uses both linear and non-linear mixing rules for its viscosity modeling, which usually ensures the phase viscosity is some mole fraction function weighted average of the component viscosities (CMG 2011). This is adequate for most miscible systems but inadequate for emulsions due to the reason stated above. However, if we can model the viscosity of the emulsified phase separately, we can then use non-linear regression to fix what the mole fraction functions should be in order for CMG-Stars^{TM} to accurately reproduce the flowing emulsion viscosities. We see

that such mole fraction functions (based on the continuous phase) should be greater than unity. Also, we can still model enhanced oil relative permeability, albeit less effectively using the oleic phase as reference for EMULSO. Consequently, we proceeded with associating the EMULSO species to the oleic phase.

The viscosity of the emulsified oil has to be greater than that of BITUMEN (continuous phase, see Table 6.1) viscosity μ at least in the region where the bitumen viscosity has been reduced due to contact with steam. This emulsion viscosity μ^* is modeled using Taylor's (1932) equation, which is an enhancement of Einstein's (1906) and (1911) equations, taking into account the viscosity of the dispersed phase μ', where φ is the (small) fraction of the volume occupied by the dispersed phase.

$$\mu^*/\mu = 1 + \left(\mu + \frac{5}{2}\mu'\right)\varphi \Big/ \left(\mu + \mu'\right) \qquad (6.1)$$

Equation (6.1) becomes Einstein's formula when μ'/μ tends to infinity (Oldroyd 1953). Non-linear regression was then used to match the results reported in Sasaki et al. (2002) using the non-linear mixing rule for phase viscosities in CMG-Stars™. In using equation (6.1), we have assumed that the interactions between the dispersed and continuous phases in an emulsion are independent of temperature and pressure.

The effect of emulsification on recovery has to be modeled in 3 steps:

- Generation
- Propagation
- Coalescence

The actual physical mechanism for formation of emulsion droplets is likely to be instabilities caused at the steam/oil interface due to the vast differences in viscosity of the

two fluids. There should be a repose angle of the steam chamber wall at which the shear instabilities exceeds a threshold in order to initiate emulsion formation. This generation step is approximated using an appropriate "physical" reaction to form the emulsion droplets. As physical measurements for the onset of emulsion formation are unavailable, we will treat the kinetic parameters controlling the onset of emulsion droplet formation in the simulator as sensitivity parameters. The propagation step is described by dispersion, since the formed emulsions are transported through the porous media, and the coalescence step is represented by adsorption, since we cannot expect the emulsions to be stable indefinitely in the porous medium.

Table 6.1: Black-Oil Fluid Model with Emulsion Species

Phase / **Component**	**Aqueous**	**Oleic**	**Gaseous**	**Adsorbed**
WATER	X		X	
BITUMEN		X		
EMULSW	X		X	
EMULSO	X	X		X

We have used the term "physical" to describe the reactions producing the emulsion droplets, as these are not true chemical reactions; however we find such representation quite suitable for our purposes as will be discussed later. It is worthy to note that this is currently the only way to represent in-situ emulsion formation in CMG-Stars™.

We understand that the use of dispersion to model macro emulsion mass transport is fundamentally not correct, since dispersion phenomena by definition can only occur in fully miscible systems. However, we have modeled the emulsion droplets as chemical

species within the same miscible phase, and hence, this approximation maybe appropriate. This is the closest process in CMG-Stars™ that can model the relatively higher velocity in the oil phase (than ordinary convection due to the growth of the steam chamber) of the emulsion droplets to the condensate interface. This is necessary (as we will show later) to prevent the emulsion droplets from being entrained inside the steam chamber.

The adsorption step is crucial for two main reasons. First, it helps in limiting the effective life of the emulsion droplets for transmitting heat into the bitumen. Second, the relative permeability of bitumen is increased due to an increase in wettability upon coalescence of the emulsion droplets on the rock surface. However, it is expected that the volume of water condensed due to the adsorption process will be quite small to cause any significant change in the bitumen relative permeabilities.

6.2.1 Emulsion Generation

The emulsions are actually produced at the condensate interface. A fraction of condensed water, (EMULSW) due to instability at the interface, forms water-in-oil (W/O) emulsion droplets, EMULSO. If we assume that the condensate is pure water (or brine), then a possible approach to model this transition so as to conserve mass is

$$1\ \text{EMULSW} \rightarrow 1\ \text{EMULSO} \qquad \Delta H_{EMULS} = +\text{ve} \tag{6.2}$$

Here, ΔH_{EMULS} is the enthalpy of emulsification and its sign is justified by the fact that these emulsion droplets are actually heat sources that propagate into the bitumen. However, in specifying ΔH_{EMULS}, we are constrained by the fact that the emulsion droplets do not carry

any more temperature than what is available at the steam-oil interface. If we assume this reaction to be simple, then the reaction kinetics can be described as

$$-r_{\mathrm{EMULSW}} = kC^{\alpha}_{\mathrm{EMULSW}} \tag{6.3}$$

If the condensate interface is composed of pure water (or brine), then the reaction must be elementary and $\alpha = 1$. However, the interface also contains low viscosity oil, and hence, we can expect a slight deviation from unity. The fitting parameters for the generation process will then be the mole fraction of EMULSW in injected steam ω, the rate constant k, reaction order α and enthalpy of emulsification $\Delta H_{\mathrm{EMULS}}$. Unfortunately, we do not have data for any of these and they will be treated as history match parameters.

K-values were used for partitioning EMULSO into the bitumen phase, and we found sixteen (16) K-value parameters adequate to model the pressure and temperature dependent mass transfer behavior of the EMULSO component at the condensate interface. A smaller number of K-values or K-value correlations could have been used that would still give a similar match for the cumulative oil recovery curve, but this would have been at a cost of accuracy in tracking the emulsion droplets at the steam-condensate-oil interface (see **Fig 6.15**).

6.2.2 Emulsion Propagation

3-D dispersion coefficients are used to describe the propagation of EMULSO through the bitumen phase. However, because the reservoir is assumed homogenous, the same value was used in all three (3) grid directions.

6.2.3 Emulsion Coalescence

Langmuir adsorption isotherm is used to describe EMULSO coalescence on the rock surface with compositions independent of temperature. This required seven (7) parameters characteristic of the isotherm and modeled in CMG-Stars™. An additional five (5) parameters were used to describe oil relative permeability enhancement by the use of two (2) relative permeability interpolation sets. Since Langmuir adsorption isotherm is used to describe equilibrium adsorption, we expect that not all the EMULSO component that is propagated through the interface will be adsorbed. However, any EMULSO adsorbed must be irreversible and this was ensured by forcing the residual adsorption to be equal to the maximum adsorption capacity (CMG, 2011).

A total of thirty two (32) fitting parameters were used to model the process of emulsion generation, propagation and coalescence and a schematic of the entire modeling process is shown in **Fig 6.2**.

6.3 Modeling Procedure

Due to a general lack of understanding of the emulsification process and its effect on recovery, we attempted to characterize the process based on available experimental or field data. Such an attempt will enhance our understanding of the underlying physics, quantify (at least in an approximate sense) the effect of emulsification on recovery and give us a feel for the sensitivities of model parameters on the emulsification process which in turn can be invaluable in designing future experiments to fully and accurately describe the process.

As in any characterization procedure, we however have to define a criterion for uniqueness and reasonableness of solution. We will address uniqueness by constraining

our model to the cumulative oil recovery measured in the laboratory experiment by Sasaki et al. (2002), and matching the corresponding production rate and water-oil ratio (WOR) data. The choice to fit with cumulative oil recovery ensures that the total recovery predicted by the mechanistic model is not greater than that of the actual experiment results. Reasonableness in the values of obtained model parameters is assumed if they are physically representative of the operating scale. We have used only the experimental data of Sasaki et al. (2002) to demonstrate the procedure in this work as this is the only data available where it was impossible to match SAGD rates due to the formation of W/O emulsions.

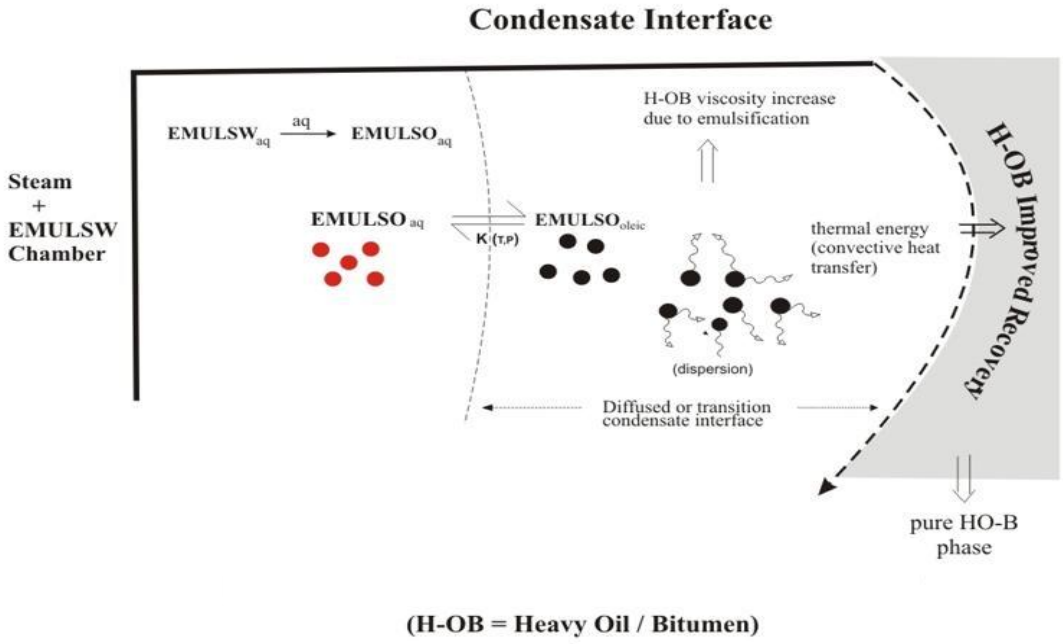

Figure 6.2: Schematic representation of the model for the water-in-oil emulsification mechanism at the steam chamber interface

6.4 Experimental Model

Sasaki et al. (1996, 2001 and 2002) performed SAGD experiments on a 300 x 300 mm 2-D square reservoir model. The model thickness was 4.5 mm and the distance between the injector and producer was set at 100 mm. Glass beads were used with a porosity of about 38% and permeability of 142,000mD, obtained using the Carman-Kozeny equation. Pure steam (100% quality) was injected at 105^0C and 121.3kPa, with the pressure difference between the injector and producer maintained at 20kPa. A schematic of Sasaki et al.'s (2002) experimental model showing the steam chamber is given in **Fig. 6.14**. Their cumulative recovery data is shown in **Figs. 6.6** through **6.10**.

6.5 Simulation Model

A 19 x 9 x 19 3-D grid model with equal sized grid blocks of dimensions 2 cm in the I-K direction (see **Fig 6.3** below) and 0.15 cm in the J direction was used to simulate the above experiment using CMG-Stars™. The 3-D grid was chosen to simulate convective heat loss from the acrylic resin model more accurately (Sasaki et al., 2001). The reservoir itself was contained in the grid block range (X = 3 to 17, Z = 3 to 17) which is colored blue (thermal rock type 1) in **Fig 6.3** and the rest being acrylic resin (red and thermal rock type 2). The 5th layer in the Y direction is the one that has the sand properties. The rest of the layers in the Y direction are present to model the heat transfer to the acrylic sand box material accurately. The reservoir range was also refined (2 x 2 x 2) to better simulate the reaction, heat and mass transfer going on at the steam chamber interface. The proposed model simulates transient conduction heat losses through the acrylic resin model more accurately, but differs (with respect to gridding) from the simulation model presented in Sasaki et al. (2001). The injector well is placed 10 grid

(refined) blocks above the producer while the producer was placed 3 grid blocks above the bottom of the reservoir to simulate Sasaki et al.'s model (2002). Both wells were placed centrally with respect to the reservoir as seen in **Fig 6.3**. The laboratory scale was used for the simulations.

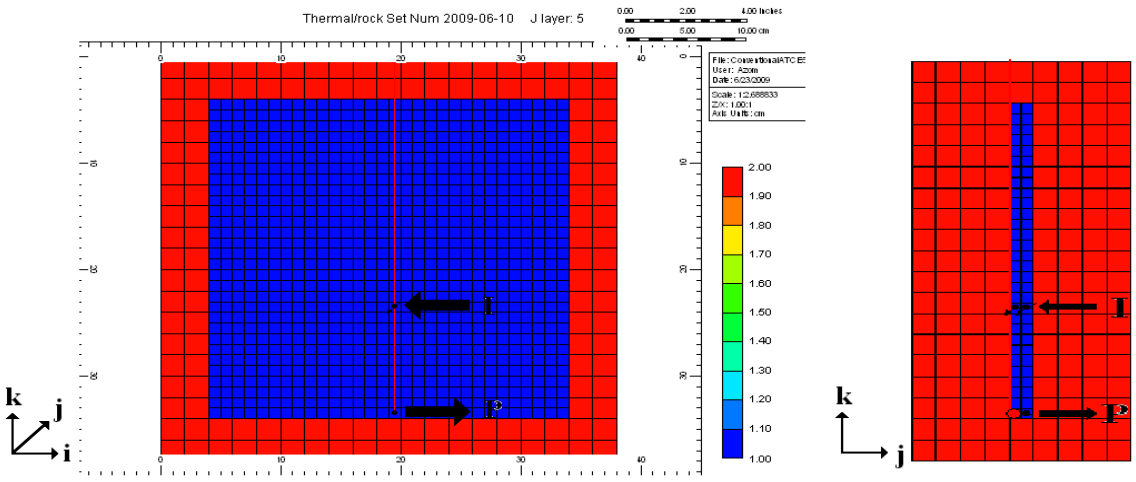

Figure 6.3: 2-D simulation grid showing well placement

Sasaki et al. (2001) report that linear relative permeability curves gave higher cumulative oil recovery and a better match to the observed production profile. We used this (**Fig 6.4**) as our base case (without adding emulsion species). We also used the more conservative (and more realistic) case of non-zero end points which they report gave a cumulative oil production of about 35 cm^3 which is less than the observed cumulative production of about 66 cm^3 in the experiment. Oil relative permeability enhancement was modeled using a convex relative permeability curve (**Fig 6.5**) which is characteristic of emulsified systems (Kovscek 2009)[11].

[11] Tony Kovscek pointed out that the convex oil relative permeability curves applied to oil-in-water (O/W) emulsion systems, but we will assume it to be so too for W/O emulsion systems and use a sensitivity analysis to determine its significance.

Steam injection was constrained using the experimental measured rates (in terms of cold water equivalent, CWE). Steam trapping was also ensured in the producer by setting a differential temperature constraint of 5^0C between the steam saturation temperature at the well bottom-hole pressure and the temperature of produced water. Both procedures are described in Sasaki et al. (2001).

6.6 Results and Discussion

Prior to modeling in-situ formation of water-in-oil (W/O) emulsions during SAGD recovery, we asked ourselves if there was any other reasonable mechanism that could explain the deviation of the simulation results reported in Sasaki et al. (2001) from the observed experimental data. This included allowing for possible measurement errors by Sasaki et al. (2001). To investigate these, we varied several reservoir parameters independently to obtain values that would better match the experimental results. The results are shown in **Figs 6.6** to **6.10**. The term "conventional" in all the figures represents the simulation results without taking into account emulsification. None of the fitting parameters gave reasonable results for this history match. For example, **Fig 6.6** shows that a permeability increase of more than 200% is necessary to fit the cumulative oil recovery of Sasaki et al. (2001), while **Fig 6.7** shows we will require a porosity increase of more than 150%. **Fig 6.8** shows similar analysis as above, but taking into account the fact that a variation is porosity is related to a variation in permeability for a pack of glass beads. We used the Carman-Kozeny relationship to tie both variations and we see that a more than 10% increase in porosity with a corresponding permeability increase of more than 54% gives recovery that is far less than that from the experiment. **Figs. 6.6**, **6.7** and **6.8** taken together tell us that porosity or permeability enhancement

cannot be the main mechanism of recovery for Sasaki et al.'s experiment. **Fig 6.9** shows that we need to reduce the overall heat transfer coefficient by a factor of more than 100% (i.e. no heat loss from the resin to the surrounding air, which would be analogous to the resin being a perfect insulator) and reduce the thermal conductivity of the resin by more than 75% to fit the experimental cumulative recovery curve. This tells us that simple conductive and/or convective heat transfer cannot fully explain the underlying mechanism of recovery. Also, if we decrease further the thermal conductivity of the resin to 90% with the overall heat transfer coefficient still reduced by 100% we see that at the end of the experiment, more oil is produced and the oil production profiles do not match over the time interval as seen in **Fig 6.9**. **Fig 6.9** also shows the cumulative oil recovery during the conduction dominated flow period which is followed by recovery during the convection dominated period (determined by the change in slope of the cumulative recovery curve). The results in **Fig 6.9** are important because they show that whatever the mechanism responsible for the improved recovery, it must exhibit time dependent variations in heat transfer since the cumulative oil recovery profile exhibits significant temporal curves. The physics of emulsification can explain such variations and the results of a history match using the mechanistic model are given in **Figs 6.11** through **6.13**.

Fig 6.11 shows the conventional simulation and our mechanistic simulation results compared against Sasaki et al.'s experimental results (2001). The mechanistic model gives a better match especially at early and late times. The oil production profiles generally exhibit two slopes corresponding to the two distinct periods of conductive and convective heating, as can be deduced from Butler's equation (1985). The early time match shows that in addition to better predicting recovery, the mechanistic model also predicts better, the time taken to transition to convective heating. The late time match is however suspect as can be seen from **Fig 6.12**, which shows the mechanistic model

predicts higher oil rates than the experiment. This could be due to some of the emulsion droplets (which did not coalesce) reaching the boundary of the reservoir which might not be the case with the experiment. The middle zone (**Fig 6.11**) clearly shows the existence of another mechanism that has not been adequately captured in our model. This mechanism could be thermo-capillary imbibition described in Chapter 4 as it could explain the reduced bitumen rates before convection by emulsification became the dominant heat transfer mechanism at later times. Notice that we could have tuned our results better, but that would have caused a prediction of total recovery greater than that obtained from the experiment.

Fig 6.12 shows the mechanistic model predicts the oil rates better than the model without emulsification. These results provide an indication of the importance of the additional heat transfer due to water droplets on recovery. The results also indicate that other effects such as permeability enhancement due to the coalescence of emulsion droplets need to be modeled more accurately so that the oil production increase due to emulsification is not exaggerated.

Water-Oil Ratio (WOR) would give an indication of the effect of emulsification on the steam chamber displacement and the interfacial recovery mechanisms. **Fig 6.13** shows that the mechanistic model results in lower WOR because of the transport of some of the condensed water into the bitumen phase in the form of emulsion droplets. In the simulation model without emulsification, on the other hand, the condensed steam is produced un-mitigated and that causes the WOR to continuously increase.

Figs 6.14 and **6.15** show the steam chamber for the experimental and mechanistic models at the end of the experiment $(t = 550 \text{ min})$. We see that the mechanistic model predicts the instability (steam fingering) occurring at the top of the steam chamber (**Fig 6.15**). **Fig 6.16** shows the spatial location of the modeled emulsion droplet species

(EMULSO). These droplets are seen to largely exist at the steam chamber interface as expected. This result is important because it signifies that the dispersion coefficients and the degree of adsorption used to match recovery were just about right to prevent steam from entraining the emulsion droplets and segregated flow of the emulsions in the oleic phase due to gravity. Such flow of the emulsions mainly along the steam chamber interface was also observed by Sasaki et al. (2002) in their experiments. The relatively larger thickness of the steam chamber interface at the bottom than at the top (**Fig 6.16**) suggests that emulsification tends to increase countercurrent flow (and hence, efficiency of heat transfer) of steam and condensate/flowing bitumen along the steam chamber walls. This must be caused by increased drag on the walls of the chamber due to the downward flow of emulsion droplets by gravity.

The onset of emulsification is not expected to be uniform throughout the steam chamber interface, and should in general be dependent on the magnitude of shear forces acting at the interface. This needs to be further investigated.

Table 6.6 shows the important results of the tuned parameters, and we see that each of them is physically realistic given the operating scale of the experiment. The significance of each of these parameters will be discussed in a sensitivity study below.

In an attempt to understand why the presence of W/O emulsions improves heat transfer at the steam chamber interface, we modeled a time snapshot of Sasaki et al.'s (2001) experiment using COMSOL^{TM} Multiphysics. **Fig 6.18** shows a COMSOL^{TM} Multiphysics simulation of the half chamber width where heat transfer has been coupled with porous media fluid flow by gravity. We approximated the fluid distribution as that in our simulations of Sasaki et al.'s (2001) experiment and introduced the emulsion droplets as small liquid water spheres having the same temperature as steam. **Fig 6.19** shows that the effective heat transfer coefficient increases as the fractional volume of the emulsions

in the bitumen phase increases and reveals an almost two-fold increase from the case without emulsions (i.e. at zero emulsion volume %). This is because the more the volumes of emulsion droplets, the more is the convective heat transfer component. This effect also plateaus at about 14% volume fraction and hence, there will exist an optimal emulsion concentration for the purposes of improved heat transfer at the steam chamber interface. **Fig 6.20** shows that the effective heat transfer coefficient also increases as the radius of the emulsion droplets increases and reveals an almost two-fold increase from the case without emulsions for a given fractional volume of emulsion droplets. This is because of increased surface area to heat transfer, thereby increasing heat transfer to the bitumen phase. **Figs 6.18** to **6.20** taken together explains why the presence of emulsion droplets enhances SAGD rates as the effective heat transfer coefficient at the steam chamber interface increases due to the presence of the emulsion droplets. This can also be better understood from the context of Butler's drainage equation (2.1) where a 100% increase in the effective thermal diffusivity will trump any increase in the effective viscosity of emulsified bitumen at steam temperature and the effective Butler m parameter due to the presence of emulsion droplets in the bitumen phase.

Table 6.2: Properties of experimental sand pack (courtesy Sasaki et al. (2001a)

Parameter	**Values**
Porosity, fraction	0.38
Average Permeability, K	1.42 x 105mD
Thermal Conductivity, λ	0.7 J/cm.min.^{0}C
Volumetric Heat Capacity	1.99 J/cm3.^{0}C
Resin Thermal Conductivity	0.13 J/cm.min.^{0}C
Resin Volumetric Heat Capacity	1.67 J/cm3.^{0}C
Overall Heat Transfer Coefficient from resin to surrounding air	0.041 J/cm^2.min

Table 6.3: Bitumen properties (courtesy Sasaki et al. (2001a)

Parameter	**Values**
Density	0.998 g/cm3
Molecular Weight	490 g/gmole
Compressibility	7.0 x 10-7 kPa-1
Thermal Expansion Coefficient	6.0 x 10-4 0C-1
Heat Capacity	411.7 J/gmol 0C
Critical Pressure	1,115 kPa
Critical Temperature	4940C
Capillary Pressure	0.0 kPa
Phase Equilibrium Constant	0.0

Table 6.4: Bitumen viscosity (courtesy Sasaki et al. (2001a)

Temp.	**Viscosity**	**Temp.**	**Viscosity**
^{0}C	cP	^{0}C	cP
15	15,000	65	996
20	9,200	75	624
25	6,913	85	418
35	4,015	95	286
45	2,412	105	200
55	1,495	120	60

Table 6.5: Initial conditions and saturation endpoints (courtesy Sasaki et al. (2001a)

Parameter	**Values**
Temperature	20.0 ^{0}C
Pressure	101.3 kPa
Oil Saturation fraction	1.0
Water Saturation fraction	0.0
Gas Saturation fraction	0.0
Reference Pressure	101.3 kPa
Reference Temperature	20.0 ^{0}C
S_{or} fraction	0.05
S_{wc} fraction	0.10
S_{gc} fraction	0.05

Table 6.6: Showing the final model results and tuned parameters

Parameter	**Tuned Values**
Rate Constant, k	0.12 min^{-1}
Reaction Order, α	1
Dispersion coefficients, D_L	1 cm^2/min
Enthalpy of Emulsification, ΔH_{EMULS}	30 J/gmol

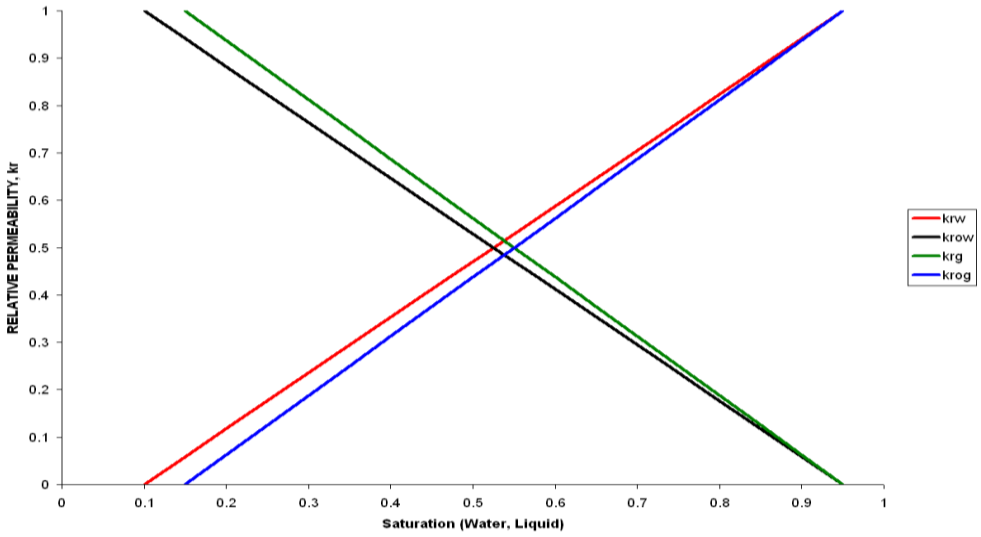

Figure 6.4: Linear relative permeability curves for sand pack model (used by Sasaki et al. 2001a)

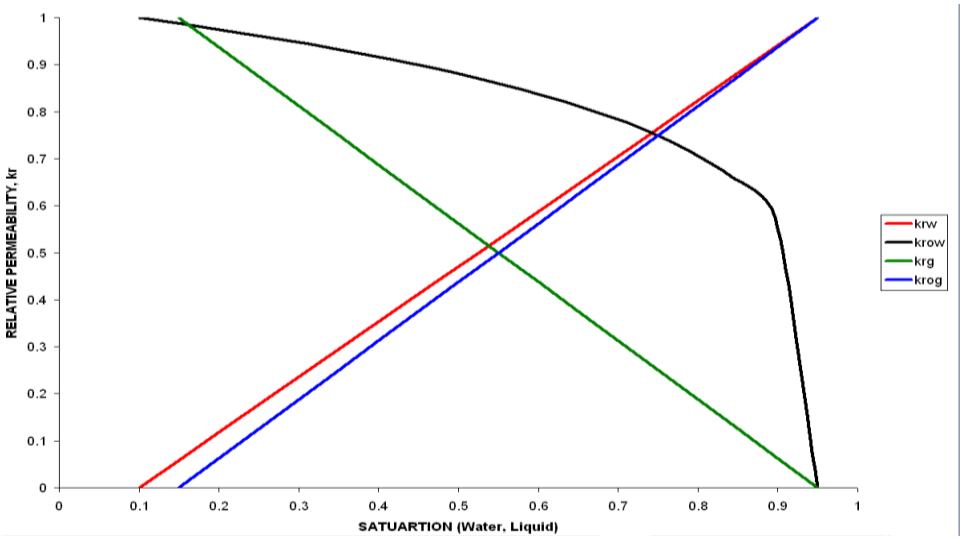

Figure 6.5: Modeling permeability enhancement to oil on coalescence of EMULSO (Kovscek, 2009)

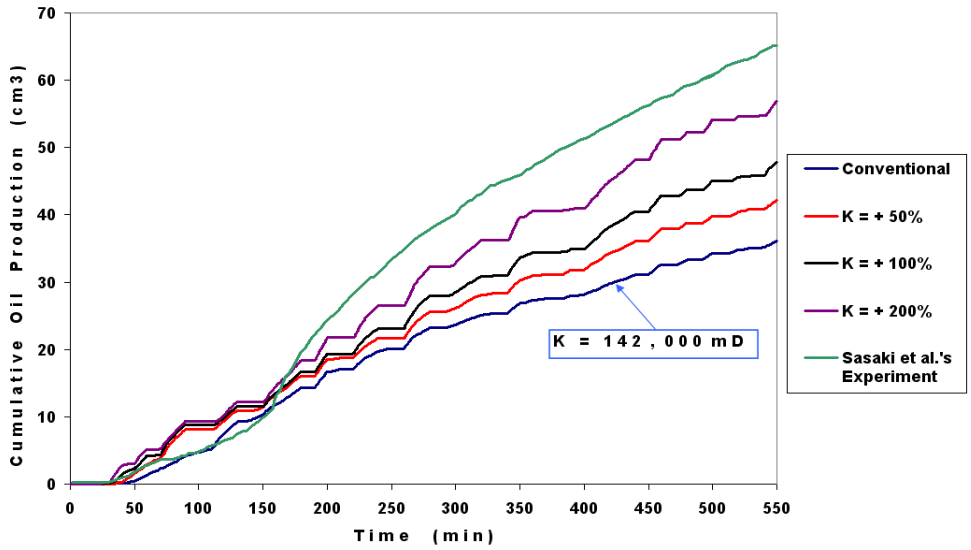

Figure 6.6: Comparison plot for cumulative oil recovery showing necessary fitting values of permeability without emulsion modeling

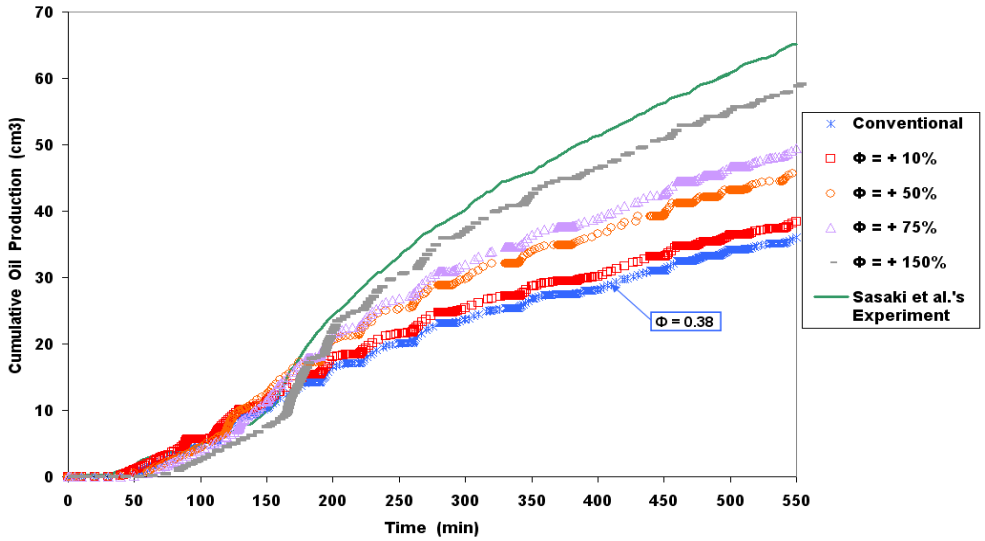

Figure 6.7: Comparison plot for cumulative oil recovery showing necessary fitting values of porosity without emulsion modeling

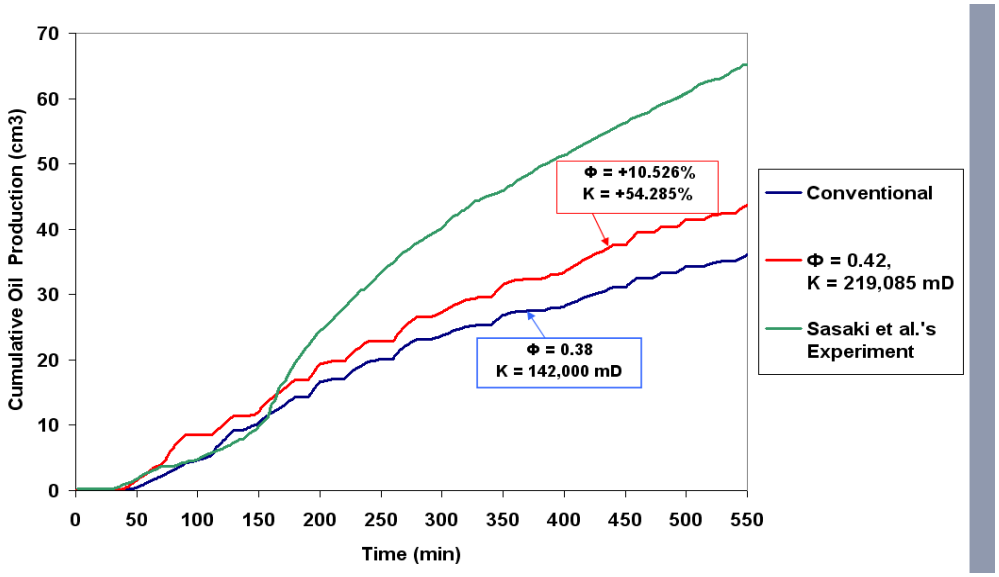

Figure 6.8: Comparison plot for cumulative oil recovery showing sensitivity to joint porosity and permeability modeling using the Carman-Kozeny relation without emulsion modeling

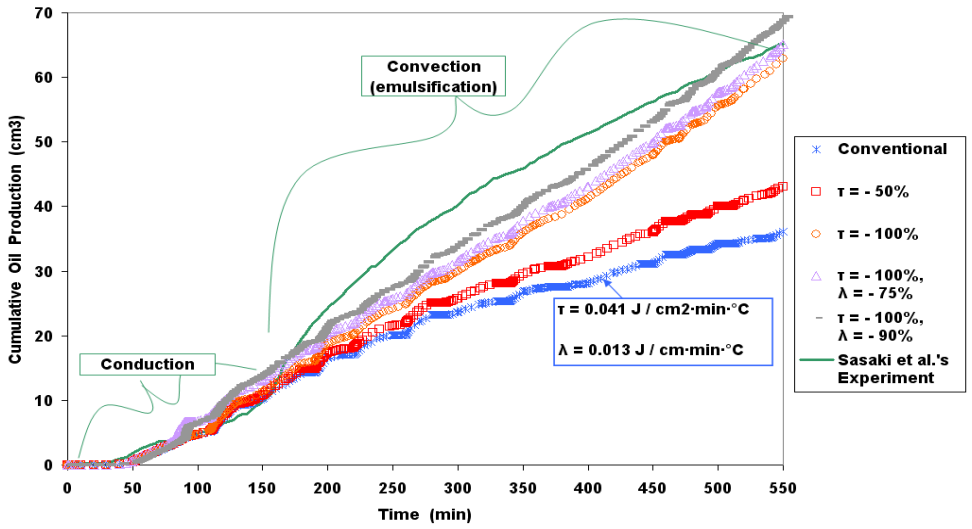

Figure 6.9: Comparison plot for cumulative oil recovery showing necessary fitting values for overall heat transfer coefficient τ and resin thermal conductivity λ without emulsion modeling

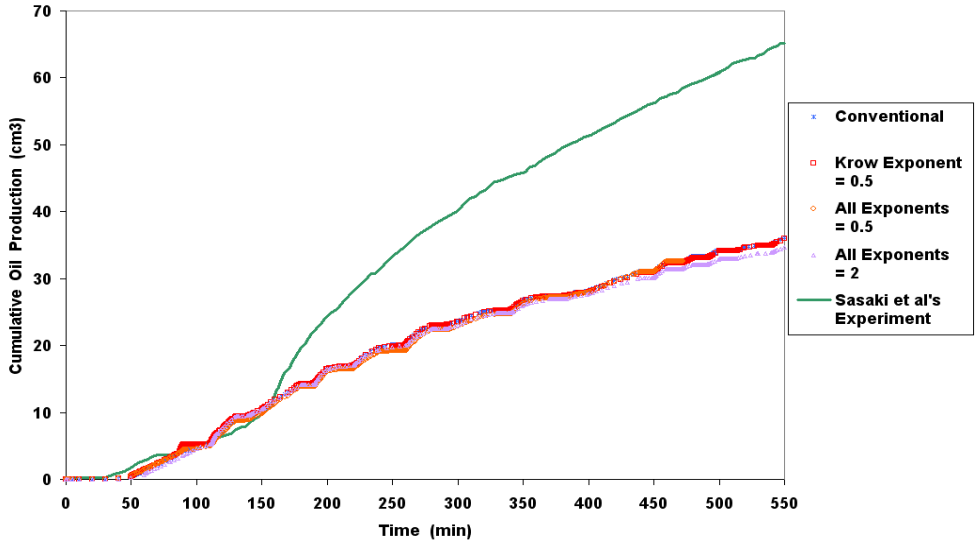

Figure 6.10: Comparison plot for cumulative oil recovery showing the sensitivity to the relative permeability exponent without emulsion modeling

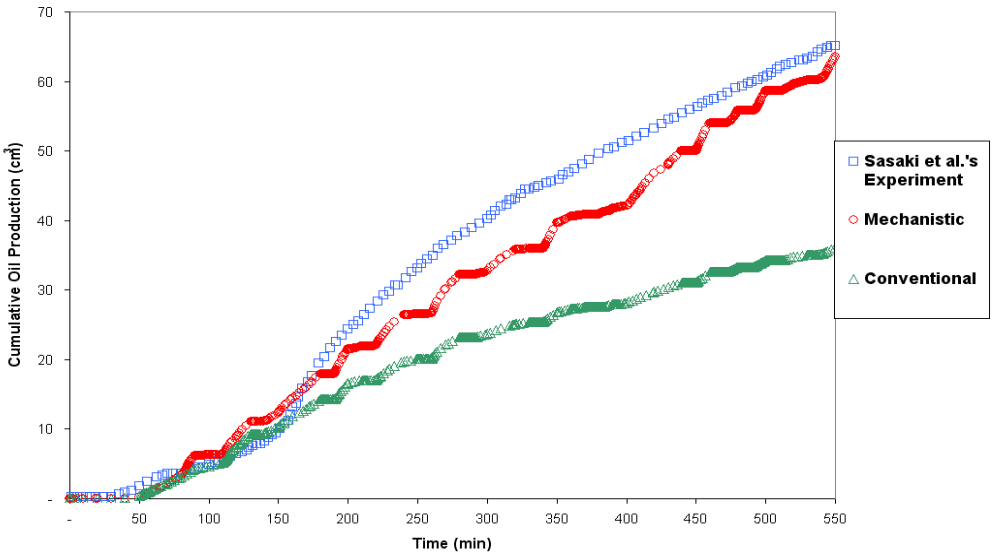

Figure 6.11: Comparison plot for cumulative oil recovery with the mechanistic model for emulsion formation, propagation and coalescence

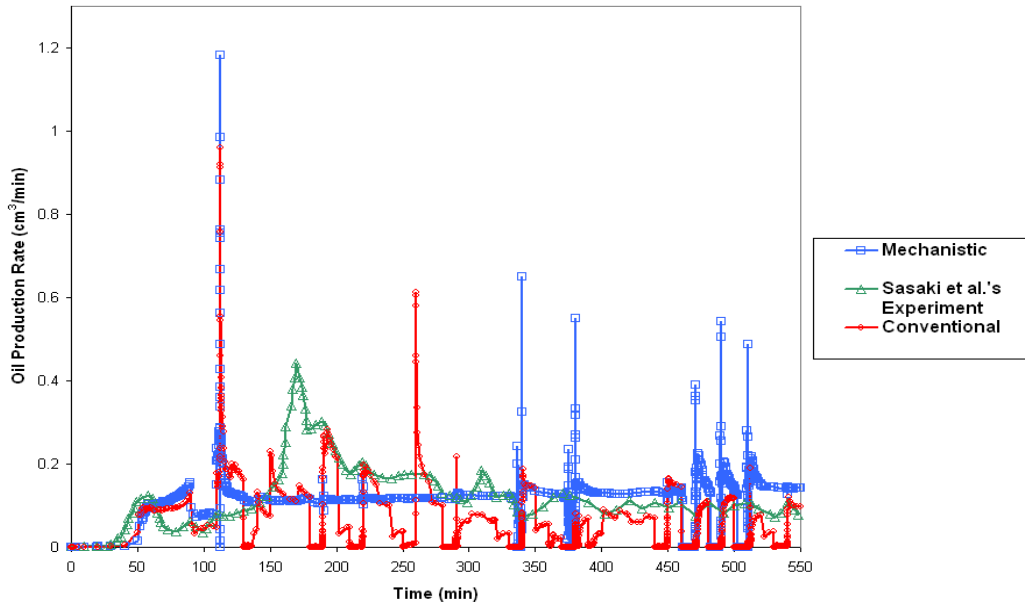

Figure 6.12: Comparison plot for oil production rate with the mechanistic model for emulsion formation, propagation and coalescence

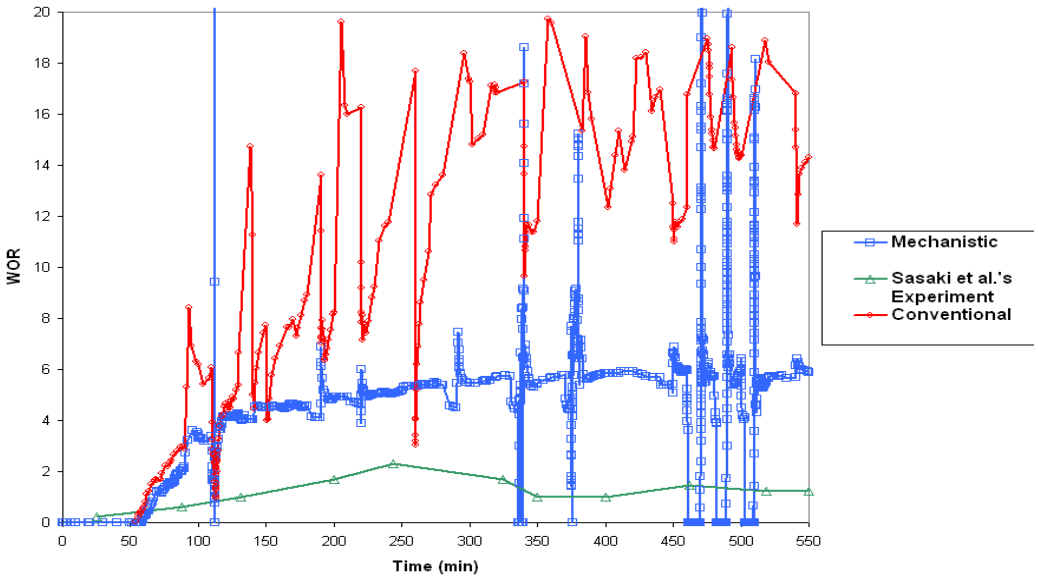

Figure 6.13: Comparison plot for water-oil-ratio (WOR) with the mechanistic model

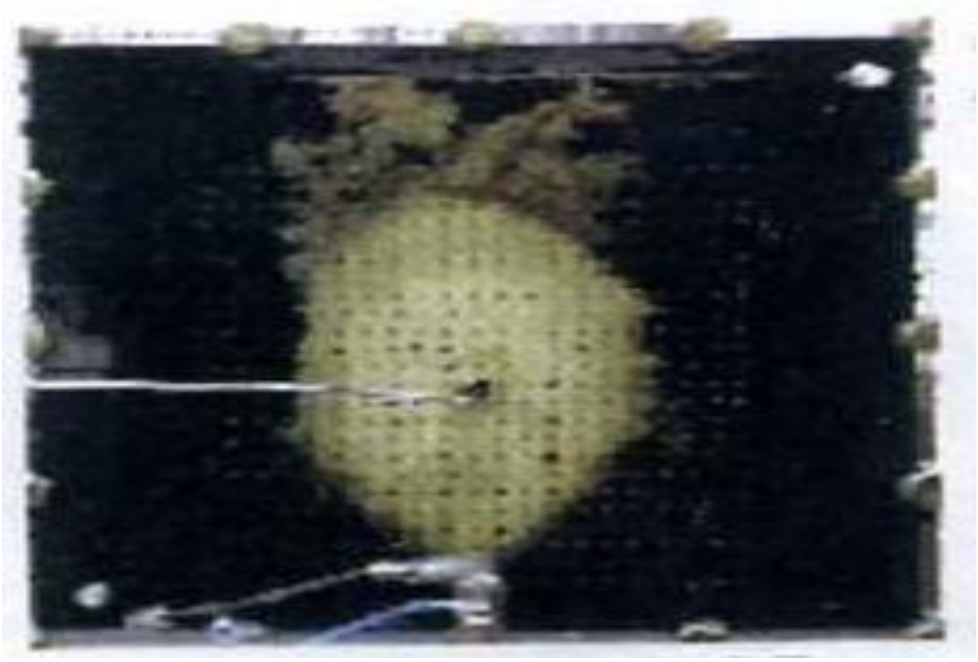

Figure 6.14: Steam chamber for experimental model at $t = 550\,\text{min}$ (courtesy Sasaki et al., 2001a) © 1996 Society of Petroleum Engineers

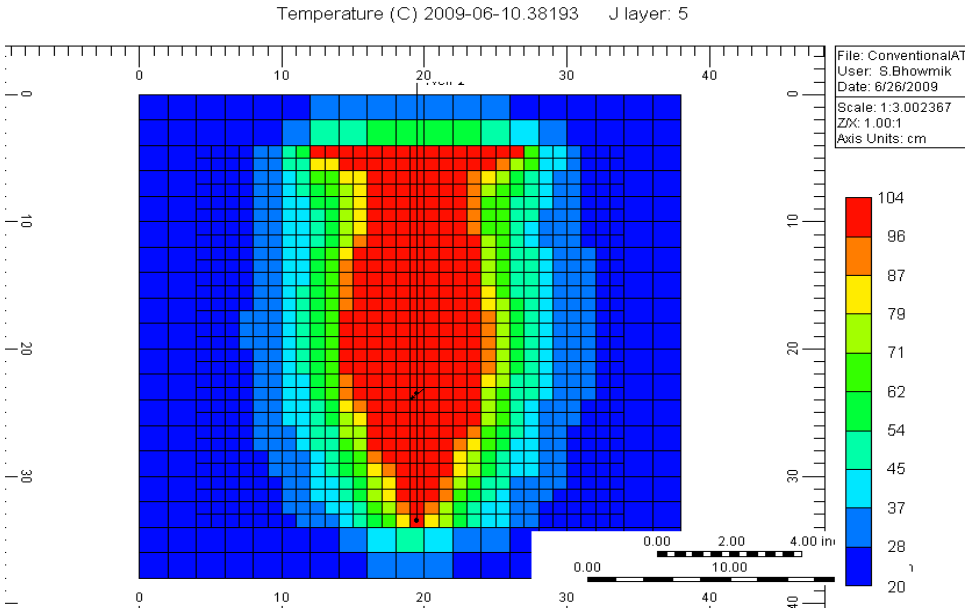

Figure 6.15: Steam chamber for mechanistic simulation model at $t = 550$ min

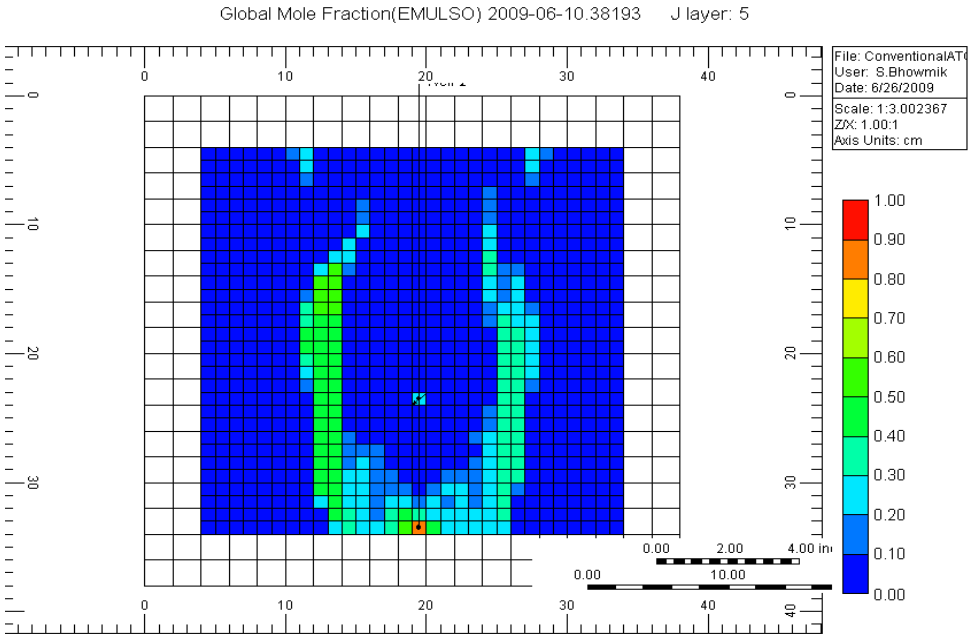

Figure 6.16: Spatial localization of emulsion (EMULSO) droplets at $t = 550$ min

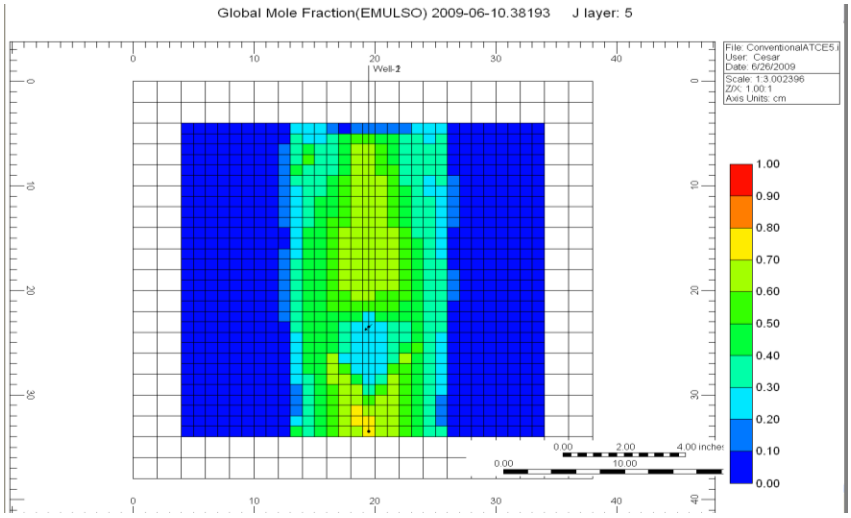

Figure 6.17: Spatial localization of emulsion (EMULSO) droplets with dispersion coefficient $D = 0$ cm^2/min at $t = 550$ min

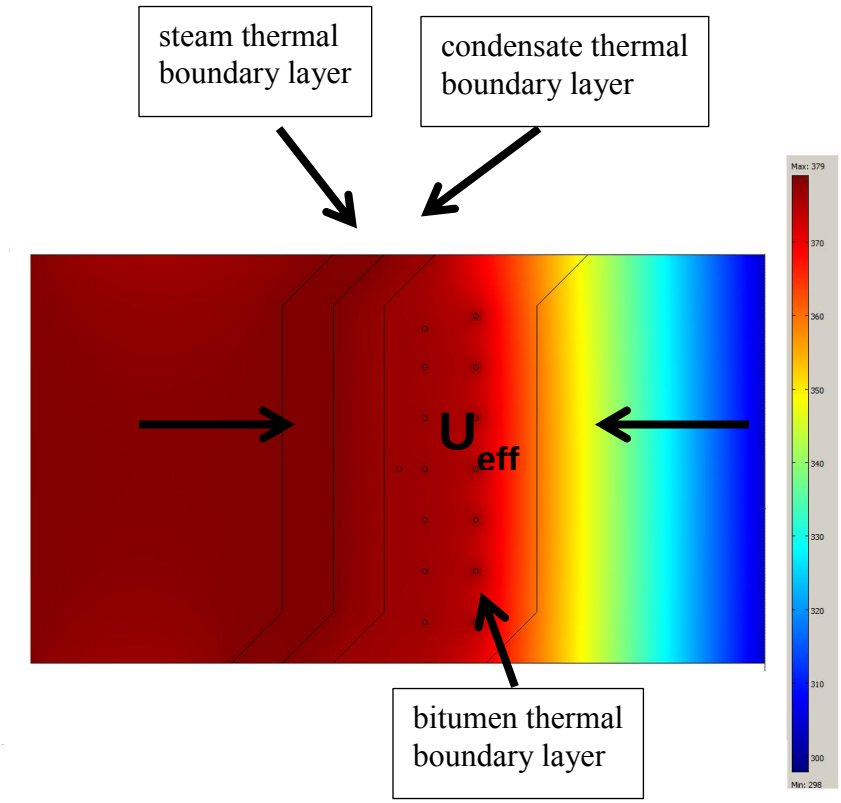

Figure 6.18: Half width of the steam chamber showing temperature (K) profiles using COMSOL^{TM} Multiphysics

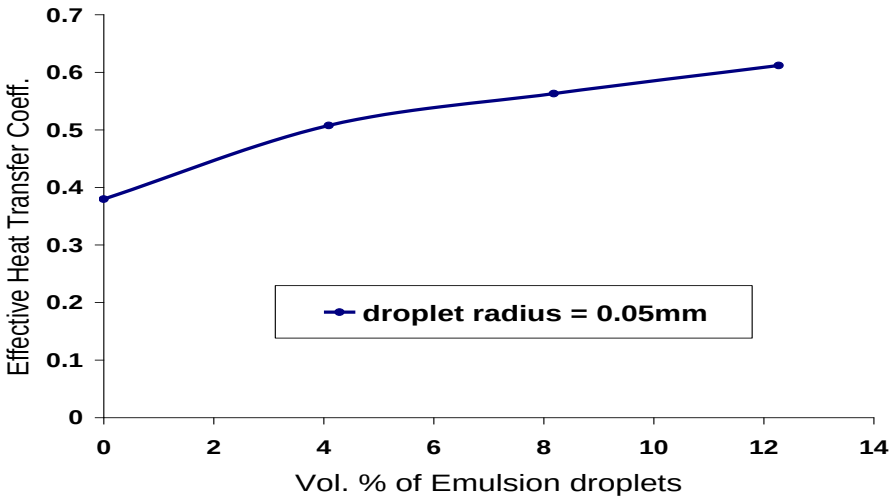

Figure 6.19: Effective heat transfer coefficient (W/m-K) vs. volume % of emulsion droplets for 0.05 mm droplets using COMSOL^{TM} Multiphysics

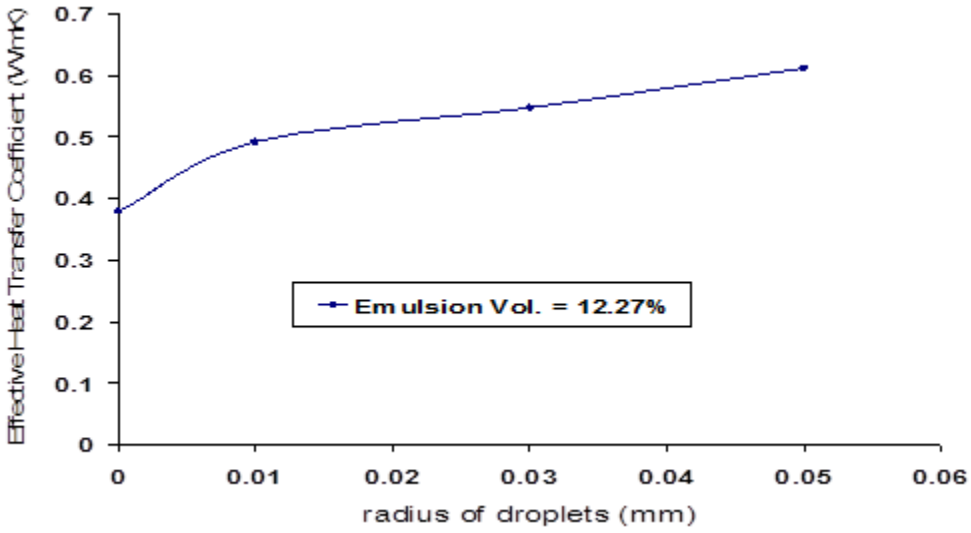

Figure 6.20: Effective heat transfer coefficient vs. radius of emulsion droplets for 12.27% emulsion volume using COMSOL^{TM} Multiphysics

6.6.1 Sensitivity analysis

We investigated the sensitivity of the recovery to various fitting parameters. Such analysis is necessary to expand our understanding of the emulsification process and to streamline the scope of future research. In the following, we systematically and independently varied all the fitting parameters. Stability was crucial in these simulations, and a change in one parameter sometimes caused the simulator to report higher material balance errors. In order to avoid this, we constrained our analysis only to results that resulted in stable and accurate simulations.

Fig 6.21 shows a fairly uniform increase in recovery with a decrease in reaction order. This increase is expected (concentration of EMULSW is always less than unity and hence a decrease in reaction order will always lead to an increase in reaction rate) but its uniformity indicates there is little resistance to spontaneous emulsification at the interface of the steam chamber (i.e. mass transfer is playing an insignificant role in the kinetics of emulsification for this system). Also, the uniformity can also mean that the reaction order is dependent more on the properties of the reservoir and less on the properties of the fluid that are changing with time. However, because the specification of chemical reaction is only to mimic the physical process of emulsion formation, the sensitivity of the recovery to various factors affecting viscous or density instability at the interface will be the subject of future research.

Fig 6.23 shows an interesting feature – the possible existence of a threshold above which emulsification disproportionately enhances recovery. Unlike the reaction order, the rate constant and enthalpy of emulsification could be dependent more on the changing fluid properties (steam and bitumen) than on the reservoir properties.

Fig 6.25 shows that recovery is enhanced when the emulsion droplets do not leave the steam chamber interface by dispersion (corresponding to the case with dispersion

coefficient equal to zero). A plausible mechanism for this is steam entrainment of the emulsion droplets. As injected steam rises to the top of the reservoir, it tends to entrain lower energy state emulsion droplets, until such droplets attain sufficient energy (determined by the dispersion coefficient) to break-through the interface of the steam chamber. If this higher energy state is not achieved, rising steam then tends to spread the droplets evenly inside the chamber which then increases the effective volume of cold bitumen in contact with the hot emulsion droplets thereby enhancing recovery. **Fig 6.17** shows such entrainment in action when there is no dispersion. We see the emulsion droplets largely reside inside the steam chamber.

Fig 6.28 shows that an enthalpy of emulsification of 0 to 30 KJ/gmol could have obtained the same match in **Fig 6.11** and that there exists a threshold enthalpy value of 30 KJ/gmol for the emulsification process beyond which the emulsification reaction ceases to be typical i.e. it ceases to be a good surrogate for the physical emulsification process itself. This can be better understood when compared with the enthalpy of vaporization of water which is 40.65 KJ/g-mol.

In all the sensitivities (**Figs 6.22**, **6.24**, **6.27** and **6.30**), we see that whenever recovery is enhanced, the water-oil-ratio (WOR) is reduced which is consistent with the flow behavior of water-in-oil (W/O) emulsions.

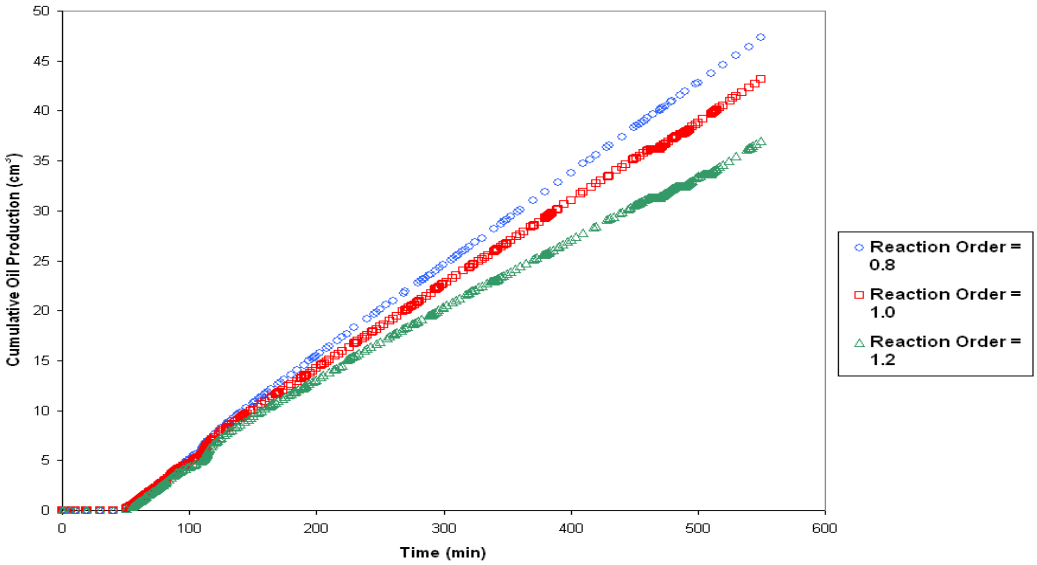

Figure 6.21: Sensitivity of cumulative oil recovery to the order of reaction.

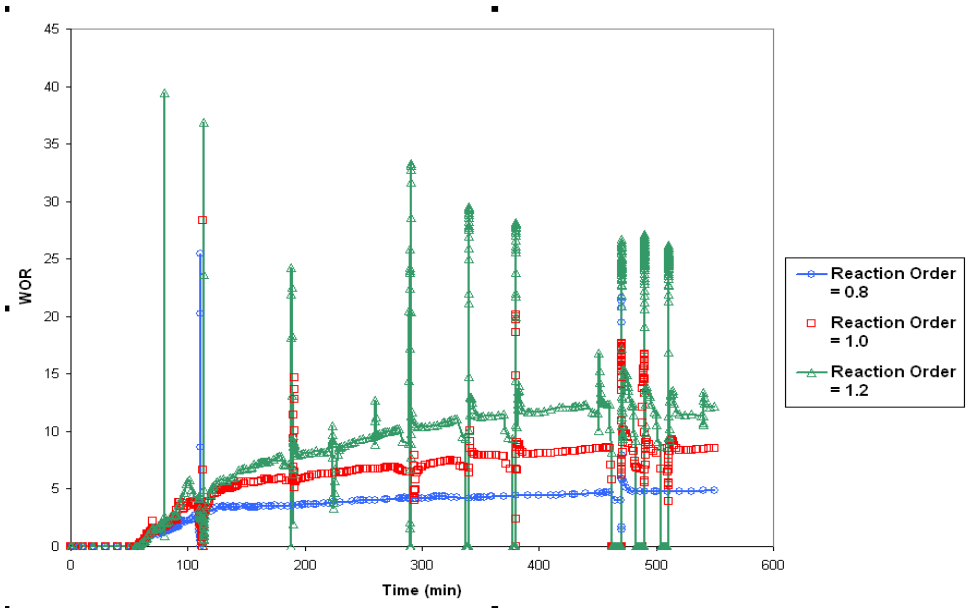

Figure 6.22: Sensitivity of the water-oil ratio (WOR) to the order of reaction

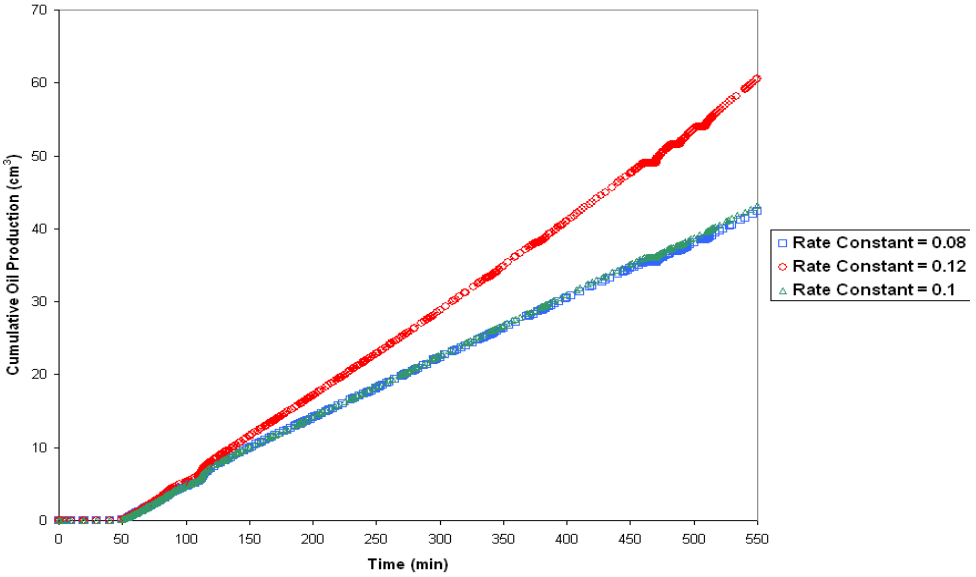

Figure 6.23: Sensitivity of cumulative oil production to the reaction rate constant

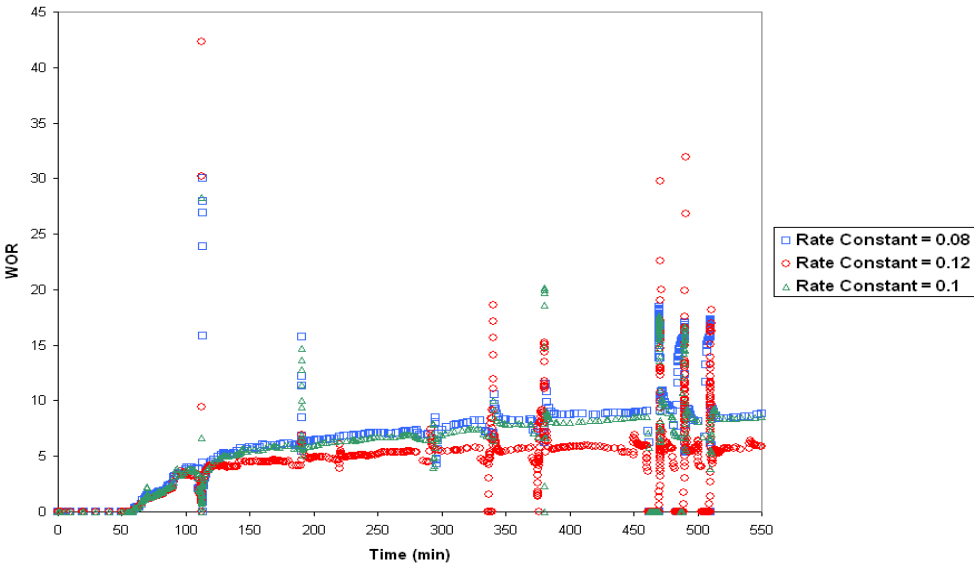

Figure 6.24: Sensitivity of the water-oil ratio to the reaction rate constant

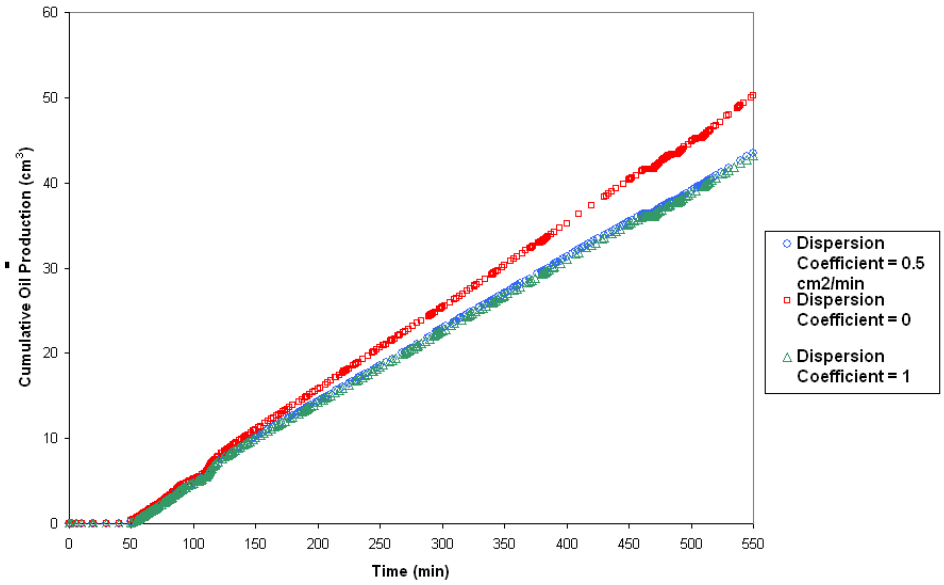

Figure 6.25: Sensitivity of the cumulative oil recovery to the dispersion coefficient of the emulsion droplets in oil

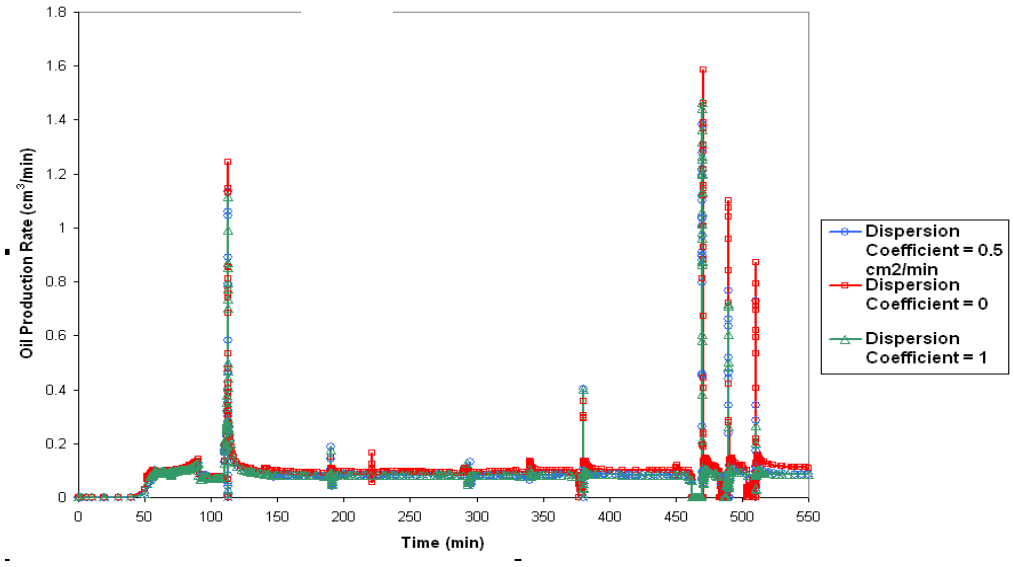

Figure 6.26: Sensitivity of oil production rate to the dispersion coefficient of the emulsion droplets in oil

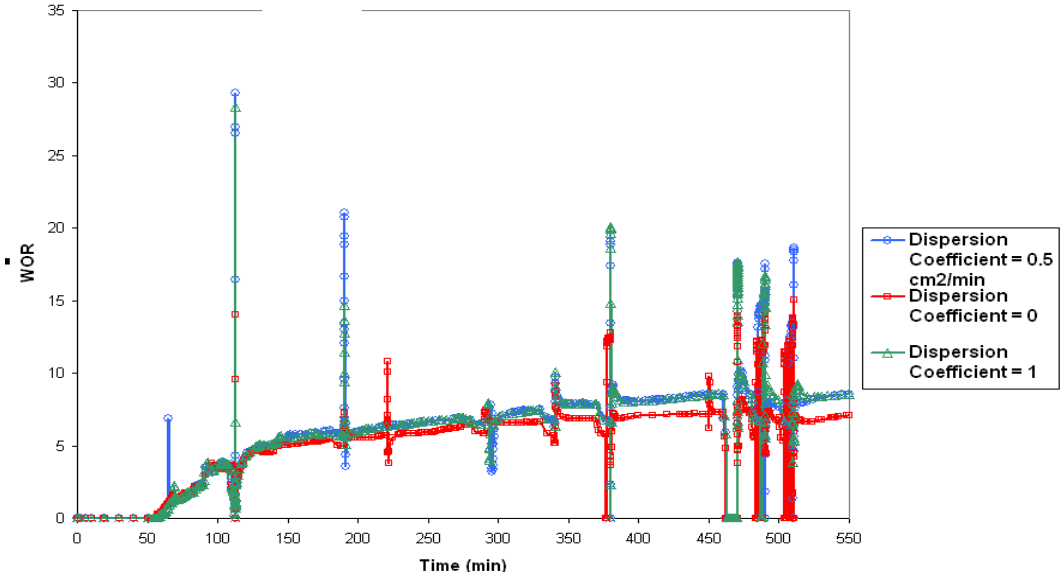

Figure 6.27: Sensitivity of the water-oil ratio to the dispersion coefficient of the emulsion droplets in oil

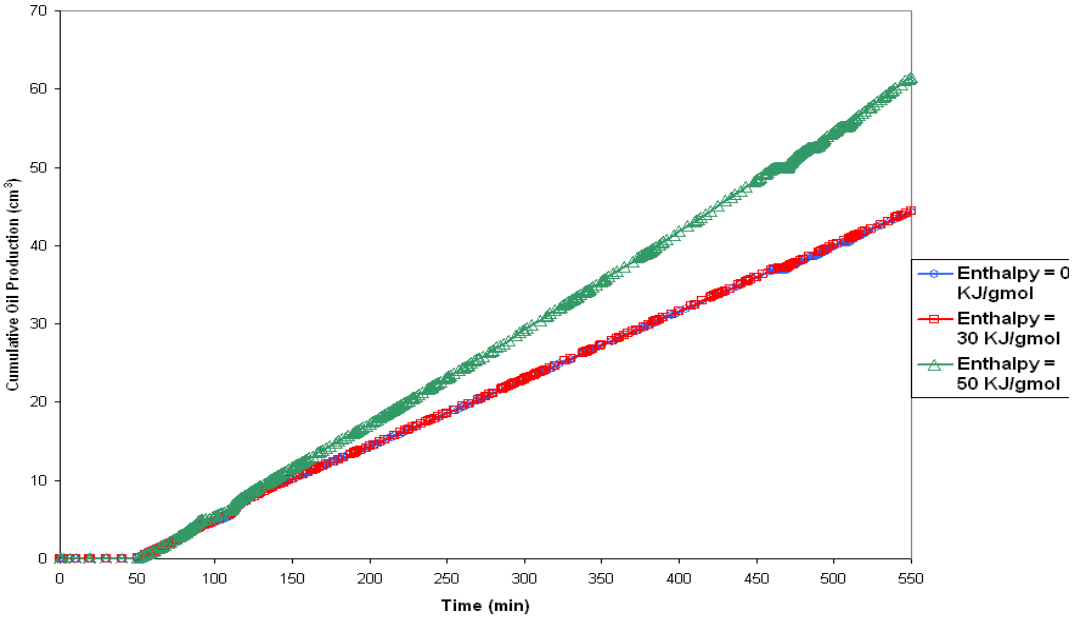

Figure 6.28: Sensitivity of the cumulative oil recovery to the enthalpy of emulsification

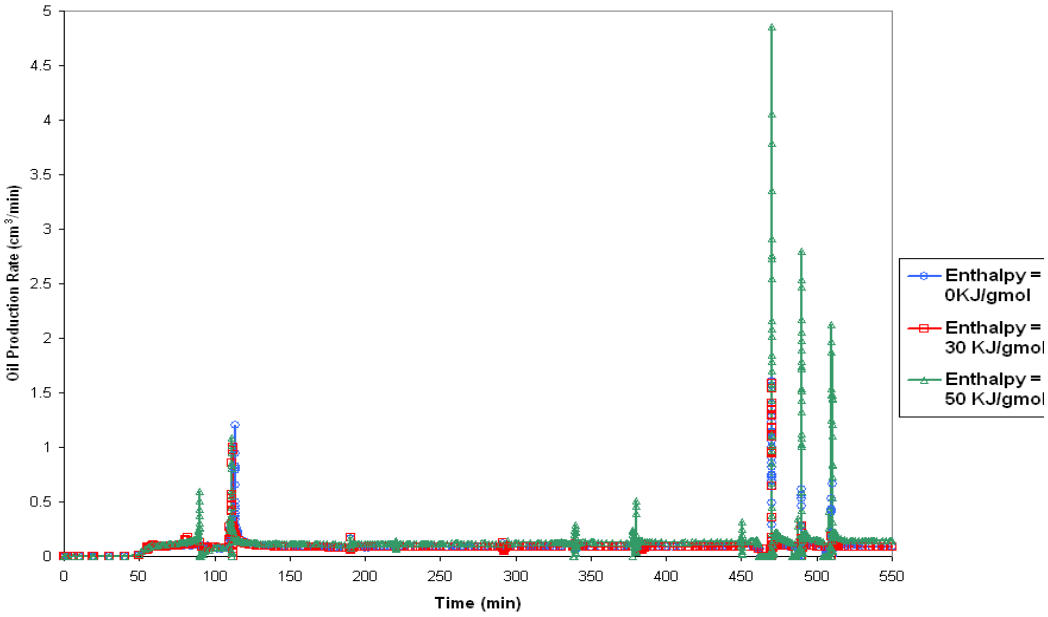

Figure 6.29: Sensitivity of the oil production rate to the enthalpy of emulsification

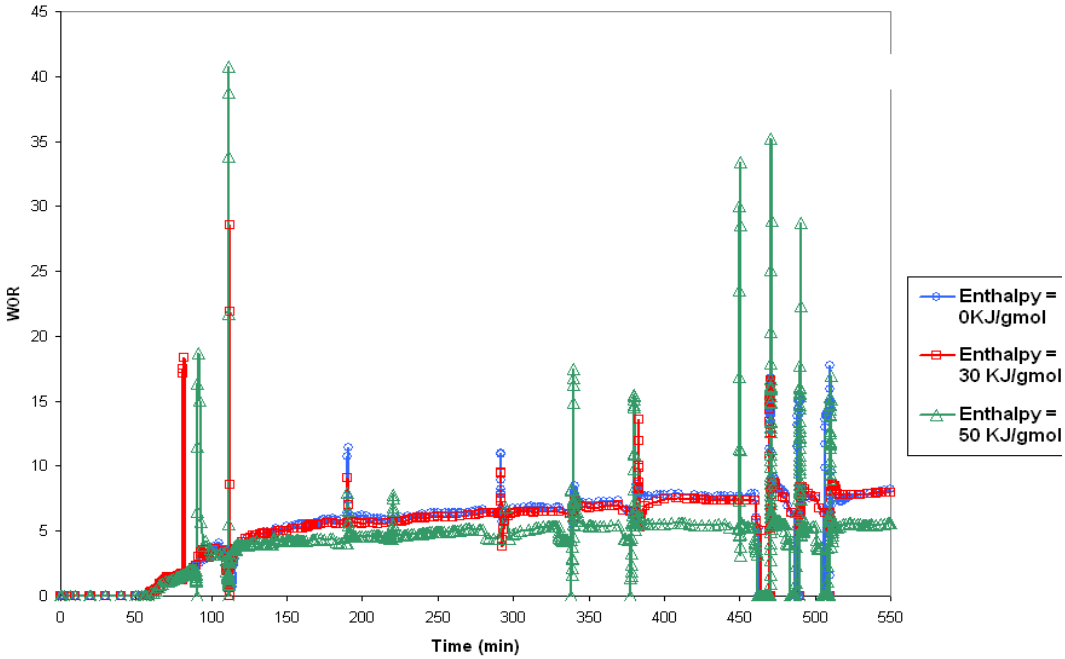

Figure 6.30: Sensitivity of the water-oil ratio to the enthalpy of emulsification

6.7 Summary and Significance of Work

An attempt has been made to model the effect of emulsion formation and transport during the steam-assisted gravity drainage (SAGD) process on recovery. A detailed framework, which involves process characterization using thirty-two (32) tuning parameters, was developed. Model validation shows very promising results and indicates that the emulsification process during SAGD might have a significant contribution towards cumulative oil recovery.

The rate constant and reaction order dictate the speed or frequency of emulsion generation at the interface of the steam chamber. However, the reaction order is expected to be fairly constant if our assumption of an elementary reaction holds, and will be dependent mainly on the properties of the reservoir. If this is the case, then for a given reservoir, the rate constant will determine the frequency of emulsion generation, and will be dependent on the properties of the heavy oil, steam temperature and pressure. The dispersion coefficients determine the speed with which the emulsion droplets move through (and leave) the steam chamber interface and hence heat transfer. The enthalpy of emulsification represents instantaneous energy transferred to flowing bitumen close to the interface. This is different from heat transferred by conduction and convection which are time dependent. From our simulations, we observe that a typical range for ΔH_{EMULS} is 10 J/gmol to 30 KJ/gmol.

This work can be used to model improved recovery due to the presence of water-in-oil (W/O) emulsions during SAGD at both the experimental and field scales. Field-scale simulations will however require an effective scale-up process since the emulsion droplets will be so much smaller than the average grid-block size.

Future experiments that make observations regarding the initiation of emulsion formation as related to the steam chamber geometry and the heat transfer across the steam-bitumen boundary will be invaluable. With these additional observations, a more comprehensive theory for the formation and transport of W/O emulsions at the walls of the steam chamber and the associated heat transfer mechanisms can be developed.

Chapter 7: Conclusions and Recommendations

In this chapter, we will summarize key conclusions and give recommendations for future work.

7.1 Conclusions

In this work, we have studied improvements to the modeling of the SAGD process by incorporating the effect of anisotropy, capillarity and W/O emulsification on SAGD rates. We also extended the capillarity model to the ES-SAGD process. A central insight from this work is that the SAGD process differs from most other enhanced oil recovery (EOR) techniques in that it is a short length scale process and hence other short length-scaled phenomena usually ignored in other EOR or conventional processes should not be ignored for the SAGD process. We now present the key conclusions of this work under these headings.

7.1.1 The Effect of Anisotropy

The effect of anisotropy on SAGD rates is time dependent generally obeying a sigmoid or elliptic function. Since for anisotropic porous media, the directions of resultant gravity head (RGH) and the resultant oil discharge (ROD) do not coincide, two models describing anisotropy during SAGD was developed for both single layer and multi-layered reservoirs.

The RGH and ROD models give similar results for $k_v/k_h > 0.7$ but can give dramatically different results for lower anisotropy ratios.

For multi-layered reservoirs, it is possible to define an equivalent anisotropy ratio, but such equivalence does not apply to the ROD model.

We also showed that structured grid finite difference models might be unable to predict accurately the effect of anisotropy due to the grid orientation effect and more research still needs to be done to determine the more appropriate model between the RGH and ROD models for the SAGD process.

This work will find invaluable use in well spacing design and in proxy models for predicting the SAGD recovery.

7.1.2 The Effect of Heat Transfer on Capillarity during SAGD

Heat transfer plays an important role on capillary behavior during the SAGD process. The existence of interfacial tension gradients due to temperature gradients ahead of the steam chamber front creates the Marangoni effect of thermo-capillary imbibition of the condensate into the bitumen phase.

This imbibition process is scale dependent and controlled by the Marangoni or thermo-capillary number and explains why several models which do well at experimental scales perform poorly at field scales and vice versa.

This work also shows that laboratory experiments used to predict field recovery must be properly scaled to include, with the Butler scaling groups, all the dimensionless groups developed in this work as phenomena completely absent at the experiment scale can occur at the field scale for improperly scaled experiments.

This work will find strong application is scaled experiment design and improved SAGD field scale recovery predictions.

7.1.3 The Effect of Heat Transfer on Capillarity during ES-SAGD

Heat transfer also plays a role in the capillary behavior of the ES-SAGD process. Our model predicts that there exists a thermo-capillary number threshold below which there is no benefit of the ES-SAGD process over SAGD.

Unlike for the SAGD process where heterogeneity is detrimental to SAGD rates as more condensate will imbibe into the bitumen phase with increased heterogeneity, heterogeneity has a more complex effect on ES-SAGD rates as it can also aid in the transport of solvent farther away from the steam chamber interface thereby aiding recovery.

An important result from this work is that it shows succinctly that the ratio of solvent viscosity to bitumen viscosity at steam temperature also controls the additional recovery from ES-SAGD over SAGD. If this ratio is close to unity, there is no benefit to use the ES-SAGD process and the smaller this value is than unity, the better the performance of the ES-SAGD process over SAGD. This is because the length scale of both the SAGD and ES-SAGD processes are very short (effectively controlled by the thermal conductivity and dispersive length scales), hence only the bitumen with viscosities at temperatures close to the steam temperature will be contacted by the solvent.

This work will also find strong application in scaled experiment design and improved field scale recovery predictions and can be incorporated in a fast ES-SAGD proxy for history matching, optimization and uncertainty analysis.

7.1.4 The Effect of Emulsion Formation and Transport during SAGD

The formation of water-in-oil (W/O) emulsions at the steam chamber interface during SAGD enhances heat transfer during SAGD by inducing convective heat

transport. These W/O emulsions are hot water droplets dispersed into the bitumen phase and help to enhance SAGD rates irrespective of the increased bitumen phase viscosity due to the emulsion droplets because the effective heat transfer coefficient across the steam chamber interface can effectively be doubled in the presence of W/O emulsions.

More work still needs to be done to determine if oil-in-water (O/W) emulsions also form at the steam chamber interface during SAGD or if other complex combinations do form. Also, it will be important to determine the incipient condition that triggers these emulsions to form.

This work can be used to model improved recovery due to the presence of W/O emulsions during SAGD at both experiment and field scales. Field-scale simulations will however require an effective scale-up process since the emulsion droplets will be so much smaller than the average grid-block size.

7.2 Recommendations for Future Work

This work can be extended further in a variety of ways, the most important being the coupling of the three (3) phenomena studied. For example, the effect of capillarity can be affected by anisotropy during SAGD since it will determine the effective permeability used to define the thermo-capillary number. This effective permeability will be the orthogonal components of the RGH and ROD models and given by equations (3.55) and (3.56) respectively. Other couplings are also possible and should be explored.

We will now discuss individual possible extensions to this work under the natural headings of this dissertation.

7.2.1 The Effect of Anisotropy

This wok did not fully resolve which of the RGH or the ROD models is best suited for the SAGD process. Experimentation or Finite Element Method (FEM) based numerical simulation should be used to explore this further.

We also only presented 2D models for the effect of anisotropy but most reservoirs are 3D. It will be useful to extend our anisotropic models to 3D.

7.2.2 The Effect of Capillarity

We ignored the effect of wettability change in our model accounting for thermo-capillary imbibition during SAGD. In reality, wettability also changes as interfacial tension changes but probably not at the same time scale. Including the effect of wettability might require either a transient extension of our model or it might be illuminating to look at the "maximum" effect of wettability change by assuming it changes at the same time scale as interfacial tension.

We extended the thermo-capillary model to the ES-SAGD process in this work, but this can also be done to other solvent aided SAGD processes with some modifications. For example, extensions to the lighter solvent aided processes like Steam and Gas Push (SAGP) and Solvent alternating Solvent (SAS) processes will require the additional use of gas/oil capillary pressure data since significant diffusion of the gas phase occurs ahead of the steam chamber (Al-Murayri et al. 2011) and for the Amine-Enhanced Steam-Assisted Gravity Drainage (AE-SAGD) process (Srivastava et al. 2010), an additional constitutive equation relating the dependence of capillary pressure on amine or surfactant concentration is needed.

7.2.3 The Effect of Emulsification

It is still not clear which emulsion type is predominantly produced during SAGD. SAGD experiments seem to produce W/O emulsions while field scale recoveries seem to produce O/W emulsions. This discrepancy seems to suggest that steam quality might be playing an important role in the emulsification process since experiments are usually run at high steam qualities while field scale recoveries will predominantly be operated at lower steam qualities. More experiments will need to be performed to verify this.

In this dissertation, we assumed that emulsification is triggered at time $t = 0$. This might however not be the case as there will generally exist conditions that trigger the emulsification process that would not have existed before steam injection. This will require a combination of force balances across the steam chamber interface and some instability analysis.

Extending the emulsion model we used in this work to field scales presents the interesting challenge that the size of the average grid block for field scale simulations will be far greater than the size of the emulsion droplets. Hence simulating the emulsion problem at field scales will require some scale up process. A cohesive but novel theory and method will be required for this.

Appendix A

We derive formally the resultant gravity head (RGH) and the resultant oil discharge (ROD) models. Our derivations follow that of Das (2013) but with a SAGD frame of reference.

From **Fig 3.1**, the oil velocities in the different directions can be written as

$$v_x = -k_h \frac{\partial h}{\partial x} \tag{A.1}$$

$$v_z = -k_v \frac{\partial h}{\partial z} \tag{A.2}$$

$$v_{RGH} = -k_{eff_{RGH}} \frac{\partial h}{\partial \psi_{RGH}} \tag{A.3}$$

$$v_{ROD} = -k_{eff_{ROD}} \frac{\partial h}{\partial \psi_{ROD}} \tag{A.4}$$

The velocity in the RGH direction can be decomposed further into

$$v_{RGH} = v_z \sin\beta + v_x \cos\beta \tag{A.5}$$

Substituting (A.1), (A.2) and (A.3) into (A.5) yields:

$$k_{eff_{RGH}} \frac{\partial h}{\partial \psi_{RGH}} = k_v \frac{\partial h}{\partial z} \sin\beta + k_h \frac{\partial h}{\partial x} \cos\beta \tag{A.6}$$

From geometry considerations

$$\frac{\partial h}{\partial x} = \frac{\partial h}{\partial \psi_{RGH}} \cos\beta \tag{A.7}$$

and

$$\frac{\partial h}{\partial z} = \frac{\partial h}{\partial \psi_{RGH}} \sin\beta \tag{A.8}$$

Substituting (A.7) and (A.8) into (A.6) yields:

$$k_{eff_{RGH}} = k_v \sin^2\beta + k_h \cos^2\beta \tag{A.9}$$

which is the required derivation for the RGH model. Similarly for the ROD model, an effective gradient in the available head for discharge can be written as

$$\frac{\partial h}{\partial \psi_{ROD}} = \frac{\partial h}{\partial z} \sin\alpha + \frac{\partial h}{\partial x} \cos\alpha \tag{A.10}$$

From (A.1), (A.2) and (A.4), we get

$$\frac{\partial h}{\partial x} = -\frac{v_x}{k_h} \tag{A.11}$$

$$\frac{\partial h}{\partial z} = -\frac{v_z}{k_v} \tag{A.12}$$

$$\frac{\partial h}{\partial \psi_{ROD}} = -\frac{v_{ROD}}{k_{eff_{ROD}}} \tag{A.13}$$

Also from geometry considerations, we get

$$v_x = v_{ROD} \cos\alpha \tag{A.14}$$

$$v_z = v_{ROD} \sin\alpha \tag{A.15}$$

Substituting equations (A.11) to (A.15) into (A.10) yields:

$$\frac{1}{k_{eff_{ROD}}} = \frac{\sin^2\alpha}{k_v} + \frac{\cos^2\alpha}{k_h} \tag{A.16}$$

which is the required derivation for the ROD model.

Appendix B

B.1 Coordinate Transform

We consider the coordinate transformation from a fixed frame (x,y) into a moving frame (ξ,ψ), attached to a moving front, as shown in **Fig. B.1**

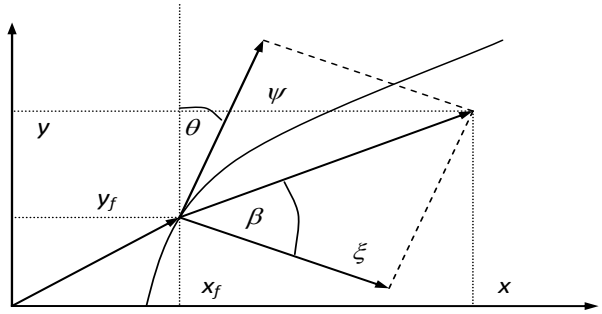

Figure B.1: Fixed and moving coordinate systems

The moving coordinate system is chosen such that ψ is the direction parallel to the front, and ξ the direction perpendicular to the front. It follows readily that:

$$x = x_f + \left(\xi^2 + \psi^2\right)^{1/2} \cos\left(\beta - \theta\right) \tag{B.1}$$

$$y = y_f + \left(\xi^2 + \psi^2\right)^{1/2} \sin\left(\beta - \theta\right) \tag{B.2}$$

where $\left(x_f, y_f\right)$ are the coordinates of the origin of the moving coordinate system, θ is the angle between the ψ direction and the y direction, and

$$\beta = \arctan\frac{\psi}{\xi} \tag{B.3}$$

Using the trigonometric relations:

$$\cos(\beta-\theta)=\cos\beta\cos\theta+\sin\beta\sin\theta \tag{B.4}$$

$$\sin(\beta-\theta)=\sin\beta\cos\theta-\cos\beta\sin\theta \tag{B.5}$$

(B.1) and (B.2) can be written as:

$$x=x_f+\left(\xi^2+\psi^2\right)^{1/2}\left(\cos\beta\cos\theta+\sin\beta\sin\theta\right) \tag{B.6}$$

$$y=y_f+\left(\xi^2+\psi^2\right)^{1/2}\left(\sin\beta\cos\theta-\cos\beta\sin\theta\right) \tag{B.7}$$

Using relation (B.3), it follows that:

$$\left(\xi+\psi\right)^{1/2}\cos\beta=\xi \tag{B.8}$$

$$\left(\xi+\psi\right)^{1/2}\sin\beta=\psi \tag{B.9}$$

Substituting (B.8) and (B.9) in (B.6) and (B.7) gives

$$x=x_f+\xi\cos\theta+\psi\sin\theta \tag{B.10}$$

$$y=y_f-\xi\sin\theta+\psi\cos\theta \tag{B.11}$$

which can be written in vector form as

$$\mathbf{x}=\mathbf{x}_f+\mathbf{R}^{-1}\mathbf{X} \tag{B.12}$$

where $\mathbf{x}_f$ is the translation $\mathbf{x}_f = \left(x_f, y_f\right)^T$, $\mathbf{x} = \left(x, y\right)^T$, $\mathbf{R}^{-1}$ the rotation matrix, and $\mathbf{X} = \left(\xi, \psi\right)^T$

$$\mathbf{R}^{-1} = \begin{bmatrix} \cos\theta & \sin\theta \\ -\sin\theta & \cos\theta \end{bmatrix} \tag{B.13}$$

The inverse transform of (B.12) is

$$\mathbf{X} = \mathbf{R}\left(\mathbf{x} - \mathbf{x}_f\right) \tag{B.14}$$

where

$$\mathbf{R} = \begin{bmatrix} \cos\theta & -\sin\theta \\ \sin\theta & \cos\theta \end{bmatrix} \tag{B.15}$$

B.2 Mass Conservation Equation in a Moving Frame

We consider the following mass conservation equation:

$$\frac{\partial C}{\partial t} + \nabla \cdot \left(\mathbf{u}C - D\nabla C\right) = 0 \tag{B.16}$$

where C is a form of concentration and is temperature in our case, $\mathbf{u} = \left(u, v\right)^T$ the convection velocity, and D a diffusion coefficient and is thermal diffusivity in our case. The first term of this equation can be written as $\left(\partial C/\partial t\right)_{x,y}$. Now, the total differential of C is:

$$dC = \left(\frac{\partial C}{\partial t}\right)_{x,y} dt + \left(\frac{\partial C}{\partial x}\right)_t dx + \left(\frac{\partial C}{\partial y}\right)_t dy \tag{B.17}$$

Dividing by a time differential and taking ξ and ψ constant yields:

$$\left(\frac{dC}{dt}\right)_{\xi,\psi} = \left(\frac{\partial C}{\partial t}\right)_{x,y} + \left(\frac{\partial C}{\partial x}\right)_t \left(\frac{\partial x}{\partial t}\right)_{\xi,\psi} + \left(\frac{\partial C}{\partial y}\right)_t \left(\frac{\partial y}{\partial t}\right)_{\xi,\psi} \tag{B.18}$$

Using equations (B.10) and (B.11) yields:

$$\left(\frac{dC}{dt}\right)_{\xi,\psi} = \left(\frac{\partial C}{\partial t}\right)_{x,y} + \left(\frac{\partial C}{\partial x}\right)_t \frac{\partial x_f}{\partial t} + \left(\frac{\partial C}{\partial y}\right)_t \frac{\partial y_f}{\partial t} \tag{B.19}$$

Now, the total differential of C is given by

$$dC = \left(\frac{\partial C}{\partial t}\right)_{\xi,\psi} dt + \left(\frac{\partial C}{\partial \xi}\right)_t d\xi + \left(\frac{\partial C}{\partial \psi}\right)_t d\psi \tag{B.20}$$

Dividing by a time differential and taking x and y constant yields:

$$\left(\frac{\partial C}{\partial t}\right)_{x,y} = \left(\frac{\partial C}{\partial t}\right)_{\xi,\psi} + \left(\frac{\partial C}{\partial \xi}\right)_t \left(\frac{\partial \xi}{\partial t}\right)_{x,y} + \left(\frac{\partial C}{\partial \psi}\right)_t \left(\frac{\partial \psi}{\partial t}\right)_{x,y} \tag{B.21}$$

In vector form we can write:

$$\left(\frac{\partial C}{\partial t}\right)_{x,y} = \left(\frac{\partial C}{\partial t}\right)_{\xi,\psi} + \nabla' C \cdot \left(\frac{\partial \mathbf{X}}{\partial t}\right)_{x,y} \tag{B.22}$$

where we have dropped the "constant-time" indication on $\nabla' C$, defined as

$$\nabla' C \equiv \left[\left(\frac{\partial C}{\partial \xi} \right)_t , \left(\frac{\partial C}{\partial \psi} \right)_t \right]^T \tag{B.23}$$

Using equation (B.14), equation (B.23) can be written as:

$$\left(\frac{\partial C}{\partial t} \right)_{x,y} = \left(\frac{\partial C}{\partial t} \right)_{\xi,\psi} - \mathbf{U} \cdot \nabla' C \tag{B.24}$$

where

$$\mathbf{U} = \mathbf{R} \frac{\partial \mathbf{X}_f}{\partial t} \tag{B.25}$$

is the velocity of the front, expressed in the directions ξ and ψ. The convection term of (B.16) can be written as follows:

$$\nabla \cdot (\mathbf{u} C) = \frac{\partial}{\partial x} \left(\frac{dx_p}{dt} C \right) + \frac{\partial}{\partial y} \left(\frac{dy_p}{dt} C \right) \tag{B.26}$$

where $\left(x_p, \mathrm{y}_p \right)$ is the position of a fluid particle in a moving coordinate system. Using partial derivatives, with (B.12) and (B.14) yields:

$$\begin{aligned}\nabla\cdot(\mathbf{u}C) = &\frac{\partial}{\partial\xi}\left(\left[u_f+\cos\theta\frac{d\xi_p}{dt}+\sin\theta\frac{d\psi_p}{dt}\right]C\right)\cos\theta+\\ &\frac{\partial}{\partial\psi}\left(\left[u_f+\cos\theta\frac{d\xi_p}{dt}+\sin\theta\frac{d\psi_p}{dt}\right]C\right)\sin\theta\\ &-\frac{\partial}{\partial\xi}\left(\left[v_f-\sin\theta\frac{d\xi_p}{dt}+\cos\theta\frac{d\psi_p}{dt}\right]C\right)\sin\theta\\ &+\frac{\partial}{\partial\psi}\left(\left[v_f-\sin\theta\frac{d\xi_p}{dt}+\cos\theta\frac{d\psi_p}{dt}\right]C\right)\cos\theta\end{aligned} \tag{B.27}$$

The front velocities are by definition not a function of ξ and ψ, so that from (B.27) it follows that

$$\nabla\cdot(\mathbf{u}C) = \nabla'\cdot[\mathbf{u}C] \tag{B.28}$$

where ∇' and $\mathbf{u}$ are respectively a space derivative operator and a fluid velocity in the moving reference frame. It is also relatively straightforward to show that the diffusion term is not affected by the coordinate transform, so that the conservation equation in the moving system becomes:

$$\frac{\partial C}{\partial t}-\mathbf{U}\cdot\nabla' C+\nabla'\cdot(\mathbf{u}C-D\nabla' C)=0 \tag{B.29}$$

Appendix C

C.1 Experimental Modeling of the SAGD process

We present an experimental study of the SAGD process which was intended to be used to study emulsification behavior during SAGD. As will be seen from the temperature maps obtained during the experiment, we had trouble obtaining the classic inverted triangle shape for the steam chamber that is central to the derivations for recovery rate and steam chamber growth rate presented in this dissertation (and in Butler's work). Furthermore, our main motivation for performing the experiments was to observe and measure any additional heat transfer that occurs at the steam-bitumen interface due to the formation and transport of water-in-oil (W/O) emulsion droplets. The measurement set up that we designed was insufficient to conclude that any enhanced heat transfer occurs at the interface due to the transport of emulsion droplets. Given that the results obtained by performing the experiments were inconclusive, we felt it best to document the details of the experiments in this appendix rather than in the main body of the dissertation.

The experimental setup is shown in **Fig C.1** which follows a typical SAGD process. Water is injected into an actuator through a pump to a steam generator which can generate steam at varying qualities. A pressure transducer and solenoid valve is used to prevent high pressures building up in the system and is connected to the reservoir (called steam chamber in **Fig C.1**) which in turn is connected to a LabView 2009 Data Acquisition System (DAQ) and an automatic fluid collection system that can be timed. The DAQ was programmed to measure the temperature of the reservoir and the pressure difference between the injector and producer. The reservoir has spacing for 100 thermocouples, but only 50 thermocouples were used in this experiment and ordinary

Kriging used to compute the temperatures of the remaining 50 unused thermocouple locations.

C.1.2 Experimental Description

We describe each part of the experimental setup in this section. The reservoir is a 10in x 10in square model made of polycarbonate glass material. On the back is drilled 100 equally spaced thermocouple locations with design distances shown in **Fig C.2**. The dimensions of the reservoir model are also shown in **Fig C.2**.

The fluid collection system is an automatic collector that can collect fluids at timed intervals with a maximum time interval of 600 seconds. The DAQ is the main electrical control for the experiment and is capable of recording temperature and pressure data by converting voltage readings using a series of shunts and resistors. The pressure transducer and solenoid valves are for steam pressure control. The polycarbonate glass material is rated for 35psia and steam pressure is not allowed to rise above 20psia in our experiments. This reduced the possible range of steam injection temperatures that could be tested in the experiment.

The water tank or reservoir is used to store water required to produce steam, and its volume was designed with the pump rate and expected duration of the experiment in mind. After some iteration, the pump rate was kept constant at 10cc/min. The actuator was used to connect the pump to the steam generator.

The steam generator used was capable of producing both saturated and superheated steam. It had the capacity to run on 100% power or less. However, to ensure only saturated steam is produced throughout the duration of the experiment for the given operating pressure, a requisite steam generation power must be determined iteratively.

This is because back pressure effects causes superheated steam to be produced at higher steam generation powers.

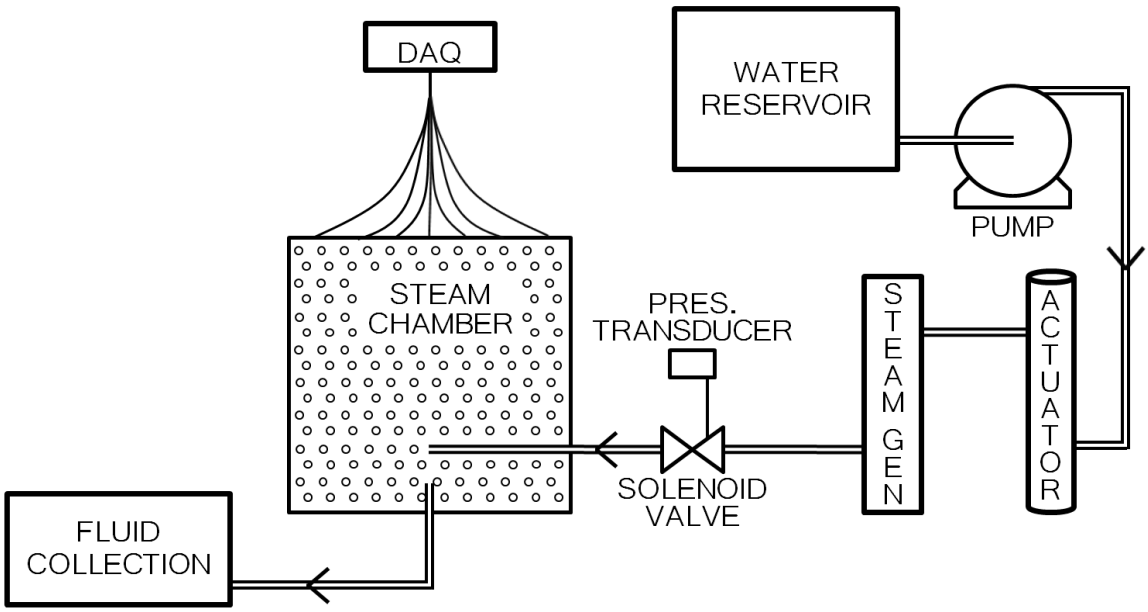

Figure C.1: Schematic of SAGD experimental model

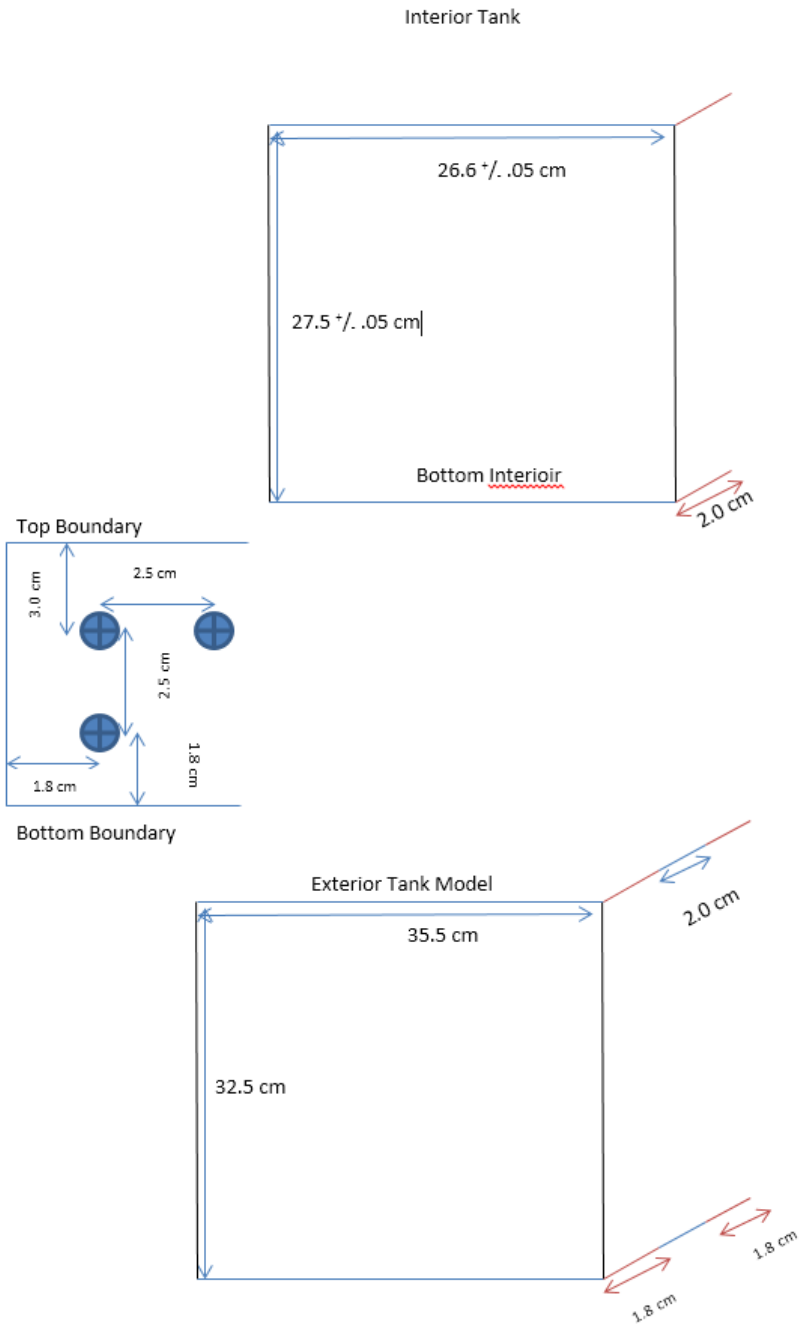

Figure C.2: Schematic of the square reservoir model used for the experiment with some important dimensions

C.1.2 Experimental Procedure

Each of the 50 thermocouples was first calibrated using a steam bath and at room temperature. One of the thermocouples got damaged and we were hence left with only 49 thermocouples to work with. The pressure transducer was also calibrated using a voltmeter. After calibration, the experimental setup was connected and ready for steam injection.

Steam was injected into the reservoir at 10% power of the steam generator, after it was determined that such power was sufficient to prevent the production of superheated steam for about 5 hours of performing the experiment. The fluid collection system was used to collect the produced fluids at varying intervals with the fluid rates obtained by dividing the amount of fluid produced by the time interval at which it was produced. The fluids produced were mostly in the form of oil-in-water (O/W) emulsions (probably because we injected low quality steam) that could not easily be broken even with calcium chloride de-emulsifying agent.

The temperatures in the steam chamber was recorded from the 49 thermocouples by the DAQ and was interpolated to the entire reservoir by Ordinary Kriging using the SGSIM geostatistical modeling software.

C.1.3 Experimental Results

The results from our experiment were mainly the temperature-time profiles and are presented in **Figs D.2** to **D.11**. They show the evolution of the steam chamber with time through the temperature profile of the reservoir. **Fig D.2**, the initial condition of the reservoir, shows some variation but this is clearly due to random noise either in the true reservoir temperatures or in the thermocouple calibration process. True variations in reservoir temperatures are seen with time and reveals that the steam chamber achieved

horizontal growth at about 30 minutes of steam injection. The growth of the steam chamber is seen not to be uniform especially during its vertical growth and is a consequence of microscopic heterogeneities inherent in the porous media packing process.

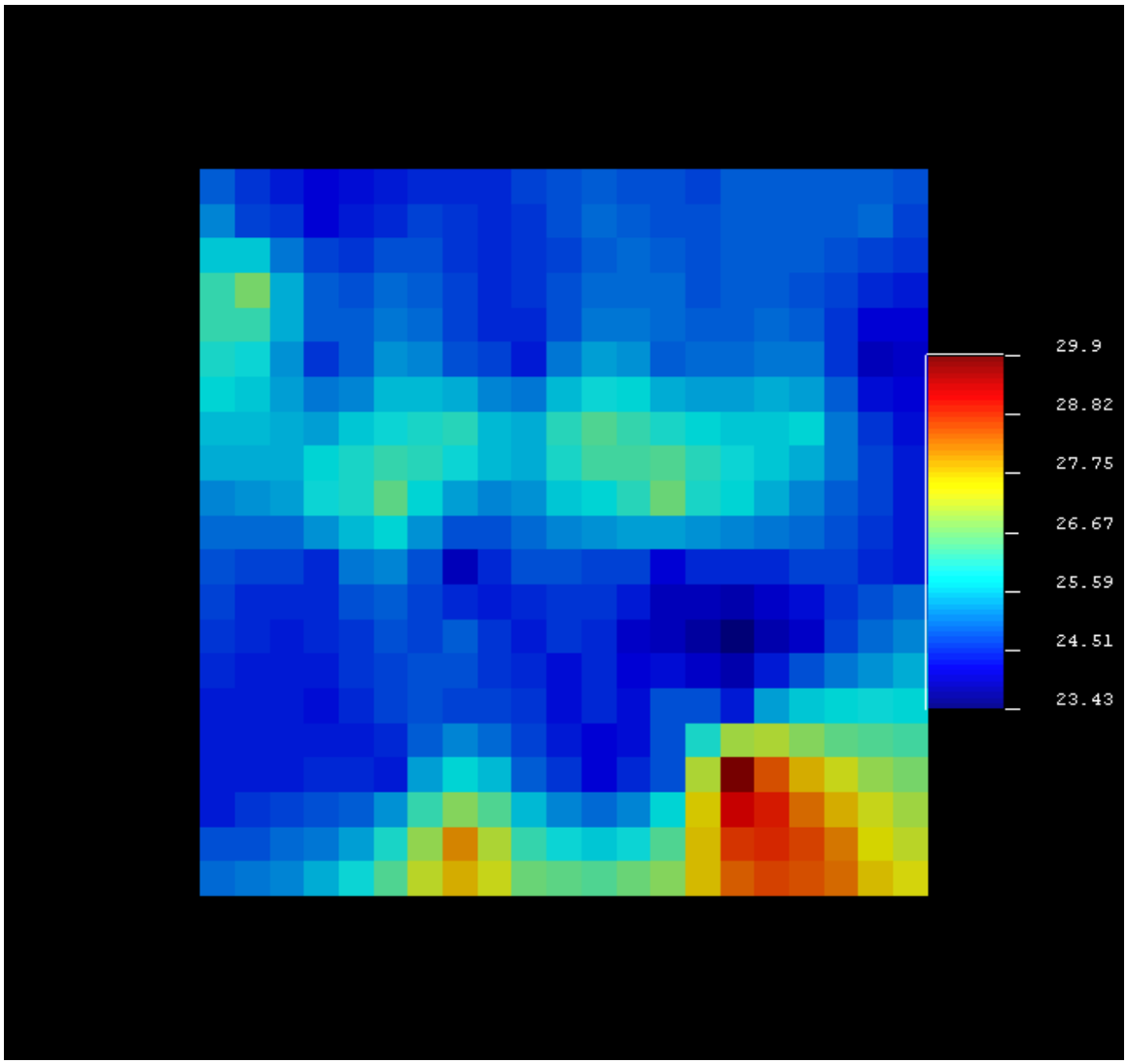

Figure C.3: Temperature profile from SAGD experiment at time $t = 2$ minutes

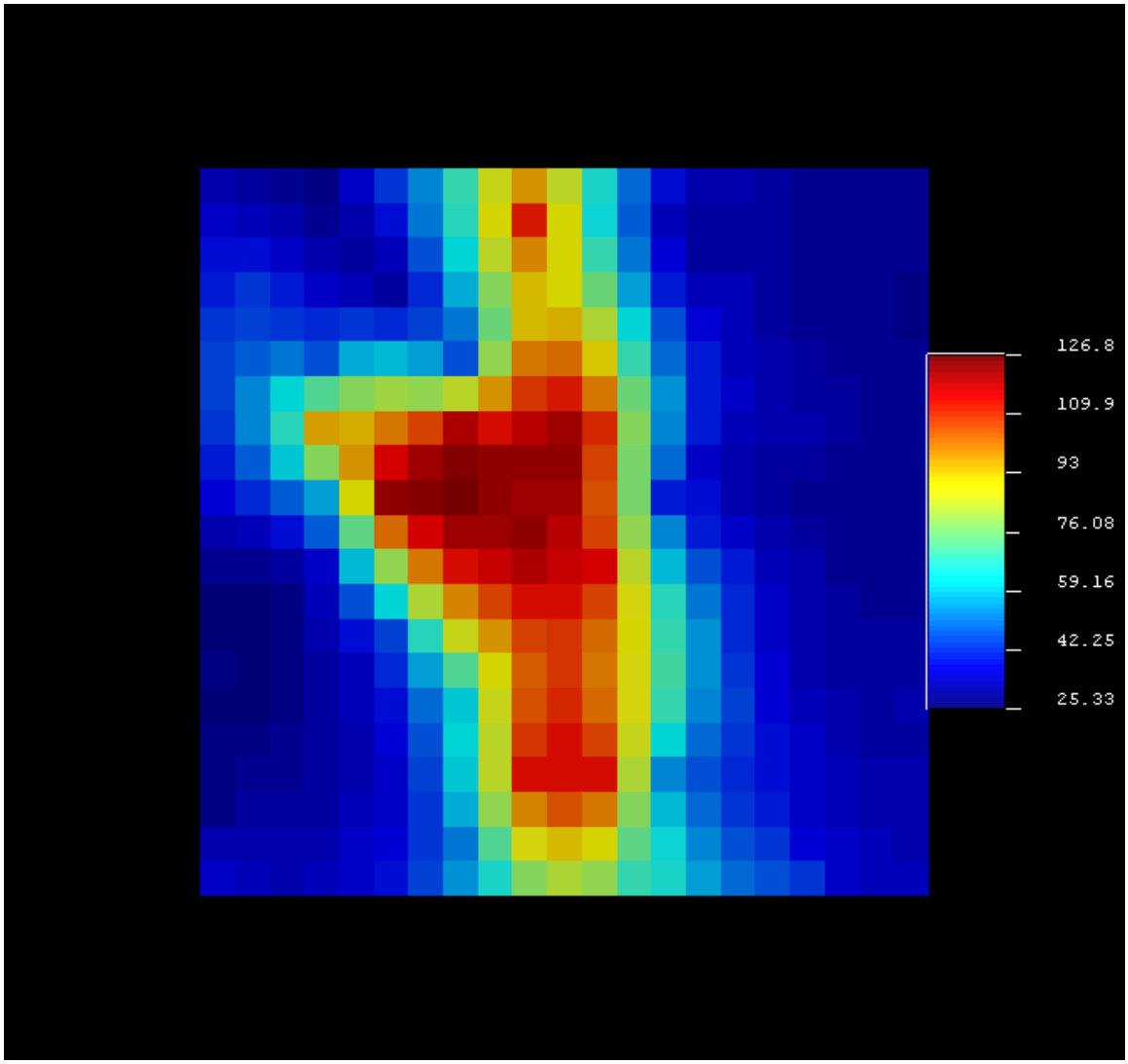

Figure C.4: Temperature profile from SAGD experiment at time $t = 12$ minutes

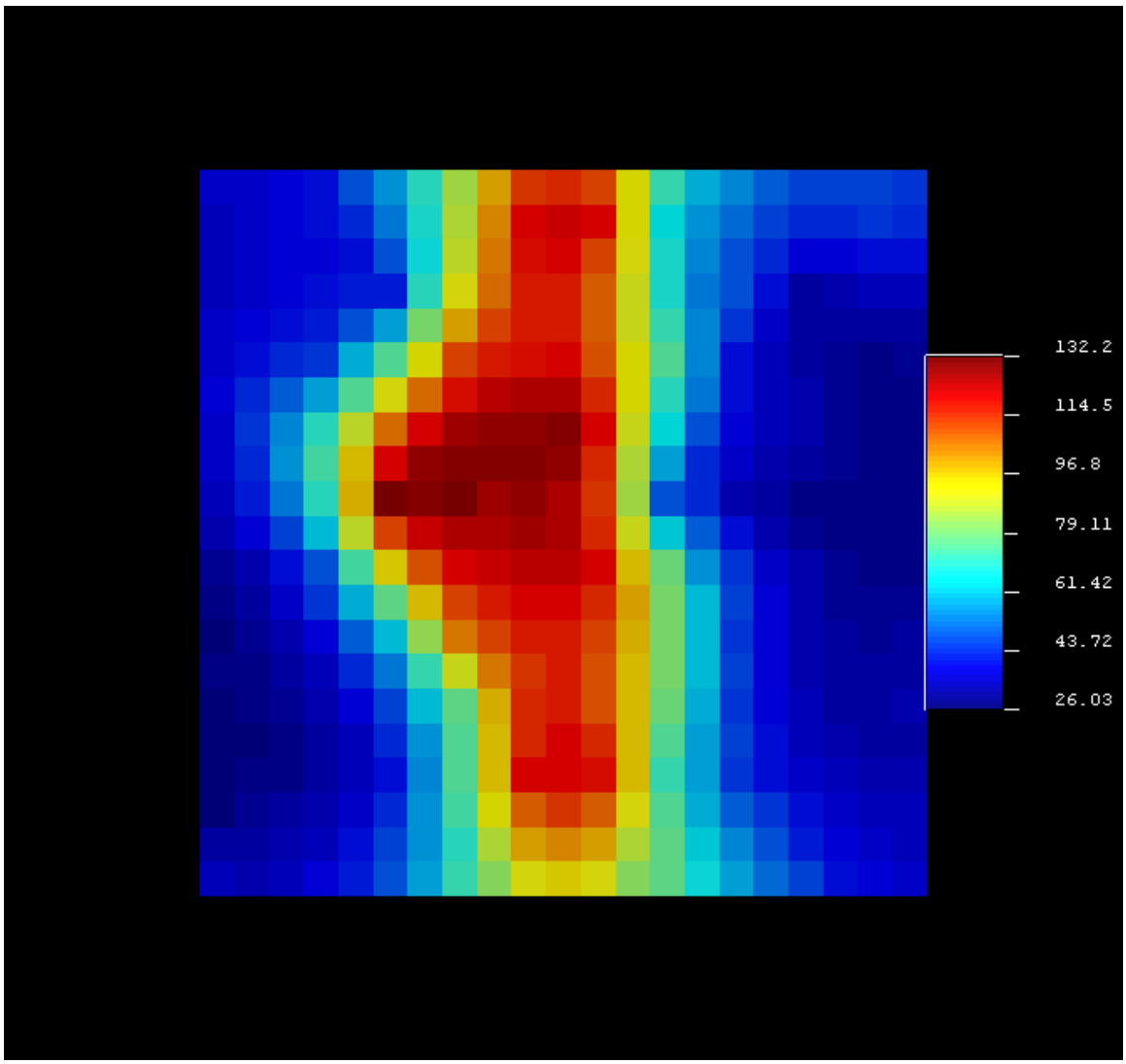

Figure C.5: Temperature profile from SAGD experiment at time $t = 22$ minutes

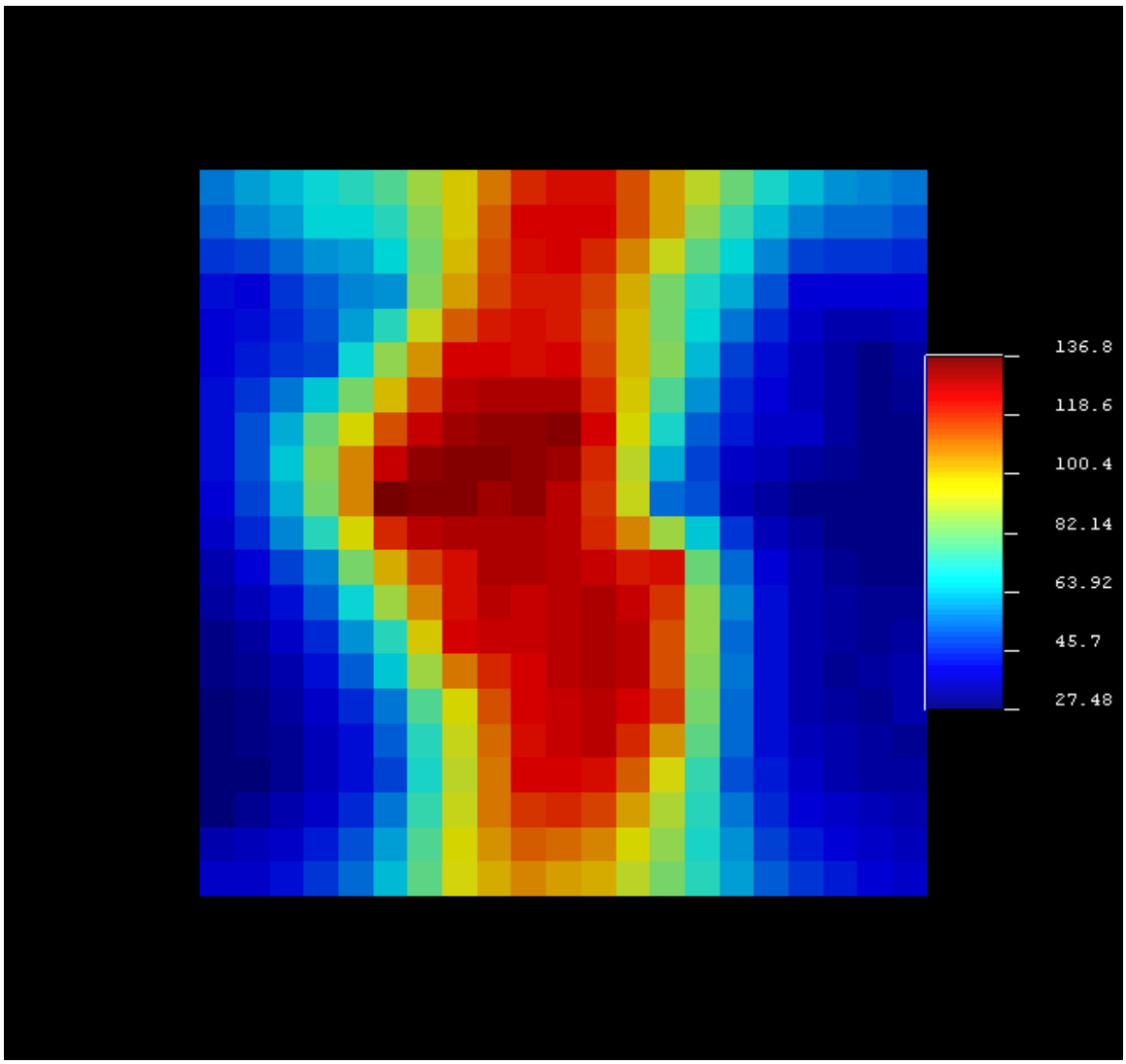

Figure C.6: Temperature profile from SAGD experiment at time $t = 32$ minutes

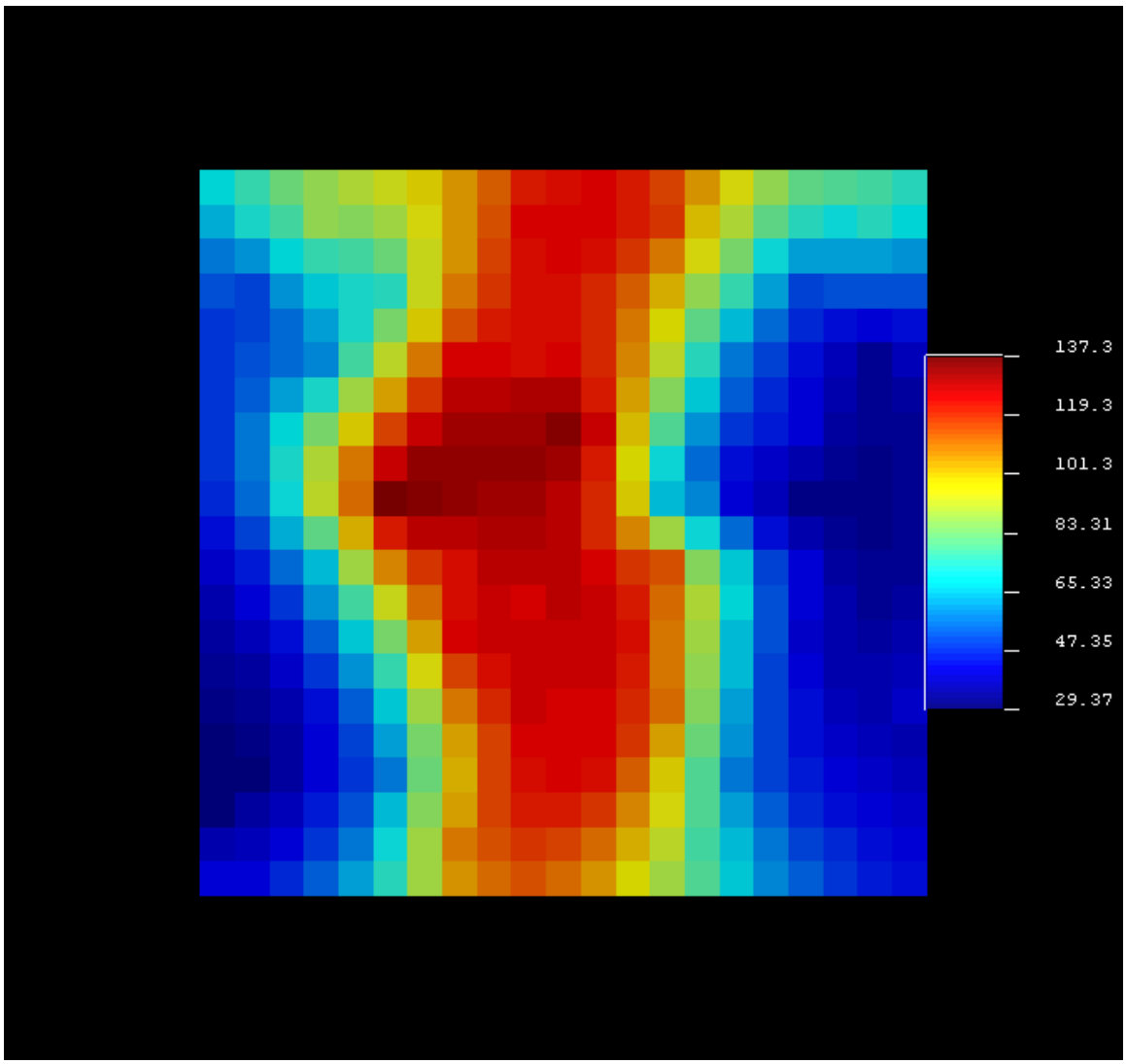

Figure C.7: Temperature profile from SAGD experiment at time $t = 42$ minutes

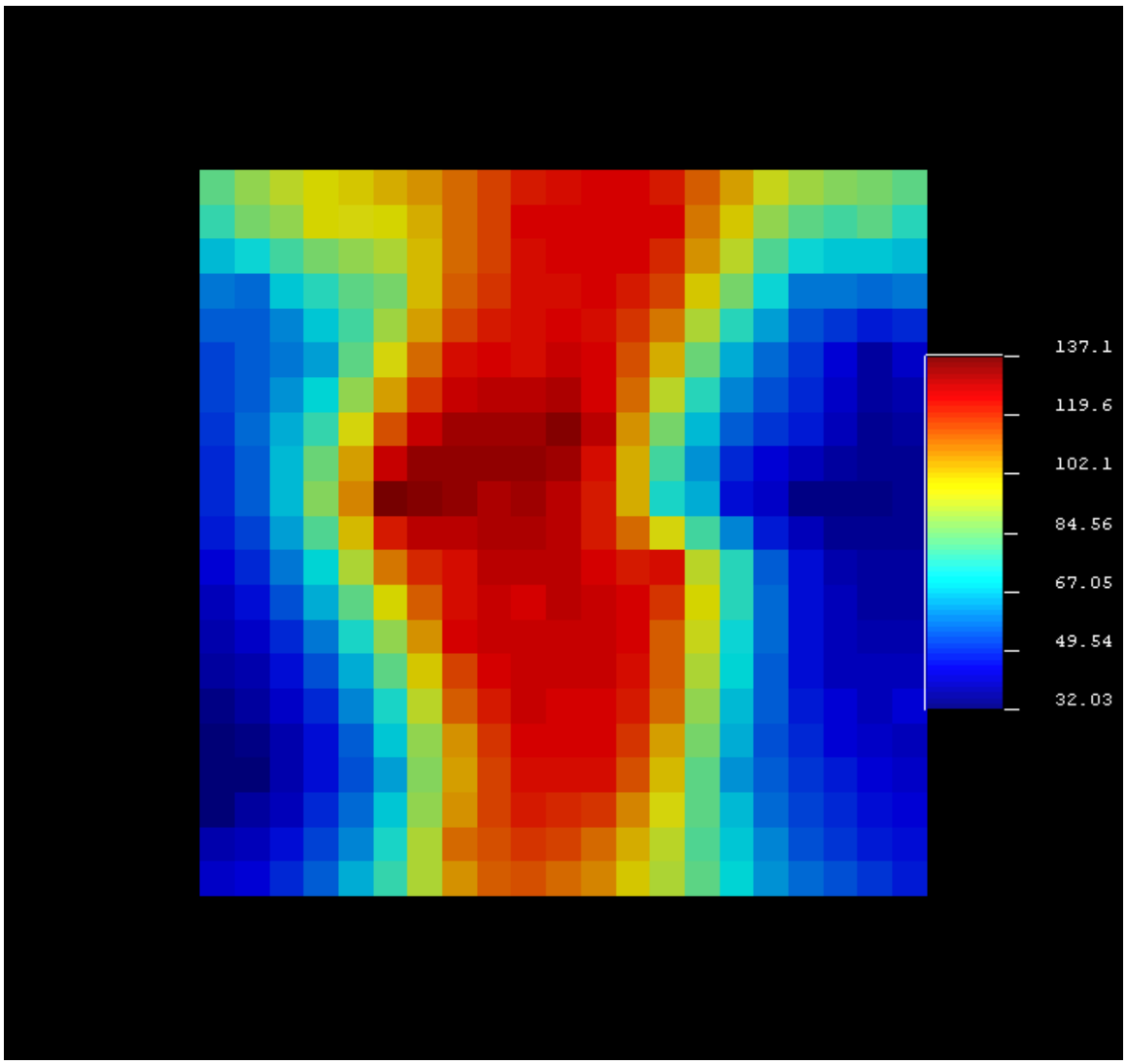

Figure C.8: Temperature profile from SAGD experiment at time $t = 52$ minutes

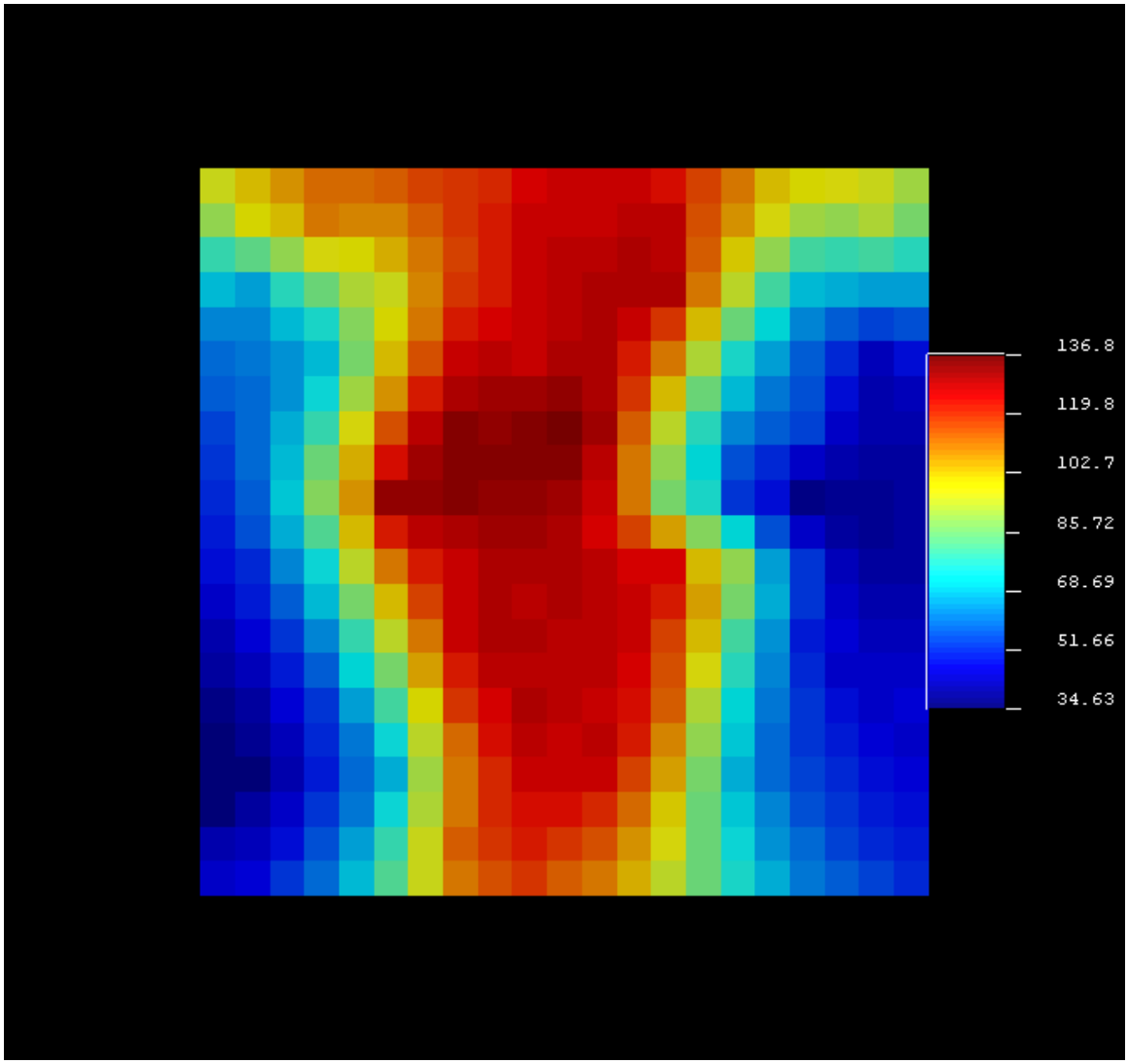

Figure C.9: Temperature profile from SAGD experiment at time $t = 62$ minutes

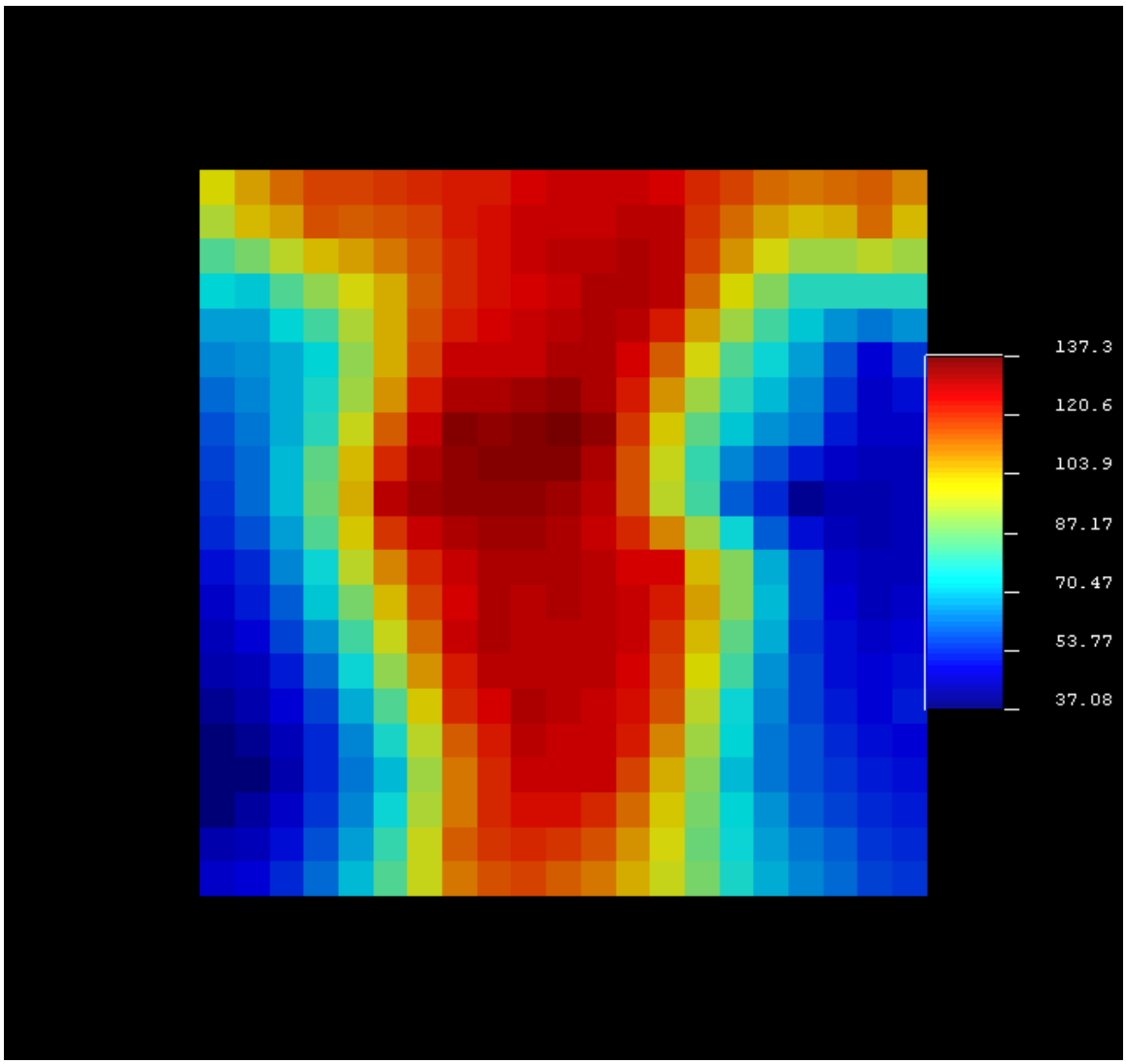

Figure C.10: Temperature profile from SAGD experiment at time $t = 72$ minutes

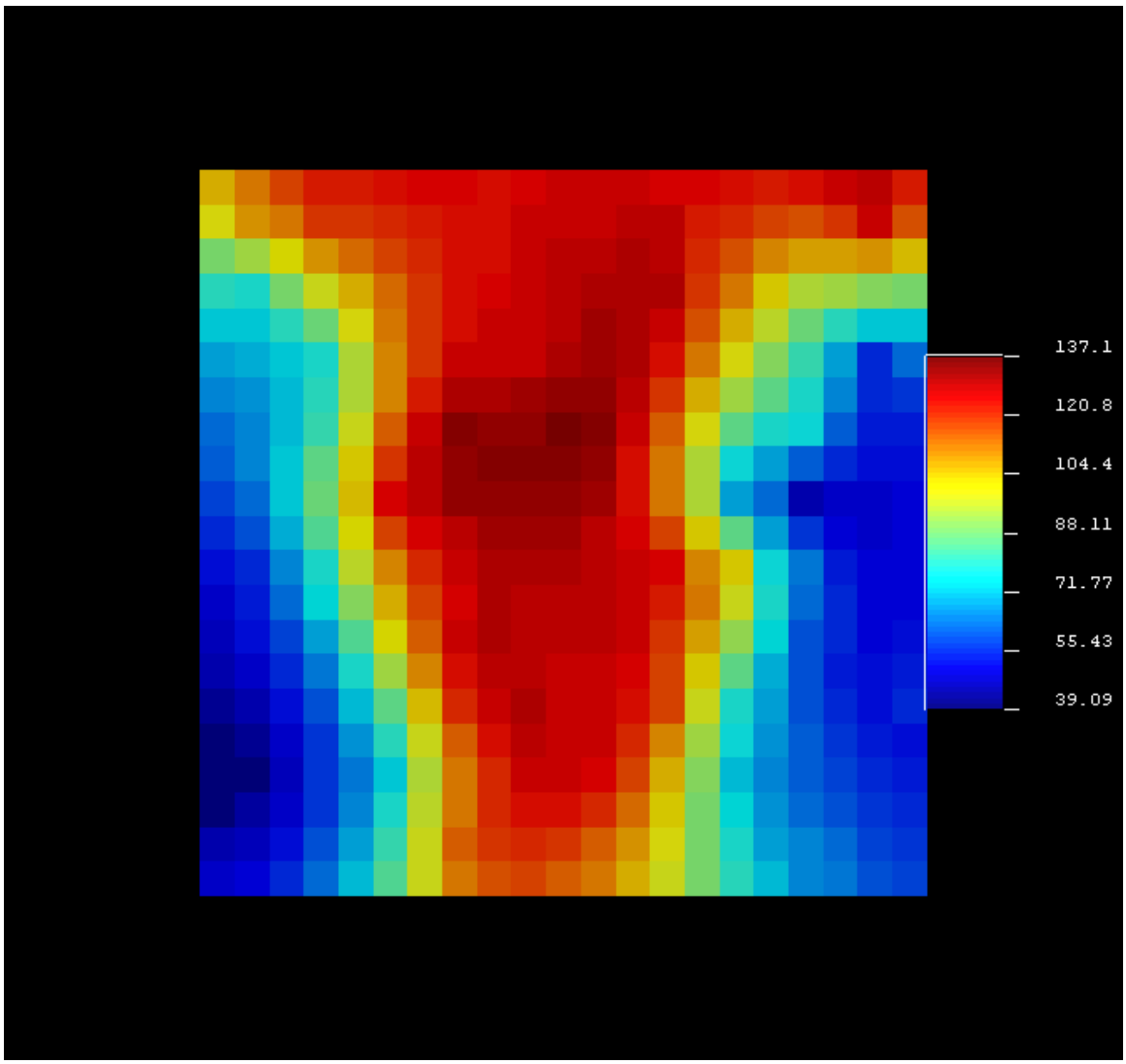

Figure C.11: Temperature profile from SAGD experiment at time $t = 82$ minutes

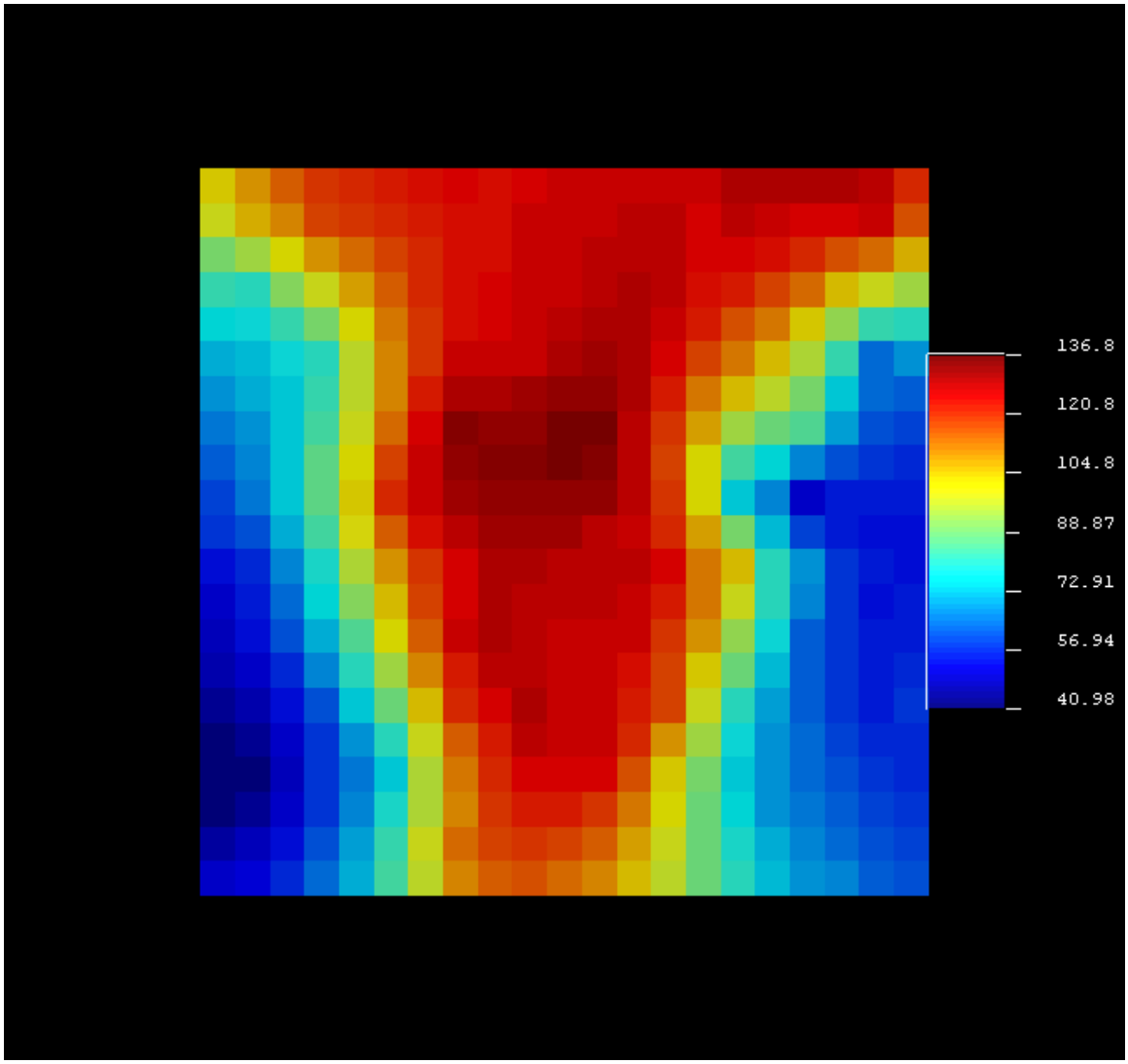

Figure C.12: Temperature profile from SAGD experiment at time $t = 92$ minutes

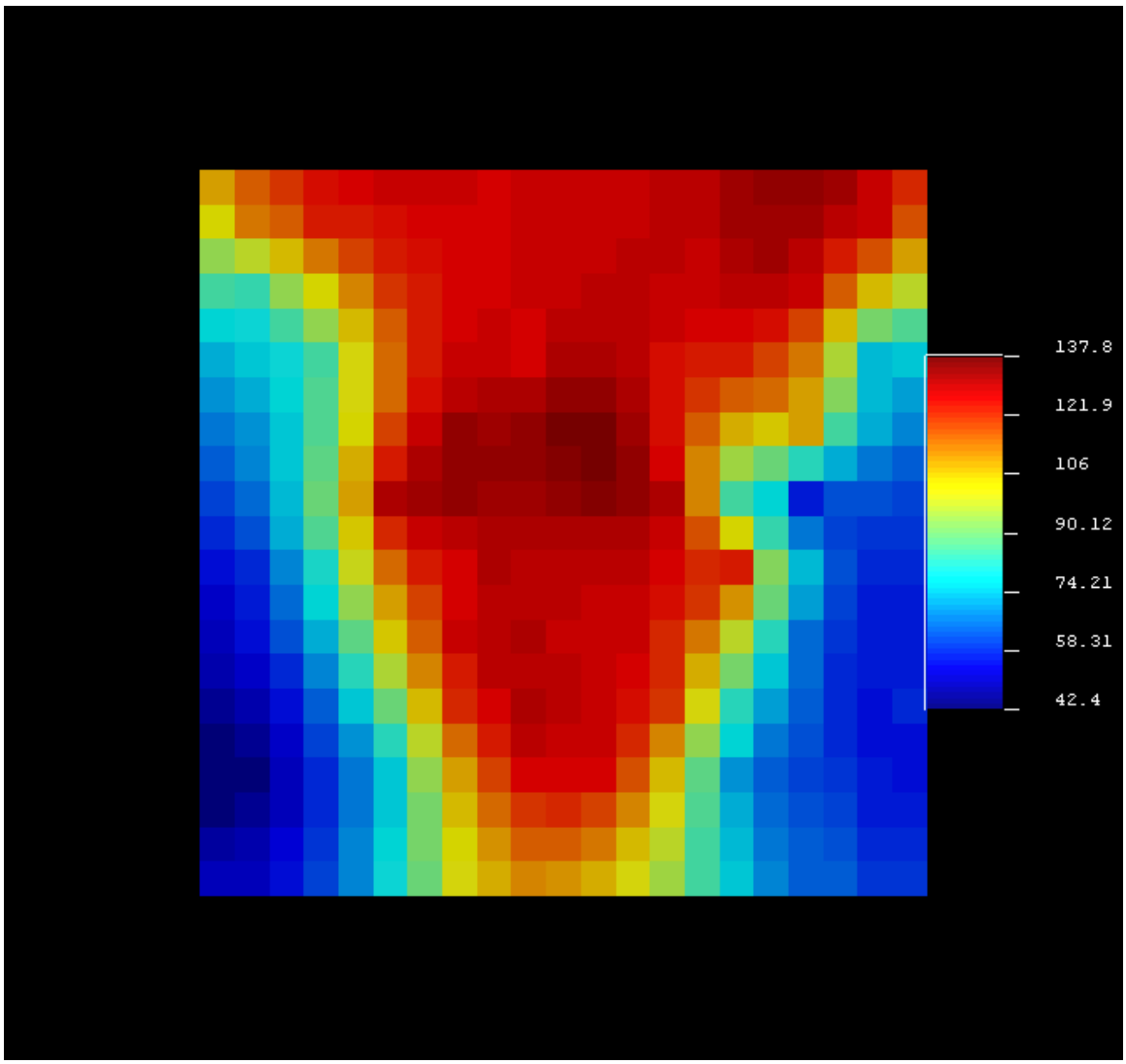

Figure C.13: Temperature profile from SAGD experiment at time $t = 102$ minutes

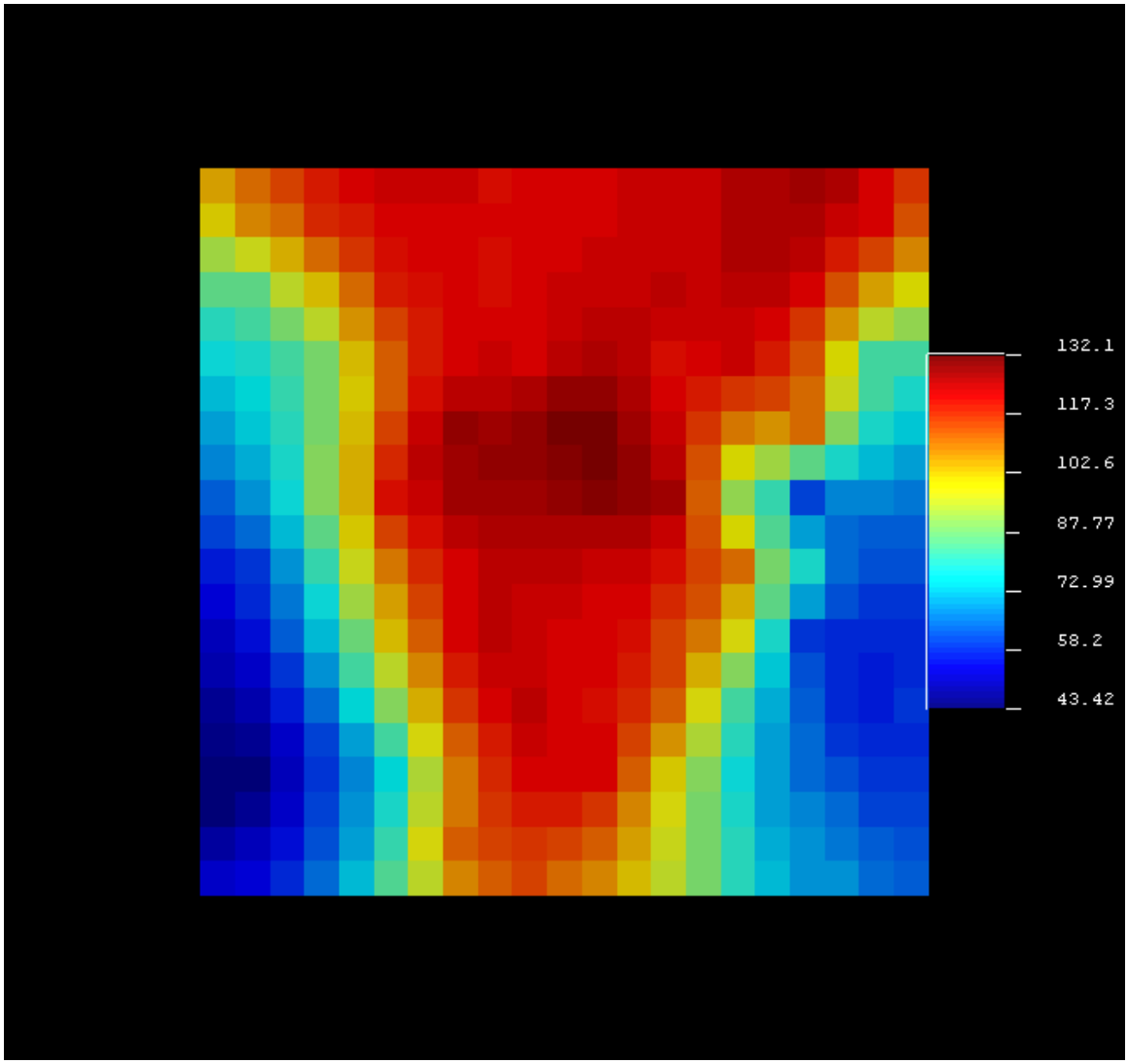

Figure C.14: Temperature profile from SAGD experiment at time $t = 112$ minutes

Bibliography

Aherne, A., Maini, B., 2008. Fluid Movement in the SAGD Process: A Review of the Dover Project. Journal of Canadian Petroleum Technology 47 (1) Jan.

Akin, S., 2005. Mathematical Modeling of Steam-Assisted Gravity Drainage. SPE Reservoir Evaluation & Engineering 8 (5) Oct.

Al-Bahlani, A.-M., Babadagli, T., 2009. SAGD laboratory experimental and numerical simulation studies: A review of current status and future issues. Journal of Petroleum Science and Engineering 68, 135–150.

Al-Murayri, M., Harding, T., Maini, B., 2011. Impact of Noncondensable Gas on Performance of Steam-Assisted Gravity Drainage. Journal of Canadian Petroleum Technology 50 (7) Jul.

Ananth Govind, P., Das, S., Srinivasan, S., Wheeler, T. J., 2008. Expanding Solvent SAGD in Heavy Oil Reservoirs. Society of Petroleum Engineers, SPE 117571-MS.

Arendo, V., Goulay, C., Stobie, G., Wall, T., Couput, J. P., 2005. The Challenges Facing Multiphase Metering in Oil-Sands Thermal Developments. Society of Petroleum Engineers, SPE 97751-MS.

Arya, Atul, Tom Hewett, Ronald Larson, and Larry Lake. 1988. "Dispersion and Reservoir Heterogeneity." SPE Reservoir Engineering 3 (1) (February).

Aster R. C., (2012), "Parameter Estimation and Inverse Problems", 2nd edition, Academic Press

Azad, A., 2012. Rapid SAGD Simulation Simulation Considering Geomechanics for Closed Loop Reservoir Optimization, PhD Dissertation, University of Alberta, Alberta, Canada.

Azad, A., Chalaturnyk, R., 2010. A Mathematical Improvement to SAGD Using Geomechanical Modelling. Journal of Canadian Petroleum Technology 49 (10) Oct.

Barillas, J.L.M., Dutra Jr., T.V., Mata, W., 2006. Reservoir and operational parameters influence in SAGD process. Journal of Petroleum Science and Engineering 54, 34–42.

Beetge, J., 2005. Emulsion Stability Evaluation of SAGD Product with the IPR-CEF Technique. Society of Petroleum Engineers, SPE 97785-MS.

Begg, S. H., and Chang, D. M., 1985. A Simple Statistical Method for Calculating the Effective Vertical Permeability of a Reservoir Containing Discontinuous Shales. Society of Petroleum Engineers SPE 14271-MS.

Bennison Trevor, 1998. Prediction of Heavy Oil Viscosity. Presented at the IBC Heavy Oil Field Development Conference, London.

Birrell, G., 2003. Heat Transfer Ahead of a SAGD Steam Chamber: A Study of Thermocouple Data From Phase B of the Underground Test Facility (Dover Project). Journal of Canadian Petroleum Technology 42 (3) Mar.

Bogdanov, I. I., K. El Ganaoui, and A. M. Kamp. 2007. "COMSOL 2D Simulation of Heavy Oil Recovery by Steam." In COMSOL Users Conference. Grenoble: COMSOL Multiphysics.

Bosch, R., Axcell, E., Little, V., Cleary, R., Wang, S., Gabel, R., Moreland, B., 2004. A Novel Approach for Resolving Reverse Emulsions in SAGD Production Systems. The Canadian Journal of Chemical Engineering 82, 836–839.

Bowman, C.W., 1967. Molecular and Interfacial Properties of Athabasca Tar Sands. Presented at the 7th World Petroleum Congress, World Petroleum Congress, Mexico City, Mexico.

Butler, R.M., Mcnab, G.S., Lo, H.Y., 1981. Theoretical studies on the gravity drainage of heavy oil during in-situ steam heating. The Canadian Journal of Chemical Engineering 59, 455–460.

Butler, R. M., and Stephens, D. J., 1981. The Gravity Drainage of Steam-heated Heavy Oil to Parallel Horizontal Wells. Journal of Canadian Petroleum Technology, 90-96, (April-June).

Butler, R., 1985. A New Approach To The Modelling of Steam-Assisted Gravity Drainage. Journal of Canadian Petroleum Technology, 42-51, (May – June).

Butler, R., Mokrys, I., 1991. A New Process (VAPEX) For Recovering Heavy Oils Using Hot Water And Hydrocarbon Vapour. Journal of Canadian Petroleum Technology 30 (1) Jan-Feb.

Butler, R. M. 1991. Thermal Recovery of Oil and Bitumen. Prentice Hall.

Butler, R. M., 1999. The Steam And Gas Push (SAGP). Journal of Canadian Petroleum Technology 38 (3) Mar.

Butler, R.M., Dargie, B., CIM, P.S. of, 1994. Horizontal wells for the recovery of oil, gas, and bitumen. Petroleum Society, Canadian Institute of Mining, Metallurgy & Petroleum.

Castor, T.P., Somerton, W.H., 1977. Interfacial Instabilities in Porous Media. Society of Petroleum Engineers, SPE 6516-MS.

Chalaturnyk, R., Li, P., 2004. When Is It Important to Consider Geomechanics in SAGD Operations? Journal of Canadian Petroleum Technology 43 (4) Apr.

Chen, Q., Gerritsen, M., Kovscek, A., 2008. Effects of Reservoir Heterogeneities on the Steam-Assisted Gravity-Drainage Process. SPE Reservoir Evaluation & Engineering 11 (5) Oct.

Chung, K., Butler, R. M., 1988. Geometrical Effect of Steam Injection on The Formation Of Emulsions In The Steam-Assisted Gravity Drainage Process. Journal of Canadian Petroleum Technology 27 (1) Jan-Feb.

Chung, K., Butler, R. M., 1989. In Situ Emulsification By The Condensation Of Steam In Contact With Bitumen. Journal of Canadian Petroleum Technology 28 (1) Jan-Feb.

Chuoke, . L., Meurs, P. va., Van der Poel, C., 1959. The instability of slow, immiscible, viscous liquid-liquid displacements in permeable media. AIME 216, 188–194.

Cuthiell, D., Green, K., Chow, R., Kissel, G., McCarthy, C., 1995. THE IN SITU FORMATION OF HEAVY OIL EMULSIONS. Society of Petroleum Engineers, SPE 30319-MS.

CMG. 2011. “CMG - STARS User Manual”. Computer Modeling Group.

Dalmazzone, C., Noïk, C., Glénat, P., Dang, H.-M., 2010. Development of a Methodology for the Optimization of Dehydration of Extraheavy-Oil Emulsions. SPE Journal 15 (3) Sep.

Das, Braja M. 2013. *Advanced Soil Mechanics*. 4th ed. Crc Pr I Llc.

Deutsch, C., 2010. Estimation of Vertical Permeability in the McMurray Formation. Journal of Canadian Petroleum Technology 49 (12) Dec.

Donnelly, J., 1998. Who Invented Gravity? Journal of Canadian Petroleum Technology 37 (9) Sep.

Dykstra, H., Parsons, R.L., 1950. The Prediction of Oil Recovery by Waterflooding. Secondary Recovery of oil in the United States 160–74.

Edmunds, Neil, and Simon Gittins. 1993. "Effective Application of Steam Assisted Gravity Drainage of Bitumen to Long Horizontal Well Pairs." Journal of Canadian Petroleum Technology 32 (6) Jun.

Edmunds, N., 1999. On the Difficult Birth of SAGD. Journal of Canadian Petroleum Technology 38 (1) Jan.

Einstein, A. 1906. Ann. Phys., Lpz., 19: 289.

Einstein. 1911. Ann. Phys., Lpz., 34: 591.

Ekwere J. Peters, 2012. Advanced Petrophysics: Volume 1: Geology, Porosity, Absolute Permeability, Heterogeneity, and Geostatistics. Live Oak Book Company.

El-Khatib, Noaman. 1995. "Development of a Modified Capillary Pressure J-Function." SPE 29890-MS .

Eötvös, L. 1886. *Annalen Der Physik* 27: 448.

Farouq-Ali, S., 1997. Is There Life After SAGD? Journal of Canadian Petroleum Technology 36 (6) Jun.

Flock, D. L., Le, T. H., Gibeau, J. P., 1986. The Effect Of Temperature On The Interfacial Tension Of Heavy Crude Oils Using The Pendent Drop Apparatus. Journal of Canadian Petroleum Technology, 25 (2) Mar-Apr.

Genuchten, Van, and M. Th. 1980. "A Closed-form Equation for Predicting the Hydraulic Conductivity of Unsaturated Soils." *Soil Science Society of America Journal* 44 (5): 892–898.

Georgie, W., Smith, P.C., 2012. The Challenges in Processing Heavy Oil. Society of Petroleum Engineers, SPE 157894-MS.

Gotawala, D.R., Gates, I.D., 2008. Steam fingering at the edge of a steam chamber in a heavy oil reservoir. The Canadian Journal of Chemical Engineering 86, 1011–1022.

Gupta, S. C., Gittins, S. D., 2006. Christina Lake Solvent Aided Process Pilot. Journal of Canadian Petroleum Technology 45 (9) Sep.

Gupta, S., Gittins, S., 2012. An Investigation Into Optimal Solvent Use and the Nature of Vapor/Liquid Interface in Solvent-Aided SAGD Process With a Semianalytical Approach. SPE Journal 17 (4) Dec. (1255 - 1264)

Haldorsen, H., Lake, L., 1984. A New Approach to Shale Management in Field-Scale Models. Society of Petroleum Engineers Journal 24 (4) Aug.

Harvey, Allan H. 1996. "Semiempirical Correlation for Henry's Constants over Large Temperature Ranges." *AIChE Journal* 42 (5): 1491–1494.

Hornbrook, M.W., Dehghani, K., Qadeer, S., Ostermann, R.D., Ogbe, D.O., 1991. Effects of CO2 Addition to Steam on Recovery of West Sak Crude Oil. SPE Reservoir Engineering 6 (3) Aug.

Ito, Y., and T. Hirata. 1999. Numerical Simulation Study of a Well In the JACOS Hangingstone Steam Pilot Project Near Fort McMurray. Journal of Canadian Petroleum Technology 38 (13).

Ito, Y., and Suzuki, S., 1999. Numerical Simulation of the SAGD Process In the Hangingstone Oil Sands Reservoir. Journal of Canadian Petroleum Technology 38 (9) Sep.

Javad S., P. Oskouei, B. Maini, R. Moore, and S. Mehta. 2010. Effect of Mobile Water-Saturation on Thermal Efficiency of Steam-Assisted Gravity-Drainage Process. SPE 138846-MS.

Kamath, V.A., Sinha, S., Hatzignatiou, D.G., 1993. Simulation Study of Steam-Assisted Gravity Drainage Process in Ugnu Tar Sand Reservoir. Society of Petroleum Engineers, SPE 26075-MS.

Kisman, K.E., Yeung, K.C., 1995. Numerical Study of the SAGD Process in the Burnt Lake Oil Sands Lease. Society of Petroleum Engineers, SPE 30276-MS.

Kovscek, A. R. 2009. "Unlocking Heavy Oil and Unconventional Resources with Heat" presented at the Petroleum & Geosystems Engineering Graduate Student Seminar Series, April 27, The University of Texas at Austin.

Lake, L.W., 1996. Enhanced Oil Recovery, 1st ed. Prentice Hall.

Lantz, R.B. 1971. “Quantitative Evaluation of Numerical Diffusion (Truncation Error).” Society of Petroleum Engineers Journal 11 (3) (September).

Le Ravalec, M., Morlot, C., Marmier, R., Foulon, D., 2009. Heterogeneity Impact on SAGD Process Performance in Mobile Heavy Oil Reservoirs. Oil & Gas Science and Technology - Revue de l’IFP 64, 469–476.

Leverett, M.C., 1941. Capillary behaviour in porous solids. Transactions of the AIME 142, 159–172.

Llaguno, P., Moreno, F., Garcia, R., Mendez, Z., Escobar, E., 2002. A Reservoir Screening Methodology for SAGD Applications. Society of Petroleum Engineers. Presented at the CIPC, Calgary, Alberta, June 11 - 13.

Lyford, Paul A., H.r.c Pratt, David C. Shallcross, and Franz Grieser. 1998. “The Marangoni Effect and Enhanced Oil Recovery Part 1. Porous Media Studies.” The Canadian Journal of Chemical Engineering 76 (2): 167–174.

Mandl, G., and C. W. Volek. 1969. “Heat and Mass Transport in Steam-Drive Processes.” SPE Journal 9 (1): 59 – 79.

Marx, J. W., and R. H. Langenheim. 1959. “Reservoir Heating by Hot Fluid Injection.” Petroleum Transactions AIME 216: 312–315.

McCormack, M., 2001. Mapping of the McMurray Formation for SAGD. Journal of Canadian Petroleum Technology 40 (8) (August).

McLennan, J., Deutsch, C., Garner, D., Mus, E., Wheeler, T., Richy, J.-F., 2006. Permeability Modeling for the SAGD Process Using Minimodels. Society of Petroleum Engineers, SPE 103083-MS.

Mehdizadeh, P., 2005. High-Temperature Multiphase Flowmeters in Heavy-Oil Thermal Production. Society of Petroleum Engineers, SPE 98009-MS.

Meyer, R. F., E. D. Attansasi, and P. A. Freeman. 2007. Heavy Oil and Natural Bitumen Resources in Geological Basins of the World. Open File. US Geological Survey.

Mohammadzadeh, O., Rezaei, N., Chatzis, I., 2010. Pore-Level Investigation of Heavy Oil and Bitumen Recovery Using Hybrid SAGD Process. Society of Petroleum Engineers, SPE 130011-MS.

Najeh, A., Pishvaie, R. M., and Jabbari, H., 2009. A new semi-analytical modeling of steam-assisted gravity drainage in heavy oil reservoirs. Journal of Petroleum Science and Engineering 69, 261–270.

Nasr, T., S. Law, D., Golbeck, H., Korpany, G., 2000. Counter-current Aspect of the SAGD Process. Journal of Canadian Petroleum Technology 39 (1) Jan.

Nasr, T., Beaulieu, G., Golbeck, H., Heck, G., 2003. Novel Expanding Solvent-SAGD Process "ES-SAGD". Journal of Canadian Petroleum Technology 42 (1) Jan.

Nasr, Tawfik, and Oluropo Ayodele. 2006. New Hybrid Steam-Solvent Processes for the Recovery of Heavy Oil and Bitumen. In Society of Petroleum Engineers, SPE 101717-MS .

Nield, D.A., 1998. Modelling the Effect of Surface Tension on the Onset of Natural Convection in a Saturated Porous Medium. Transport in Porous Media 31, 365–368.

Noik, C., Dalmazzone, C., Goulay, C., Glenat, P., 2005. Characterisation and Emulsion Behaviour of Athabasca Extra-Heavy-Oil Produced by SAGD. Society of Petroleum Engineers, SPE 97748-MS.

Nukhaev, M., Pimenov, V., Shandrygin, A., Tertychnyi, V., 2006. A New Analytical Model for the SAGD Production Phase. Society of Petroleum Engineers, SPE 102084-MS.

Oldroyd, J. G. 1953. "The Elastic and Viscous Properties of Emulsions and Suspensions." Proceedings of the Royal Society of London. Series A. Mathematical and Physical Sciences 218 (1132) (June 9): 122–132.

Orr, Bryan. 2009. ES-SAGD; Past, Present and Future. In SPE Annual Technical Conference and Exhibition. New Orleans, Louisiana, USA: SPE 129518-STU.

Peaceman, D.W., 1993. Reperesentation of a Horizontal Well in Numerical Reservoir Simulation. SPE Advanced Technology Series 1 (1).

Plyasunov, Andrey V., and Everett L. Shock. 2003. "Prediction of the Vapor–liquid Distribution Constants for Volatile Nonelectrolytes in Water up to Its Critical Temperature." *Geochimica Et Cosmochimica Acta* 67 (24) (December 15): 4981–5009.

Rabiei Faradonbeh, M., Harding, T., Abedi, J., 2012. Semi-Analytical Modeling of Steam-Solvent Gravity Drainage of Heavy Oil and Bitumen, Part 1: Enhanced Flow Rate at Mobile Zone. Society of Petroleum Engineers, SPE 160316-MS.

Raghavan, R., and Marsden S.S. 1971a. "Theoretical Aspects of Emulsification in Porous Media." Society of Petroleum Engineers Journal 11 (2) (June).

Raghavan, R., Marsden, S.S., 1971b. The stability of immiscible liquid layers in a porous medium. Journal of Fluid Mechanics 48, 143–159.

Raghavan, R., 1982. The Instability of Liquid-liquid Interfaces and Model Systems for Emulsion Formation in Porous Media. University Microfilms.

Reis, J., 1992. A Steam-Assisted Gravity Drainage Model For Tar Sands: Linear Geometry. Journal of Canadian Petroleum Technology 31 (10) Oct.

Reis, J., 1993. A Steam Assisted Gravity Drainage Model For Tar Sands: Radial Geometry. Journal of Canadian Petroleum Technology 32 (8) Aug.

Sandler, Stanley I. 2006. *Chemical, Biochemical, and Engineering Thermodynamics*. John Wiley & Sons.

Sanyi, W., Eric, A., Robert, C., Virgil, L., Lon, P., 2004. Application Of A Reverse-Emulsion-Breaker At A SAGD Pilot Plant In Northern Alberta. Society of Petroleum Engineers, SPE 86932-MS.

Sasaki, K., Akibayahsi, S., Yazawa, N., Doan, Q., Farouk Ali, S., 2001a. Numerical and Experimental Modelling of the Steam Assisted Gravity Drainage (SAGD). Journal of Canadian Petroleum Technology 40 (1) Jan.

Sasaki, K., Akibayashi, S., Yazawa, N., Doan, Q.T., Ali, S.M., 2001b. Experimental Modeling of the SAGD Process - Enhancing SAGD Performance with Periodic Stimulation of the Horizontal Producer. SPE Journal 6 (1) Mar.

Sasaki, K., Satoshi, A., Nintoku, Y., Fuminori, K., 2002. Microscopic Visualization with High Resolution Optical-Fiber Scope at Steam Chamber Interface on Initial Stage of SAGD Process. Society of Petroleum Engineers, SPE 75241-MS.

Serhat, A., Castanier, L., Brigham, W., 1999. Effect of Temperature on Heavy Oil/Water Relative Permeabilities. Society of Petroleum Engineers, SPE 54120-MS.

Sharma, B., Santanu, K., Patil, S., Kamath, V., Dandekar, A., 2002. A Simulation Study of Novel Thermal Recovery Methods in the Ugnu Tar Sand Reservoir, North Slope, Alaska. Society of Petroleum Engineers, SPE 76729-MS.

Sharma, J., Gates, I., 2010a. Steam-Solvent Coupling at the Chamber Edge in an In Situ Bitumen Recovery Process. Society of Petroleum Engineers, SPE 128045-MS.

Sharma, J., Gates, I.D., 2010b. Multiphase flow at the edge of a steam chamber. The Canadian Journal of Chemical Engineering 88, 312–321.

Sharma, J., Gates, I., 2011. Convection at the Edge of a Steam-Assisted-Gravity-Drainage Steam Chamber. SPE Journal 16 (3) Sep.

Sharma, J., Moore, R., Mehta, S., 2012. Effect of Methane Co-injection in SAGD − Analytical and Simulation Study. Society of Petroleum Engineers Journal 17 (3) Sep.

Shin, H., Choe, J., 2009. Shale Barrier Effects on the SAGD Performance. Society of Petroleum Engineers, SPE 125211-MS.

Srivastava, Piyush, Vladimir Sadetsky, Justin Debord, Brian Stefan, and Bryan Orr. 2010. Development of a Steam-Additive Technology To Enhance Thermal Recovery of Heavy Oil. In Society of Petroleum Engineers, SPE 133465-MS.

Taylor, G. I. 1932. "The Viscosity of a Fluid Containing Small Drops of Another Fluid." Proceedings of the Royal Society of London. Series A 138 (834) (October 1): 41–48.

Thimm, H. 2001. A General Theory of Gas Production in SAGD Operations. Journal of Canadian Petroleum Technology 40 (11) Nov.

Thimm. 2006. Henry's Law Near the Critical Point of Water-Applications in Solvent Co-Injection With SAGD. Journal of Canadian Petroleum Technology 45 (1) Jan.

Torabzadey, S.J. and Handy L. L., 1984. The Effect of Temperature and Interfacial Tension on Water/Oil Relative Permeabilities of Consolidated Sands. SPE 12689-MS.

Veil, J. A., Quinn, J. J., 2008. Water Issues Associated with Heavy Oil Production. Prepared of the U.S. Department of Energy, national Energy Technology Laboratory.

Wagner, Wolfgang, and A. Pruss. 1993. “International Equations for the Saturation Properties of Ordinary Water Substance. Revised According to the International Temperature Scale of 1990. Addendum to J. Phys. Chem. Ref. Data 16, 893 (1987). Journal of Physical and Chemical Reference Data 22 (3): 783.

Wu, C.H., M.K. Beladi, G.P. Xue, M. Barrufet, I. Chawla, and K. Liu. 1997. Three Phase K-Values of Heavy Paraffins and Crude Oil Pseudocomponents in Presence of Water. In Society of Petroleum Engineers, SPE 37537-MS.

Xu, Yuming. 1990. Thermodynamic Investigations: 1. Gases and Vapours in Liquids; 2. Calorimetric Studies. Ph.D., Alberta, Edmonton, AB: Alberta.

Yang, G., Butler, R. M., 1992. Effects of Reservoir Heterogeneities on Heavy Oil Recovery by Steam-Assisted Gravity Drainage. Journal of Canadian Petroleum Technology 31 (8) Aug.

Vita

Prince Nnamdi Azom was born in Nigeria and received his Bachelor of Science degree in Chemical Engineering from the University of Lagos also in Nigeria, graduating with a First Class (Hons.) in December 2006. He started his graduate studies at the University of Texas at Austin in August 2007 and in May 2011, applied and obtained his Master's degree in Petroleum Engineering on his way to obtaining his PhD degree in the same discipline. He had several internships during his graduate studies with Afren Resources, USA and worked briefly as a Research Engineer at the Open & Experimental Center for Heavy Oil (CHLOE), Pau, France in 2010. He is also the author of numerous technical papers on modeling unconventional reservoirs. He is happily married with a son and currently lives with his family in Alberta, Canada.

Permanent e-mail address: prince.azom@utexas.edu

This thesis was typed by the author.